Structural Design Parameters of Current WSDOT Mixtures

Jacob Meader

A thesis
submitted in partial fulfillment of the
requirements for the degree of

Master of Science in Civil Engineering

University of Washington
2013

Committee:
Marc Eberhard
Donald Janssen

Program Authorized to Offer Degree:
Civil Engineering

DISCLAIMER

The contents of this report reflect the views of the authors, who are responsible for the facts and the accuracy of the data presented herein. The contents do not necessarily reflect the official views or policies of the Washington State Department of Transportation or Federal Highway Administration. This report does not constitute a standard, specification, or regulation.

Executive Summary

PROBLEM STATEMENT

Typically, designers specify a minimum compressive strength for concrete (at 28 days) for each portion of a structure. The other performance characteristics of the concrete, such as tensile strength, elastic modulus, shrinkage and creep parameters, are then estimated based on compressive strength alone.

This practice may not reflect actual performance, because (1) the concrete strength of a mixture will usually exceed the specified strength, (2) concrete properties vary from batch to batch, and (3) the properties of a mixture can vary based on mixture characteristics other than compressive strength.

RESEARCH GOALS

The goals of this research were to

- characterize the structural characteristics of the Washington State Department of Transportation (WSDOT) Class 4000 concrete mixture
- evaluate the variations in these properties according to variations in mixture proportions
- evaluate the accuracy of relevant provisions in the AASHTO Load and Resistance Factor Design (LRFD) specifications
- where necessary, provide guidance for improving estimates of these properties.

RESEARCH APPROACH

Class 4000 concrete mixtures were sampled from five WSDOT bridge construction projects located throughout Washington State. Coarse aggregate from the same sources used in each of these WSDOT projects (and from two additional sources) was then used to cast laboratory mixtures with a variety of mix proportions. For each of the seven aggregate types, the researchers evaluated the properties of four mixtures. Two mixtures of these mixtures had a constant water-cementitious ratio, but the paste

contents differed. The remaining two mixtures had the same paste content, but the water-cementitious ratios differed.

The concrete performance properties were evaluated by using standardized testing procedures. Tests on laboratory and field mixtures included:

- Compressive strength (ASTM C39),
- Flexural strength (ASTM C78),
- Split-tensile strength (ASTM C496),
- Elastic modulus (ASTM C469),
- Drying shrinkage (ASTM C157), and
- Creep (ASTM C512).

The collected aggregate sources were also tested for absorption and specific gravity (ASTM C127).

FINDINGS AND RECOMMENDATIONS:

Compressive Strength

For a given concrete age, the compressive strength of a mixture depended mainly on its water-cementitious ratio and to a lesser extent, on the aggregate source. The compressive strength did not vary consistently with paste content.

The concrete mixtures cast for this research gained strength faster at early ages than suggested by the specifications. The time dependence of the compressive strength was modeled well by the ACI 209.2R-08 specifications (A-17), but only if the equation constants were optimized. It is likely that variations in cement type and cement refinement process since the development of the ACI 209.2R-08 equation have led to acceleration in the rate of strength gain.

WSDOT should consider estimating early strength gain using parameters that are representative of current materials used in Washington state.

Tensile Strength

The following conclusions were drawn from the results of split-tension and flexural tests:

- The flexure strengths and split-tensile strengths increased with increasing compressive strength, as expected.
- The flexural strength of the mixtures was approximately equal (on average) to 1.58 times the split-tension strength. The correlation between the two strengths was close to that suggested by ASTM STP 169D.
- The variability of the strengths of the split tension specimens (average variation of 8.3%) generally exceeded that of the flexural strength samples (4.0%).

The AASHTO LRFD code specifications for normal-weight concrete (5.4.2.6) greatly underestimated the flexural strengths of the field samples (lower by an average of 33%). In contrast, the equation that was developed for high-strength concrete over-predicted the field sample flexure strengths (by an average of 13%).

Elastic Modulus

The following findings were reached regarding variations in the elastic modulus.

- The elastic modulus consistently increased with increasing compressive strength.
- The effect of the paste content on the elastic modulus was not consistent.

Regardless of compressive strength, paste content or aggregate source, the elastic moduli for all the laboratory mixtures exceeded the values predicted by the AASHTO LRFD specifications (5.4.2.4-1) by 10.4%, on average. Surprisingly, this discrepancy was not identified for the field mixtures. The average difference between the measured and calculated elastic moduli for the field mixtures was only 4.2%.

Further research would be needed to determine the causes of the discrepancy between the elastic moduli for the laboratory cast and field-cast mixtures.

Shrinkage

The drying shrinkage strain increased with:

- increasing water-to-cementitious ratio,
- increasing paste content,
- decreasing volume-to-surface ratio, and
- decreasing compressive strength.

The specification procedures greatly overestimated the measured time-related shrinkage stains (by approximately 45%). The AASHTO drying shrinkage strain predictions improved when the measured Day 28 compressive strengths were used, but the predicted and measured strain still differed typically by about 20%.

Two methods were developed to improve predictions of long-term deformations (one year drying duration). The first method extrapolates long-term deformations from short duration tests by optimizing the two coefficients from a modified formula based on the ACI 209R-92 specifications (2-7). A second method was developed to predict long-term deformations directly from key mixture characteristics. Predicted one-year drying strains were within an accuracy of 6.6% for the mixtures tested.

WSDOT should consider the use of these alternate methods for establishing the long-term shrinkage strains for mixtures made with local materials.

Creep

Based on the results of the six creep tests, the following conclusions were drawn.

- The elastic, drying shrinkage and creep strains all varied according to the aggregate type, compressive strength, and paste content.
- The specific creep (ratio of creep strain to applied stress) varied little for the range of mixtures considered. At day 365, the average specific creep was 0.48 and it had a coefficient of variation of 7.2%.
- The creep coefficient (ratio of creep strain) was also insensitive to changes in the mixture properties. At day 365, the creep coefficient had an average of 2.08 and a coefficient of variation of 8.1%.

Using design values of the concrete compressive strength (4,000 psi), and calculated values of the elastic modulus and creep coefficient, the measured creep strains consistently exceeded (on average, by 21%) the values predicted following the AASHTO specifications,. The errors in the estimates of creep strains appear to stem mainly from differences between assumed and measured values of the concrete compressive strength and elastic modulus. Estimates of long-term creep deformations could be best improved by making accurate estimates of the actual concrete strength and estimates of the actual elastic modulus.

Table of Contents

List of Figures

List of Tables

Chapter 1: Problem Statement

The structural performance of a concrete mixture can be characterized by a number of properties, including its compressive strength and tensile strength, as well as deformation-related properties, such as the modulus of elasticity, drying shrinkage and creep parameters. These properties depend mainly on the mixture proportions, including the water-to-cementitious ratio and the amount of cementitious binder (paste), as well as the coarse aggregate size and type. Variations in these mixture characteristics can affect both the performance of the concrete and the accuracy of estimates of these properties.

In current design practice, agencies usually specify a compressive strength (typically at 28 days of curing) and use equations to predict other performance characteristics from the strength. However, current specifications relate most of the structural performance properties to compressive strength, with little regard to mixture proportions. Therefore, because under-strength concrete is penalized, the actual concrete strength often exceeds the design strength, which can lead to inaccuracies in strength-based performance predictions when the design strength is used instead of the actual strength. In addition, mixtures with the same strength can have different paste contents, different aggregate sources, and normal production variability. All of these factors can lead to variations from the properties assumed in design.

The goals of this research were to

- characterize the structural behavior of the Washington State Department of Transportation (WSDOT) Class 4000 concrete mixture
- evaluate the variations in these properties according to variations in mixture proportions
- evaluate the accuracy of relevant provisions in the AASHTO Load and Resistance Factor Design (LRFD) specifications
- where necessary, provide guidance for improving estimates of these properties.

The concrete performance properties that were investigated in this research were compressive strength, tensile strength, elastic modulus, drying shrinkage, and creep. Samples of WSDOT Class 4000 mixtures were taken throughout Washington state from five WSDOT bridge construction projects to document the effects of variations in aggregate sources. Laboratory

mixtures were cast by using the same aggregate sources from the WSDOT projects. In the laboratory mixtures, the paste content and water-cementitious ratio were varied over a wide range to further evaluate the sensitivity of concrete properties to the mixture proportions.

In this report, instances when performance predictions were sufficiently accurate are noted, and when current code specifications for performance predictions could be improved, modifications are recommended to improve the accuracy of concrete property estimates throughout Washington state. By examining a range of mixture proportions and coarse aggregates for WSDOT mixtures, it may be possible to improve predictions for the properties of future concrete mixtures made with similar materials. Use of both material properties and the compressive strength of a concrete mixture would greatly improve the accuracy of related performance property estimates.

Chapter 2: Background and Literature Review

The concrete performance properties that were investigated in this research were the compressive strength, tensile strength, elastic modulus, drying shrinkage, and creep. The AASHTO, ACI, and ASTM specifications contain provisions for estimating the expected values of each of these properties. This chapter defines the terminology and describes the code-prescribed predictive equations for each performance characteristic.

2.1 COMPRESSIVE STRENGTH

This research project was concerned with Class A(AE) concrete mixtures, as defined by AASHTO. Specifically, the concrete mixtures were designed to have a compressive strength of 4,000 psi at 28 days of curing, a water-cementitious ratio of less than 0.45, and the inclusion of air entraining admixture to produce an air content of approximately 6 percent ± 1 percent. ACI 318 Section 5.6.3.3 b states that the compressive strength of a single sample at 28 days of curing cannot fall below 500 psi of the specified design strength (4,000 psi). If any sample fails to meet ACI 318 specifications, an investigation of the mixture must be undertaken.

ACI 209 specifications (A-17) suggest a method of modeling the compressive strength gain over time for a concrete mixture. The formula from ACI 209 is shown in Equation 2.1.

$$\frac{f_{time}}{f_{28}} = \frac{time}{K_1 + K_2 \times time} \qquad \text{(Equation 2.1)}$$

The two constants, K_1 and K_2, are optimized to fit the normalized data set for each concrete mixture. ACI 209 suggests values for the K_1 and K_2 constants of 4.0 and 0.85, respectively. These suggested values are for Type I cement and were developed many years ago. The cement used for casting the field and laboratory mixtures was Type I/II, but cements today tend to be ground finer, which typically results in higher early strengths.

The provisions and recommendations for compressive strength are evaluated in Chapter 3.

2.2 TENSILE STRENGTH

Two test methods are commonly used to measure the tensile strength of concrete: the flexural strength test (ASTM C78) and the split-tension test (ASTM C496). The split-tension test indirectly measures the tensile strength of the concrete, and the flexural strength test determines the modulus of rupture. The modulus of rupture (σ_{FLEX}) can be estimated for normal-weight concrete in the AASHTO LRDF specifications (Section 5.4.2.6) with Equation 2.2.

$$\text{Normal Weight, } \sigma_{FLEX} \text{ psi} = 240 \times \sqrt{f_c} \text{ (ksi)} \qquad \text{(Equation 2.2)}$$

Equation 2.3 can be used to estimate the modulus of rupture for high-strength concrete, as defined in the AASHTO commentary (Section C5.4.2.6).

$$\text{High Strength, } \sigma_{FLEX} \text{ psi} = 370 \times \sqrt{f_c} \text{ (ksi)} \qquad \text{(Equation 2.3)}$$

ACI 318 (Section R8.6) specifies a relationship for estimating the split tensile strength (σ_{ST}) for normal-weight concrete, as shown in Equation 2.4.

$$\sigma_{ST} \text{ psi} = 6.7 \times \sqrt{f_c} \text{ (psi)} \qquad \text{(Equation 2.4)}$$

ASTM STP 169D suggests there is a linear correlation between the split-tension and flexural strength results, as shown in Equation 2.5.

$$\sigma_{ST} \text{ psi} = 0.65 \times \sigma_{FLEX} \text{ (psi)} \qquad \text{(Equation 2.5)}$$

Equation 2.5 can be rewritten in the form of Equation 2.6, in which the flexural strength is predicted from the split-tension strength.

$$\sigma_{FLEX} \text{ psi} = 1.54 \times \sigma_{ST} \text{ (psi)} \qquad \text{(Equation 2.6)}$$

The accuracy of these provisions and recommendations is evaluated in Chapter 4.

2.3 ELASTIC MODULUS

According to the AASHTO LRFD provisions (Section 5.4.2.4-1), the elastic modulus for a concrete mixture can be estimated as shown in Equation 2.7.

$$E_c \text{ (ksi)} = 33{,}000\, K_1 w_c^{1.5} \sqrt{f'_c} \text{ (ksi)} \qquad \text{(Equation 2.7)}$$

where: $K_1 =$ factor for aggregate taken as 1.0 unless determined by physical testing

$w_c^{1.5}$ = unit weight of concrete (kcf)

For normal-weight concrete (approximately 0.145 kcf), the resulting elastic modulus equation becomes $1{,}820 \sqrt{f'_c}$ (ksi) (C5.4.2.4-1). The more commonly used model for estimating the elastic modulus is defined in ACI 318 (Section 8.5.1) and can be seen in Equation 2.8.

$$E_c \text{ (psi)} = 57{,}000 \sqrt{f'_c} \text{ (psi)} \qquad \text{(Equation 2.8)}$$

Both the ACI and AASHTO LRDF specifications estimate the elastic modulus of a concrete mixture on the basis of the compressive strength, so the two models are compared in Figure 2.1.

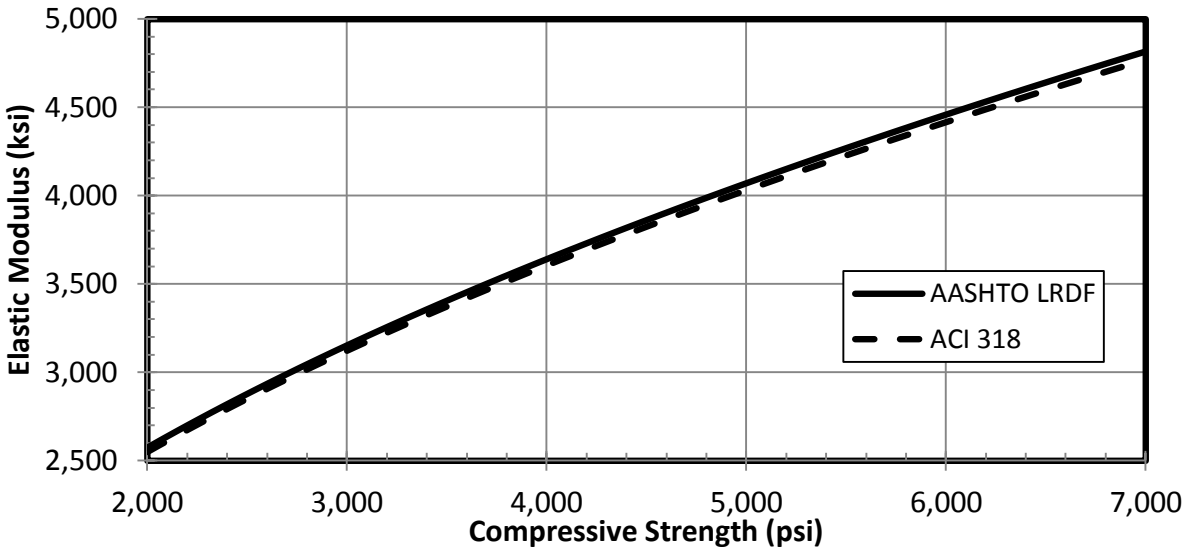

Figure 2.1: AASHTO and ACI 318 Estimated Elastic Moduli

The figure shows that the two models are nearly identical and that the AASHTO LRFD predicts values for the elastic modulus that are approximately 1 percent higher than the values suggested by ACI 318. This small difference results from rounding of the ACI 318 specifications (Section 8.5.1) for normal weight concrete (145 pounds per cubic foot). The differences between the two equations are small, so this research concerned itself only with the validity of the AASHTO LRDF specifications.

Both the AASHTO specifications (Section 5.4.2.4-1) and the ACI 318 specifications (Section 8.5.1) denote the compressive strength of the concrete mixture as f'_c, which is the design strength. This is not the correct interpretation of the research based on work by Paul (1960), which used the average compressive strength, f_c.

The evaluation of the elastic modulus provisions is provided in Chapter 5.

2.4 DRYING SHRINKAGE

AASHTO LRFD specifications (Section 5.4.2.3.3) estimate the drying shrinkage strains for a concrete sample for a particular drying duration. Equation 2.9 shows the form of the predictive formula.

$$\varepsilon_{sh} = k_{hs} k_s k_f k_{td} 0.48 \times 10^{-3} \qquad \text{(Equation 2.9)}$$

where: $k_{hs} = 2.00 - 0.014H$

$$k_s = \frac{t}{26e^{0.36\,(V/S)} + t} \quad \frac{1064 - 94\,(V/S)}{923}$$

$$k_f = \frac{5}{1 + f'_{ci}}$$

$$k_{td} = \frac{t}{61 - 4f'_{ci} + t}$$

H = relative humidity (percent)

V/S = volume-to-surface ratio (in.)

f'_{ci} = specified compressive strength of the concrete at the time of initial loading or prestressing; if the concrete age at the time of initial loading is unknown, it may be taken as $0.80f'_c$.

ACI 209R-92 specifications (2-7) suggest a method of normalizing and fitting drying shrinkage and creep strain data over time. The equation fits a curve to the shrinkage data by optimizing two constants, denoted as f and $\varepsilon_{ult.}$ and shown in Equation 2.10.

$$\varepsilon_{time} = \frac{time^{\alpha}}{f + time^{\alpha}} \times \varepsilon_{ult.} \qquad \text{(Equation 2.10)}$$

where: $\alpha =$ recommended as 0.90 to 1.10
$f =$ time (in days), recommended as 20 to 130 days.
$\varepsilon_{ult.} =$ The ultimate strain the drying shrinkage samples are expected to reach if left alone to dry indefinitely.

A small modification to Equation 2.10 and the assumption α is 1.0 generates more meaningful results from the optimized constants. Equation 2.11 shows the predictive equation with the defined constants from Equation 2.10.

$$\varepsilon_{time} = \frac{time}{t_{50}+time} \times \varepsilon_{ult.} \qquad \text{(Equation 2.11)}$$

where: $t_{50} =$ The time (in days) for the curve to reach 50 percent of the ultimate value
$\varepsilon_{ult.} =$ The ultimate strain the drying shrinkage samples are expected to reach if left alone to dry indefinitely.

2.5 CREEP

The creep strain is defined as the time-dependent, load-induced strain from a sustained loading applied to concrete samples. Creep strain is determined by subtracting the elastic and drying shrinkage strains from the measured strains of an unsealed, loaded cylinder. The strains from the drying shrinkage and creep cylinders (sealed and unsealed) were fit to Equation 2.11 to model the behavior of the strain over time for the different types of cylinders.

The creep coefficient is defined as the creep strains for a mixture divided by the average elastic strain value. AASHTO LRFD (Section 5.4.2.3.2) defines an equation for estimating the creep coefficient of a mixture over time, which has the form shown in Equation 2.12.

$$\Psi\ (t, t_i) = 1.9 k_s k_{hc} k_f k_{td} t_i^{-0.118} \qquad \text{(Equation 2.12)}$$

where: $k_s = 1.45 - 0.13(V/S) \geq 1.0$

$k_{hc} = 1.56 - 0.008H$

$$k_f = \frac{5}{1 + f'_{ci}}$$

$$k_{td} = \frac{t}{61 - 4f'_{ci} + t}$$

ti = time cured (days) when load was applied

V/S = volume-to-surface ratio (in)

H = relative humidity (percent)

f'_{ci} = specified compressive strength of the concrete at the time of initial loading or prestressing; if the concrete age at the time of initial loading is unknown, it may be taken as $0.80f'_c$.

Chapter 3: Test Program

The initial phase of the project was to sample Class 4000 concrete mixtures from five WSDOT bridge construction projects located throughout Washington state. Coarse aggregate from each of the WSDOT projects was then acquired to cast laboratory mixtures with a variety of mix proportions.

The following sections identify the locations of the WSDOT project sites and aggregate pits that were sampled (Section 3.1), the laboratory mixture proportions (Section 3.2), the types of tests that were performed and their schedules (Section 3.3), and the procedures followed to conduct each test (Section 3.4).

3.1 WSDOT PROJECTS SAMPLED

Class 4000 mixtures on bridge construction projects were sampled at five locations around Washington state. Table 3.1 describes the projects that were sampled and identifies the WSDOT administrative region for each project. Figure 3.1 shows the location of each construction site and WSDOT's six regions.

Table 3.1: Description of WSDOT Projects Sampled

Project Name	City	Aggregate Name	Pit Name	Project Number	Project Region
Alaskan Way Viaduct	Seattle	DuPont (3/4")	B-335	C7847	Northwest
SR 522, Snohomish	Snohomish	DuPont (3/4")	B-355	C8128	Northwest
US 395, Freya to Farewell	Spokane	Sullivan Road	C-173	C7967	Eastern
US 2, Tumwater Canyon	Wenatchee	Rock Island	DO-209	C8139	North Central
SR 14, Camas/Washougal	Washougal	Santosh	OR-27	C8105	Southwest

Figure 3.2 Locations of WSDOT Projects Sampled

Following the UW sampling, WSDOT staff cast additional compression cylinders at subsequent dates (in most cases, additional sets of samples were taken on five days) at the field sites to allow the research team to measure the day-to-day variability of the field mixtures.

3.2 LABORATORY MIXTURES

Four coarse aggregate sources used in the Class 4000 concrete mixtures at five of the projects were collected for further laboratory testing. The Alaskan Way Viaduct and SR 522 Snohomish projects used the same aggregate pit (DuPont [3/4-in.]). Three additional coarse aggregate sources were sampled for this research. One of the additional coarse aggregates was a pea gravel to measure the effects of decreasing the aggregate size. A second aggregate source was selected to sample the South Central region of Washington state. The third additional aggregate source (Okanogan Valley) was sampled from the North Central Region. Table 3.2 lists the aggregate sources sampled for this project, and Figure 3.2 shows the location of each aggregate pit.

Table 3.2: Aggregate Sources Sampled

Aggregate Name	Pit Number	WSDOT Region
DuPont (3/4”)	B-335	Olympic
DuPont (3/8”)	B-335	Olympic
Sullivan Road	C-173	Eastern
Okanogan Valley	U-119	North Central
Rock Island	DO-209	North Central
Pasco	FN-50	South Central
Santosh	OR-27	Oregon Region 1

Figure 3.3: Locations of Aggregate Sources Sampled

For each aggregate source, laboratory mixtures were proportioned to produce four mixtures (high and low paste contents, as well as high and low strengths) at levels expected to cover the extreme ranges of paste contents and water-cementitious ratios for a 4,000 psi design mixture. The collected aggregate sources were tested for absorption and specific gravity (ASTM C127) to account for the moisture content and maintain a constant coarse-to-fine aggregate ratio. For all of the mixtures, the coarse-to-fine aggregate ratio was 0.60, an air content of 5 percent

was maintained by including an air entraining admixture, and cement Type I/II was used for casting.

Table 3.3 lists the proportions of the conventional laboratory mixtures. The pea gravel [DuPont (3/8-in.)] required alterations to the mix proportions to account for the smaller aggregate size and can be seen in Table 3.4.

Table 3.3: Conventional Laboratory Concrete Mixture Proportions

Mixture	Paste Content (%)	Cement Factor	Water-Cementitious Ratio
High Paste	30.5	7.9	0.38
Low Paste	24.0	6.2	0.38
High Strength	27.0	7.9	0.30
Low Strength	27.0	6.1	0.49

Table 3.4: Pea Gravel Laboratory Concrete Mixture Proportions

Mixture	Paste Content (%)	Cement Factor	Water-Cementitious Ratio
High Paste	33.2	8.5	0.38
Low Paste	26.1	6.7	0.38
High Strength	28.2	7.8	0.33
Low Strength	29.3	6.5	0.49

3.3 TESTS PERFORMED

Six standardized tests (compressive strength, flexural strength, split-tension strength, elastic modulus, drying shrinkage, and creep) were conducted to characterize the hardened properties of each laboratory concrete mixture. The testing regime for each of the performed tests is listed in Table 3.5 for the laboratory mixtures and in Table 3.6 for the field samples.

Table 3.5: Testing Schedule for Laboratory Mixtures

	Laboratory Mixtures			
Test Performed	**Day 7**	**Day 14**	**Day 28**	**Day 56**
Compressive Strength	X	X	X	X
Elastic Modulus	X	X	X	X
Drying Shrinkage (Test Start Date)			X	
Creep (Test Start Date)		X		

Table 3.6: Testing Schedule for Field Samples

	Initial Field Sampling				Field Variability			
Test Performed	**Day 7**	**Day 14**	**Day 28**	**Day 56**	**Day 7**	**Day 14**	**Day 28**	**Day 56**
Compressive Strength	X	X	X	X				X
Elastic Modulus	X	X	X	X				X
Split Tension Strength			X	X				
Flexure Strength			X	X				
Drying Shrinkage (Test Start Date)			X					

3.4 SPECIMEN PREPARATION AND TESTING

The standardized procedures followed to prepare and test concrete samples for each of the six tests are described in the following subsections.

3.4.1 Compressive Strength Test Procedure

The compressive strength tests were performed on 6-in. x 12–in. concrete cylinders that were cast per ASTM C192 procedures. Compression cylinders from laboratory mixtures were cast with reusable steel molds, whereas the field cylinders were cast with single-use plastic molds.

Upon removal of the concrete cylinders from the molds, the samples were immediately capped with a sulfur-based compound following the ASTM C617-specified procedure. The cylinders were then stored in a moisture room (as defined by ASTM C192) until the respective cure duration had passed. Compression tests were performed on a minimum of two concrete samples; three samples were used if the failure load varied by more than 5 percent between the two cylinders. The procedure followed to conduct the compression tests is defined in ASTM C39.

3.4.2 Tensile Strength Test Procedure

Split-tension tests were performed on 6-in. x 12–in. cylinders, and flexural strength samples were cast as 6-in. x6-in. x21-in. beams following the ASTM C192 procedure. The concrete cylinders and beam samples for the tensile strength tests were cast only from field mixtures. The beam samples were cast in reusable steel molds, and the cylinder samples were cast in single-use plastic molds. The samples were allowed to cure for 16 hours onsite before they were transported back to the University of Washington. The concrete samples were left in the molds during transportation to reduce the possibility of damaging the samples.

Upon arrival at the university, the concrete cylinders and beams were removed from the molds and stored in the moisture room to cure until the test date. Split-tension tests were performed on two cylinders after curing for 28 and 56 days following ASTM C496. Flexure tests were performed by the third-point loading method as defined in ASTM C78, on three beam samples after curing for 28 and 56 days.

3.4.3 Elastic Modulus Test Procedure

For the field and laboratory mixtures, two additional 6-in. x 12–in. cylinders were cast, following ASTM C192 procedures, to test the elastic modulus. The cylinders were capped with the sulfur-based compound, per ASTM C617, upon removal from the molds. The samples were stored in the same moisture room as the compression cylinders. On each test date, the elastic moduli of the two cylinders were measured in accordance with ASTM C469: the cylinders were loaded to 50 percent of the failure load and unloaded for two cycles. The elastic modulus

cylinders were then placed back in the moisture room to continue curing until the following testing date.

The applied load and deformation of the cylinder were recorded for 1-second intervals. The load and deformation were then converted into stress and strain values. The elastic modulus was determined by fitting the stress and strain data from 50 microstrain to 40 percent of the failure stress for the mixture at that test date.

3.4.4 Drying Shrinkage Test Procedure

The drying shrinkage was monitored for field and laboratory mixtures. Three beam samples were cast from each mixture that were 3 in. x 4 in. x 16 in., as per ASTM C157, in reusable steel molds. The concrete beams were removed from the molds after curing for 16 to 24 hours. Upon removal, the shrinkage samples were stored in a saturated Calcium Hydroxide water bath for curing the first 28 days.

On Day 28 of curing, the beams were removed from the water and towel dried to saturated surface-dry conditions. The weight and length of each beam was measured twice to establish an initial length and weight. The samples were then set inside a temperature controlled room, as defined by ASTM C157, and began air drying. The monitoring schedule for the shrinkage beams was to then measure the weight and length of the beams once a day for the first week, then once a week for the first month, and then once a month for the first year of air drying.

3.4.5 Creep Test Procedure

Creep testing was performed on laboratory high- and low-paste mixtures. Three distinct aggregate sources were selected for the creep testing. For each mixture, six additional concrete cylinder samples were cast from the mixture. These cylinders were cast in reusable steel molds and prepared for the creep rigs by applying the sulfur-based capping compound as per ASTM C617, upon removal from the molds. The six creep cylinders were then stored in the moisture room to cure.

Two cylinders were removed from the moisture room on the twelfth day of curing. The surface of these samples was dried and coated with an epoxy sealant. The sealant was allowed to harden for 24 hours before a second epoxy coat was applied on Day 13. This second coat was

allowed to harden for another 24 hours. Once the two sealed cylinders had finished drying on Day 14, the remaining four creep cylinders were taken out of the moisture room and the surfaces were allowed to dry. All six of the creep cylinders were placed on a wooden rack, and steel gauge studs were epoxied onto each of the cylinders' side. The studs were placed at 10-inch spaces along the length of each cylinder. The cylinders were then rotated 90 degrees, and another set of studs was glued onto the side of the cylinder. This process was repeated until the cylinders had studs placed on each quadrant. A picture of the creep cylinders with the attached gauge studs can be seen in Figure 3.3.

Figure 3.4: Gauge Stud Placement on Typical Creep Cylinder

The creep cylinder ends were capped with sulfur, so the rigs were assembled by stacking four cylinders (two sealed and two non-sealed) overtop each other. The remaining two non-sealed cylinders were placed adjacent to the creep rig. These two cylinders were used to measure the drying shrinkage for the creep samples. Figure 3.4 shows a typical creep rig set-up, with a non-sealed cylinder at the bottom of the stack and sealed and non-sealed cylinders stacked interchangeably.

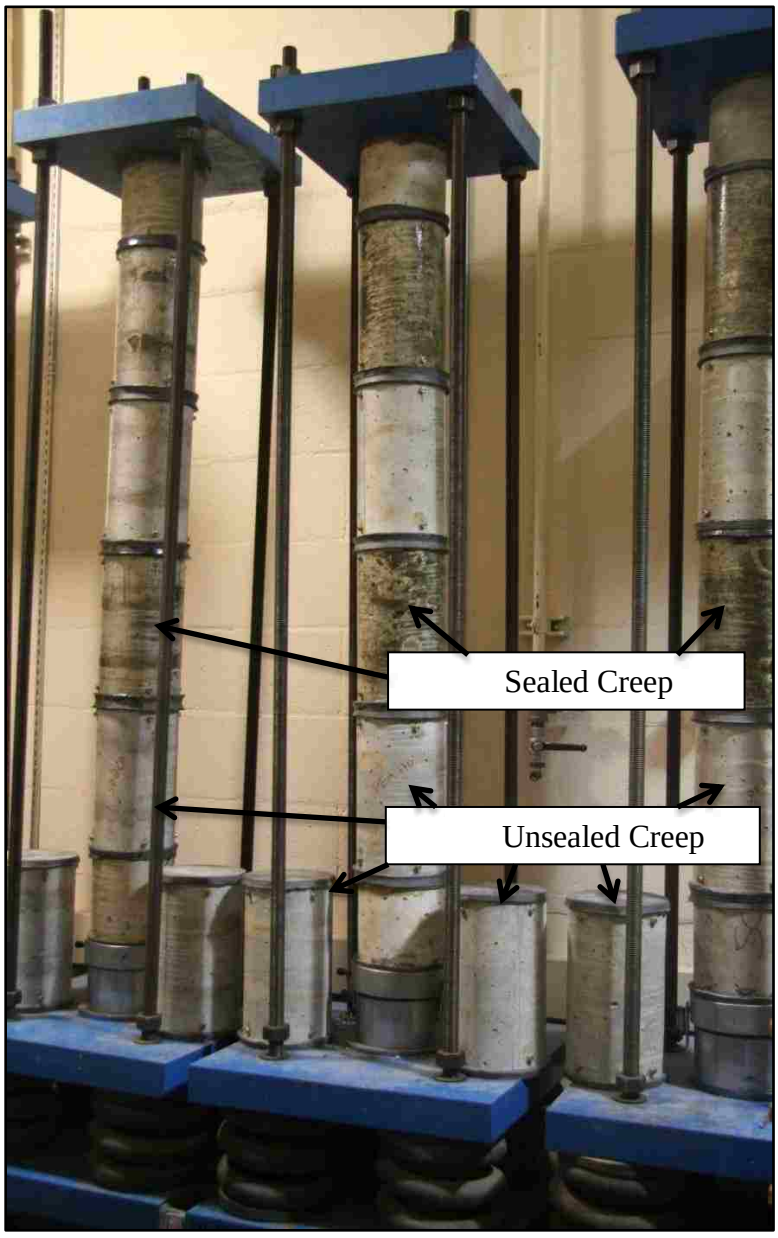

Figure 3.5: Typical Creep Rig Assembly

Once the creep rig had been assembled, measurements for each of the six cylinders were taken. These measurements were repeated until a consistent initial length for each set of gauge studs was determined. The creep rig was then loaded with a hydraulic ram to a target load of 35 percent of the Day 14 failure stress. This failure stress was determined from the mixture's compression test performed on alternative samples. The lengths of the four creep cylinders were measured while the loading from the hydraulic ram was still applied. Locking nuts were tightened to maintain the applied load on the creep rig once the pressure had been released from the ram. The lengths of the creep cylinders were measured a final time once the load from the ram had been removed.

This measurement and loading procedure was repeated for each monitor date. The schedule for monitoring each creep rig was twice on the first day of assembly, followed by once a day for the first week, then once a week for the first month, and then once a month for the following year.

Chapter 4: Compressive Strength

The compressive strength of concrete is strongly correlated with other properties. This chapter discusses the compressive strengths of the concrete mixtures used in this study, as well as the effects of time, water-cementitious ratio, paste content, and coarse aggregate. The influence of these factors on strength variability is also examined.

A single laboratory aggregate source is discussed in Section 4.1 to illustrate the data-analysis procedure. Section 4.2 summarizes the results for the remaining aggregate sources and identifies trends. The field mixture data are presented in Section 4.3. The results from all of the compressive strength tests are reported in Appendix A.

4.1 LABORATORY DATA FOR DUPONT (3/4-IN.) AGGREGATE SOURCE

The DuPont ¾-inch aggregate is discussed in detail, since two of the sampled WSDOT projects used this aggregate. The three-quarter inch designation in the naming system for DuPont denotes the maximum aggregate size. The size was included in the aggregate designation to distinguish it from the pea gravel (3/8-in. max size) from the same pit location that was also considered in this research.

4.1.1 Measured Compressive Strengths

As mentioned in Section 2.3, compressive tests were performed on lab mixtures at days 7, 14, 28, and 56. The compressive strengths for the four DuPont (3/4-in.) laboratory mixtures (high paste, low paste, high strength, low strength), along with the mixture proportions, are reported in Table 4.1 and Figure 4.1.

Table 4.1: Measured Compressive Strengths: DuPont (3/4-in.)

Mixture	Paste Content (%)	Water-Cementitious Ratio	Day 7 (psi)	Day 14 (psi)	Day 28 (psi)	Day 56 (psi)
High-Paste	30.5	0.38	5,350	4,990 *	6,530	7,020
Low-Paste	24.0	0.38	3,400	3,710	4,400	4,710
High- Strength	27.0	0.30	5,070	5,680	6,040**	7,560
Low-Strength	27.0	0.49	2,840	3,210	3,750	4,000

* Day 14: High Paste mixture had low break, not used to fit EQ 2.1
** Day 28: High Strength mixture had low break, best-fit value used for calibrating EQ 2.1

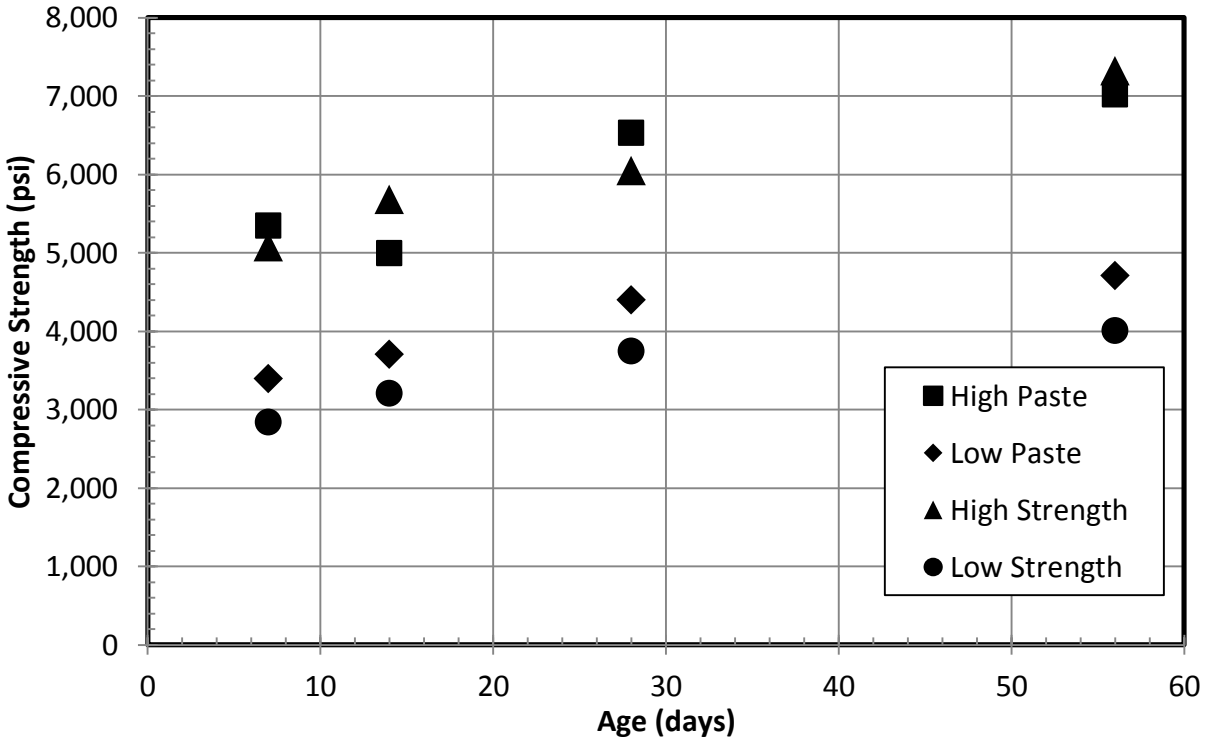

Figure 4.1: Compressive Strengths: DuPont (3/4-in.) Mixtures

The compressive strength of the mixtures at Day 28 (f_{28} **)** ranged from 3,750 psi to 6,530 psi. By Day 56, the strengths of all mixtures had reached or exceeded the design strength of 4,000 psi. The compressive strengths of the high-paste and high-strength mixtures were similar. The low-paste and low-strength mixtures also had strengths similar to each other. These two mixtures had strengths approximately 2,000 psi lower than the strength of the high-paste and high-strength mixtures.

The Day 28 strengths for the four DuPont (3/4-in.) mixtures are plotted against the water-cementitious ratio in Figure 4.2. The best-fit line for the four mixtures had the following form:

$$f_{28\ Day} = A - B \times w/cm \qquad \text{(Equation 4.1)}$$

where: A = 10,000 psi
B = 12,500 psi

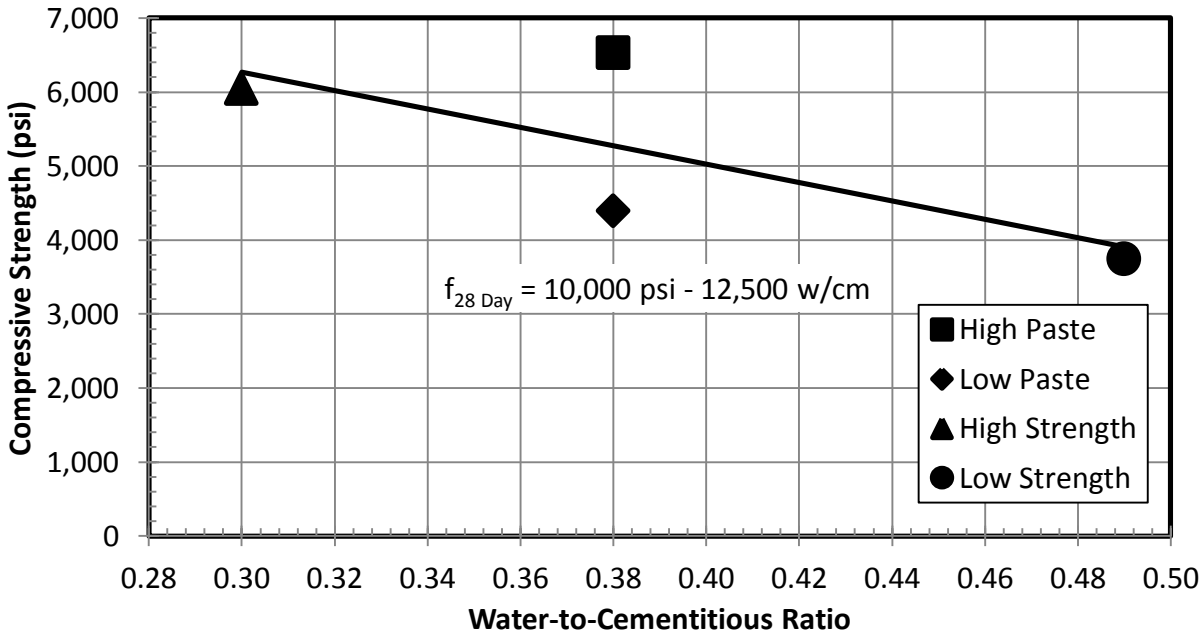

Figure 4.2: Day 28 Comp. Strength vs. W/CM Ratio: DuPont (3/4-in.) Mixtures

The figure shows that the compressive strength decreased with increasing water-cementitious ratio, as expected. The high- and low-paste mixtures both had a water-to-cementitious ratio of 0.38, so the difference between the strengths of these two mixes was attributed to differences in the paste content. If a medium-paste mixture with the same water-to-cementitious materials ratio had been cast, its compressive strength would have been expected to lie between the high- and low-paste mixture strengths and to fall near the fitted line.

4.1.2 Rate of Strength Gain

The normalized rate of strength gain was determined for each mixture by dividing the compressive strength on each testing day by the Day 28 strength. The normalized rate of strength

gain for each of the four testing days was then fit to a curve in the form of Equation 2.1, as explained in Section 2.1.

For the DuPont (3/4-in.) low-paste mixture, the results from the four compression testing days were evaluated to determine the K1 and K2 constants in Equation 2.1. The resulting optimal values are provided in Equation 4.2, and the fitted curve is plotted in Figure 4.3. The normalized compressive strength data are also shown in the figure to show the goodness of fit.

$$\text{DuPont } (3/4-\text{in.}) \text{ Low} - \text{Paste: } \frac{f_{time}}{f_{28}} = \frac{\text{time}}{3.22 + 0.89 \times \text{time}} \qquad \text{(Equation 4.2)}$$

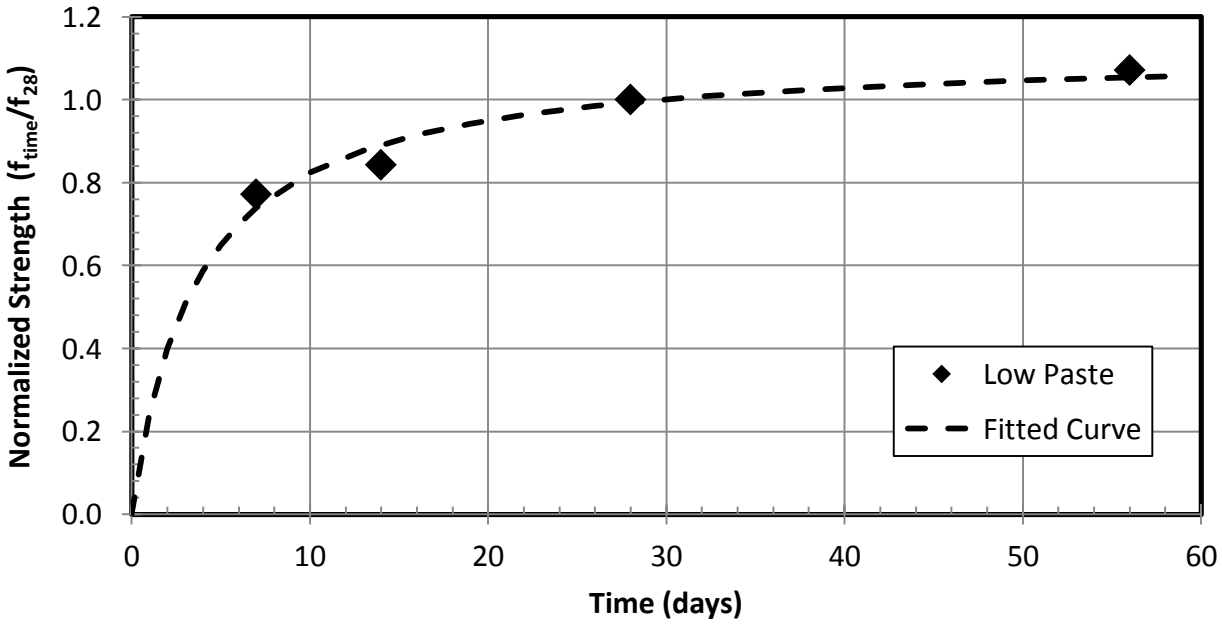

Figure 4.3: Rate of Strength Gain Fitted Curve: DuPont (3/4-in.) Low-Paste Mixture

This procedure was repeated for the other three DuPont (3/4-in.) mixtures. The low break for Day 14 of the high-paste mixture was excluded from the data set when K1 and K2 were fit. The low break for Day 28 of the high-strength mixture was accounted for by excluding the Day 28 break from the data set and optimizing K1 and K2 by normalizing to the Day 56 strength. With the normalized fitted curve for the high-strength mixture, the strength at Day 28 was estimated by the value provided from the curve.

The constants for the four fitted curves are listed in Table 4.2, along with the mean compressive strength at Day 28 for each mixture. Figure 4.4 shows the four fitted curves for the DuPont (3/4-in.) laboratory mixtures.

Table 4.2: Optimized Constants for DuPont (3/4-in.) Aggregate

Mixture	f_{28} (psi)	K1	K2	f_7/f_{28}	f_{56}/f_{28}
High-Paste	6,530	2.23	0.91	0.82	1.07
Low-Paste	4,400	3.23	0.89	0.77	1.07
High-Strength	6,740*	3.64	0.87	0.77	1.09
Low-Strength	3,750	3.26	0.89	0.76	1.07
Average	5,360	3.09	0.89	0.78	1.08
St. Deviation	1,500	0.60	0.02	0.03	0.01
Coef. of Variation	28.1%	19.5%	1.7%	3.9%	0.7%

** Determined from fitted curve*

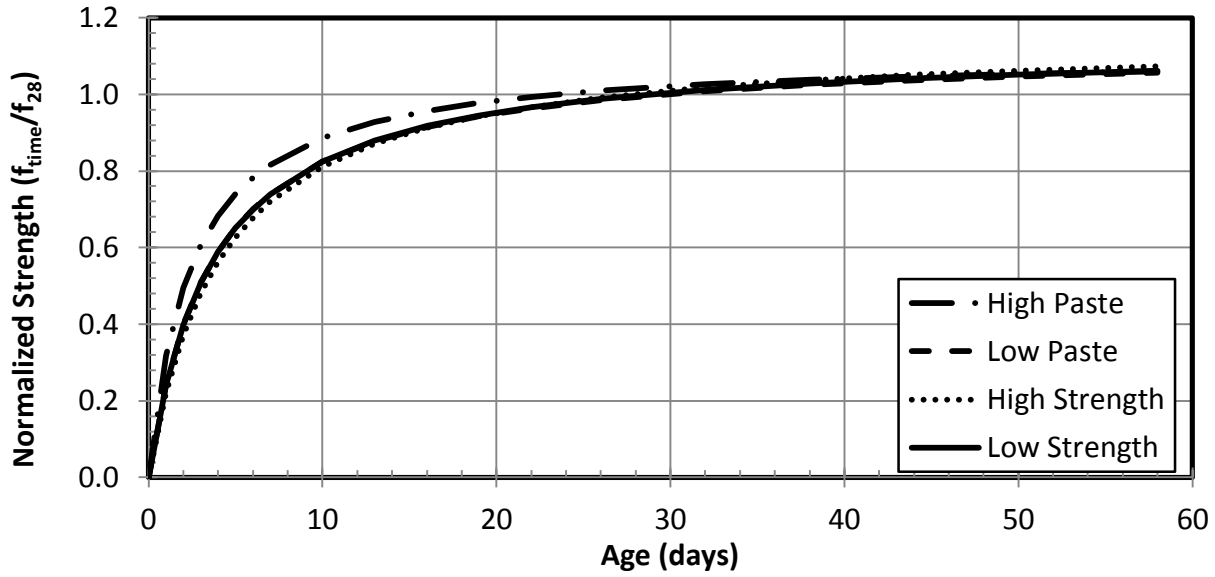

Figure 4.4: Rate of Strength Gain Fitted Curves: DuPont (3/4-in.) Mixtures

The ratio of the Day 7 strength to the Day 28 strength was nearly identical for the low-paste, high-strength, and low-strength mixtures. At Day 7, the mean compressive strength for these three mixtures was on average 77.5 percent of the 28 day strength. The high-paste mixture gained strength slightly more rapidly. The same ratio for the high-paste mixture was 81.9

percent. At Day 56, the normalized strength for all four mixtures was similar (average of 1.08 percent).

As mentioned in Section 2.1, the ACI 209 specifications (A-17) suggest values for the K1 and K2 constants of 4.0 and 0.85, respectively. A curve plotted with these suggested constants from ACI 209 are compared with the DuPont (3/4-in.) low-paste fitted curve in Figure 4.5.

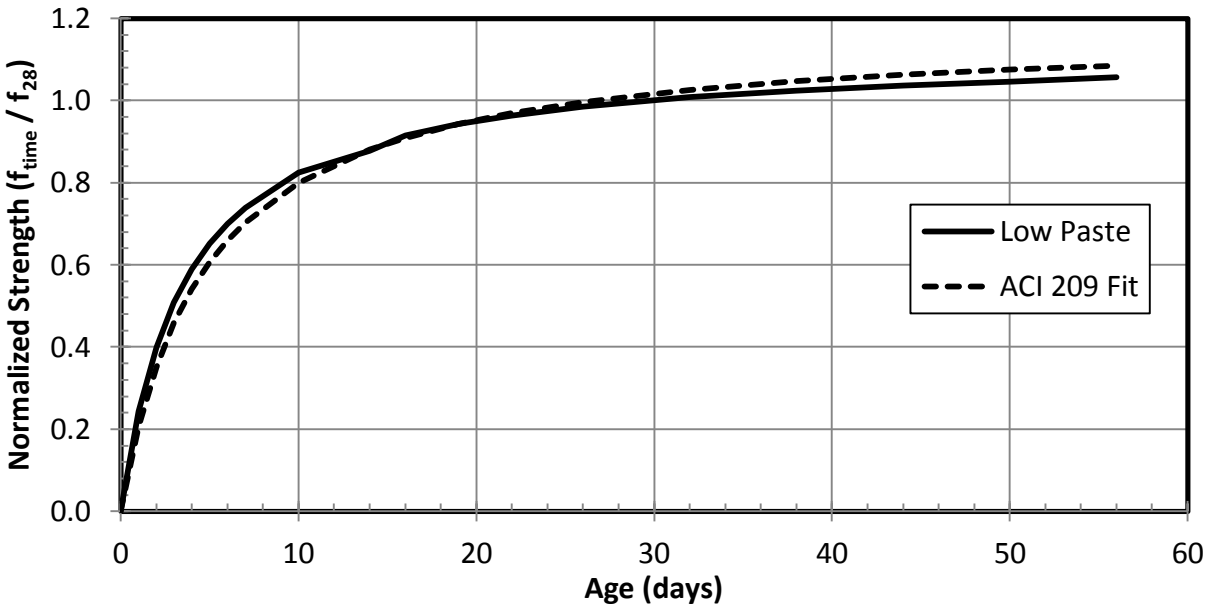

Figure 4.5: ACI 209 Specification Comparisons: DuPont (3/4-in.) Low-Paste

The ACI 209 equation slightly under-predicted the rate of strength gain for the DuPont (3/4-in.) low-paste mixture until Day 14. Beyond Day 14, the ACI 209 fit slightly over-predicted the rate of measured strength gain. The difference between the low-paste mixture and the ACI 209 at Day 7 was 3.6 percent, and at Day 56 it was 2.9 percent.

4.2 LABORATORY DATA FOR ALL AGGREGATE SOURCES

The process outlined in Section 4.1 was repeated for all of the remaining aggregates. Appendix A provides the details of the test results.

4.2.1 Summary of Measured Compressive Strengths

The Day 28 compressive strengths for each aggregate's high- and low-strength mixtures are shown in Figure 4.6. The high- and low-strength mixtures had different water-cementitious ratios, but they had the same paste content.

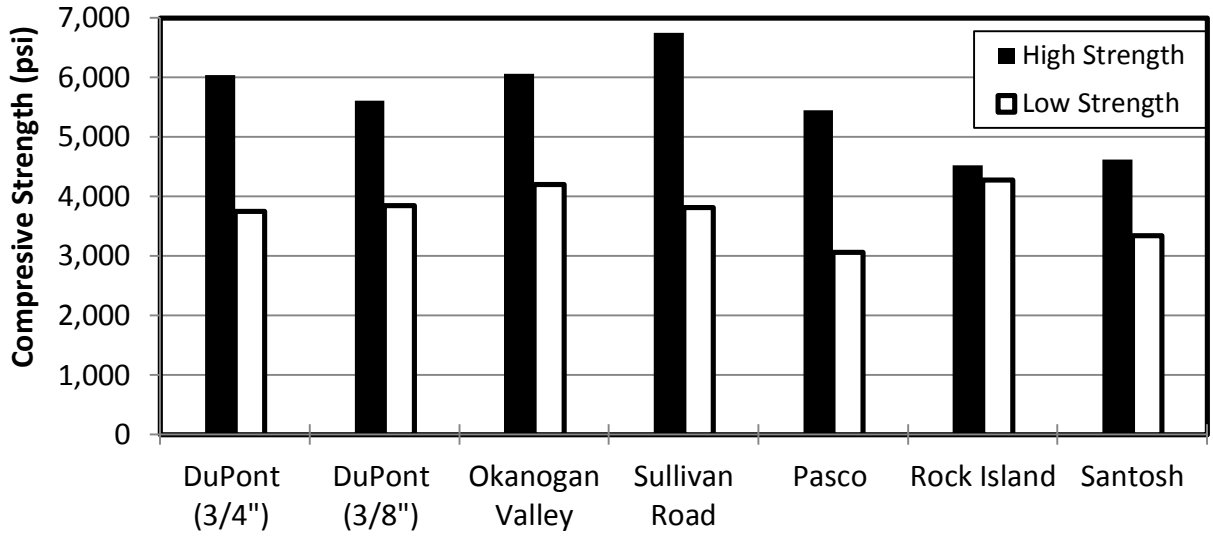

Figure 4.6: Day 28 Comp. Strength: All Aggregates High- and Low-Strength Mixtures

As expected, the strengths of the high-strength mixtures exceeded the strengths of the low-strength mixtures for every aggregate source. The high-strength mixtures had compressive strengths that ranged from 4,500 psi to 6,800 psi, with an average strength of 5,600 psi at Day 28. The low-strength mixtures had a compressive strength range of 3,100 psi to 4,300 psi, with a mean strength of 3,800 psi at Day 28. In the case of the Rock Island aggregate, the percentage difference between the high- and low-paste mixtures was only 5.4 percent. The compressive strength of all of the high-strength mixtures exceeded 4000 psi at 28 days. In contrast, the strengths of only the Okanogan Valley and Rock Island low-strength mixtures exceeded 4,000 psi at 28 days of curing.

For each aggregate source, a line in the form of Equation 4.1 was fit to the Day 28 compressive strengths versus the water-cementitious ratios for the four laboratory mixtures. The resulting lines for the seven aggregate sources are plotted in Figure 4.7. Appendix A provides individual figures for the Day 28 compressive strengths versus the water-cementitious ratios of the four laboratory mixture for each aggregate source.

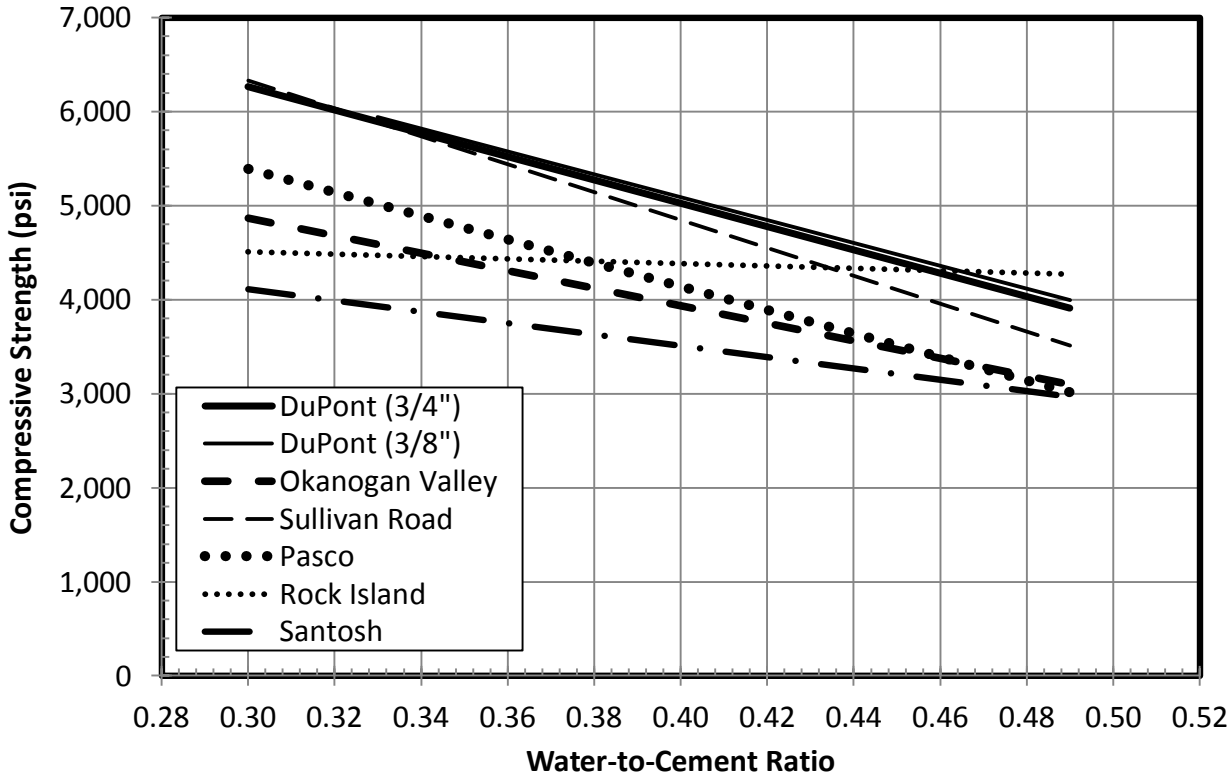

Figure 4.7: Day 28 Comp. Strength vs. Water-Cementitious Ratio: All Aggregates

With the exception of the Rock Island aggregate source (and to a lesser extent, the Santosh source), all of the lines had similar slopes. The Rock Island mixtures had a small slope (Figure A.11). The compressive strength change per change in 0.1 water-cementitious ratios ranged from 930 psi to 1,250 psi, with an average of 1,120 psi. The nearly constant slopes for each of the aggregates implied that rate of change in compressive strength as a function of the water-cementitious ratio was insensitive to the aggregate source; however, the compressive strength varied for each aggregate source. For example, the strengths of the mixtures that included aggregates from the Santosh source were consistently lower than those of other sources.

The mean compressive strength of each aggregate's high- and low-paste mixture at Day 28 can be seen in Figure 4.8. The high- and low-paste mixtures differed in paste content, but they had the same water-cementitious ratio.

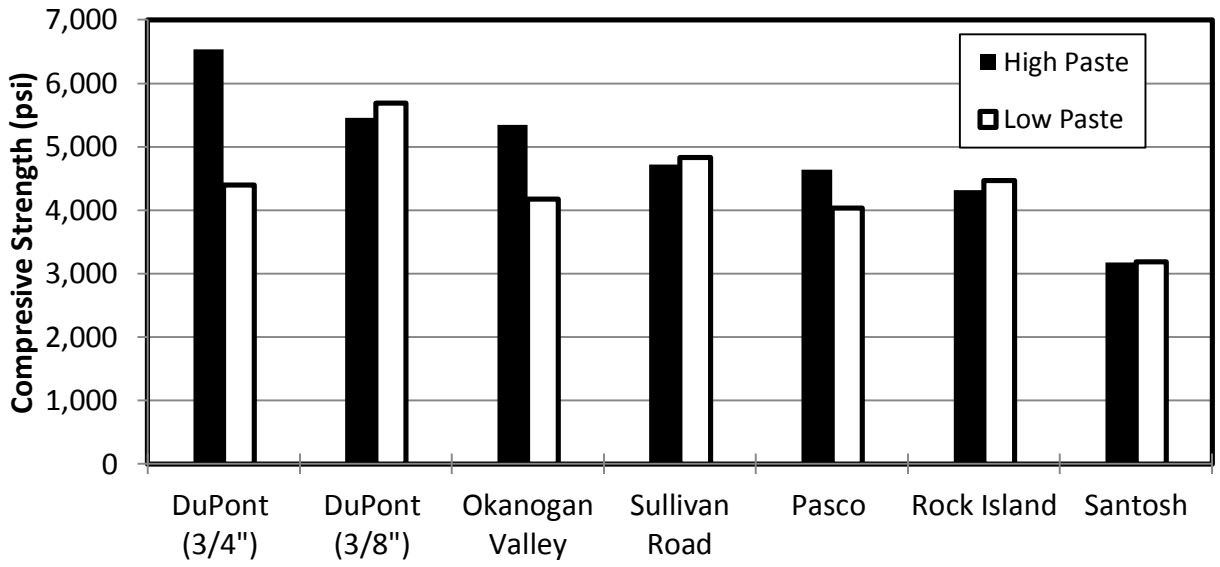

Figure 4.8: Day 28 Comp. Strength: All Aggregates High- and Low-Paste Mixtures

The compressive strengths of the high-paste mixtures ranged from 3,200 psi to 6,500 psi, with an average of 4,900 psi. The low-paste mixtures had a compressive strength range of 3,200 psi to 5,700 psi, with a mean strength of 4,400 psi. Variations in the paste content did not have a consistent effect on the compressive strength.

4.2.2 Rate of Strength Gain

The compressive strength results from each laboratory mixture were normalized and fit to Equation 2.1, as detailed in Section 4.1.2. The optimized coefficients and curve fits for each of the mixtures can be seen in Appendix A. The ratios of Day 7 to Day 28 strengths for the high- and low-strength mixtures are shown in Figure 4.9.

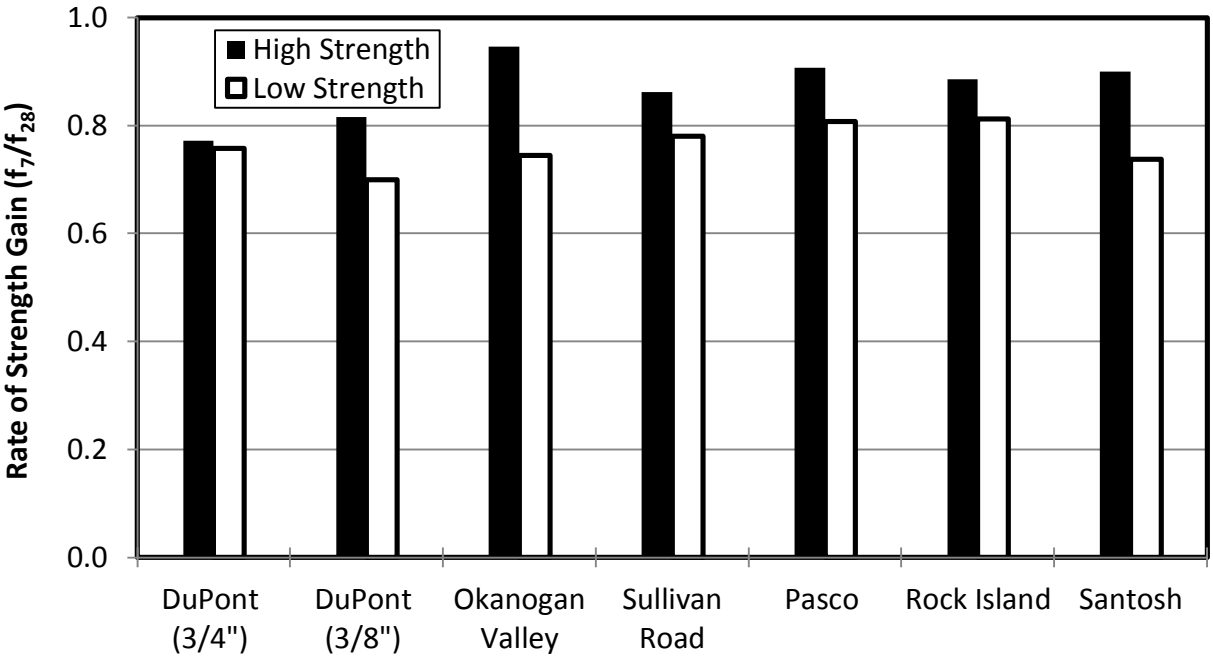

Figure 4.9: Rate of Strength Gain: All Aggregates High- and Low-Strength Mixtures

The rate of strength gains for the high-strength mixtures consistently exceeded the rate of strength gains for the low-strength mixtures. Since the paste contents were constant, the difference in rate of strength gains between the high- and low-strength mixtures was attributed to the effect of the water-cementitious ratio as well as cement content. The ratio between the high and low strength mixture's rate of strength gain had a range of 1.09 to 1.22 with a mean of 1.16.

The ratio of Day 7 to Day 28 strengths for each of the high-and low-paste mixtures can be seen in Figure 4.10. The high-and low-paste mixtures had the same water-cementitious ratio with only variations in the paste content.

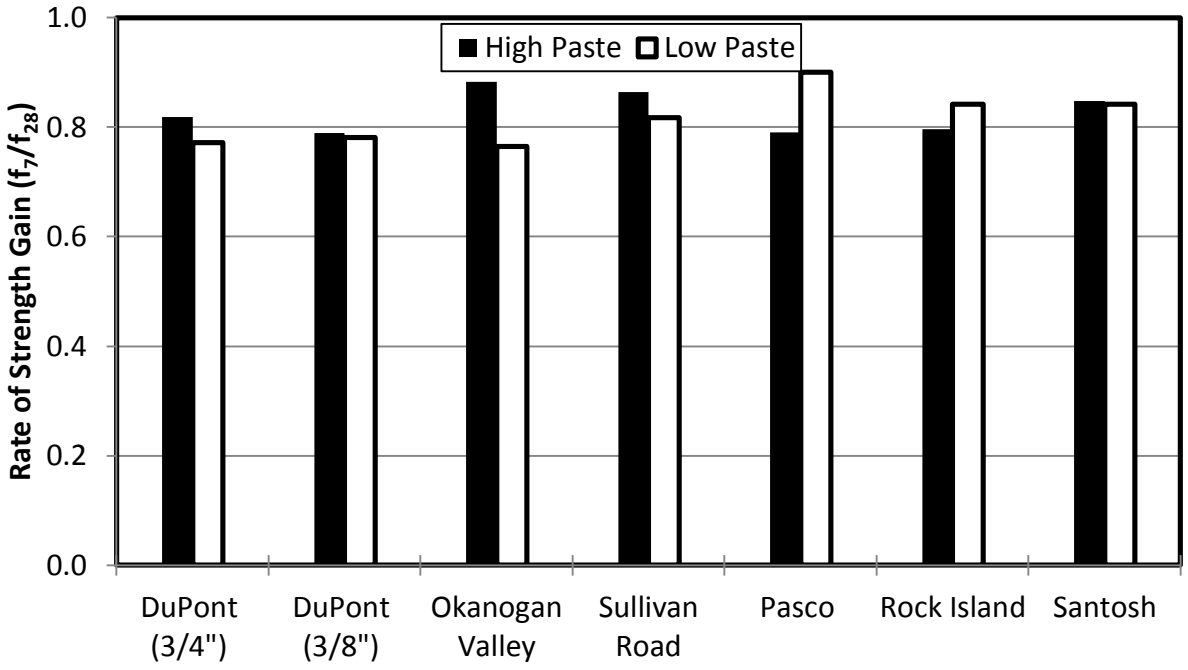

Figure 4.10: Rate of Strength Gain: All Aggregates High- and Low-Paste Mixtures

The Day 7 rate of strength gain for the high-paste mixtures ranged from 0.79 to 0.88, with a mean normalized strength of 0.83. The low-strength mixtures had a rate of strength gain that ranged from 0.77 to 0.90, with an average rate of 0.82. There were no consistent differences between the normalized rates of strength gain for the high- and low-paste mixtures.

4.3 DATA FOR FIELD SAMPLES

This section discusses the results from the compressive tests performed on the field samples for each of the five WSDOT projects.

4.3.1 Measured Compressive Strengths

The compressive strengths for all five of the WSDOT projects collected by the UW are reported in Table 4.3 and in Figure 4.11. Table 4.3 also lists the paste content and water-cementitious ratio for the mixture sampled at each project. The Tumwater Canyon project was the only construction job that included fly ash in the mixture. The reported paste content includes the converted fly ash as a component of cement.

Table 4.3: Field Sample Compressive Strengths

Project	Aggregate Name	Paste Content (%)	W/CM Ratio	Day 7 (psi)	Day 14 (psi)	Day 28 (psi)	Day 56 (psi)
Freya to Farewell	Sullivan Road	25.5	0.31	4,650	5,180	5,420	5,900
Alaskan Way	DuPont (3/4")	25.2	0.31	4,250	5,010	5,290	5,660
Tumwater Canyon	Rock Island	25.9*	0.40*	3,030	3,670	3,680**	4,410
Snohomish	DuPont (3/4")	24.6	0.32	5,090	5,700	6,300	6,370
Camas / Washougal	Santosh	27.8	0.41	3,020	3,420	4,070	4,380

** Wenatchee mixture included fly ash*
*** Day 28: Wenatchee mixture had low break, best-fit value used for calibrating EQ 2.1*

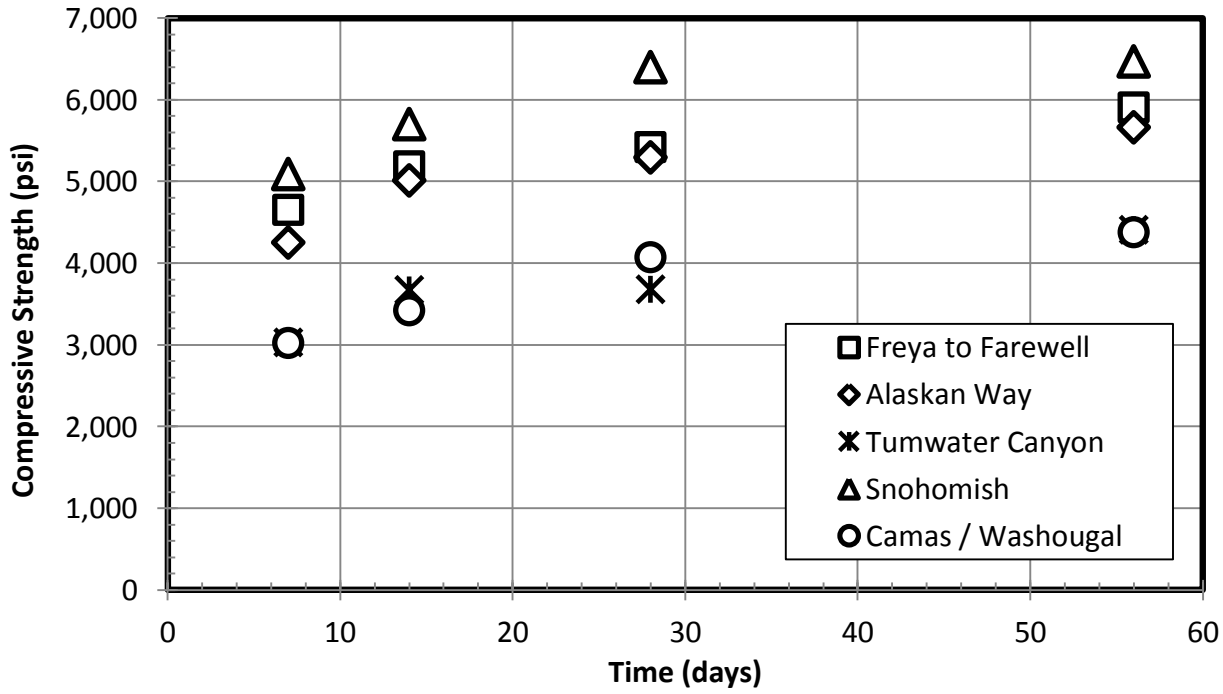

Figure 4.11: Field Sample Compressive Strength over Time

The compressive strengths of the Tumwater Canyon and Camas/Washougal project concrete were similar, whereas the Freya to Farewell, Alaskan Way, and Snohomish projects all had compressive strengths that were around 2,000 psi higher. The Day 28 compressive strength

for each project is plotted versus the water-cementitious ratio for each mixture in Figure 4.12. The field strength results were fit to Equation 4.1, and the resulting line is also included in the figure.

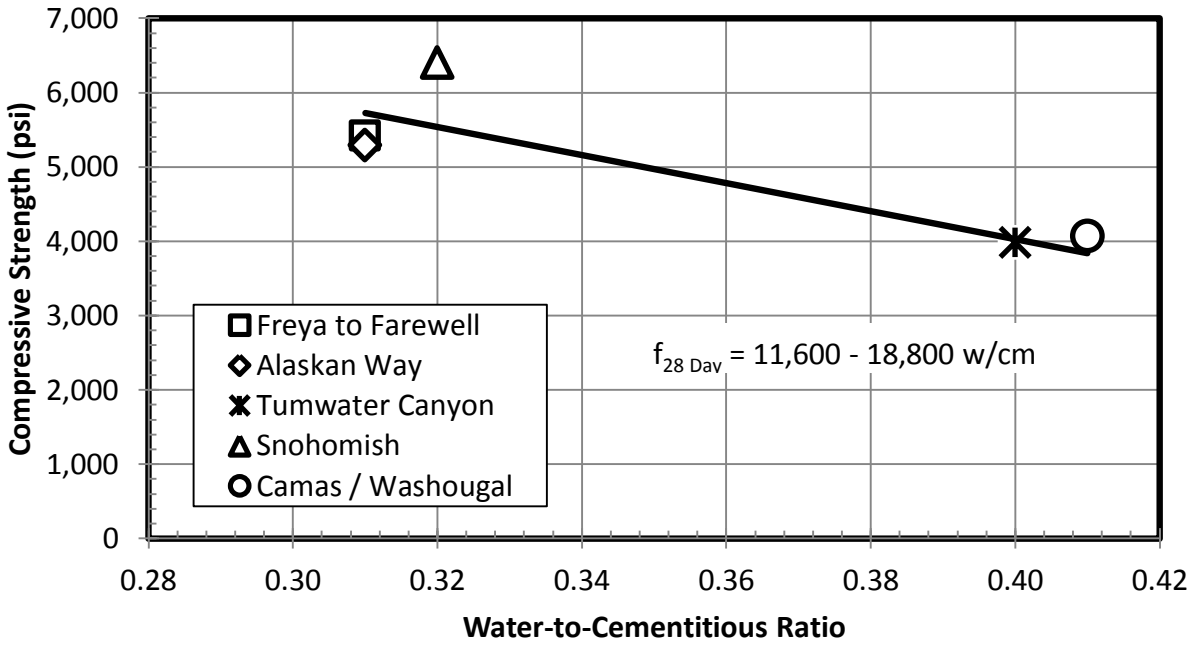

Figure 4.12: Day 28 Comp. Strength vs. Water-Cementitious Ratio: Field Samples

The Class 4000 concrete mixtures had a water-cementitious ratio that ranged from 0.31 to 0.42 among the five projects. The slope of the line suggests that increases in the water-cementitious ratio decreased the compressive strength, as expected.

4.3.2 Rate of Strength Gain

The field data were normalized by dividing each project's monitored strengths by the Day 28 strength. The normalized data sets were fit to Equation 2.1 by optimizing the K1 and K2 constants. Table 4.4 lists the two constants along with the Day 28 compressive strength for each project. The fitted curves for the projects are plotted in Figure 4.13. Tumwater Canyon had a low break on Day 28, so the strength was altered by normalizing the data with the Day 56 strength. The altered Day 28 break was estimated by the fit curve, which was used to then renormalize the data set.

Table 4.4: Predictive Equation Constants for Field Samples

Project	f_{28} (psi)	K1	K2	f_7/f_{28}	f_{56}/f_{28}
Freya to Farewell	5,420	1.88	0.90	0.84	1.06
Alaskan Way	5,290	2.42	0.90	0.80	1.07
Tumwater Canyon	3,980**	3.26	0.86	0.76	1.01
Snohomish	6,300	2.22	0.94	0.80	1.08
Camas / Washougal	4,070	3.70	0.87	0.74	1.08
Average	4,970	2.69	0.89	0.79	1.06
St. Deviation	1,100	0.76	0.03	0.04	0.03
Coef. Of Variation	22.1%	28.2%	3.7%	4.6%	2.6%

*** Day 28: Wenatchee had a low break. Best-fit value estimated*

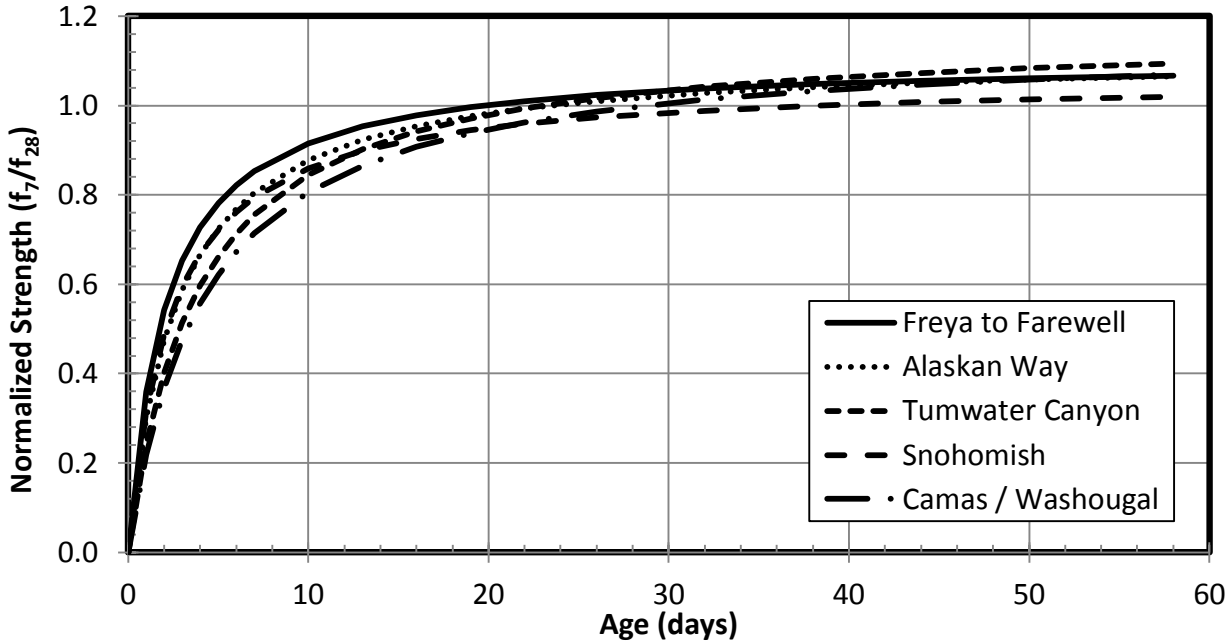

Figure 4.13: Rate of Strength Gain Fitted Curves: Field Samples

After the first week, the normalized rate of strength gain for the field mixtures had less than a 5.0 percent coefficient of variation. Despite the field mixtures having large variations in mixture proportions, aggregate type, and compressive strengths, only the initial rate of strength gain varied among them. These variations in the initial strength gain were to be expected, given the analysis of figures 4.9 and 4.10. The initial rate of strength gain increased with decreasing water-cementitious ratios. The field mixture proportions ranged from a water-cementitious ratio

of 0.31 to 0.41, with the lowest ratio for the Freya to Farewell project and the highest ratio for Camas/Washougal, so the results were as expected.

4.3.3 Variability

The measured compressive strength of a concrete mixture varies each time it is cast and tested. Knowledge of the expected range of strengths is critical to understanding the differences between the actual and design strengths. This difference is important, because many calculated performance characteristics of the concrete are estimated on the basis of the design strength. The variability of the WSDOT Class 4000 mixture was monitored by casting five additional sets of concrete samples on different construction days at each of the projects. These additional samples were tested after 56 days of curing, and the strengths can be seen in Table 4.5.

Table 4.5: Field Sample Day 56 Compressive Strength Variation

	Freya to Farewell (psi)	Alaskan Way (psi)	Tumwater Canyon (psi)	Snohomish (psi)	Camas / Washougal (psi)
Initial Sampling	5,900	5,660	4,410	6,370	4,380
Subsequent Sampling	5,550	6,950	4,690	4,820	4,090
	5,050	5,170	4,530	5,130	4,530
	5,390	5,300	5,210	4,910	4,280
	4,790	5,850	4,970	5,210	4,520
	4,980	6,070	5,190	4,730	4,650
Mean	5,280	5,830	4,830	5,200	4,410
St. Deviation	410	640	340	600	200
Coef. of Variation	7.8%	11.0%	7.0%	11.6%	4.5%

The concrete mixtures all achieved the design strength of 4,000 psi; however, the actual strengths of the mixtures varied. For example, the Alaskan Way Viaduct project had compressive strengths ranging from 5,170 psi to 6,950 psi, which is a difference of 1,780 psi (difference of 25.6 percent). The average coefficient of variation of all five certified mixtures was 7.8 percent. This suggests that the compressive strength of all five of the concrete mixtures varied by different casting dates. These variations in strength arose from the moisture content of the aggregate during mixing, penalties the concrete providers faced for under-strength

performance, and methods of dealing with complications from weather conditions (i.e., using hot water to speed up the rate of hydration when casting on cold days).

4.4 ANALYSIS OF COMPRESSIVE STRENGTH RESULTS

As expected, the effect of water-cementitious ratio was consistent for the laboratory and field mixtures (figures 4.2, 4.6, 4.7 and 4.12). Strength decreased as the water-cementitious ratio increased. The variation in strength as a function of the water-cementitious ratio was not constant for each aggregate source (Figure 4.7). The Rock Island and Santosh aggregate sources were less sensitive to modifications to the water-cementitious ratio, so making higher-strength concrete with these aggregate types might be more difficult. The effect of the water-cementitious ratio on the rate of strength gain (Day 7 to Day 28 strength ratio) was consistent for the aggregates (Figure 4.9); the higher-strength mixtures had a higher rate of strength ratio than the lower-strength mixtures.

The compressive strength and rate of strength gain appeared to be insensitive to variations in the paste content. This may have been due to differences in stiffness between coarse aggregates and paste. Stiffer aggregates (DuPont [3/4-in.]) achieve higher strength with higher paste contents, while less stiff aggregates (Sullivan Road) can achieve better strength with less paste. The compressive strength for the high-paste mixture was not consistently stronger than the low-paste mixture for a single aggregate source and water-cementitious ratio (Figure 4.8). The high-paste mixture's rate of strength gain for the normalized Day 7 strength did not always exceed that of the low-paste mixture for a given aggregate (Figure 4.10).

The normalized compressive strength data fit the ACI 209 specifications (A-17, Equation 2.1) well, despite the differences in cement type and changes in the cement refinement process (figures 4.3 and 4.5). The difference in cement and cement refinement processes was reflected in the initial rate of strength gain (ratio of Day 7 to Day 28 strengths). ACI 209 recommends values for the K_1 and K_2 constants as 4.0 and 0.85, respectively. The optimized K_1 and K_2 values for the laboratory data had an average value of 2.4 and 0.90, a difference of 39.0 percent and 5.5 percent, respectively.

Chapter 5: Tensile Strength

This chapter discusses flexure and split-tension tests of five field concrete mixtures sampled in this study. The paste content and water-cementitious ratio varied among the sampled projects, as seen in Table 5.1. Since only five projects were sampled, it was not possible to identify the effects of paste content or water-cementitious ratio on tensile strength.

Table 5.1: Field Mixture Proportions

Project	Paste Content (%)	Water-Cementitious Ratio
Freya to Farewell	25.5	0.31
Alaskan Way	25.2	0.31
Tumwater Canyon	25.9*	0.40*
Snohomish	24.6	0.32
Camas / Washougal	27.8	0.41

** Tumwater Canyon mixture included fly ash.*

The tensile and compressive strength results for the field samples for Day 28 and Day 56 are listed in Table 5.2. Section 5.1 and Section 5.2 discuss the flexure test and split-tension test analysis, respectively. The relationship between the flexure and split-tension strengths is investigated in Section 5.3.

Table 5.2: Flexural and Compressive Strength Results

		Alaskan Way	Snohomish	Tumwater Canyon	Freya to Farewell	Camas / Washougal
Flexural Strength (psi)	Day 28	780	680	620	830	670
	Day 56	820	680	620	850	700
Split-Tension (psi)	Day 28	540	450	390	540	350
	Day 56	510	500	350	510	410
Compressive Strength (psi)	Day 28	5,290	6,400	3,680	5,420	3,880
	Day 56	5,660	6,470	4,410	5,900	4,380

Table 5.1 lists the Day 28 and 56 strengths for each test. As expected, the flexural and compressive strengths for the field mixtures increased slightly between Day 28 and Day 56. In contrast, the split-tensile strengths did not consistently increase with time. For the Alaskan Way,

Tumwater Canyon, and Freya to Farewell field mixtures, the split-tensile strength decreased slightly between days 28 and 56. This behavior may be attributable to the large variability among the strengths of the individual split-tension specimens. These test results are analyzed in further detail in the Section 5.2.

5.1 FLEXURE TESTS

As described in Section 2.3, flexure tests were performed for each mixture on three beam samples at 28 and 56 days. The failure loads within each set of three samples varied little; they had an average coefficient of variation of only 3.9 percent. The mean flexural strengths for each of the field mixtures at Day 28 and Day 56 are shown in Figure 5.1.

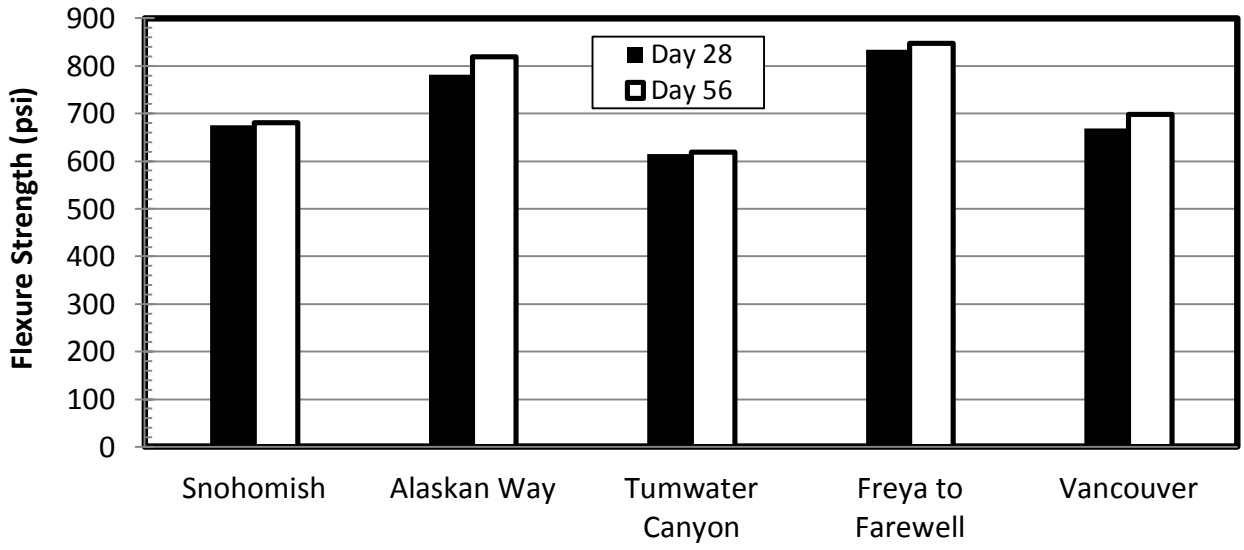

Figure 5.1: Field Sample Flexural Strengths

The measured flexural strengths ranged from 620 to 850 psi, with a mean strength of 725 psi. The tensile strength of each field mixture varied little with time. The increase in flexural strength from Day 28 to Day 56 ranged from 0.6 percent to 4.7 percent, depending on the mixture, with an average increase of 2.5 percent.

Figures 5.2 and 5.3 show the measured flexural strength versus compressive strength for Day 28 and Day 56, respectively. The flexural strengths calculated from AASHTO specifications

for normal-weight concrete (Equations 2.2) and high-strength concrete (Equation 2.3) are included in these figures.

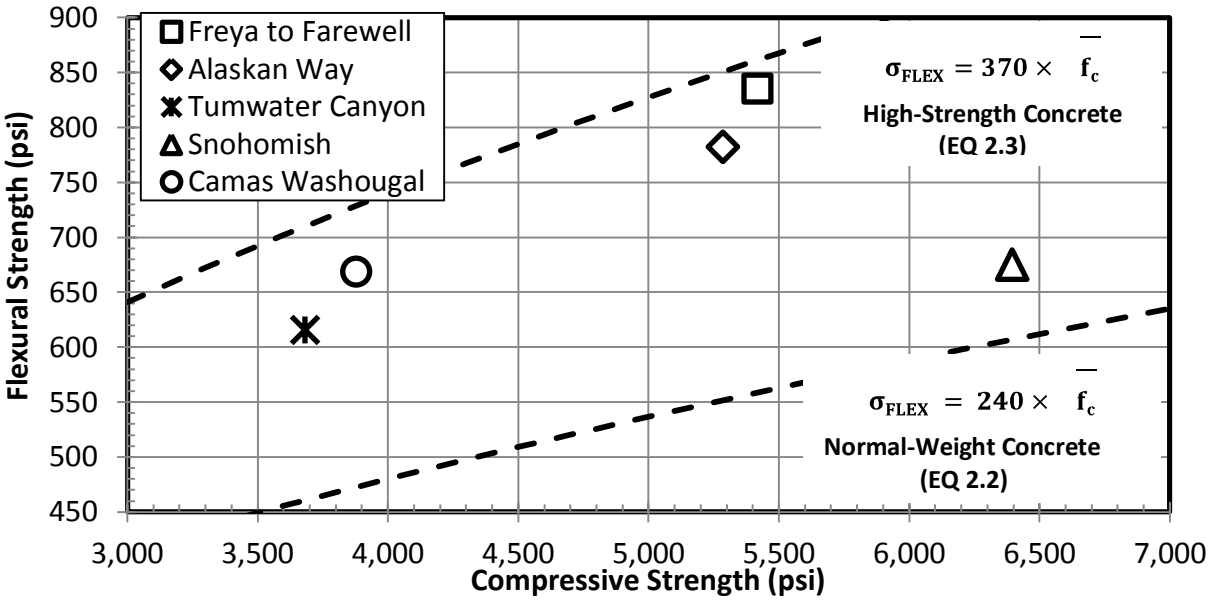

Figure 5.2: Day 28 Flexure Strength vs. Compressive Strength

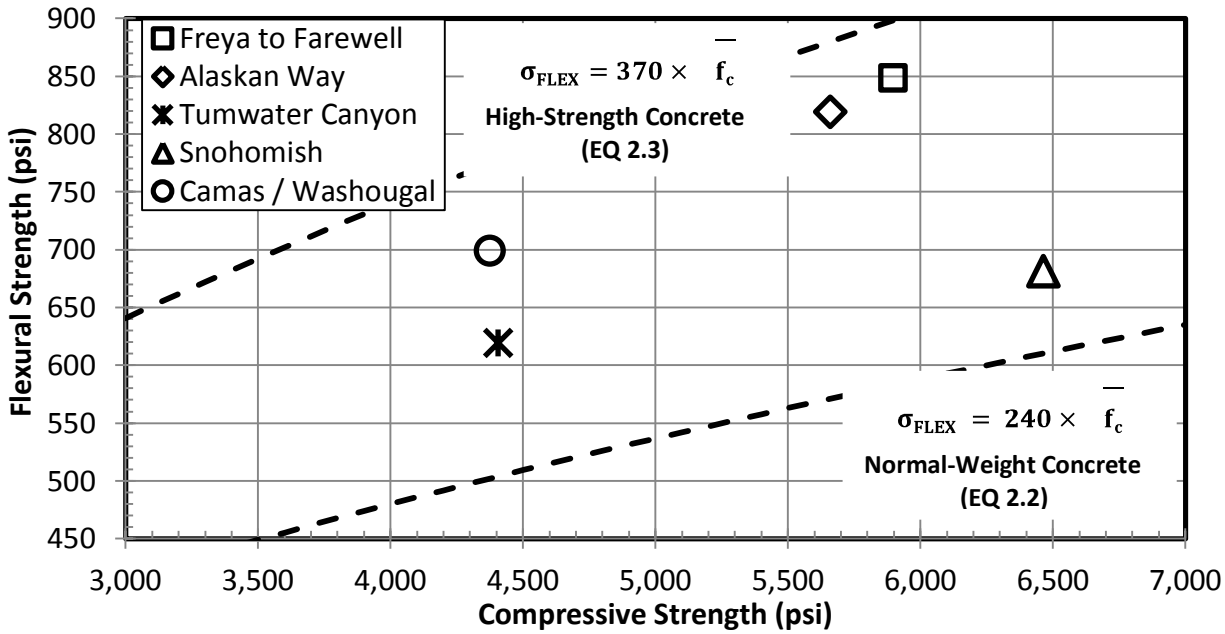

Figure 5.3: Day 56 Flexure Strength vs. Compressive Strength

For both ages, the two AASHTO equations provided upper and lower bounds for the measured flexural strengths. The flexural strengths of the field samples consistently exceeded the strengths computed for normal-weight concrete (Equation 2.2). The percent difference between the actual and the predicted strength from Equation 2.2 was an average of 33.0 percent for the field mixtures. In comparing the tensile strength of the field mixtures with Equation 2.3, which is defined for high-strength concrete, the percentage error between the actual and predicted strengths was 13.1 percent on average. The Snohomish mixture had a much lower tensile strength than expected, at both Day 28 and Day 56. The reason for this difference in behavior is unknown.

An alternative equation was developed by optimizing the constants for Equation 2.2 on the basis of the field mixture test results. The resulting formula, to estimate the flexural strength of a mixture based on the compressive strength, can be seen in Equation 5.1.

$$\sigma_{FLEX} \text{ psi} = 420 \times \sqrt[3]{\overline{f_c}} \text{ (ksi)} \qquad \text{(Equation 5.1)}$$

Maintaining the same exponent for the compressive strength resulted in Equation 5.2, but resulted in a worse fit to the data.

$$\sigma_{FLEX} \text{ psi} = 320 \times \overline{f_c} \text{ (ksi)} \qquad \text{(Equation 5.2)}$$

Figures 5.4 and 5.5 show Day 28 and Day 56 flexural strengths versus compressive strengths for the field mixtures, respectively, with Equation 5.1 included in the figures.

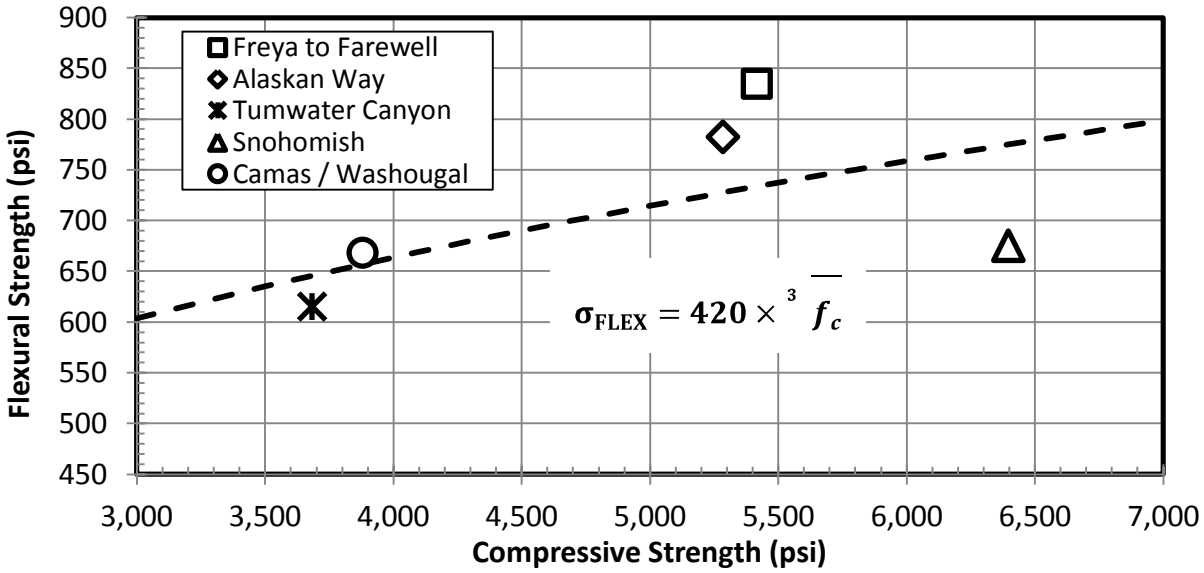

Figure 5.4: Day 28 Flexure Strength vs. Compressive Strength-Optimized Equation

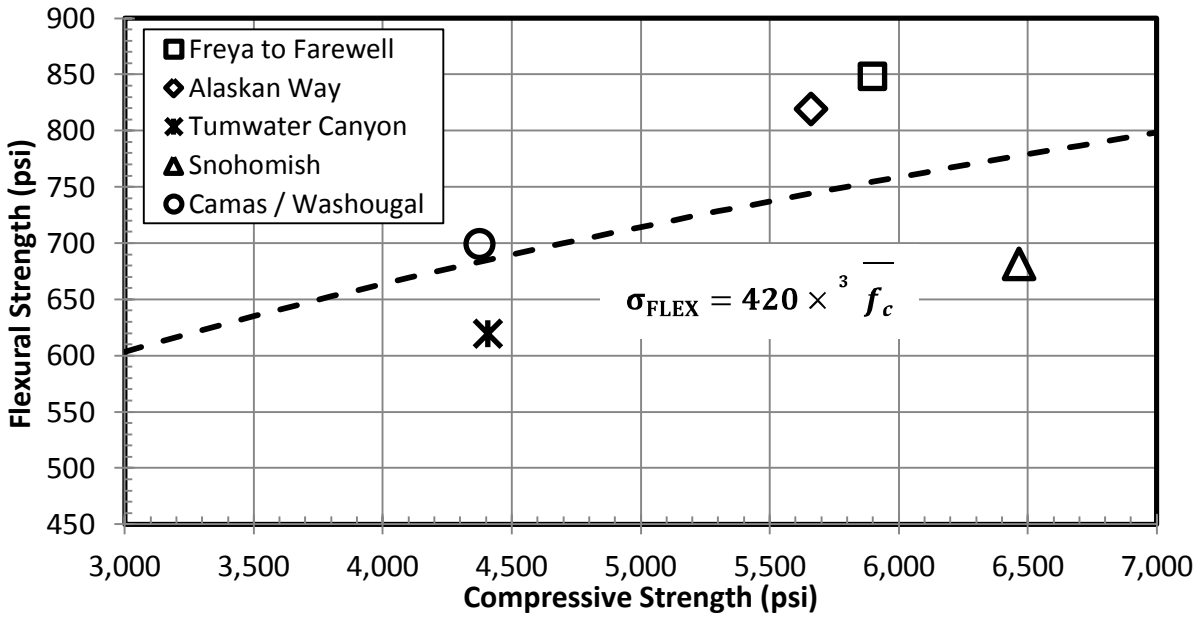

Figure 5.5: Day 56 Flexure Strength vs. Compressive Strength-Optimized Equation

Equation 5.1 estimates the average flexural strength of the field mixtures. The percentage difference from the actual to the estimated strength ranged from 4.7 percent to 12.9 percent, with an average difference of 8.3 percent for Day 28 and Day 56 tests. These figures show that

Equation 5.1 better modeled the flexural strength based on the compressive strength than either equation from the AASHTO specifications.

5.2 SPLIT-TENSION TESTS

The split-tension tests were performed on two cylinder samples on Day 28 and Day 56. The measured strengths for the two samples differed by as much as 31.6 percent, with an average difference of 10.7 percent between samples. The mean split-tension strengths for Day 28 and 56 are shown in Figure 5.6.

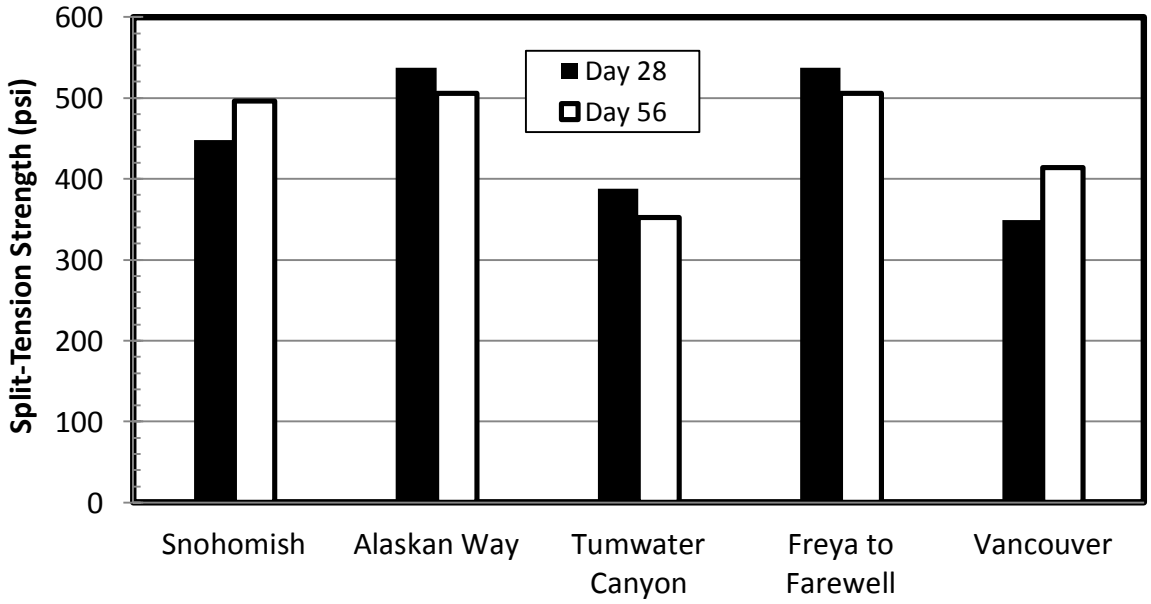

Figure 5.6: Field Sample Split Tensile Strengths

The split-tension strength ranged from 350 psi to 540 psi with a mean strength of 450 psi. The two split-tension breaks for a single test varied for each mixture by 52 psi on average. The tensile strength gain over time was not consistent for the field mixtures. The change in strength from Day 28 to Day 56 ranged from a loss of 9.1 percent to a gain of 10.7 percent, with a mean strength gain of 1.6 percent. For a single mixture, the difference in split-tension strengths from Day 28 to Day 56 ranged from 5 psi to 65 psi, with an average difference of 37 psi. The variability between samples exceeded the change in strength over time, so no consistent trend was determined.

Figure 5.7 shows the Day 28 and Figure 5.8 the Day 56 split-tension results; both are plotted against the measured compressive strength. The calculated values following AASHTO specifications (Equation 2.4) are included in the figures.

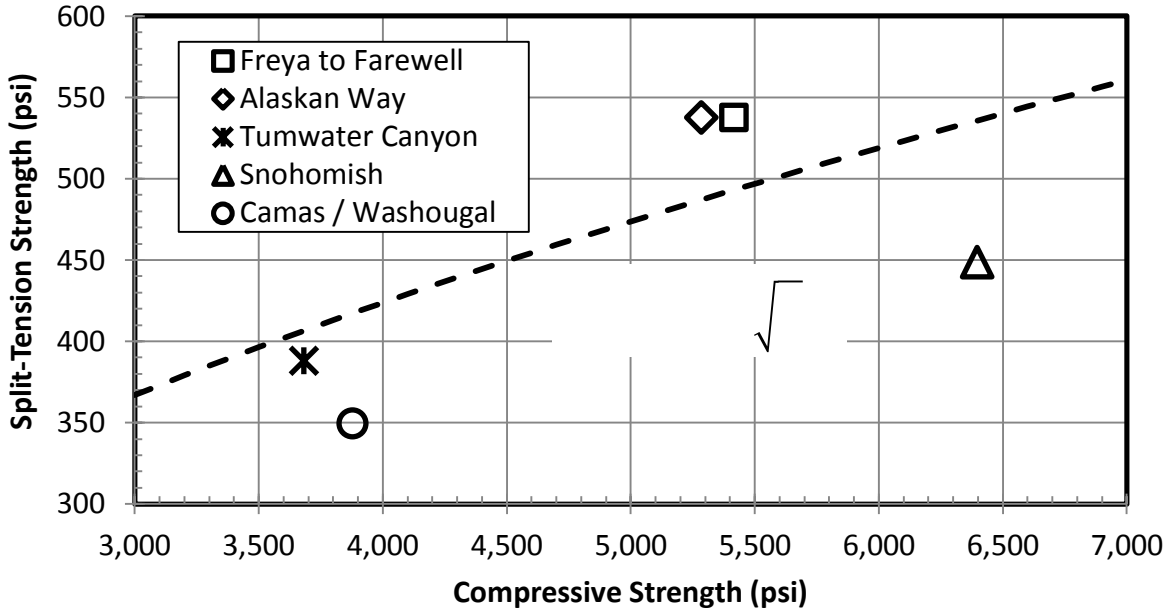

Figure 5.7: Day 28 Split-Tension vs. Compressive Strength

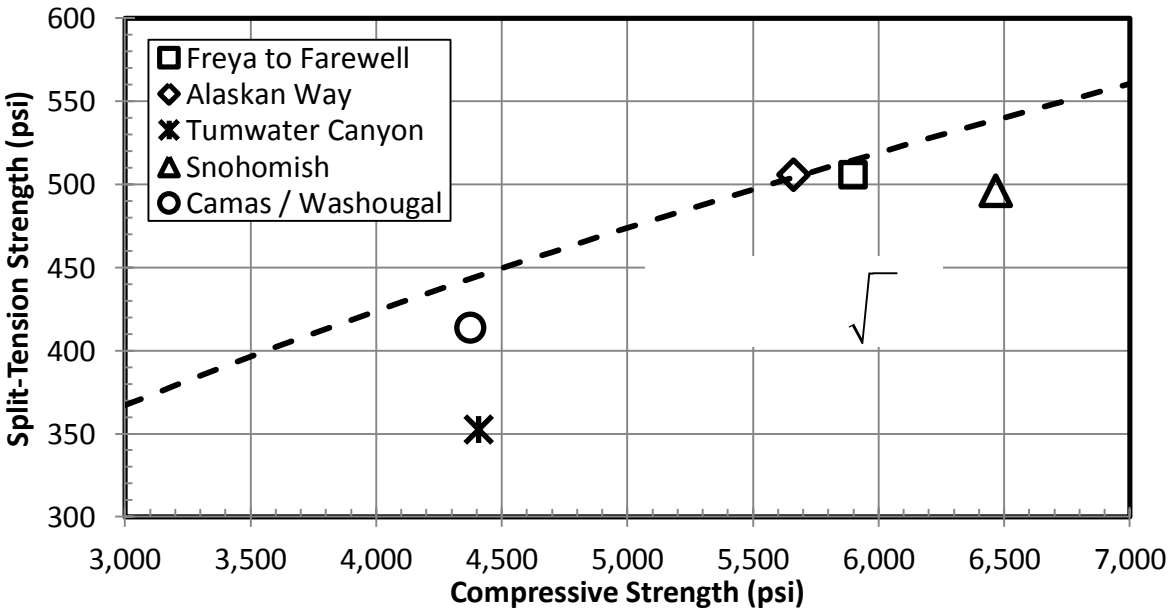

Figure 5.8: Day 56 Split-Tension vs. Compressive Strength

With the exception of Day 28 breaks for the Freya to Farewell and Alaskan Way projects, Equation 2.4 consistently over-predicted the tensile strength of the field mixtures. Equation 2.4 fit the split-tension data well and had an average difference between the estimated and actual tensile strength of 11.3 percent for Day 28 and 7.5 percent for Day 56. The largest deviations from Equation 2.4 occurred with the breaks for Snohomish on Day 28 (difference of 16.3 percent) and Tumwater Canyon on Day 56 (difference of 20.8 percent).

5.3 RELATIONSHIP BETWEEN SPLIT-TENSION AND FLEXURE STRENGTHS

The following section describes the relationship between the tensile strengths predicted by the split-tension and flexural tests. This relationship is important because it is much easier to cast and test cylinder samples than flexural beams. The split-tension and flexural strengths were correlated, and a linear fit between the two tests is shown by Equation 5.2.

$$\sigma_{FLEX}\ \text{psi} = 1.58 \times \sigma_{ST}\ \text{psi} \qquad \text{(Equation 5.2)}$$

As mentioned in Section 2.2, ASTM STP 169D suggests a value of 1.54 to correlate the two tensile strength test results (difference of 2.5 percent). Equation 5.2 was plotted against the Day 28 and Day 56 test results, as shown in figures 5.9 and 5.10, respectively.

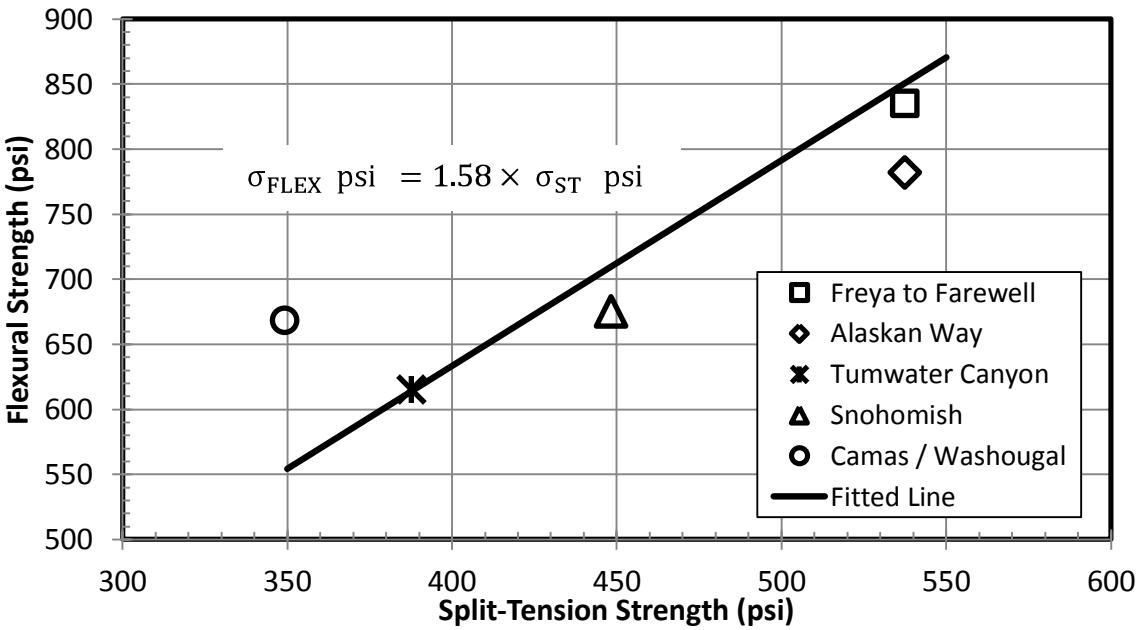

Figure 5.9: Day 28 Split-Tension vs. Flexural Strength

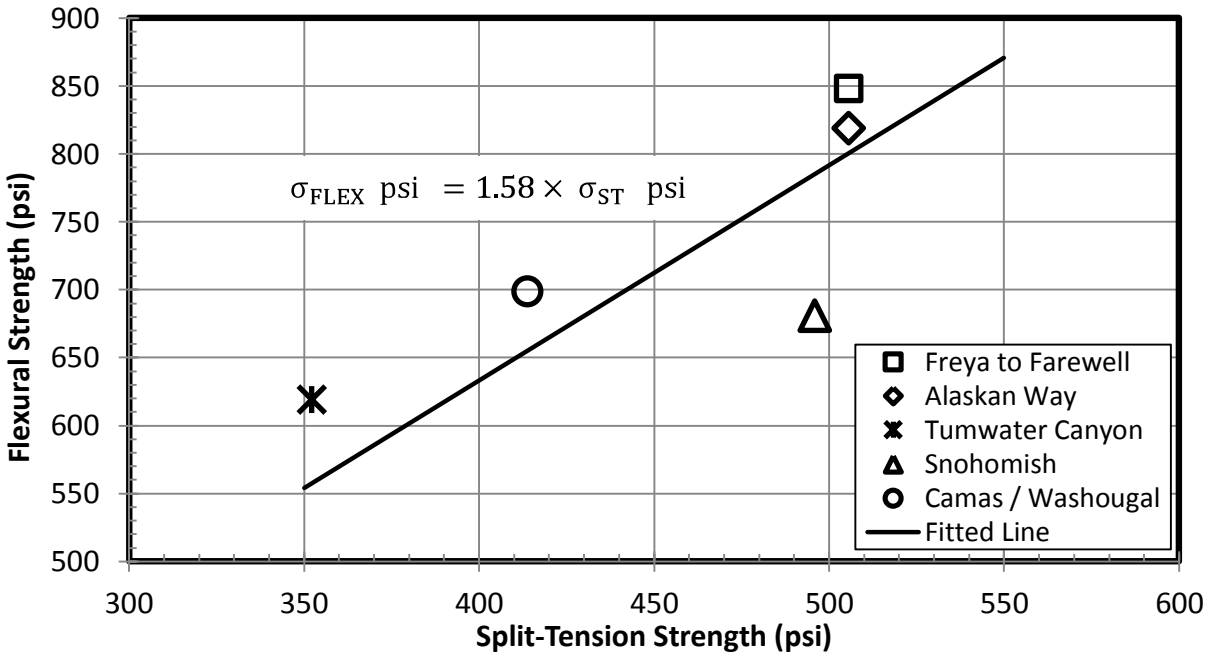

Figure 5.10: Day 56 Split Tension vs. Flexural Strength

Equation 5.2 fit the data set well, with the exception of the Day 28 break for Camas/Washougal and Day 56 Snohomish break. Including all data points, the percentage error in the predicted values from Equation 5.2 was an average of 7.6 percent for all of the mixtures. The correlation coefficient was 7.2 percent for Day 28 and 8.0 percent for Day 56.

5.4 SUMMARY OF TENSILE STRENGTH RESULTS

The variation in flexural strengths among test specimens was small, with an average variation of only 4 percent. The flexural strength increased a little between Day 28 and Day 56, as expected. AASHTO code specifications for normal-weight concrete (Equation 2.2) under-predicted the field sample strengths (figures 5.2 and 5.3). Equation 2.3, which is for high-strength concrete, over-predicted the field sample strengths but had a smaller percentage difference than Equation 2.2 (figures 5.2 and 5.3). The optimized Equation 5.1 fit the mean flexural strength of the field mixtures and had a lower percentage difference than either Equations 2.2 or 2.3 (figures 5.4 and 5.5).

The split-tension results showed large variation among samples. That variability in tensile strength among samples had an average difference of 8 percent. Because of that large variation,

it was not possible to measure a consistent trend in strength over time for the field mixtures. The ACI specifications for estimating split-tensile strength (Equation 2.4) matched the field samples within a 10 percent error (figures 5.7 and 5.8).

The measured split-tension and flexural strengths of the field concrete mixtures were fit well by Equation 5.2 (figures 5.9 and 5.10). The correlation between the split-tension and flexural strength tests found in the laboratory data was similar to the value suggested by Equation 2.6 (difference of 2.5 percent). Because of the variability of the split-tension results, further testing is required if the modulus of rupture is to be accurately predicted from the split-tension strength tests.

Chapter 6: Elastic Modulus

This chapter discusses the results from the elastic modulus tests that were performed in this study. The influences of the water-cementitious ratio, paste content, and coarse aggregate on elastic modulus were evaluated.

Section 6.1 documents the data for a single aggregate source to illustrate the process used to analyze the data. Section 6.2 summarizes and documents the data for the remaining aggregate sources. The field mixture data are covered in Section 6.3. The details of the elastic modulus tests are located in Appendix B.

6.1 LABORATORY DATA FOR DUPONT (3/4-IN.) AGGREGATE SOURCE

This section discusses the results from the elastic modulus tests performed on the DuPont (3/4-in.) mixtures and the method of analyzing the data.

6.1.1 Measured Elastic Modulus

Elastic modulus tests were performed on two 6-in. x 12–in. cylinders for the laboratory and field samples at days 7, 14, 28 and 56. The results of the elastic modulus tests on the four DuPont (3/4-in.) mixtures are reported in Table 6.1, along with key mixture proportions.

Table 6.1: Measured Elastic Moduli: DuPont (3/4-in.) Mixtures

Mixture	Paste Content (%)	Water-Cementitious Ratio	Day 7 (ksi)	Day 14 (ksi)	Day 28 (ksi)	Day 56 (ksi)
High Paste	30.5	0.38	4,460	4,900	5,160	5,260
Low Paste	24.0	0.38	3,910	4,280	4,560	4,610
High Strength	27.0	0.30	4,550	4,650	5,090	5,530
Low Strength	27.0	0.49	3,810	4,050	4,240	NA*

**The data for Day 56 for low-strength mixture were omitted from the data set because the strain gauge was not properly attached to the cylinders.*

The elastic moduli for the Day 28 results ranged from 4,240 to 5,160 ksi, with an average of 4,750 ksi. Figure 6.1 plots these data against the water-cementitious ratio for each mixture. The figure also includes a fitted line of the form of Equation 6.1.

$$E_{28\ Day} = A + B \times w/cm \qquad \text{(Equation 6.1)}$$

where: A = 6,850 ksi
B = -4,600 ksi

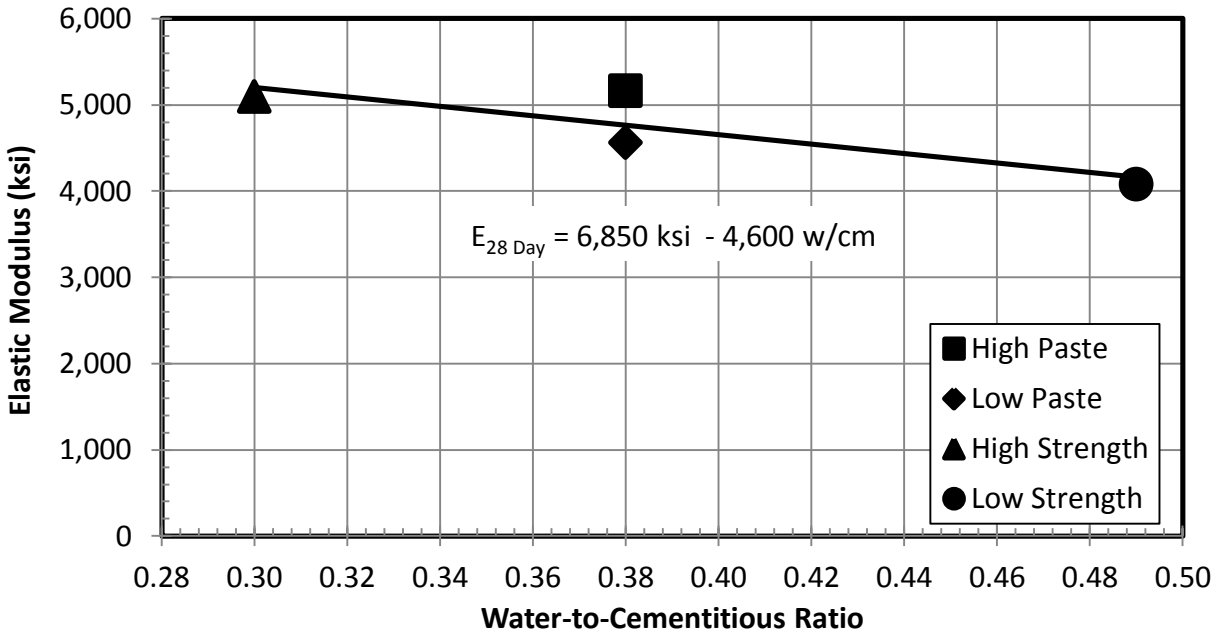

Figure 6.1: Day 28 Elastic Moduli vs. W / CM Ratios: DuPont (3/4-in.) Mixtures

The elastic moduli decreased with increases in the water-cementitious ratio, as expected because of the reduction in compressive strength. Since the high- and low-paste mixtures had the same water-cementitious ratio, the difference in elastic moduli (11.5 percent) was likely attributable to differences in compressive strength.

Figure 6.2 is a plot of the DuPont (3/4-in.) elastic moduli versus the compressive strength for all four test days and includes the curve from AASHTO (5.4.2.4-1, Equation 2.7). The data point for Day 28 results are identified by an increased size and hollowed symbol.

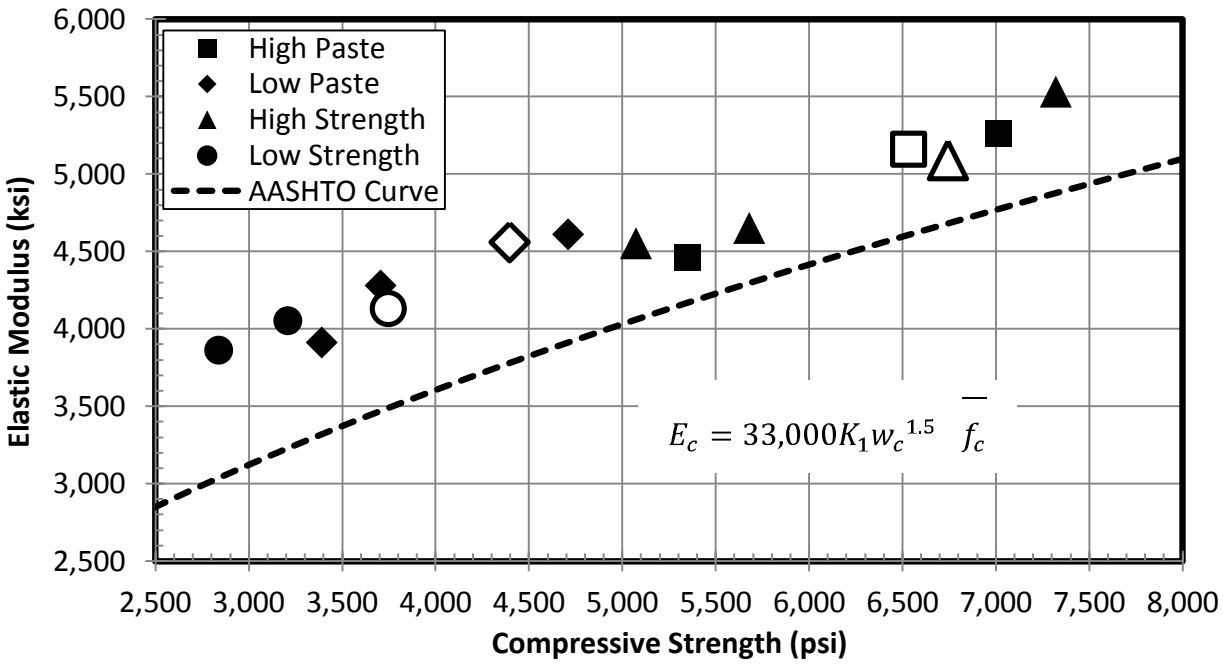

Figure 6.2: Elastic Moduli vs. Compressive Strengths: DuPont (3/4-in.) Mixtures

The elastic modulus for the DuPont (3/4-in.) aggregate exceeded by 14.6 percent, on average, the calculated values for the AASHTO relationship (Equation 2.7). The measured elastic moduli were normalized by dividing by the estimated elastic moduli from Equation 2.7 to evaluate the accuracy of this equation. The resulting normalized elastic moduli ratios for the DuPont (3/4-in.) mixtures are listed in Table 6.2.

Table 6.2: Measured to Calculated Elastic Moduli Ratio: DuPont (3/4-in.) Mixture

	Day 7	Day 14	Day 28	Day 56	Average
High Paste	1.07	1.22*	1.12	1.10	1.13
Low Paste	1.18	1.23	1.21	1.18	1.20
High Strength	1.12	1.08	1.09	1.13	1.11
Low Strength	1.25	1.25	1.21	NA	1.24
Average	1.16	1.20	1.16	1.14	
St. Deviation	0.08	0.08	0.06	0.04	
Coef. of Variation	6.8%	6.5%	5.5%	3.4%	

**Day 14 compressive strength was low for DuPont (3/4-in.) High-Paste*

The low-paste and low-strength mixtures had similar elastic moduli ratios that were on average 1.22. The high-paste and high-strength mixtures had similar ratios with an average ratio of 1.10. The Day 28 normalized elastic moduli (ratio of measured elastic modulus to AASHTO predicted value) are plotted against the compressive strength for each of the DuPont (3/4-in.) mixtures in Figure 6.3.

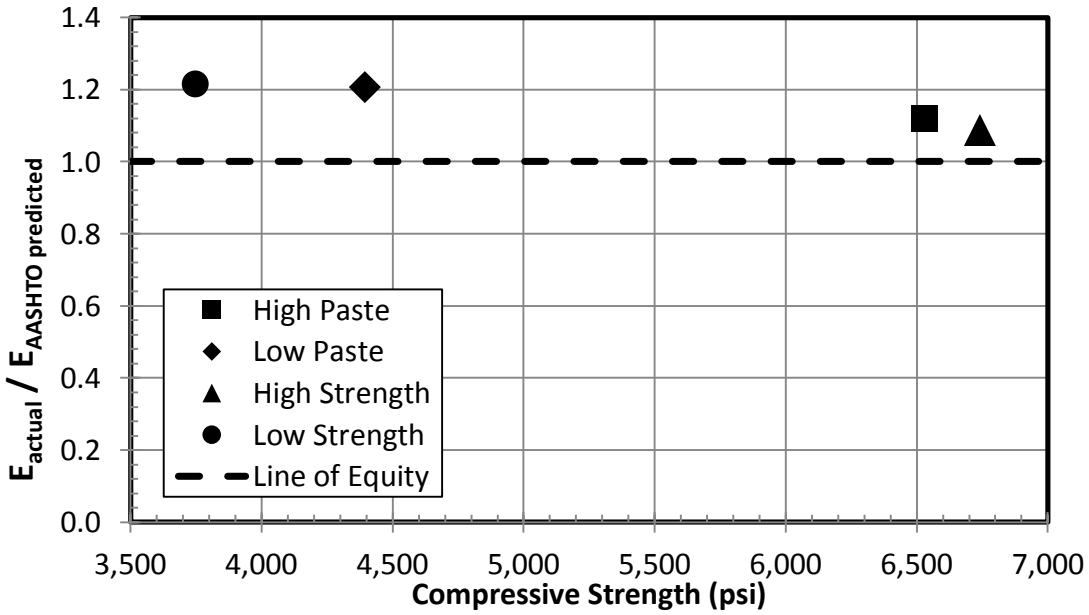

Figure 6.3: Day 28 Elastic Modulus Ratio: DuPont (3/4-in.) Mixtures

The AASHTO 5.4.2.4-1 curve under-predicted the DuPont (3/4-in.) concrete samples, but for higher-strength mixtures, the estimated elastic modulus was more accurate. This implies that the exponent and/or coefficient for the AASHTO code favor a range of compressive strengths and could be altered to improve the accuracy for a larger range of strengths.

6.1.2 Rate of Stiffness Gain

The results from the elastic modulus tests were normalized by dividing each by the Day 28 value. The normalized elastic moduli were optimized to a non-linear curve fit, as explained in Section 2.3, and took the form shown in Equation 6.2. The DuPont (3/4-in.) low-paste mixture's K1 and K2 constants are included below the formula. Figure 6.4 displays the fitted curve along with the normalized elastic moduli data.

$$\frac{E_{time}}{E_{28}} = \frac{time}{K1 + K2 \times time} \qquad \text{(Equation 6.2)}$$

where: K1 = 1.42
K2 = 0.95

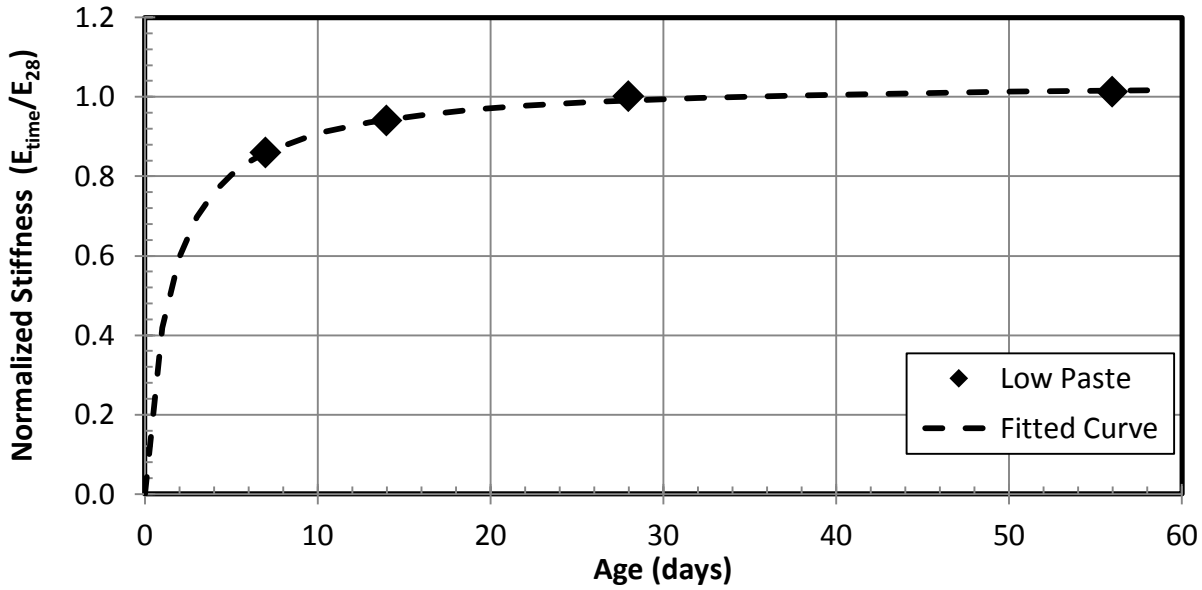

Figure 6.4: Rate of Stiffness Gain Fitted Curve: DuPont (3/4-in.) Low-Paste Mixture

The rate of stiffness gain for the DuPont (3/4-in.) low-paste mixture rapidly reached a plateau. The rate of stiffness gain can be compared to the rate of strength gain for the DuPont (3/4-in.) low-paste mixture, which is plotted in Figure 6.5.

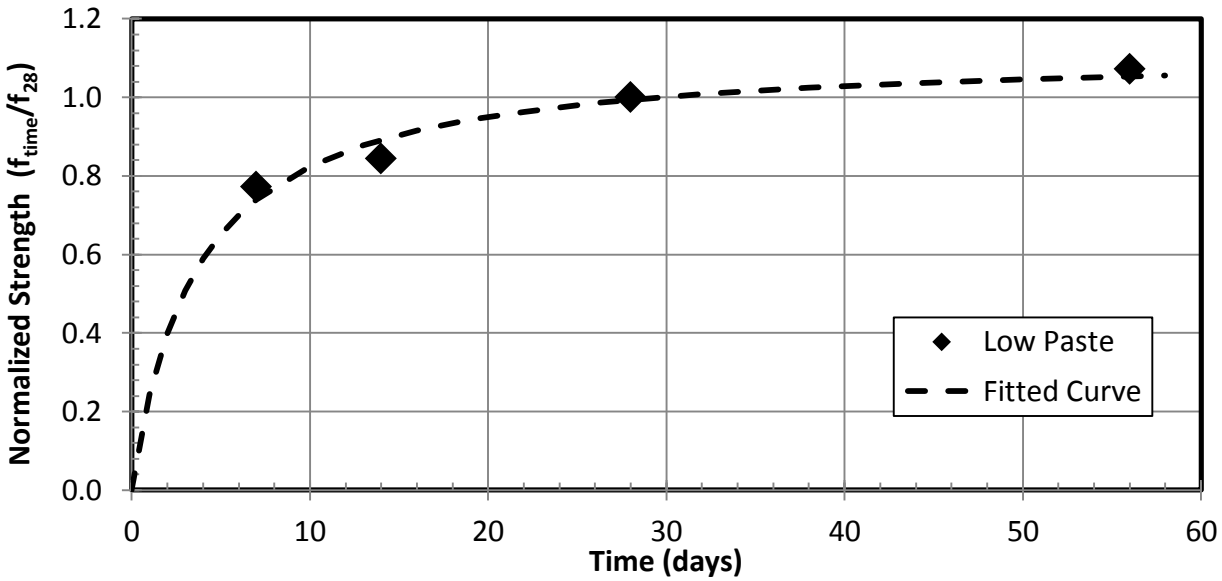

Figure 6.5: Rate of Strength Gain Fitted Curve: DuPont (3/4-in.) Low-Paste Mixture

Figures 6.4 and 6.5 show that the rate of stiffness gain leveled out faster than the compressive strength. The ratio of the elastic modulus measured at Day 7 to that measured at Day 28 was 0.94, whereas the same ratio was 0.72 for compressive strength. This trend continued, and the normalized elastic modulus ratio for Day 56 to Day 28 was 1.01, while the compressive strength had a ratio of 1.07.

The process of optimizing the constants for each of the DuPont (3/4-in.) mixtures was repeated, and the constants for all of the mixtures are shown in Table 6.3. The mean elastic moduli for the Day 28 results are included in the table. Figure 6.6 shows the fitted curves for the four mixtures.

Table 6.3: Optimized Constants for DuPont (3/4-in.) Aggregate

Mixture	E_{28} (ksi)	K1	K2	E_7/E_{28}	E_{56}/E_{28}
High Paste	5,160	1.47	0.95	0.86	1.02
Low Paste	4,560	1.43	0.96	0.86	1.01
High Strength	5,090	1.70	0.92	0.89	1.09
Low Strength	4,130	0.60	0.98	0.90	1.01**
Average	4,740	1.30	0.95	0.88	1.03
St. Deviation	484	0.48	0.02	0.02	0.04
Coef. of Variation	10.2%	37.1%	2.5%	2.4%	3.5%

***Determined from fitted curve*

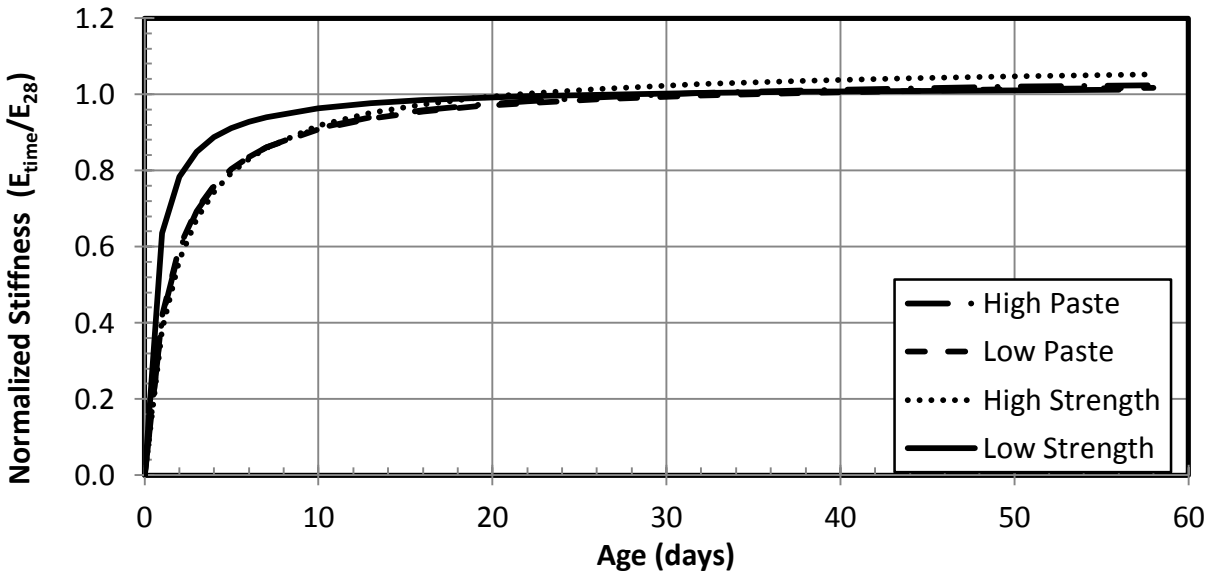

Figure 6.6: Rate of Stiffness Gain Fitted Curves: DuPont (3/4-in.) Mixtures

The normalized elastic moduli curves for the high-paste, low-paste, and high-strength mixtures were almost identical. At Day 7, the mean normalized stiffness for those three mixtures was 87.3 percent. The low-strength mixture gained stiffness faster than the other mixtures initially (normalized ratio of Day 7 to Day 28 of 90.0 percent) but matched the other mixtures after Day 14.

6.2 LABORATORY DATA FOR ALL AGGREGATE SOURCES

The process outlined in Section 6.1 was repeated for all of the aggregates. The details for the tests are provided in Appendix B.

6.2.1 Measured Elastic Moduli

For each aggregate source, the elastic moduli for the high- and low-strength mixtures at Day 28 are shown in Figure 6.7. The paste content was constant for both the high- and low-strength mixtures, with only the water-cementitious ratios varying.

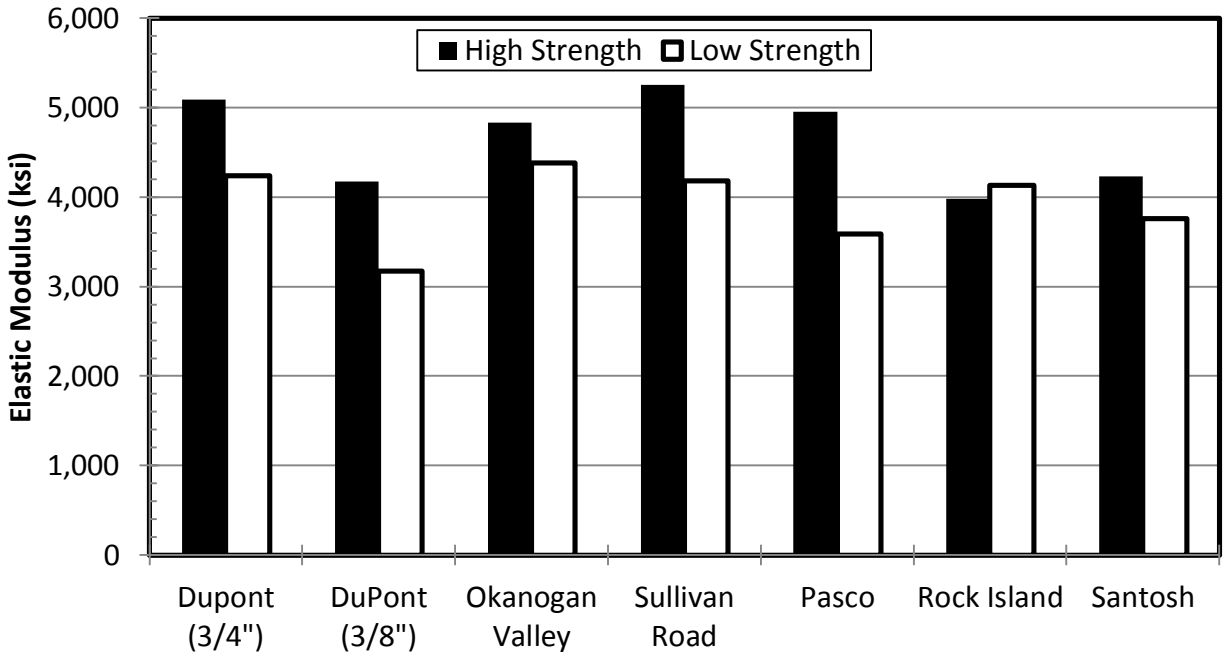

Figure 6.7: Day 28 Elastic Moduli: All Aggregates—High- and Low-Strength Mixtures

The high-strength mixtures had elastic moduli that ranged from 3,980 ksi to 5,250 ksi, with an average of 4,680 ksi. The elastic moduli for the low-strength mixtures ranged from 3,400 ksi to 4,380 ksi, with an average of 3,950 ksi. With the exception of the Rock Island mixtures, the elastic modulus for the high-strength mixtures exceeded that of the low-strength mixtures. The difference in compressive strength between the high- and low-strength mixtures for the Rock Island aggregate was only 5.4 percent, whereas the other aggregates had an average strength difference of 33.6 percent.

The Day 28 elastic moduli were analyzed against the water-cementitious ratio and fit to the line for Equation 6.1 for each aggregate source. Figure 6.8 shows the resulting linear fits for the seven aggregate sources. The individual plots for the elastic moduli versus water-cementitious ratios can be seen in Appendix B for the various aggregate sources. There was little change in elastic moduli as a function of water-cementitious ratio for Rock Island mixtures, which can be seen in Figure B.5.

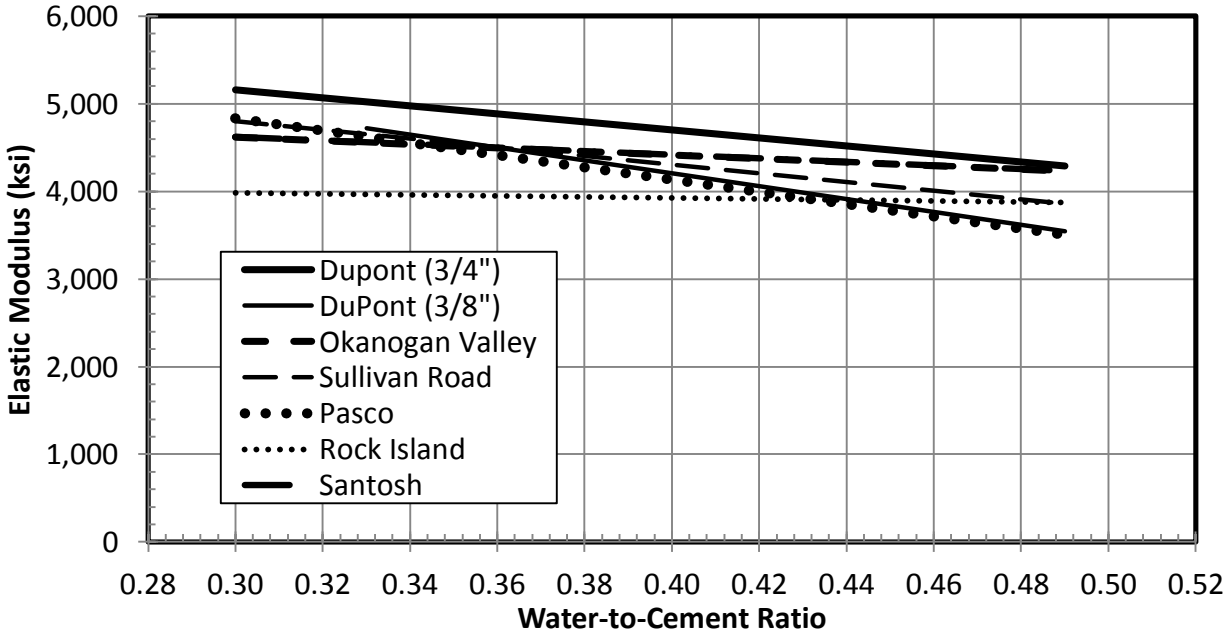

Figure 6.8: Day 28 Elastic Modulus vs. Water-Cementitious Ratio: All Aggregates

Excluding the Rock Island aggregate, raising the water-cementitious ratio decreased the elastic modulus for the aggregates. An increase of 0.1 in the water-cementitious ratio reduced the elastic moduli in a range of 205 ksi to 735 ksi, with an average decrease of 470 ksi. The average change in compressive strength per change of 0.1 water-cementitious ratios was 1,200 psi. This suggests that for the range of water-cementitious ratios between 0.30 and 0.49, the elastic modulus increases at approximately 40 percent of the rate of the compressive strength. This supports the finding that elastic modulus increases more slowly than the strength, and an exponent of less than 1.0 should be used to correlate the strength to the elastic modulus.

Figure 6.9 shows each aggregate's Day 28 elastic moduli for the high- and low-paste mixtures. The variation in paste content is shown for these two mixtures since they had the same water-cementitious ratio.

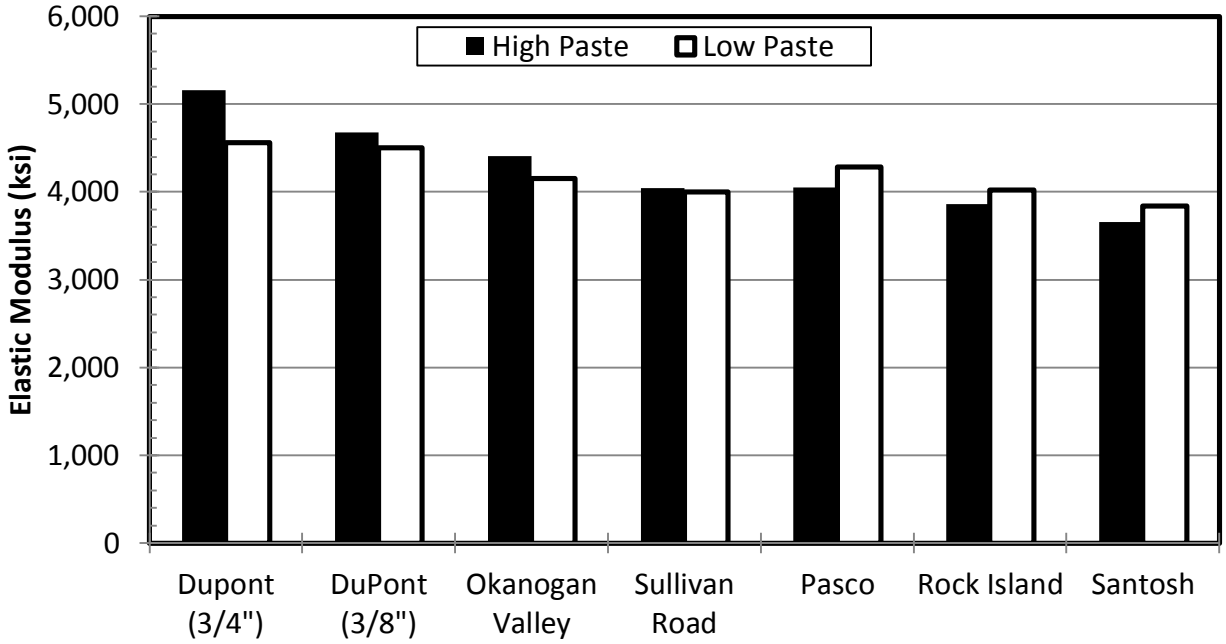

Figure 6.9: Day 28 Elastic Moduli: All Aggregates—High- and Low-Paste Mixtures

The elastic moduli of the high-paste mixtures ranged from 3,660 ksi to 5,160 ksi, with an average of 4,370 ksi. The low-paste mixtures had elastic moduli that ranged from 3,840 ksi to 4,560 ksi, with an average of 4,190 ksi. The elastic modulus for a low-paste mixture is more heavily influenced by the stiffness of the aggregate, whereas a high-paste mixture combines the stiffness from the aggregate and the paste. Because of the relatively low stiffness of cement paste in comparison to the coarse aggregate, it is expected that a lower paste mixture will have a higher elastic modulus than a higher paste mixture of similar strength. Though the high- and low-paste mixtures had the same water-cementitious ratio, the strength of the high-paste mixtures varied from 3.2 percent lower to 32.7 percent higher than those of the low-paste mixtures. The variation in strength between the high- and low-paste mixtures affected the elastic moduli, so a consistent pattern could not be determined for the effect of only the paste content on the elastic modulus.

The ratio of Day 28 measured elastic modulus to the AASHTO estimated elastic moduli from Equation 2.7 was calculated for each mixture. Figure 6.10 shows ratios of elastic moduli for the high- and low-strength mixtures of each aggregate source. The individual ratios of measured to predicted elastic moduli for each test date are listed in Appendix B.

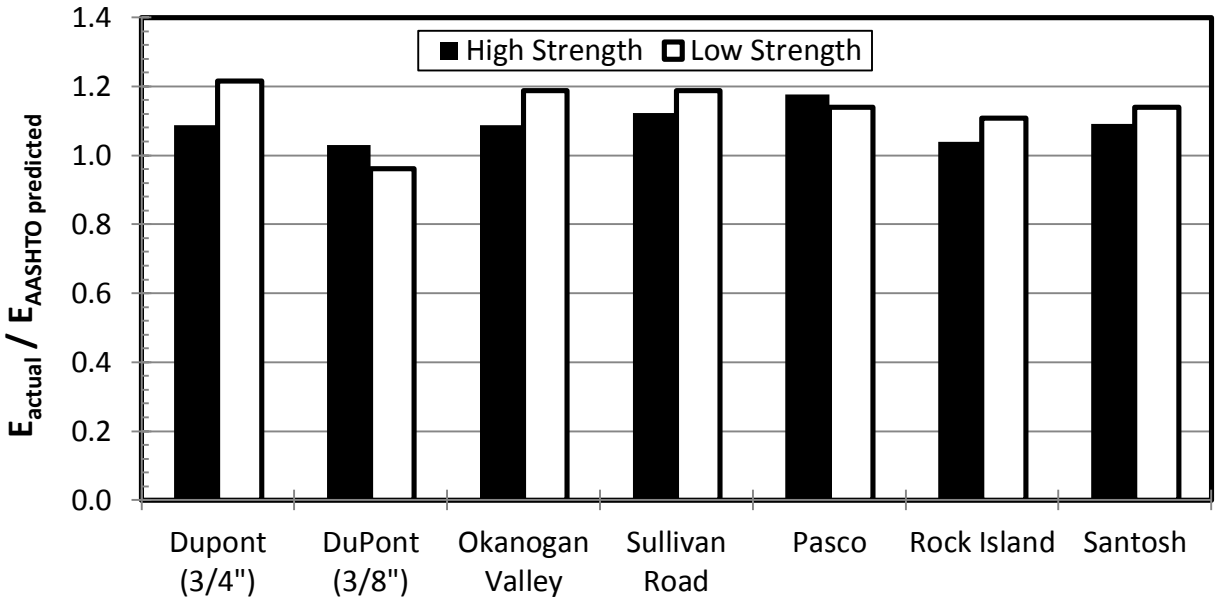

Figure 6.10: Day 28 Elastic Modulus Ratio: All Aggregate—High- and Low-Strength

With the exception of the DuPont (3/8-in.) and Pasco aggregate sources, the ratio of measured to estimated elastic moduli was larger for the low-strength mixtures than for the high-strength mixtures. The low-strength mixture for DuPont (3/8-in.) was also the only sample for which the measured elastic modulus did not exceed the estimated value from Equation 2.7. The paste contents for the pea gravel low-strength mixtures were higher (29.3 percent vs. 27.0 percent, tables 3.3 and 3.4) than for the other mixtures, which may explain this behavior. The high-strength mixtures had an elastic moduli ratio that ranged from 1.03 to 1.18, with an average of 1.09. The low-strength mixtures had an elastic moduli ratio that ranged from 0.96 to 1.21, with an average of 1.13. As expected, this suggests that Equation 2.7 estimates the higher strength mixtures more accurately than it does lower strength mixtures.

Figure 6.11 shows the ratio of measured to AASHTO estimated elastic moduli for the high- and low-paste mixtures.

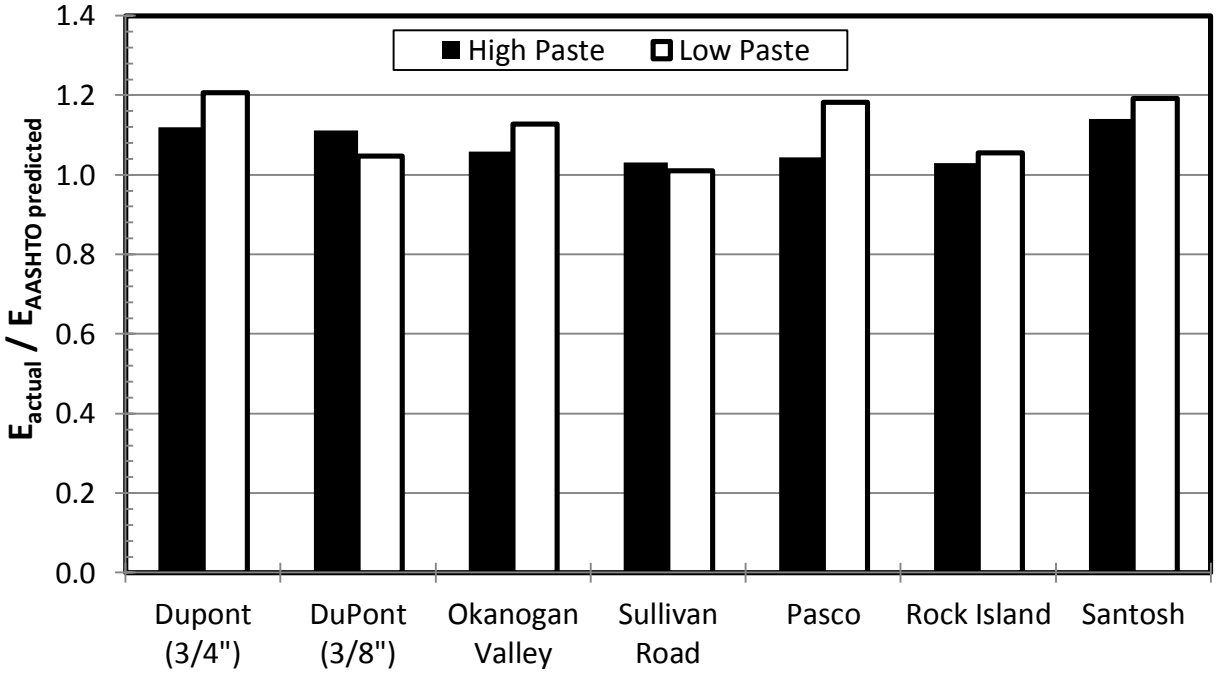

Figure 6.11: Day 28 Elastic Modulus Ratio: All Aggregate—High- and Low-Paste

Excluding the DuPont (3/8-in.) and Sullivan Road aggregate, the ratio between the measured and estimated elastic modulus was larger for the low-paste mixtures than for the high-paste mixtures. The high-paste mixtures had a ratio that ranged from 1.03 to 1.14, with an average of 1.08. The low-paste mixtures had a range of 1.01 to 1.21 and an average ratio of 1.12. This follows the same suggestion that the AASHTO specifications for estimating the elastic modulus based on compressive strength (Equation 2.7) are more accurate for higher strength concrete mixtures.

6.2.2 Rate of Stiffness Gain

The measured elastic moduli for each mixture were normalized by dividing the data by the respective Day 28 elastic moduli. Figure 6.12 shows the normalized elastic moduli for the high- and low-strength mixtures as a ratio of Day 7 to Day 28 values for each of the aggregates. Each mixture's normalized elastic modulus data were fit to Equation 6.2; the optimized K1 and K2 coefficients and fitted curves can be seen in Appendix B.

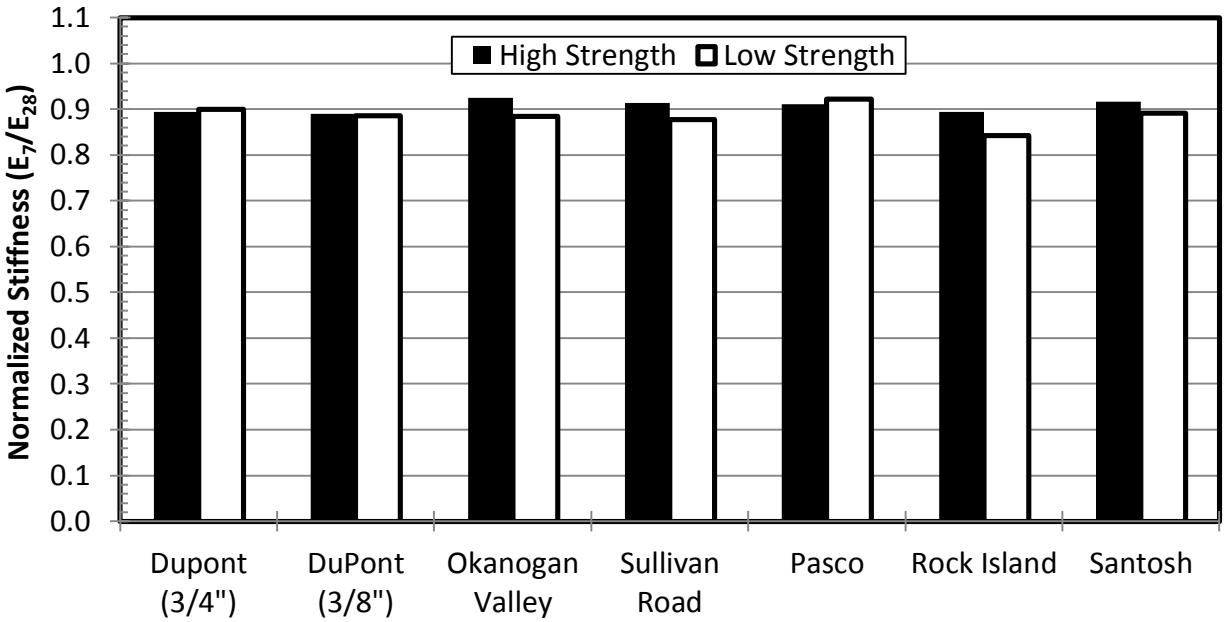

Figure 6.12: Day 28 Rate of Stiffness Gain: All Aggregates-High- and Low-Strength

The ratio of Day 7 to Day 28 stiffness was nearly identical for the high-strength and low-strength mixtures. The normalized stiffness ratio for the Day 7 to Day 28 elastic moduli of the high-strength mixture ranged from 0.89 to 0.92, with an average ratio of 0.91. The low-strength mixtures had a ratio that ranged from 0.84 to 0.92, with an average of 0.89. The percentage difference between the high and low strength mixtures ranged from 0.6 percent to 5.8 percent, with a mean of 2.7 percent. The variation in water-cementitious ratio, aggregate type, and cement content did not have a large effect on the early rate of stiffness gain for mixtures with constant paste content.

Figure 6.13 shows the normalized Day 7 to Day 28 ratio of the elastic moduli for the high- and low-paste mixtures.

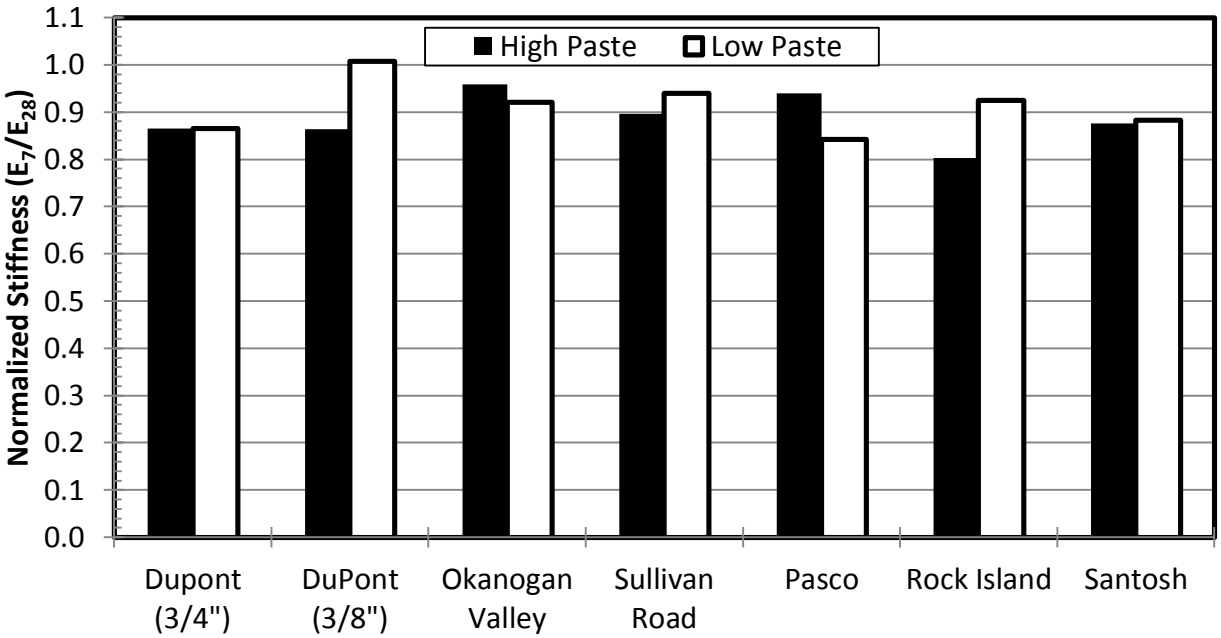

Figure 6.13: Day 28 Rate of Stiffness Gain: All Aggregates-High- and Low-Paste

The normalized Day 7 to 28 rate of stiffness gain for the high-paste mixtures ranged from 0.80 to 0.96, with an average rate of 0.89. The low-paste mixtures had a normalized stiffness gain that ranged from 0.84 to 1.01, with an average of 0.91. The percentage difference between the high- and low-paste mixtures ranged from 0.0 percent to 14.3 percent, with an average of 6.7 percent. There was no consistent pattern across the different aggregate sources, so the effect of the paste content on the rate of stiffness gain was not determined.

6.3 DATA FOR FIELD SAMPLES

This section discusses the results from the elastic modulus tests performed on the field samples for each of the five WSDOT projects.

6.3.1 Measured Elastic Moduli

The mixture proportions and elastic moduli for each testing day are shown for the five WSDOT projects in Table 6.4.

Table 6.4: Measured Elastic Moduli: Field Mixtures

Project	Paste Content (%)	Water-Cementitious Ratio	Day 7 (ksi)	Day 14 (ksi)	Day 28 (ksi)	Day 56 (ksi)
Freya to Farewell	25.5	0.31	3,710	3,870	4,200	4,490
Alaskan Way	25.2	0.31	4,760**	4,880	5,030	5,200
Tumwater Canyon	25.9*	0.40	3,160	3,210	3,400	3,450
Snohomish	24.6	0.32	4,200	4,460	4,800	5,240**
Camas / Washougal	27.8	0.41	3,280	3,370	3,680	3,870

** Tumwater Canyon mixture included fly ash*
*** Day 7 and Day 56: strain gauges not properly attached*

The elastic moduli for Day 28 ranged from 3,400 to 5,030 ksi, with an average of 4,220 ksi.

The tests on Day 7 for Seattle and Day 56 for the Snohomish mixtures did not have the strain gauge properly attached, so the elastic moduli were larger than expected (see Figure 6.15). The two data points were omitted when each mixture was optimized and fit to Equation 6.2 and were reevaluated with the curve from the respective mixture.

The Day 28 elastic moduli were plotted against the water-cementitious ratios for the field mixtures, as shown in Figure 6.14. A line was fit to the field sample data by using Equation 6.1, as shown in the figure. The elastic modulus for the field mixtures decreased with an increase in the water-cementitious ratio, as expected.

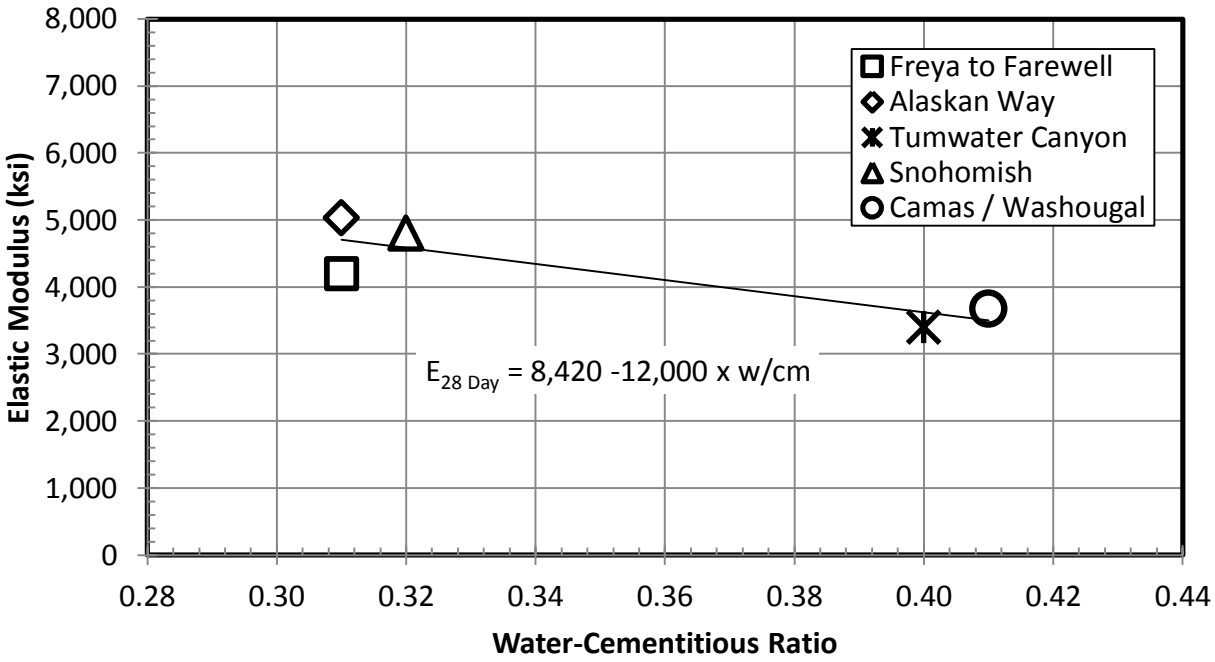

Figure 6.14: Day 28 Elastic Modulus vs. Water-Cementitious Ratio: Field Mixtures

Figure 6.15 is a plot of the elastic moduli versus compressive strengths for each of the field mixtures on all four of the testing days. The AASHTO 5.4.2.4-1 equation is included in the figure (Equation 2.7). Since the AASHTO specifications use the design compressive strength, the data point for the Day 28 test results of each field mixture are indicated by a solid fill and increasing the size.

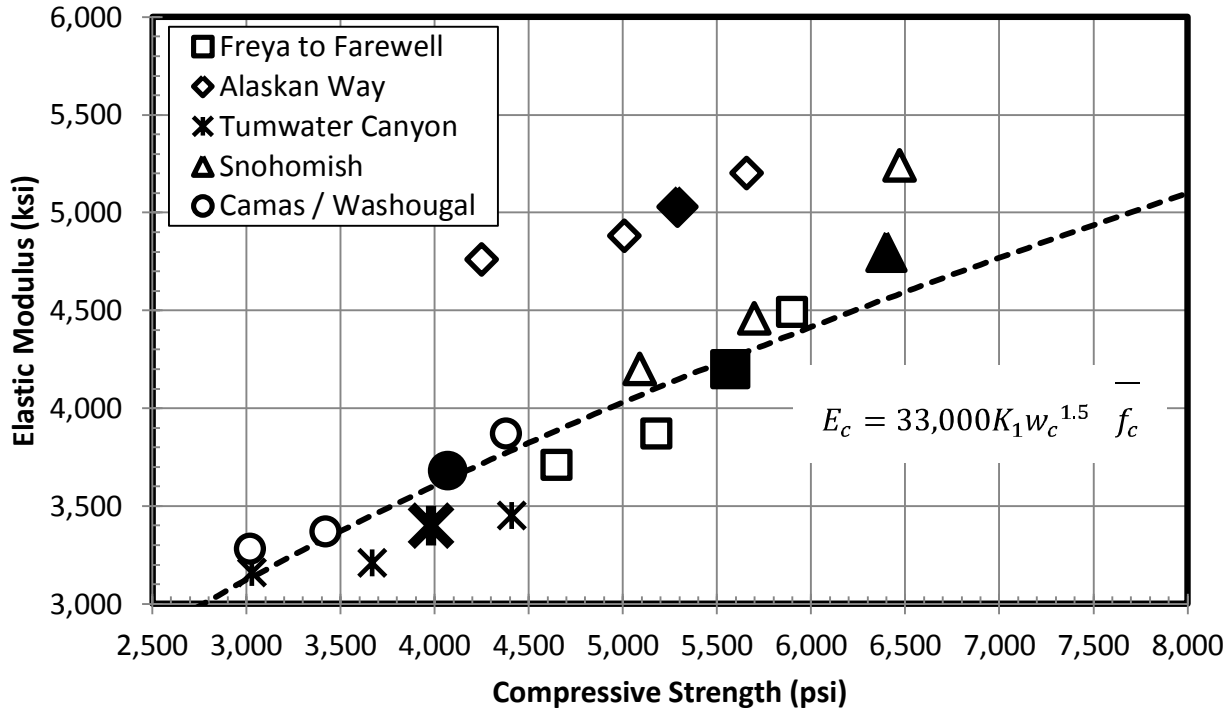

Figure 6.15: Elastic Moduli vs. Compressive Strength: Field Mixtures

The Day 7 Alaskan Way and Day 56 Snohomish elastic moduli were significantly stiffer for the respective compressive strengths because the strain gauge was improperly attached. With the exception of those two data points, the Seattle field mixture was the only concrete samples that had a significant percentage difference from the AASHTO 5.4.2.4-1 specifications. The Seattle field mixture had an average difference of 21.3 percent, whereas the remaining four field mixtures had an average difference of 0.2 percent. The laboratory mixtures that utilized the same coarse aggregate as the field mixtures had an average difference of 11.1 percent from the AASHTO specifications.

The measured Day 28 elastic moduli from the field projects were normalized by the predicted elastic moduli from AASHTO specifications (Equation 2.7). Figure 6.16 shows the ratio of the Day 28 elastic moduli to the estimated elastic moduli for the field mixtures.

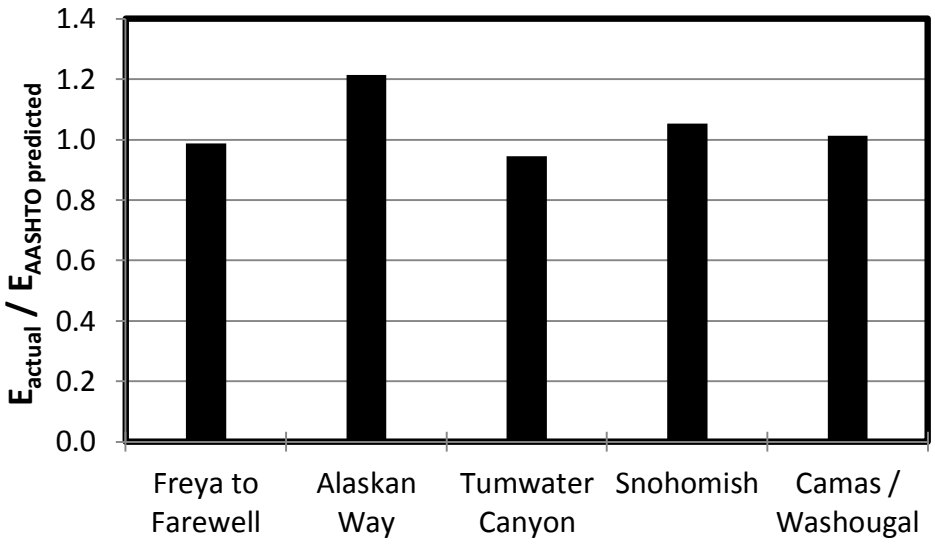

Figure 6.16: Day 28 Elastic Modulus Ratio: Field Mixtures

With the exception of the Alaskan Way mixture, Equation 2.7 estimated the elastic modulus for each of the field projects well. The average ratio for the four field sites was 1.00, whereas the ratio for the Alaskan Way mixture was 1.21. The ratios of measured to estimated elastic moduli for the field mixtures were lower than the ratios for the laboratory mixtures using the same coarse aggregate by an average of 7.8 percent.

6.3.2 Rate of Stiffness Gain

The rate of stiffness gain for each field mixture was determined by dividing each monitored test value by the respective Day 28 elastic modulus. The normalized data were fit to Equation 6.2. The resulting coefficients and mean elastic modulus for Day 28 can be seen in Table 6.5 for the field mixtures. Figure 6.17 shows the fitted curves for the field samples.

Table 6.5: Optimized Constants for Field Samples

Project	E_{28} (ksi)	K1	K2	E_7/E_{28}	E_{56}/E_{28}
Freya to Farewell	5,570	1.74	0.93	0.88	1.07
Alaskan Way	5,290	1.10	0.95	0.90**	1.03
Tumwater Canyon	3,980	0.93	0.98	0.91	1.01
Snohomish	6,400	1.38	0.96	0.87	1.02**
Camas / Washougal	4,070	1.41	0.95	0.89	1.05
Average	5,060	1.27	0.95	0.90	1.05
St. Deviation	1030	0.57	0.02	0.03	0.03
Coef. Of Variation	20.4%	23.9%	1.6%	1.4%	2.3%

** *Determined from fitted curve*

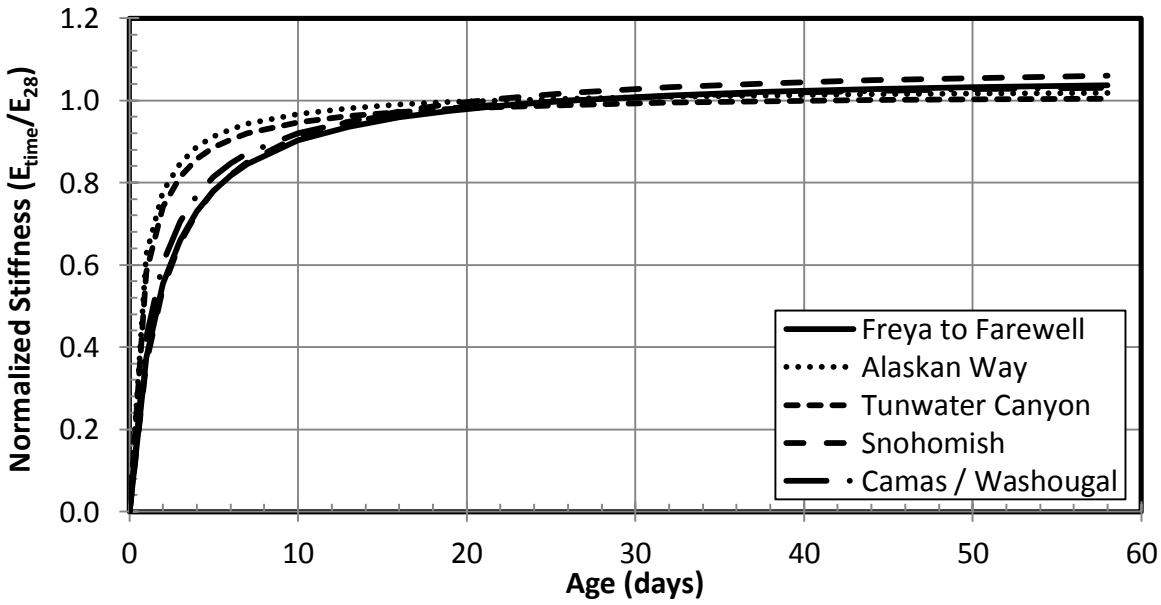

Figure 6.17: Rate of Stiffness Gain Fitted Curves: Field Mixtures

The rate of stiffness gain for the five field mixtures was very similar. After Day 7, the normalized elastic moduli had less than a 3 percent coefficient of variation. Only the initial rate of stiffness gain before Day 7 varied among field samples. This can be attributed to the variations in compressive strength or cement content.

The rate of stiffness gain for the ratio of Day 7 to Day 28 elastic moduli was plotted against the water-cementitious ratio and the paste content of the field mixtures, as shown in Figure 6.18 and Figure 6.19, respectively. As expected, the water-cementitious ratio and paste content did little to affect the rate of stiffness gain for each of the different aggregate sources.

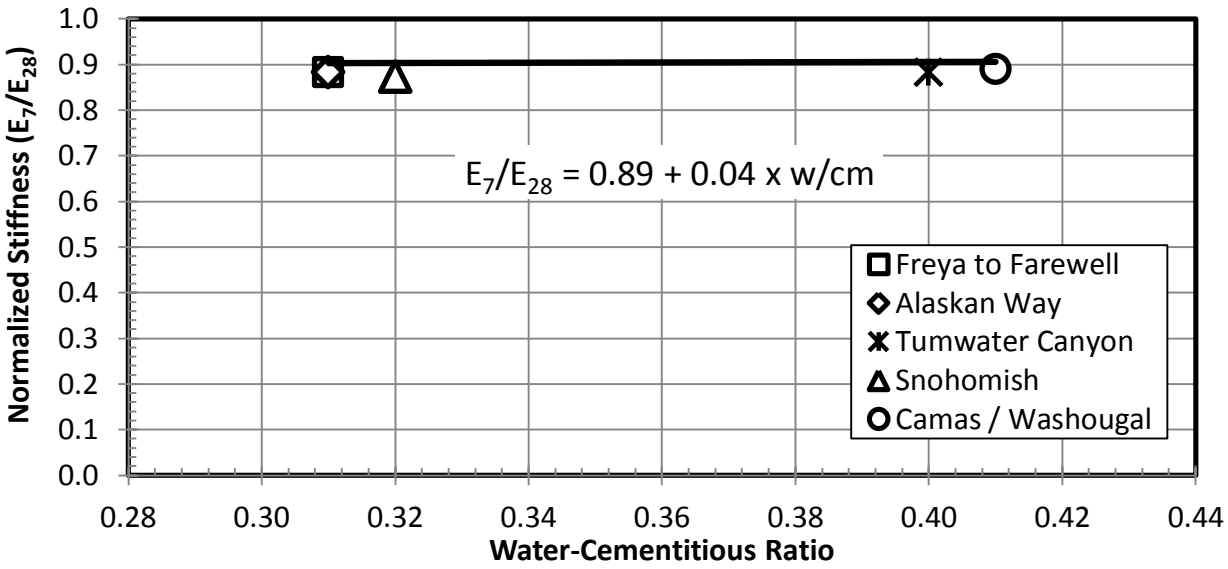

Figure 6.18: Rate of Stiffness Gain vs. Water-Cementitious Ratio: Field Mixtures

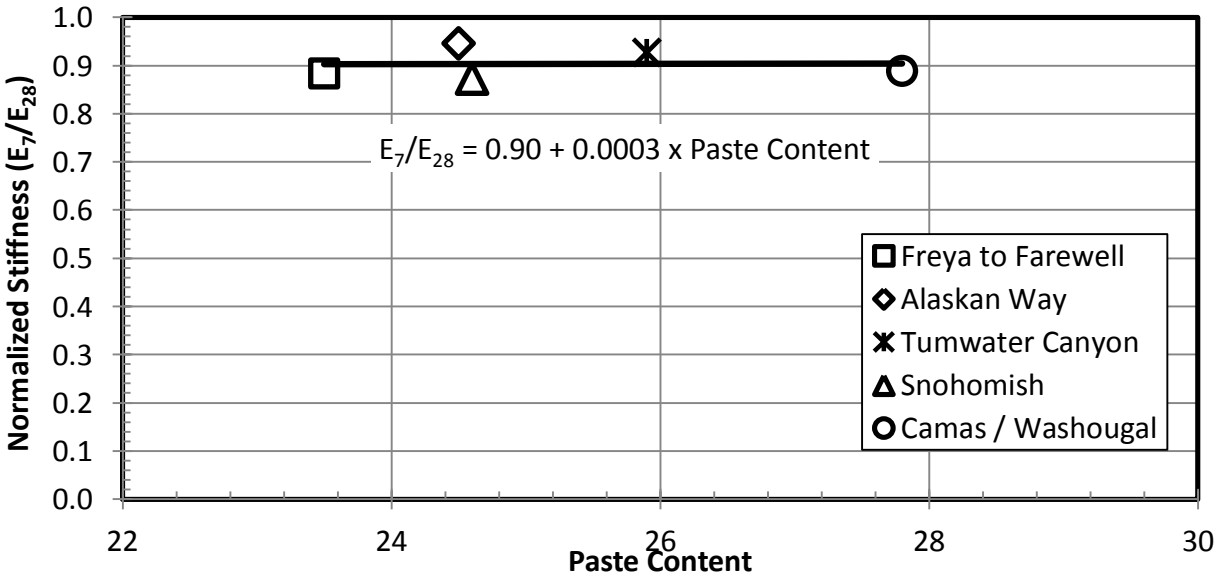

Figure 6.19: Rate of Stiffness Gain vs. Paste Content: Field Mixtures

6.3.3 Variability

To monitor the amount of variability in the elastic moduli for each of the field mixtures, samples from six different construction days were cast at each project. The same Class 4000 mixture was collected for each of the casting dates. The initial samples were tested after 7, 14, 28, and 56 days of curing while the subsequent samples were tested only on the 56th day of curing. The elastic moduli for all six of the Day 56 samples are shown in Table 6.6 for the different field mixtures.

Table 6.6: Field Sample Day 56 Elastic Modulus Variation

	Freya to Farewell (ksi)	Alaskan Way (ksi)	Tumwater Canyon (ksi)	Snohomish (ksi)	Camas / Washougal (ksi)
Initial Sampling	4,490	5,200	3,450	5,240	3,680
Subsequent Sampling	3,920	5,560	3,500	4,330	3,880
	3,770	4,760	3,740	4,470	3,920
	3,780	4,890	4,190	4,570	3,900
	3,710	5,020	3,890	4,500	4,030
	3,850	5,090	4,060	4,430	4,180
Mean	3,920	5,140	3,810	4,590	3,930
St. Deviation	290	290	300	330	170
Coef. of Variation	7.4%	5.6%	7.8%	7.2%	4.2%

The elastic moduli for each of the certified mixtures varied with each casting day. The effects of the variations in compressive strength for each of the mixtures show in the elastic modulus results. Note that the average coefficient of variation for the elastic moduli was 6.4 percent, whereas the average coefficient of variation for the compressive strengths was 8.4 percent. The lower coefficient of variation for the elastic moduli correlates to the findings of Section 6.1.2, which describes a comparison of the rate of stiffness and strength gain curves for the DuPont (3/4-in.) low-paste mixture. As shown in figures 6.4 and 6.5, the rate of stiffness gain after 28 days was minimal, but the compressive strength was still increasing. This suggests that the elastic modulus value is more defined for a given mixture after 28 days and is less inclined to vary.

6.3.4 Comparison of Laboratory and Field Data

Table 6.7 shows the average compressive strengths and elastic moduli of the Day 56 samples from the field sites. The elastic modulus predicted from the AASHTO specifications (5.4.2.4-1, Equation 2.7) and the percentage difference between the measured and estimated elastic modulus are included in the table.

Table 6.7: AASHTO Predicted Field Sample Elastic Moduli

Project	Average Comp. Strength (psi)	Average Elastic Modulus (ksi)	Predicted Elastic Modulus (ksi)	Percentage Difference
Freya to Farewell	5,280	3,920	4,180	6.2%
Alaskan Way	5,830	5,140	4,390	14.6%
Tumwater Canyon	4,830	3,810	4,000	4.8%
Snohomish	5,270	4,590	4,140	9.8%
Camas / Washougal	4,410	3,930	3,790	3.6%

The difference in estimated and actual elastic moduli ranged from 3.6 percent to 14.6 percent, with an average difference of 7.8 percent. This suggests that the AASHTO specifications (5.4.2.4-1, Equation 2.7) predict the elastic modulus well for a concrete mixture without including parameters for the aggregate source, paste content, or water-to-cementitious ratio. For the Tumwater Canyon and Freya to Farewell mixtures, AASHTO specifications over-predicted the elastic modulus (predicted values were on average 5.5 percent larger). The Alaskan Way, Snohomish, and Camas/Washougal projects had estimated elastic moduli that were under-predicted (predicted values were on average 9.3 percent smaller).

An alternative formula was derived to account for the mixture proportions and compressive strength in estimating the elastic modulus. Equation 6.3 shows the formatting and optimized constants that were derived from the laboratory mixtures based on the Day 28 results.

$$E_C = K_1 \times PC \times w/cm + K_2 \; Strength^{K_3} \qquad \text{(Equation 6.3)}$$

where: E_C = elastic modulus (ksi)
PC = paste content (percent)
w/cm= water-cementitious ratio
Strength = compressive strength (psi)
K_1 = -21.3
K_2 = 278.5
K_3 = 0.33

To validate the accuracy of Equation 6.3, the constants (K1, K2, and K3) were re-optimized on the basis of the laboratory mixtures at 56 days of curing. The elastic moduli for the field mixtures were evaluated and compared with the measured results from the samples of each project. Table 6.8 shows the Day 56 compressive strengths, measured elastic moduli, and estimated elastic moduli for the field mixtures. The percentage differences between the estimated and measured elastic moduli are included in the table.

Table 6.8: Laboratory Predicted Field Sample Elastic Moduli

Project	Paste Content (%)	W/CM Ratio	Average Comp. Strength (psi)	Average Elastic Modulus (ksi)	Predicted Elastic Modulus (ksi)	Percentage Difference
Freya to Farewell	25.5	0.31	5,280	3,920	4,530	13.5%
Alaskan Way	25.2	0.31	5,830	5,140	4,910	4.5%
Tumwater Canyon	25.9*	0.40*	4,830	3,800	4,110	7.3%
Snohomish	24.6	0.32	5,270	4,590	4,750	3.4%
Camas / Washougal	27.8	0.41	4,480	3,870	4,180	6.0%

** Tumwater Canyon mixture included fly ash*

By including the mixture proportions (paste content and water-to-cementitious ratio), the difference between estimated and actual elastic moduli ranged from 3.4 percent to 13.5 percent, with an average of 6.9 percent. With the exclusion of the Seattle concrete mixture, the formula derived in Equation 6.3 over-predicted the elastic modulus value by approximately 7.5 percent. This method is less conservative than the AASHTO specifications (5.4.2.4-1, Equation 2.7) and is dependent on the ability of the concrete batching plant to provide consistent mixture proportions.

6.4 ANALYSIS OF ELASTIC MODULUS RESULTS

The variations in the compressive strength and aggregate type significantly affected the elastic modulus (figures 6.2 and 6.15). A reduction in the water-cementitious ratio increased the compressive strength and elastic modulus (figures 4.6, 6.1, 6.8, and 6.14). The changes in compressive strength and elastic modulus due to a change in water-cementitious ratio were not similar. The effect of the paste content on the elastic modulus was not able to be determined (Figure 6.9).

The rate of stiffness gain was not affected by the compressive strength or aggregate source (figures 6.12 and 6.18). The paste content did not consistently affect the rate of stiffness gain (figures 6.13 and 6.19).

AASHTO specifications (5.4.2.4-1, Equation 2.7) estimated the elastic moduli of the field mixtures well but were less accurate for the laboratory mixtures (Table 6.2 and figures 6.10, 6.11, and 6.17). Equation 2.7 estimated the elastic modulus for higher strength mixtures more accurately than for lower strength mixtures (Figure 6.3). By accounting for the effect of the paste content on the elastic modulus in Equation 6.3, the percentage difference between the estimated value and the measured elastic modulus was 6.9 percent (the AASHTO specifications had a difference of 7.8 percent).

Chapter 7: Drying Shrinkage

The results of the drying shrinkage tests that were performed and monitored for a year's duration are discussed in this chapter. The effects of water-cementitious ratio, paste content, compressive strength, and coarse aggregate on the drying shrinkage are analyzed in this chapter.

The results from a single aggregate source are presented in Section 7.1 to document the procedure used to analyze the shrinkage data. A summary of all of the laboratory aggregate sources is discussed in Section 7.2 and includes the trends that were identified. Section 7.3 gives the shrinkage results from the field mixtures. The shrinkage that occurred over a year's duration is compared with the allowable strain for fatigue in Section 7.4. The details of the drying shrinkage tests are provided in Appendix D.

7.1 LABORATORY DATA FOR DUPONT (3/4-IN.) AGGREGATE SOURCE

Three drying shrinkage samples were cast for each laboratory and field mixture to perform the drying shrinkage tests. The three samples were submerged in a Calcium Hydroxide saturated solution to moist-cure for 28 days. After this curing period, the samples were placed in a temperature-controlled room to air dry for a year.

As explained in Section 2.4, the drying shrinkage strains were fit to a non-linear curve which can be seen in Equation 7.1. The optimized constants (t_{50} and $\epsilon_{Ult.}$) for the DuPont (3/4-in.) low-strength mixture were included to show typical values. The monitored shrinkage data and fitted curve are plotted in Figure 7.1.

$$\epsilon_{time} = \frac{time}{t_{50}+time} \times \epsilon_{Ult.} \qquad \text{(Equation 7.1)}$$

where: t_{50} = 25.5 days
$\epsilon_{Ult.}$ = 810 microstrain
time = Drying duration (days)

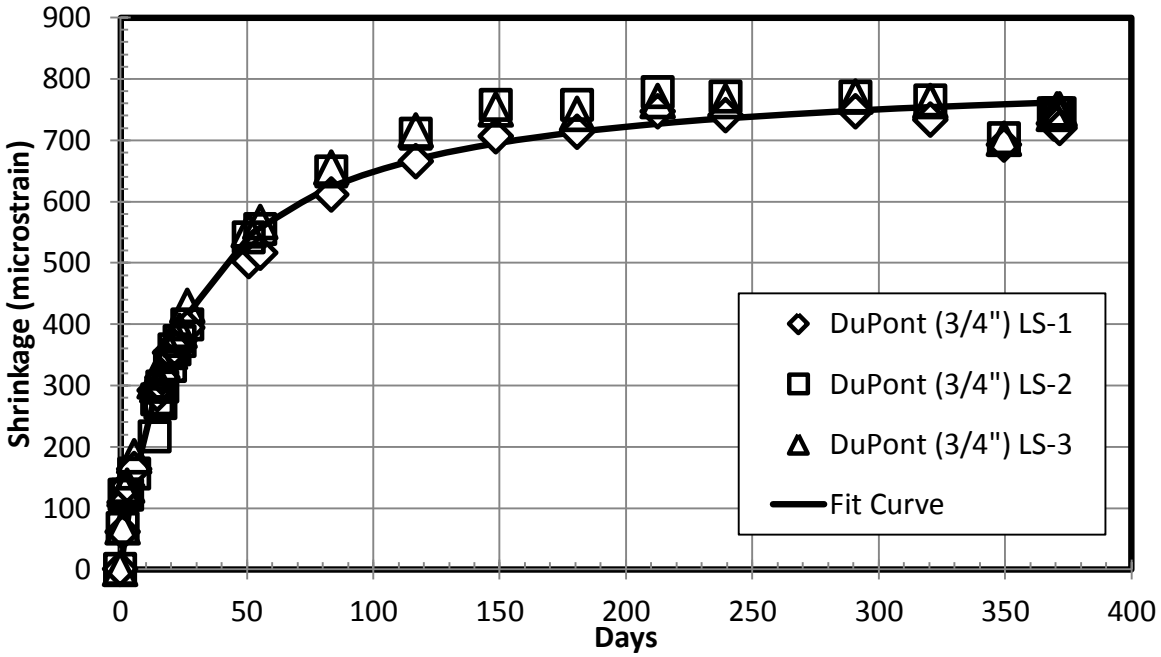

Figure 7.1: Fitted Dry Shrinkage Data: DuPont (3/4-in.) Low-Strength

The figure shows that the measured shrinkage varied little among the three shrinkage samples, and Equation 7.1 fit that drying shrinkage data well. The small drop in shrinkage that occurred around Day 350 was attributed to an increase in relative humidity within the monitoring room.

The strain data for the remaining DuPont (3/4-in.) mixtures (high and low paste and high and low strength) were fit to Equation 7.1, and the optimized constants (t_{50} and $\epsilon_{Ult.}$) for each mixture are listed in Table 7.1. The fitted Day 365 strains are also included in the table. The fitted curves for the four mixtures can be seen in Figure 7.2.

A key note to mention is that the shrinkage beams for the DuPont (3/4-in.) high-paste mixture were stored improperly for the first two weeks of air drying. Specifically, the beams were stacked on top of each other, which decreased the drying surface area of the beams. This storage may have led to a slower rate of strain gain during that early period. The procedure for storing the shrinkage beams was corrected and followed the ASTM C426 specifications for the remaining mixtures.

Table 7.1: Optimized Constants for DuPont (3/4-in.) Mixtures

	Paste Content (%)	W/CM Ratio	t_{50} (Days)	ε_{Ult} (microstrain)	Fitted ε_{365} (microstrain)	$\varepsilon_{28} / \varepsilon_{365}$
High Paste	30.5	0.38	32.9	750	690	0.50
Low Paste	24.0	0.38	15.2	670	640	0.67
High Strength	27.0	0.30	22.9	670	630	0.59
Low Strength	27.0	0.49	25.5	810	760	0.56

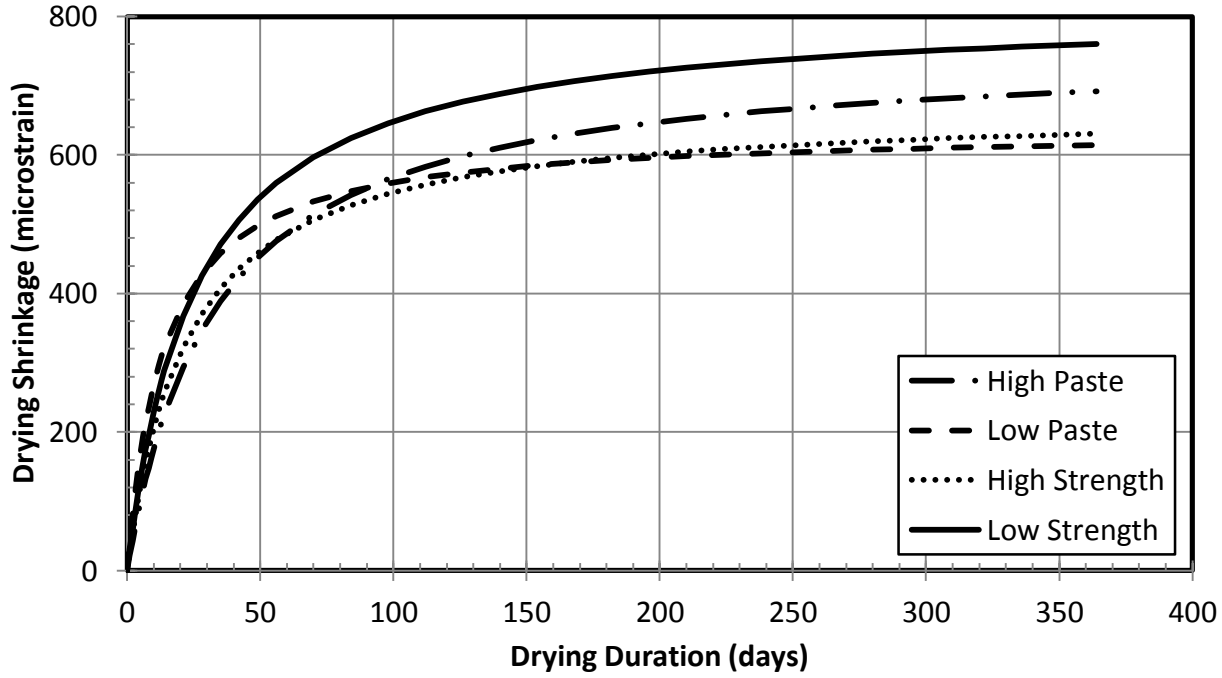

Figure 7.2: Fitted Dry Shrinkage Data: DuPont (3/4-in.) Mixtures

The fitted drying shrinkage curves for the low-strength and high-paste mixtures had the largest drying shrinkage strains after a year of drying. The high-strength and low-paste mixtures had similar ultimate strains (average of 640 microstrain) that were nearly 10 percent lower than those of the high-paste mixture. The initial rates of shrinkage for the high-paste, low-paste, and high-strength mixtures were similar, with the ratio of Day 28 to Day 365 strains an average of 0.55. The low-strength mixture had a shrinkage rate of 0.79 for the ratio of Day 28 to Day 365 strains. The significant increase in drying shrinkage was attributable to the high water-cementitious ratio for the low-strength mixture and the large paste content for the high-paste mixture.

The creep and drying shrinkage samples were stored in the same temperature-controlled room as the drying shrinkage beams. Since the drying shrinkage cylinders and beams were exposed to the same conditions for most of the year, the two shrinkage types of samples could be compared. There were two differences between the shrinkage beams and cylinders:

- The shrinkage beams were cured for 28 days before air drying (ASTM C157), whereas the shrinkage cylinders were removed from the fog room after curing for 14 days. This difference would lead to higher drying shrinkage in the cylinders than the beams.
- The drying shrinkage cylinders had a larger volume-to-surface ratio (V/S ratio of 1.5) than the beams (V/S ratio of 0.86), so the rate of shrinkage due to loss of moisture would be expected to be lower for the cylinders than the beams.

The optimized constants and fitted Day 365 strains for the DuPont (3/4-in.) high-paste mixture's drying shrinkage curves for the cylinders and beams are listed in Table 7.2 and plotted in Figure 7.3. The graph shows that there was only a small difference between the shrinkage strains in the two types of samples. The strain at Day 365 for the shrinkage cylinders slightly exceeded the strain measured for the beams by only 8.3 percent. This small difference suggests that the shorter curing period had a greater effect than the larger volume-to-surface ratio.

Table 7.2: Shrinkage Beam and Cylinder Coefficients: DuPont (3/4-in.) High-Paste

	t_{50} (Days)	ε_{Ult} (microstrain)	Fitted ε_{365} (microstrain)	$\varepsilon_{28} / \varepsilon_{365}$	Volume-to-Surface Ratio
Shrinkage Cylinders	34.5	790	750	0.49	1.50
Shrinkage Beams	32.9	750	700	0.50	0.86
Percentage Difference	4.6%	8.3%	5.3%	2.2%	

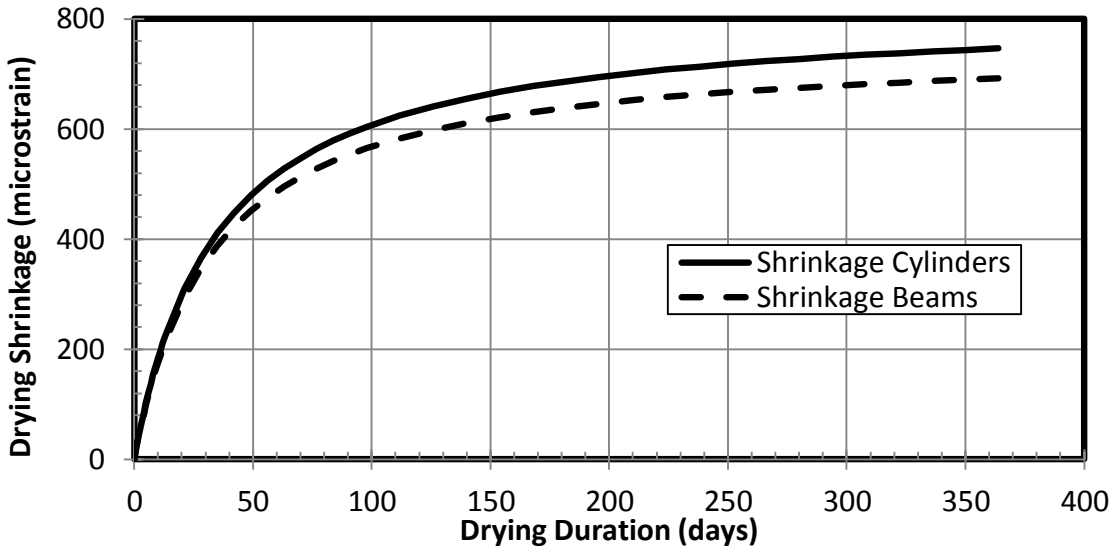

Figure 7.3: Dry Shrinkage Beam and Cylinder Curve Fits: DuPont (3/4-in.) High-Paste

As mentioned previously, the DuPont (3/4-in.) high-paste shrinkage beams were stacked on top of each other for the first two weeks. This improper storage decreased the drying surface area and may have led to a slower rate of initial strain gain. The measured shrinkage strains can be compared with AASHTO specifications (Section 5.4.2.3.3-1, Equation 2.9), which estimate the drying shrinkage strain. Given the relative humidity (RH = 45 percent), volume-to-surface ratios (Table 7.2), and design strength (4,000 psi) for the two samples, the drying strains calculated with the AASHTO specifications for the shrinkage cylinders and beams are shown in Figure 7.4. The measured drying shrinkage strains for each sample type are included in the figure.

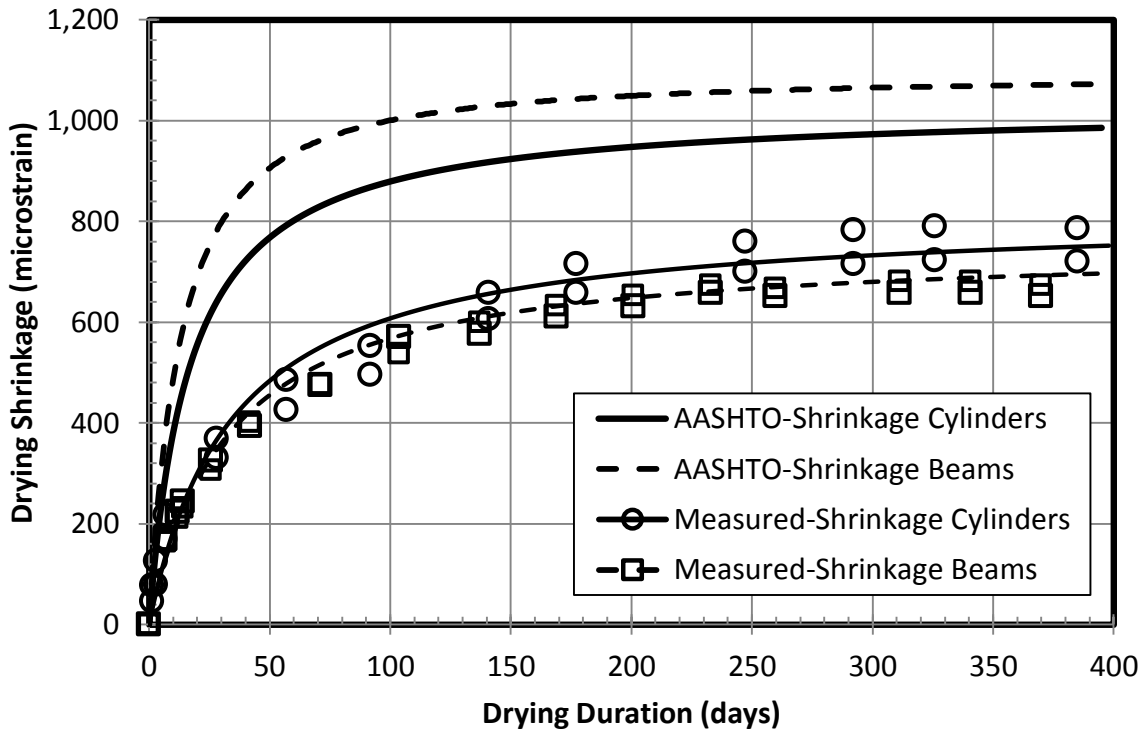

Figure 7.4: AASHTO Drying Shrinkage Strains: DuPont (3/4-in.) High-Paste Mixture

As expected, the calculated cylinder strains were slightly lower than the shrinkage beam strains (lower by an average of 11.3 percent) calculated from the AASHTO specifications. The different curing ages were not taken into consideration when the drying strains from the AASHTO specifications were estimated, so that may have affected the difference between the sample types. More importantly, the calculated drying shrinkage strains were on average 29.7 percent and 41.6 percent larger than the fitted curve strains for the shrinkage cylinders and beams, respectively. A comparison of the drying shrinkage cylinders and beams for the remaining creep mixtures can be seen in Appendix C. The effect on the AASHTO estimated strains of using the measured Day 28 compressive strengths, instead of the design strength (4,000 psi), for the DuPont (3/4-in.) mixtures can be seen in Table 7.3.

Table 7.3: AASHTO Strains from Measured Strengths: DuPont (3/4-in.) Mixtures

	f'_{28}	Fitted ε_{365} (microstrain)	Predicted ε_{365} (microstrain)	ε_{365} Difference (microstrain)	Difference (%)
High-Paste	6,530	690	670	20	2.9%
Low-Paste	4,400	650	980	330	33.7%
High-Strength	6,040	630	720	90	12.5%
Low-Strength	3,750	760	1,140	380	33.3%

The accuracy of the Day 365 AASHTO drying shrinkage strains improved when the measured Day 28 strengths for the DuPont (3/4-in.) high-paste and high-strength mixtures were used. The low-paste and low-strength mixtures were over-predicted by an average of 33.5 percent by the AASHTO specifications. The results from the AASHTO specifications for estimating the drying shrinkage did not match the measured drying shrinkage values when the measured strengths were used. The accuracy of the formula might be improved by accounting for the effects of paste content, water-cementitious ratio, and measured compressive strength of the concrete mixtures.

The fitted Day 365 strains from the DuPont (3/4-in.) mixtures are plotted against the water-cementitious ratio and paste content for the laboratory mixtures in Figure 7.5 and Figure 7.6, respectively. As expected, the fitted Day 365 drying shrinkage strains increased with an increase in water-cementitious ratio, as well as an increase in paste content.

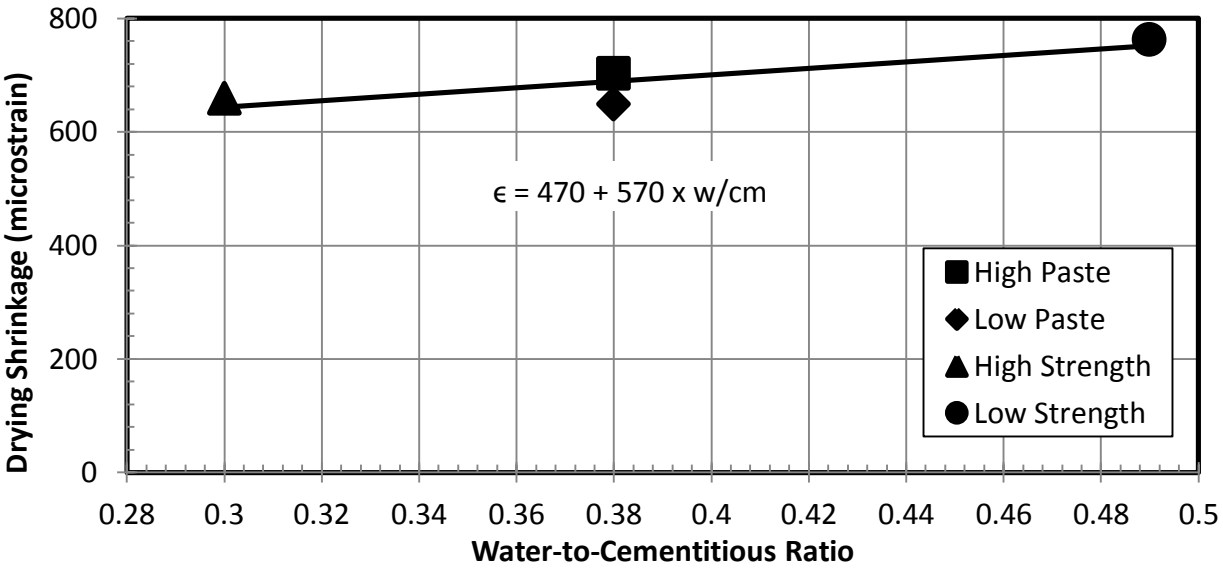

Figure 7.5: Fitted Day 365 Strains vs. W/CM Ratio: DuPont (3/4-in.) Mixtures

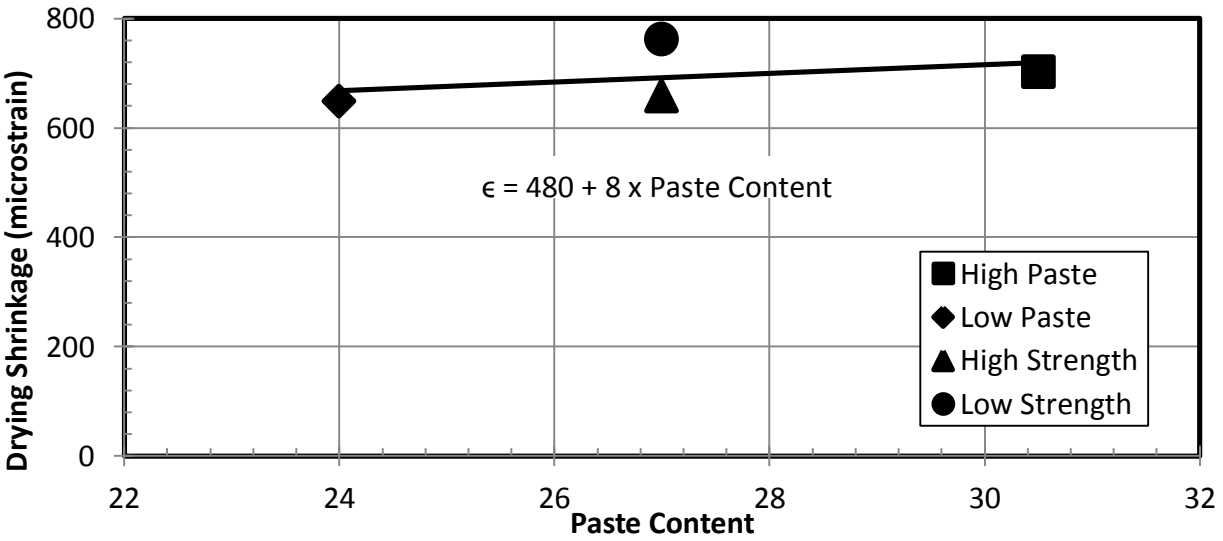

Figure 7.6: Fitted Day 365 Strains vs. Paste Content: DuPont (3/4-in.) Mixtures

Figure 7.7 shows the effects of the compressive strength on the fitted Day 365 strains for the four laboratory mixtures. The strength of each mixture was taken from the Day 28 compressive strength tests. The figure shows that the strain from drying shrinkage decreased with increasing strength. This trend was expected because compressive strength increases with

decreasing water-to-cementitious ratio; however, other factors (paste content and water-cementitious ratio) would help explain the deviation from the fitted line.

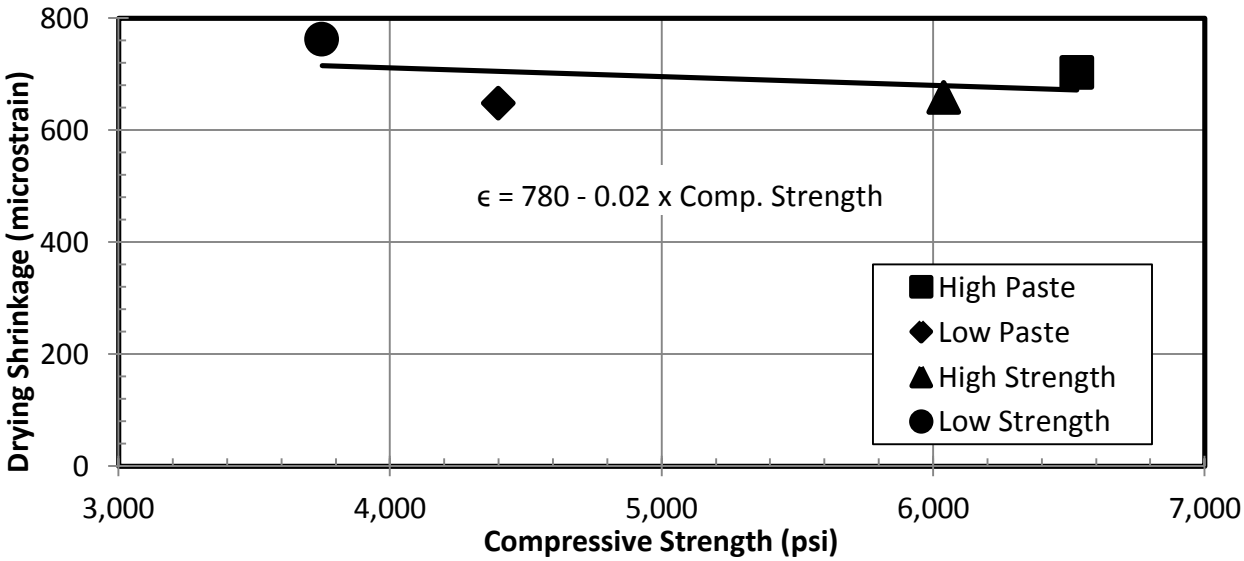

Figure 7.7: Fitted Day 365 Strains vs. Day 28 Comp. Strength: DuPont (3/4-in.) Mixtures

7.2 LABORATORY DATA FOR ALL AGGREGATE SOURCES

The process of analyzing the shrinkage data in Section 7.1 was repeated for each of the laboratory aggregates. The fitted drying shrinkage strain curves for all of the laboratory mixtures can be seen in Appendix C. The fitted Day 365 strains for the high- and low-strength mixtures for each aggregate source are shown in Figure 7.8. For these mixtures, the water-cementitious ratio varied between the high- and low-strength mixtures, but the paste content was constant.

With the exception of the Rock Island aggregate mixture, the drying shrinkage for the low-strength mixtures exceeded the shrinkage of the high-strength mixtures. The fitted Day 365 strains for the high-strength mixtures ranged from 540 to 810 microstrain, with an average of 650 microstrain. The low-strength mixtures had fitted Day 365 strains that ranged from 590 to 830 microstrain, with an average of 710. This trend was expected because the fitted Day 365 shrinkage strain would be expected to increase for increases in water-cementitious ratio.

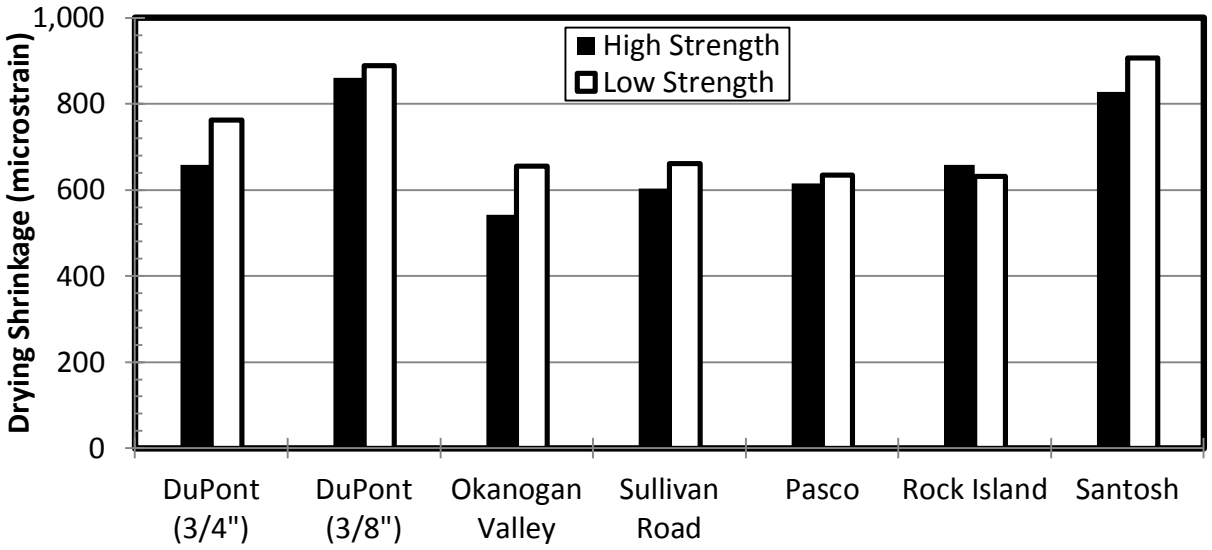

Figure 7.8: Fitted Day 365 Drying Shrinkage Strain: High- and Low-Strength Mixtures

Figure 7.9 shows the fitted Day 365 strain values of each of the aggregate sources for the high- and low-paste mixtures. The water-cementitious ratio was the same for both the high- and low-paste mixtures, and only the paste content varied.

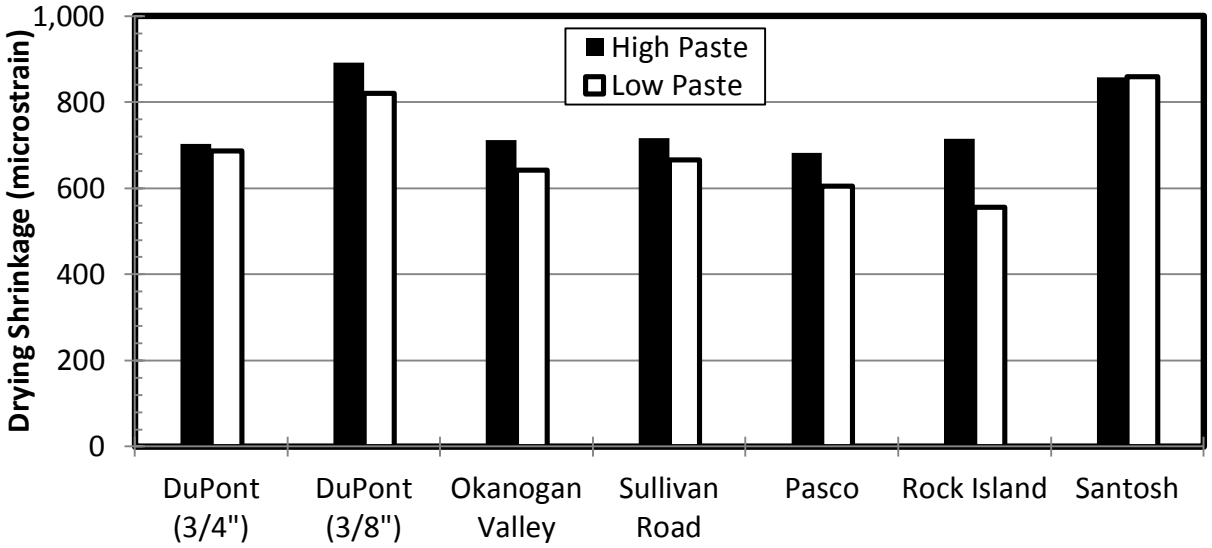

Figure 7.9: Fitted Day 365 Drying Shrinkage Strain: High- and Low-Paste Mixtures

As expected, increasing the paste content generally increased the drying shrinkage for the mixture. With the exclusion of the Santosh aggregate, the high-paste mixtures had larger fitted Day 365 strain values than the corresponding low-paste mixtures. The fitted Day 365 strain for

the high-paste mixtures ranged from 640 to 860 microstrain, with an average of 720 microstrain. The low-paste mixtures ranged from 530 to 790 microstrain, with an average of 660.

As shown by figures 7.8 and 7.9, varying the aggregate source affected the fitted Day 365 drying shrinkage strains for a given mixture. The fitted Day 365 strains from the Okanogan Valley, Sullivan Road, Pasco, and Rock Island mixtures were similar (average of 620 microstrain). The DuPont (3/4-in.) and Santosh mixtures had average fitted Day 365 strains of 700 and 780 microstrain, respectively. The DuPont (3/8-in.) mixtures had the largest fitted Day 365 strains with an average of 830 microstrain, as expected because of the higher paste contents for the smaller aggregate size.

The high- and low-paste mixtures from the DuPont (3/4-in.), DuPont (3/8-in.), and Sullivan Road aggregates were monitored for creep testing. Those creep mixtures had companion drying shrinkage cylinder that were monitored in the same room as the drying shrinkage beams. The drying shrinkage cylinders strains were normalized and fit to Equation 7.1. The optimized coefficients and fitted Day 365 strains are listed for the shrinkage cylinders in Table 7.4. The corresponding coefficients and fitted Day 365 strains for the drying shrinkage beams are listed in Table 7.5. The strains from the shrinkage cylinders and beams were plotted together for the high- and low-paste mixtures. These plots are shown in Figure 7.10 for the DuPont (3/4-in.) aggregate, Figure 7.11 for the DuPont (3/8-in.) aggregate, and Figure 7.12 for the Sullivan Road aggregate.

Note – The drying shrinkage beam samples for the DuPont (3/4-in.) high-paste mixture were stored improperly for the first two weeks, as mentioned in Section 7.1.

Table 7.4: Optimized Coefficients for Shrinkage Cylinders: All Creep Mixtures

	t_{50} (Days)	ε_{Ult} (microstrain)	Fitted ε_{365} (microstrain)	$\varepsilon_{28} / \varepsilon_{365}$
DuPont (3/4") –HP	34.5	790	750	0.49
DuPont (3/4") –LP	21.6	550	520	0.61
DuPont (3/8") –HP	23.4	840	790	0.58
DuPont (3/8") –LP	26.1	700	650	0.54
Sullivan Road –HP	28.2	660	620	0.57
Sullivan Road –LP	32.7	640	590	0.53

Table 7.5: Optimized Coefficients for Shrinkage Beams: All Creep Mixtures

	t_{50} (Days)	ε_{Ult} (microstrain)	Fitted ε_{365} (microstrain)	$\varepsilon_{28} / \varepsilon_{365}$
DuPont (3/4") -HP	32.9	750	690	0.50
DuPont (3/4") -LP	17.4	700	670	0.70
DuPont (3/8") –HP	17.0	860	820	0.67
DuPont (3/8") –LP	18.6	780	750	0.66
Sullivan Road –HP	19.1	710	670	0.67
Sullivan Road -LP	15.9	660	630	0.70

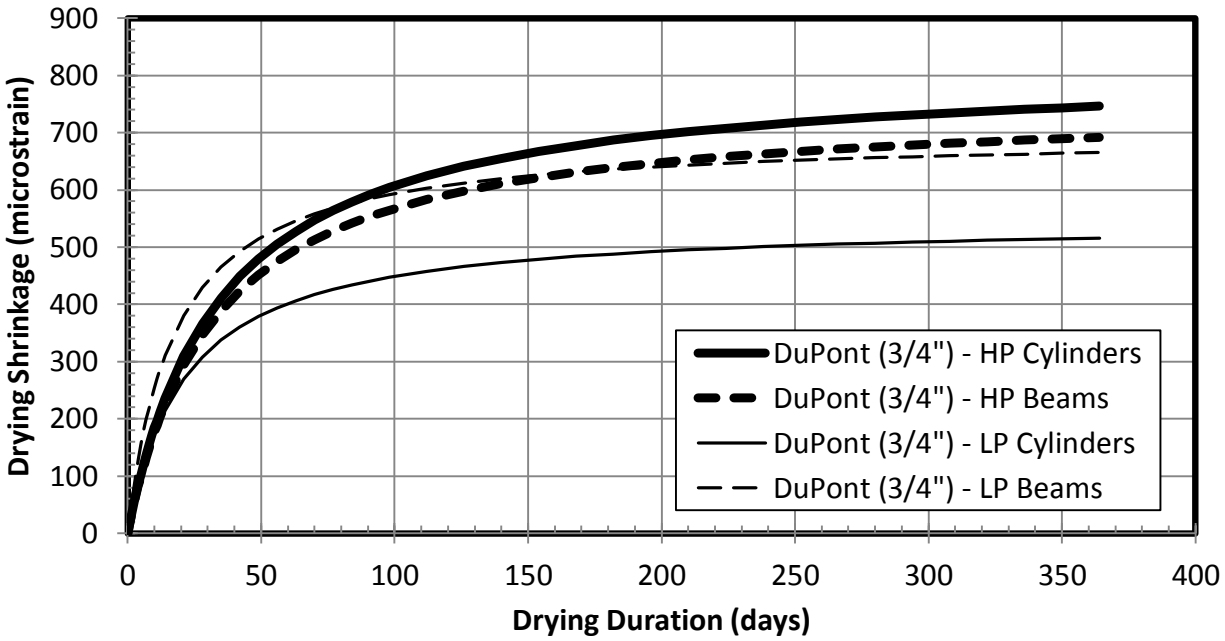

Figure 7.10: Dry Shrinkage Beam and Cylinder Strain Curves: DuPont (3/4-in.) Mixtures

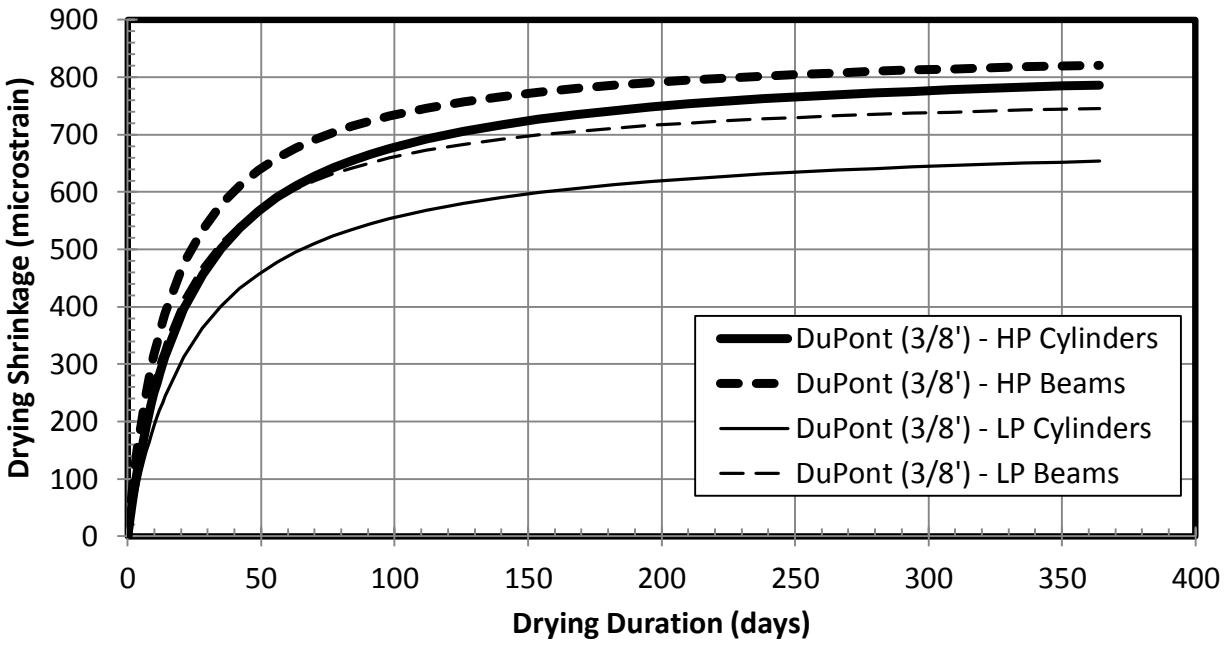

Figure 7.11: Dry Shrinkage Beam and Cylinder Strain Curves: DuPont (3/8-in.) Mixtures

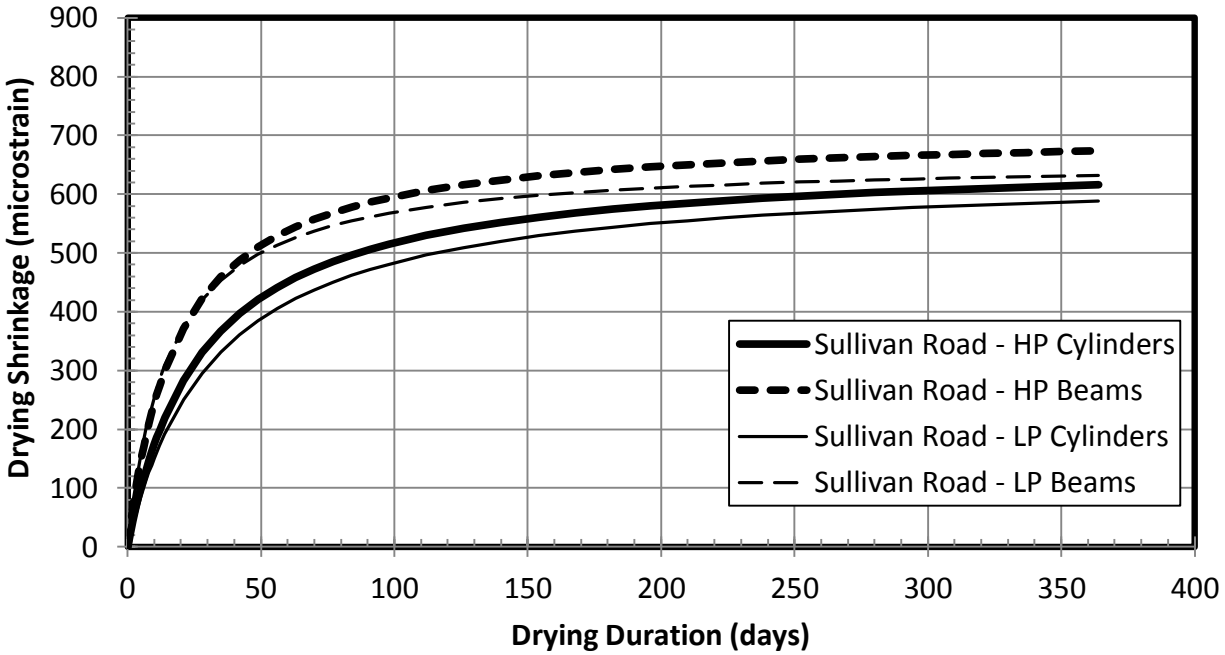

Figure 7.12: Drying Shrinkage Beam and Cylinder Strain Curves: Sullivan Road Mixtures

As expected, the shrinkage strains for the high-paste mixtures exceeded the strains for the low-paste mixtures for both the drying shrinkage beams and cylinders. For the DuPont (3/8-in.) and Sullivan Road mixtures, the strains from the shrinkage beams had a faster initial rate of

strain gain than the shrinkage cylinders. After a year's duration, the Day 365 fitted drying strains from all of the shrinkage cylinders were on average 14.2 percent lower than the drying strains for the shrinkage beams. This difference is consistent for the effect of the volume-to-surface as expected from AASHTO specifications (5.4.2.3-3-1) [average difference of 11.1%]. According to the specifications, the difference in shrinkage strains for the two V/S ratios would be expected to be 8.1 percent.

7.3 DATA FOR FIELD SAMPLES

The shrinkage results for the field mixtures were fit to Equation 7.1 following the same method as that outlined in Section 7.1. The mixture proportions, fitted Day 365 strains, and optimized constants (t_{50} and $\epsilon_{Ult.}$) for the different field mixtures are listed in Table 7.6. Figure 7.13 is a plot of the fitted curves for the field mixtures.

Table 7.6: Optimized Constants for Field Mixtures

	Paste Content (%)	**W/CM Ratio**	**t_{50} (Days)**	**ε_{Ult} (microstrain)**	**Fitted ε_{365} (microstrain)**	**ε_{28} / ε_{365}**
Freya to Farewell	25.5	0.31	18.0	820	820	0.64
Alaskan Way	25.2	0.31	13.6	710	720	0.70
Tumwater Canyon	25.9*	0.40*	8.3	830	870	0.80
Snohomish	24.6	0.32	12.5	860	870	0.72
Camas / Washougal	27.8	0.41	17.6	1,090	1,060	0.64

* *Tumwater Canyon mixture included fly ash.*

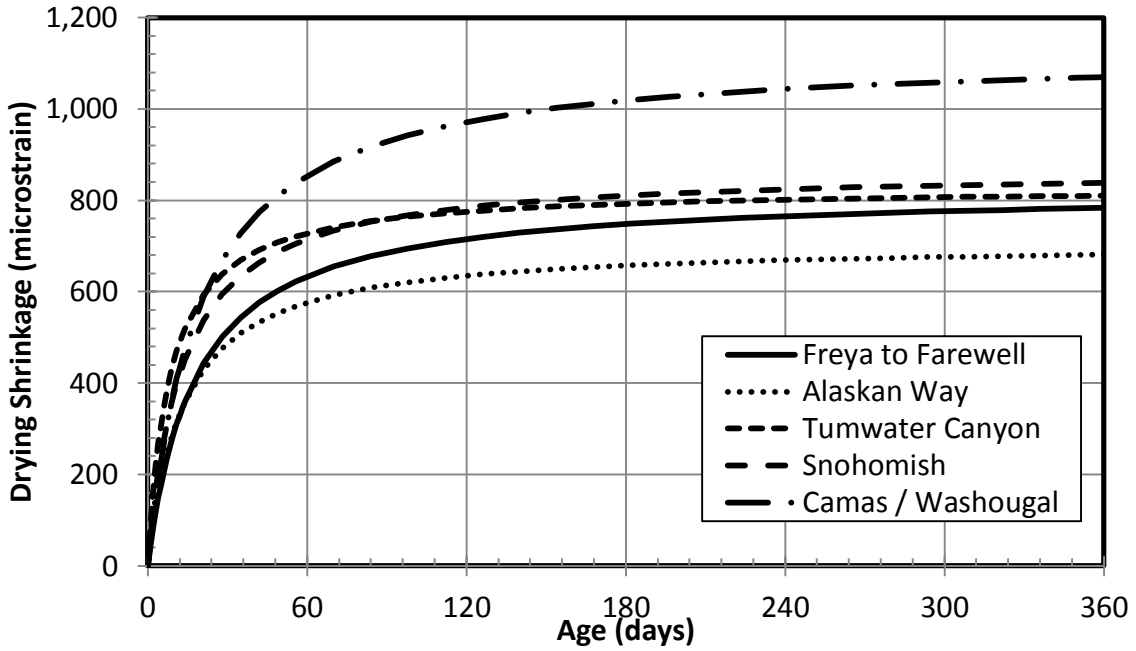

Figure 7.13: Fitted Dry Shrinkage Data: Field Mixtures

The concrete mixture for the Camas/Washougal project had the largest shrinkage strain after a year of drying (1,060 microstrain), and the Alaskan Way project had the smallest drying shrinkage (680 microstrain). The concrete from the Freya to Farewell, Tumwater Canyon, and Snohomish projects had similar shrinkage values after one year of drying, on average 840 microstrain. The concrete from the Tumwater Canyon project had the largest initial rate of shrinkage gain with a strain ratio of 0.80, while the Alaskan Way, Snohomish and Camas/ Washougal projects had an average Day 28 to Day 365 strain ratio of 0.70. Spokane's strain ratio of 0.64 was the smallest. The different aggregate sources and mixture proportions played a large role in the drying shrinkage, as expected from the laboratory results.

7.4 COMPARISON OF LABORATORY AND FIELD DATA

A formula was derived to estimate the drying shrinkage strains of the field samples after a year of drying. The formula was derived from the laboratory mixture results, fit the drying shrinkage strains to the mixture's proportions (paste content and water-cementitious ratio), and measured Day 28 compressive strength. Equation 7.2 shows the formula and associated constants from the results of the laboratory mixtures.

$$\epsilon_{365} = K_1 \times PC \times W/CM + K_2 \ f_{Day\ 28}^{\ K_3} \qquad \text{(Equation 7.2)}$$

where: ϵ_{365} = Estimated drying shrinkage strain (microstrain)
PC = Paste content (percent)
W/CM = Water-cementitious ratio
$f_{Day\ 28}$ = Average Day 28 compressive strength
K_1 = 21.2
K_2 = 32.4
K_3 = 0.33

The three coefficients for Equation 7.2 ($K_1, K_2,$ and K_3) were optimized from the fitted Day 365 drying shrinkage strains for the laboratory mixtures (with an average difference of 10.7 percent and standard deviation of 110 microstrain). The mixture proportions and measured Day 28 strengths for each field site were used to estimate the Day 365 drying shrinkage strains. The estimated strains were compared with the fitted Day 365 strains of the field mixtures. The proportions, strength, predicted and fitted strains, and percentage difference are shown in Table 7.7 for each of the field mixtures. The mixture proportions were determined from the concrete delivered to the WSDOT projects (adjusted for moisture and not the design proportions. The proportions were adjusted

Table 7.7: Predicting Day 365 Drying Shrinkage Strains for Field Mixtures

Project	Paste Content	W/CM Ratio	Comp. Strength (psi)	Predicted ε_{365} (microstrain)	Fitted ε_{365} (microstrain)	Difference (microstrain)	Difference (%)
Freya to Farewell	25.5	0.31	5,420	860	820	-40	-4.9%
Alaskan Way	25.2	0.31	5,290	850	720	-130	-18.1%
Tumwater Canyon	25.9*	0.40*	3,980**	860	870	10	1.1%
Snohomish	24.6	0.32	6,300	890	870	-20	-2.3%
Camas / Washougal	27.8	0.41	4,070	900	1,060	160	15.1%

** Tumwater Canyon mixture included fly ash.*
*** Day 28: Tumwater Canyon mixture had low break, best-fit value from strength-time curve*

The percentage difference for the projects ranged from 1.1 percent to 18.1 percent, with an average difference of 6.6 percent. With the exception of the Tumwater Canyon and the

Camas/Washougal projects, the predicted strains were lower than the actual strains. The constants derived for Equation 7.2 were based on the average results from all of the laboratory mixtures to avoid any aggregate-specific effects. As shown in Figure 7.13, the fitted drying shrinkage curves for the Alaskan Way and Camas/Washougal projects are significantly different than those for the other field mixtures. These results are consistent with the percentage differences listed in Table 7.6. The accuracy of the estimated Day 365 drying shrinkage strains varied with each field mixture, but with an average difference of 6.6 percent from the fitted and estimated strains, Equation 7.2 has the potential for future usage. By making further laboratory mixtures that vary the proportions and aggregate sources, the accuracy of Equation 7.2 may be improved.

7.5 SHRINKAGE CURVE VARIABILITY

This section investigates the effects of varying the monitored duration of drying shrinkage samples on the accuracy of the extrapolated shrinkage at one year. Six drying durations were selected to analyze the error in extrapolating the shrinkage at a year's length. To show typical results, the shrinkage data from DuPont (3/4-in.) low-strength mixture was fit to Equation 7.1 for drying durations of 28, 56, 90, 180, 270, and 365 days. The percentage difference between the extrapolated and measured fitted strain for a year's duration were averaged and are listed in Table 7.8. The differences in fitted Day 365 strains values are included in the table. The fitted curves from each of the different drying durations are shown in Figure 7.14.

Table 7.8: Percentage Difference from Varying Drying Shrinkage Monitor Durations

Monitored Duration (days)	Fitted ε_{365} (percentage difference)	Average Strains (percentage difference)
270	2.1%	1.2%
180	3.0%	4.2%
90	5.6%	6.8%
56	14.9%	9.6%
28	32.5%	20.7%

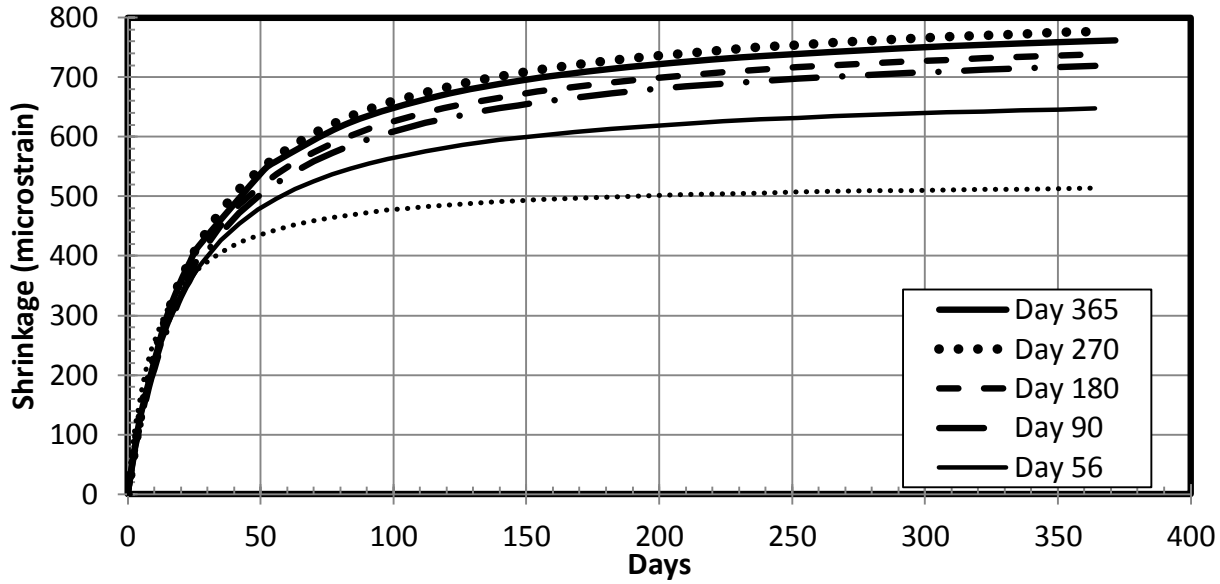

Figure 7.14: Strain Extrapolation Error: DuPont (3/4-in.) – Low Strength

With 28 days of drying shrinkage data, the average percentage difference of extrapolating the strain over a year's duration was over 20 percent. Fifty-six days of drying shrinkage data dropped the average percentage difference for extrapolating the strain to less than 10 percent. As expected, longer monitoring durations significantly improved the accuracy of the predicted drying shrinkage strains. These results were consistent with the other mixtures and aggregate sources, with longer drying durations improving the accuracy of extrapolating to a year's drying duration.

Reducing the required monitor duration for drying shrinkage samples is desirable, but extrapolating the strain values from shorter periods decreased the accuracy of the results. To improve the accuracy of estimated strains from shorter drying durations, a constant was determined for multiplying the data sets fit to Equation 7.1. For 56 days of monitoring, a coefficient of 1.1 minimized the average percentage difference of the strain values for the mixtures used in this research. For the DuPont (3/4-in.) low-strength mixture, the percentage differences for the modified strains from 56 days of monitoring are listed in Table 7.9. Figure 7.15 plots the fitted curves for the 56 days, modified 56 days, and 365 days of monitoring.

Table 7.9: Improvement from Modified Drying Shrinkage: DuPont (3/4-in.) Low-Strength

	Fitted ε_{365} (percentage difference)	Average Strains (percentage difference)
Modified 56	2.2%	4.7%
Unmodified Day 56	14.9%	9.6%

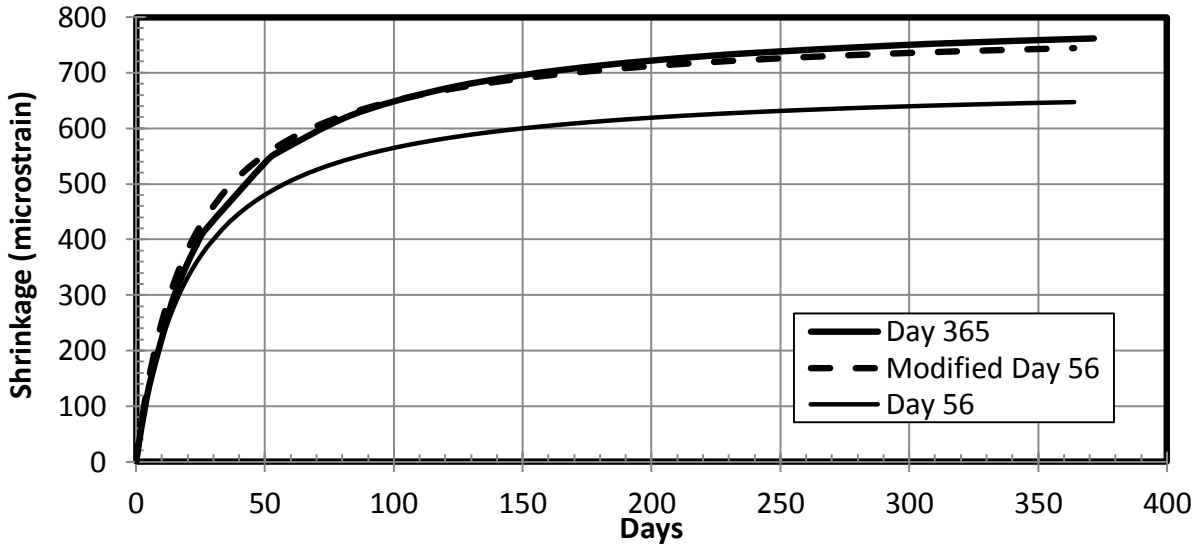

Figure 7.15: Modified Drying Shrinkage Strain: DuPont (3/4-in.) Low-Strength

The results from modifying the fitted drying shrinkage curve for 56 days of monitoring were consistent for the remaining laboratory and field mixtures. Using a coefficient of 1.1 to multiply the fitted shrinkage strain curves from 56 days of monitoring improved the extrapolated strain values at a year's duration of monitoring. The percentage differences in fitted Day 365 strains and average strain value for the modified and unmodified Day 56 drying shrinkage curve fits are listed in Table 7.10.

Table 7.10: Improvement from Modified Drying Shrinkage: All Laboratory Mixtures

	Fitted ε_{365} (percentage difference)		Average Strains (percentage difference)	
	Day 56	Modified Day 56	Day 56	Modified Day 56
DuPont (3/4")	18.8%	8.7%	14.0%	6.8%
DuPont (3/8")	18.1%	7.5%	14.0%	7.1%
Okanogan Valley	18.4%	10.2%	14.4%	8.4%

Sullivan Road	13.1%	7.0%	10.5%	6.3%
Pasco	24.7%	13.4%	20.1%	10.6%
Tumwater Canyon	32.1%	20.1%	25.1%	15.2%
Santosh	21.5%	10.5%	17.1%	8.2%

7.6 DISCUSSION OF DRYING SHRINKAGE RESULTS

In the design process, it is important to account for the strain caused from drying shrinkage. The purpose of this section is to compare the magnitude of the drying shrinkage strains to the strain limit for fatigue. The allowed stress limit when designing for fatigue is 40 percent of the design strength (AASHTO specifications 5.5.3.1). The fatigue strain limit can then be determined by dividing the design fatigue stress by the elastic modulus, as shown in Equation 7.3.

$$\text{Strain at Fatigue Stress, } \epsilon_{fatigue} = \frac{0.4\, f'_{28}}{E_{28}} \qquad \text{(Equation 7.3)}$$

The fitted Day 365 strains were divided by the strain from fatigue limits to compare the magnitude of each value. This ratio of drying shrinkage to fatigue limit strains was calculated for each of the laboratory and field mixtures. The ratio of strains for the DuPont (3/4-in.) mixtures can be seen in Figure 7.16.

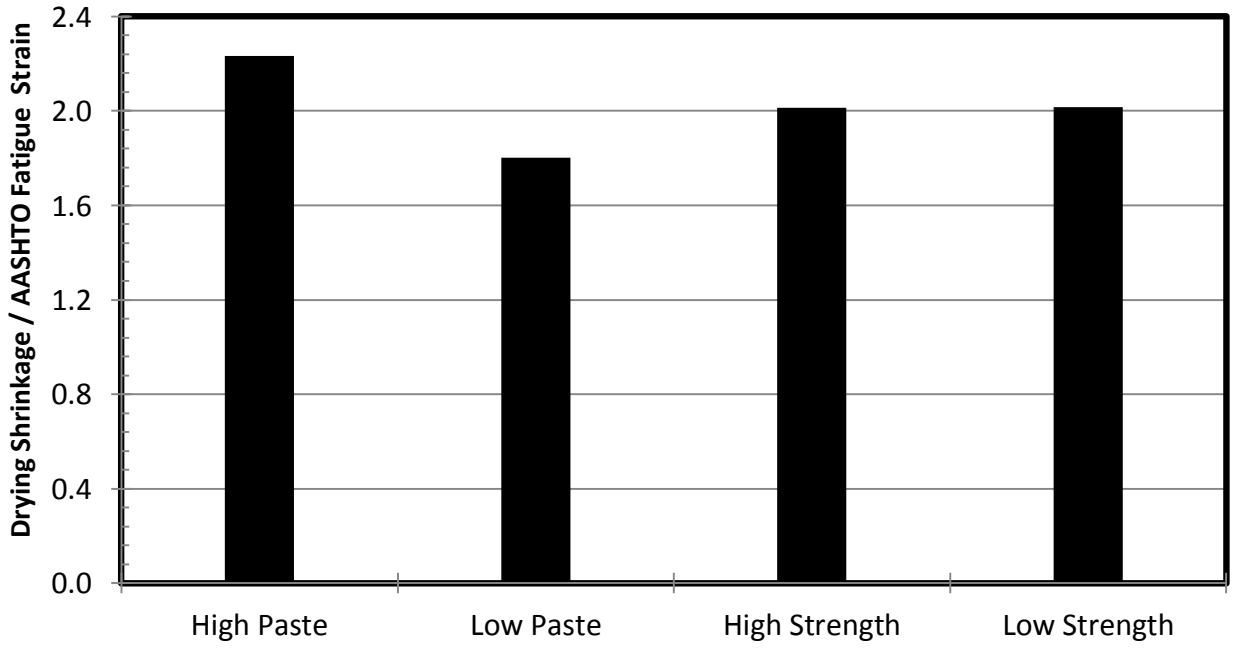

Figure 7.16: Day 28 Drying Strain to Fatigue Strain: DuPont (3/4-in.) Mixtures

The fitted Day 365 drying shrinkage strains were on average twice as large as the elastic strain at the fatigue stress. This calculation illustrates the significance of the drying shrinkage. These results were consistent throughout the laboratory mixtures, as shown in Figure 7.17 for the high- and low-strength mixtures and in Figure 7.18 for and high- and low-paste mixtures.

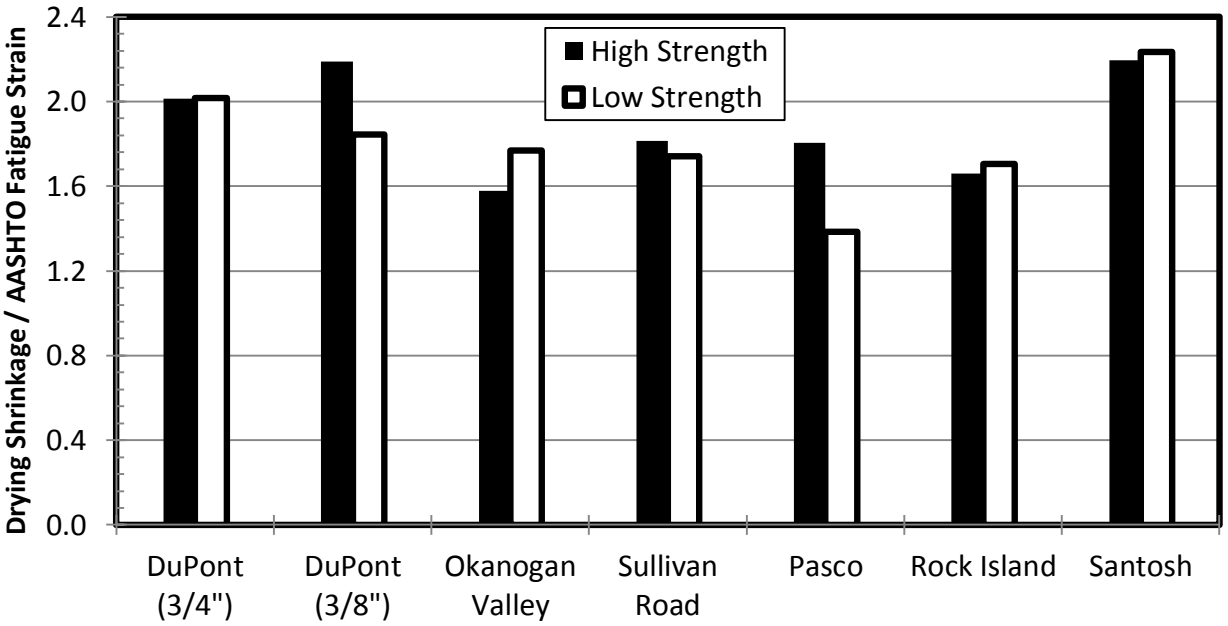

Figure 7.17: Drying Strain to Fatigue Strain: All Aggregates-High- and Low-Strength

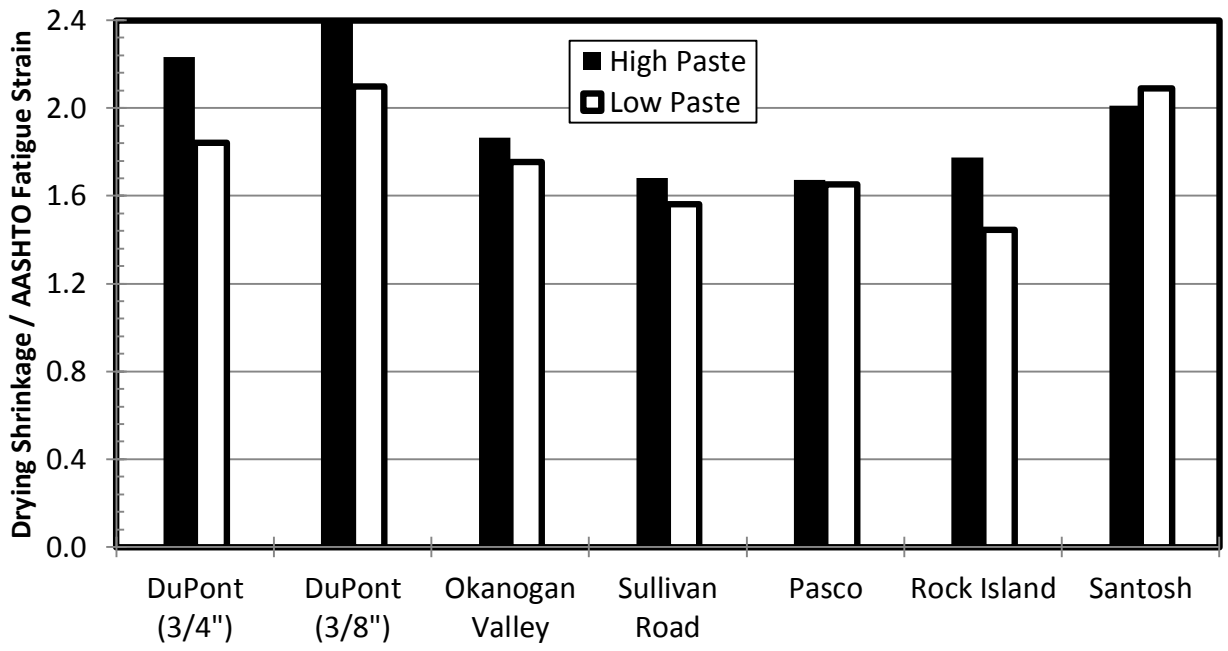

Figure 7.18: Drying Strain to Fatigue Strain: All Aggregates-High- and Low-Paste

7.6 ANALYSIS OF DRYING SHRINKAGE RESULTS

The results presented in this chapter led to the following observations:

- Variations in the aggregate type significantly affected the drying shrinkage strains (figures 7.8, 7.9, 7.17 and 7.18).
- The drying shrinkage strains increased with increasing paste content (figures 7.6 and 7.9).
- Increases in the water-cementitious ratio increased the drying shrinkage strain (figures 7.5 and 7.8).
- Increasing compressive strengths decreased drying shrinkage strains (Figure 7.7).
- Increases in the volume-to-surface ratios of drying shrinkage samples decreased the initial rate of shrinkage strain gain (figures 7.3, 7.4, 7.10, 7.11 and 7.12).

Equation 7.1 did a great job at fitting the monitored drying shrinkage strains (Figure 7.1). AASHTO specifications (5.1.2.3.3-1, Equation 2.9) did not estimate the drying shrinkage strains well (Figure 7.4). The long-term shrinkage can be predicted from short-term shrinkage monitoring, with greater accuracy than AASHTO predictions, by multiplying monitored shrinkage curves by an extrapolation correction coefficient. For only 56 days of monitoring,

extrapolated drying shrinkage strains for a year's duration were improved by multiplying by a constant of 1.1 (Figure 7.15). The accuracy of the extrapolated drying shrinkage strains were within an average of 8.9 percent difference of the strain curves from 365 days of monitoring.

Another method of estimating the Day 365 drying shrinkage strains is to use Equation 7.2. This formula accounts for the mixture proportions (paste content and water-cementitious ratio) and measured Day 28 compressive strengths to estimate the Day 365 drying shrinkage strains. Aggregate source does affect the accuracy of the estimated strain values (Table 7.7), but further research for specific aggregate sources would vary the optimized values (K1, K2, and K3), and could improve the accuracy of the equation.

Chapter 8: Creep

This chapter reports the results of a test program (Section 3.4.5) that was designed to measure the elastic strains, creep strains (composed of basic and drying creep strains), and drying shrinkage strains on six sets of samples. Creep tests were conducted for three aggregate types (DuPont 3/4-in., DuPont Pea Gravel, and Sullivan Road) for both high- and low-paste contents. For each combination of aggregate type and paste content, sealed and unsealed cylinders were loaded to approximately 35 percent of the Day 14 failure stress and then monitored for over one year. In parallel, unloaded, unsealed cylinders were monitored to measure the drying shrinkage.

The following procedure was used to determine the elastic, creep, and drying shrinkage strains for each creep rig. Since it took around five minutes to load and measure the creep samples, the initial lengths of each set of gauges were extrapolated from the measured data (Appendix D) back to a time of zero. The elastic deformations of the loaded creep cylinders (sealed and unsealed) were as assumed to be the difference between the length immediately after applying the axial load and the initial, extrapolated lengths (8.1.1 and 8.2.1). The monitored deformations of the creep and drying shrinkage cylinders were divided by the respective initial lengths to calculate the long-term strains, which were then fit to a nonlinear curve (8.1.2 and 8.2.2). Those data sets were then used to analyze the drying shrinkage (8.1.4 and 8.2.3), as well as the creep performance (8.1.5 and 8.2.4) in terms of specific creep (8.1.6 and 8.2.5) and creep coefficient (8.1.7 and 8.2.6).

The process followed to analyze the deformation data is illustrated in Section 8.1 for the DuPont (3/4-in.), high-paste mixture. The results of applying the same methodology to the data for all samples are reported in Section 8.2. During the data analysis, the researchers discovered that the integrity of the sealant on the sealed creep cylinders may have been compromised. This issue, and its effects on the calculation of basic and drying creep strains, is discussed in Section 8.1.3. Appendix E provides the details of the creep data.

8.1 LABORATORY DATA FOR DUPONT (3/4-IN.) HIGH-PASTE MIXTURE

The analysis procedure used to process the data is illustrated in this section by using deformation data for the DuPont (3/4-in.) high-paste mixture.

8.1.1 Elastic Strain

At Day 14, each creep rig was loaded to approximately 35 percent of the Day 14 failure stress. The initial strain due to loading is defined as the elastic strain. Because of the non-homogeneity of the cylinder, the load on each creep rig may not have been applied exactly at the cylinder's centroid. Variations in measured strains among the four gauges were expected.

To evaluate whether the variation in measured elastic strains among a set of gauges were sufficiently consistent for a single cylinder, a procedure was established to quantify any discrepancy, and when necessary, to modify the data. For each gauge, the discrepancy between this gauge and the others was determined by extrapolating a plane defined by the strains measured by the other three gauges. The discrepancy was estimated as the difference between the fourth gauge's strain and the planar projection at that location based on the other three gauges. This process was repeated by varying the strain gauge that was excluded when forming the strain plane. If the difference between the measured and projected strains exceeded 100 microstrain, then the error was classified as excessive, and corrective action was taken.

To improve the data set, the centroid of the strain plane was found for the cylinder by calculating the average measured strain of the four gauges. The gauge with the largest difference between the measured and average strains was altered to the value calculated by the strain plane from the remaining three gauges. This procedure had the effect of eliminating the data point with the largest discrepancy.

Table 8.1 lists the initial elastic strains measured for each of the four sets of gauges (labeled North, South, East, or West, depending on the gauge orientation) on the loaded, unsealed creep cylinders. This data set had only one data point (out of eight) that had a large discrepancy. Specifically, the West gauge on unsealed Cylinder #2 had a discrepancy of 440 microstrain, so the elastic strain was altered (to the value shown in parentheses).

Table 8.1: Measured Elastic Strain and Modulus: DuPont (3/4-in.) High-Paste Mixture

	Measured Elastic Strain (microstrain)		
	Unsealed Cylinder #1	**Unsealed Cylinder #2**	**Average**
North Gauge	310	340	330
West Gauge	340	730 (290)	320
East Gauge	380	460	420
South Gauge	410	410	410
Average Strain	360	380	370
Applied Stress (psi)	1,760	1,860	1,810

The mean elastic strain (with the modification of unsealed Cylinder #2, West gauge) from the creep rig and the Day 14 elastic modulus from standardized testing (ASTM C469) were used to estimate the actual applied stress on each creep mixture as shown in Equation 8.1.

$$f_{14\ creep} = \varepsilon_{Elastic} \times E_{14} \qquad \text{(Equation 8.1)}$$

where: E_{14} = 4,990 ksi (Table 6.1)
$\varepsilon_{Elastic}$ = 370 microstrain

For this mixture, $f_{14\ creep}$ was estimated as 1,810 psi. This calculated applied stress from the creep samples was compared with the targeted stress value of 35 percent of the Day 14 failure stress. As shown in Table 4.1 for the DuPont (3/4-in.) high-paste mixture, the Day 14 compressive strength was 4,900 psi, which resulted in a targeted stress of 1,750 psi. Therefore, the inferred average stress for the creep samples (1,810 psi) was 8.4 percent larger than that inferred from standard elastic modulus testing. The difference in stresses may have arisen from inaccuracies in the applied stress on the creep rig, the measured deformation, and the extrapolation of the initial lengths to account for early creep.

8.1.2 Time-Dependent Deformations

As explained in Section 3.4.5, the deformations of the loaded unsealed and sealed cylinders, as well as the drying shrinkage cylinders, were monitored for a year. To estimate the time-dependent deformations, the elastic deformation was subtracted from the monitored deformations. The strains for the drying shrinkage and creep cylinders were then calculated by

dividing the measured time-dependent deformations by the extrapolated initial lengths, as described in Appendix E. The time-dependent data for each cylinder type was then fit to a curve in the form of Equation 8.2.

$$\epsilon_{\text{time}} = \frac{\text{time}}{t_{50} + \text{time}} \times \epsilon_{\text{Ult.}} \qquad \text{(Equation 8.2)}$$

In this equation, ε_{50} corresponds to the ultimate strain, and t_{50} corresponds to the time at which 50 percent of the ultimate deformation has occurred. Table 8.2 lists the optimized coefficients and Day 365 long-term strains from the fitted curves for the creep and drying shrinkage cylinders. The measured time-dependent strains over a year (along with the respective fitted curves) are shown in Figure 8.1.

Table 8.2: Creep and Drying Shrinkage Coefficients: DuPont (3/4-in.) High-Paste

	t_{50} (Days)	ε_{Ult} (microstrain)	Fitted ε_{365} (microstrain)	$\varepsilon_{28} / \varepsilon_{365}$
Unsealed Creep	30.3	1,620	1,570	0.56
Sealed Creep	50.6	1,370	1,290	0.44
Drying Shrinkage	34.5	790	750	0.49

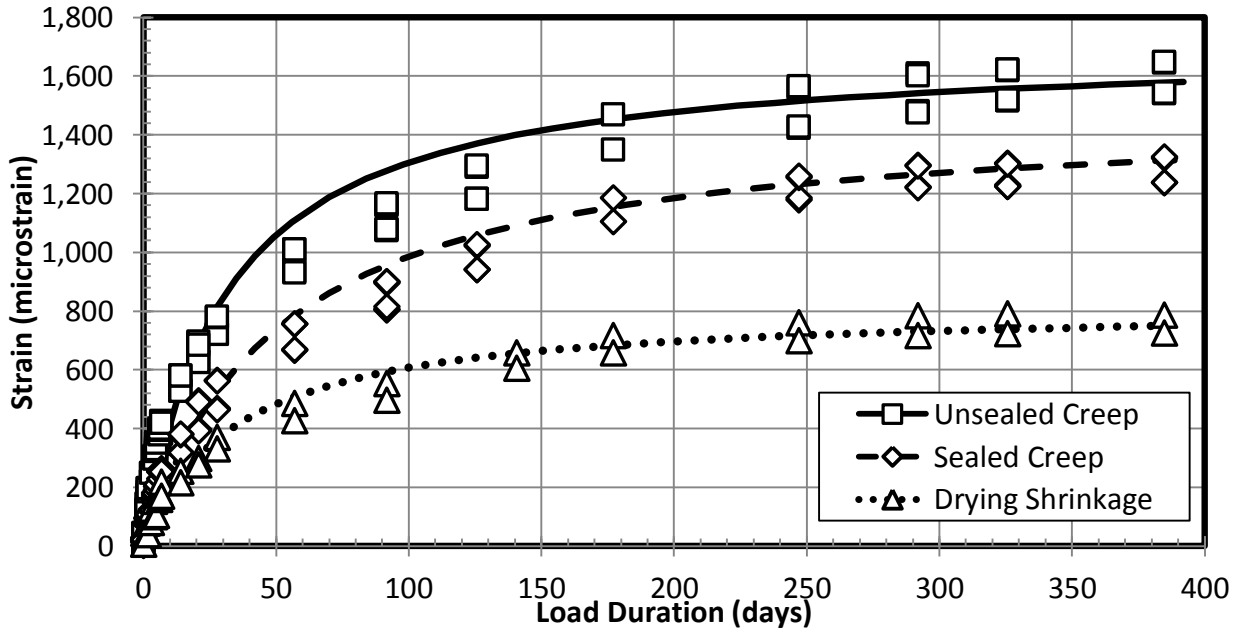

Figure 8.1: Long-Term Deformations: DuPont (3/4-in.) High-Paste

For the creep (sealed and unsealed) and drying shrinkage cylinders, the measured deformations of the two cylinders were consistent. As expected, the unsealed creep cylinders deformed more than the sealed creep cylinders. The fitted curves for the unsealed and sealed creep cylinders reached strains of 1,570 and 1,290 microstrain, respectively, after 365 days. These results are analyzed in the following sections.

8.1.3 Basic and Drying Creep

The creep strain is composed of both the basic and drying creeps. Ideally, the basic creep is the deformation measured by sealed cylinders, which should not lose any water. The drying creep is the additional long-term deformations that occur as a result of drying over and above the drying shrinkage.

During the data analysis, the researchers determined that the two layers of epoxy sealant on the sealed creep cylinders may have been compromised. This damage was attributed to exposure of the sealed cylinders to the heat lamps that were used to maintain a constant room temperature. Loss of the sealant would have allowed the concrete to begin drying. To investigate this hypothesis, the sealed and unsealed cylinders were weighed and then stored in water, and the weights of the cylinders were monitored over time. The sealed cylinders gained over 1.5 percent of their original mass in comparison to the 2.6 percent gained by the unsealed cylinders for the same time period. These data suggest that the "sealed" cylinders dried about 60 percent as much as the unsealed cylinders, when they should have not absorbed any water.

The total creep, basic and drying creep strains were fit to Equation 8.2, and the optimized coefficients are listed in Table 8.3. The data suggest that the "sealed" cylinders began drying, which caused larger strains than expected and resulted in the drying creep strain to become a negative value, which is not credible.

Table 8.3: Optimized Coefficients for Creep and Basic Creep: DuPont (3/4-in.) High-Paste

	t_{50} (Days)	ε_{Ult} (microstrain)	Fitted ε_{365} (microstrain)	$\varepsilon_{28} / \varepsilon_{365}$
Creep Strain	26.9	880	820	0.55
Basic Creep Strain	50.6	1,370	1,290	0.44
Drying Creep Strain	159.1	-710	-470	0.18

The rest of this chapter focuses on the behavior of the unsealed cylinders because the moisture conditions for the "sealed" cylinders are unknown.

8.1.4 Drying Shrinkage

The unloaded, unsealed cylinders had a drying shrinkage strain of 750 microstrain from the fitted curve after a year of monitoring. As mentioned in Section 7.1, the fitted drying shrinkage curves for the DuPont (3/4-in.) high-paste cylinders and beams were compared to evaluate the effects of varying the curing duration before air drying and the volume-to-surface ratio. The fitted Day 365 strain for the shrinkage cylinders exceeded the fitted Day 365 strain for the beams by 8.3 percent. This suggests that the shorter curing period had a greater effect than the larger volume-to-surface ratio.

An analysis of AASHTO specifications (5.4.2.3.3-1, Equation 2.9) was also performed (Section 7.1) for the drying shrinkage cylinder and beam samples of the DuPont (3/4-in.) high-paste mixture. The AASHTO specifications estimate the drying shrinkage strains for a concrete sample on the basis of the relative humidity, volume-to-surface ratio, design strength, and drying duration. Using the conditions present for this research, drying shrinkage curves were evaluated for the shrinkage beams and cylinders and were compared with the measured values. The calculated drying shrinkage strains were on average 29.7 percent and 41.6 percent larger than the fitted curve strains for the shrinkage cylinders and beams, respectively.

8.1.5 Creep Strains

The creep strains were determined by subtracting the drying shrinkage and elastic strains from the monitored strains of the unsealed, loaded cylinders. The creep-strain data were fit to Equation 8.2, and the optimized coefficients and fitted Day 365 strain are listed in Table 8.4. The total time-dependent strain (result of subtracting the elastic strain from the unsealed, loaded cylinder) and drying shrinkage strain are included in the table for comparison. Figure 8.2 plots the fitted strain curves for the total time-dependent, drying shrinkage, and creep strains.

Table 8.4: Optimized Constants for DuPont (3/4-in.) High-Paste Mixture

	t_{50} (Days)	ε_{Ult} (microstrain)	Fitted ε_{365} (microstrain)	$\varepsilon_{28} / \varepsilon_{365}$
Total Time-Dependent Strain	30.3	1,620	1,570	0.56
Drying Shrinkage Strain	34.5	790	750	0.49
Creep Strain	26.9	880	820	0.55

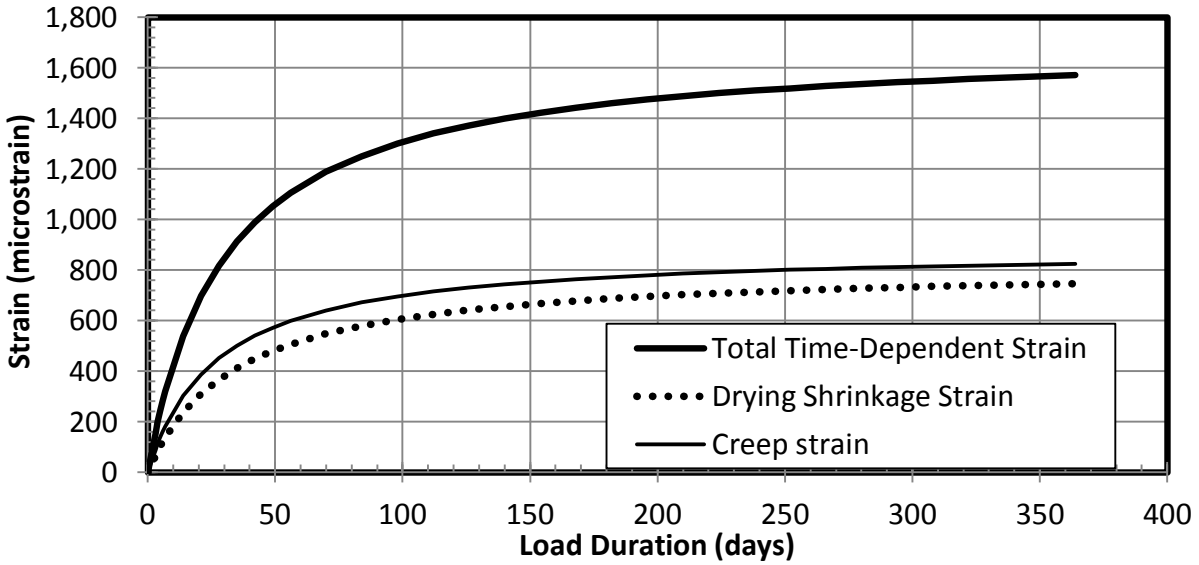

Figure 8.2: Long-Term Deformation Fitted Curves: DuPont (3/4-in.) High-Paste

This figure shows that the magnitudes of creep and drying shrinkage strains were similar for the DuPont (3/4-in.) high-paste mixture. The creep strains exceeded the drying shrinkage strains by an average of 12.6 percent.

8.1.6 Specific Creep

The specific creep data were calculated by dividing the creep strain data by the calculated applied stress (in psi) that was applied to each creep rig. The targeted stress on each creep rig was 35 percent of the Day 14 failure stress (Section 3.4.5); however, the applied stress on a creep rig may have varied and was calculated from the elastic strain measurements (Section 8.1.1). Dividing the creep strain by the applied stress creates a normalized data set, which is defined in ACI 209 as the specific creep. Specific creep provides a comparison of the creep strain for concrete mixtures with different strengths and applied loads. The specific creep data were fit to

the curve of the form of Equation 8.2, and the optimized constants for the DuPont (3/4-in.) high-paste mixture are reported in Table 8.5 and Figure 8.3.

Table 8.5: Optimized Coefficients for Specific Creep: DuPont (3/4-in.) High-Paste

	t_{50} (Days)	Ultimate (microstrain/psi)	Fitted Day 365 (microstrain/psi)	Day 28/Day 365
Specific Creep	27.0	0.45	0.43	0.55

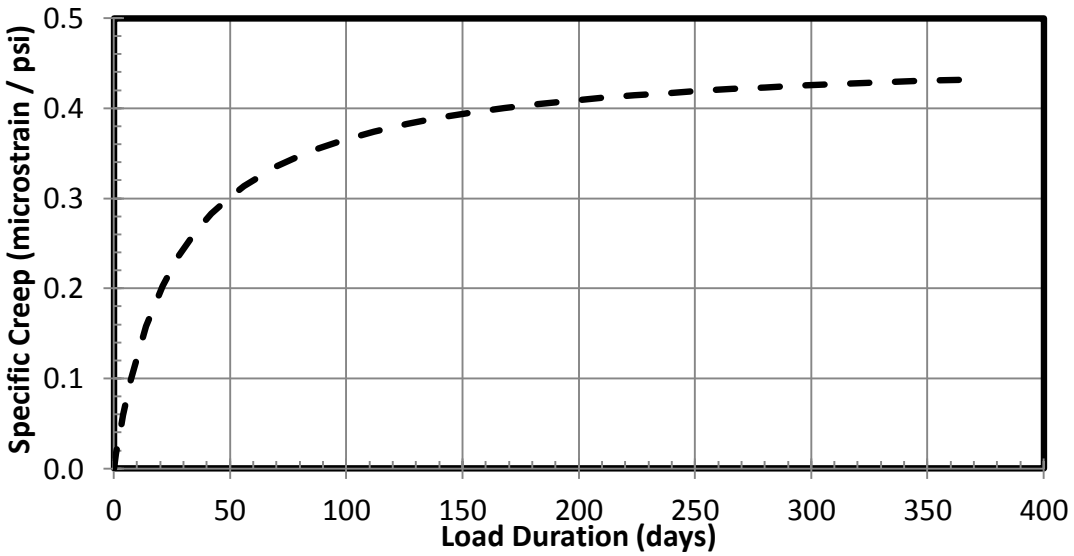

Figure 8.3: Specific Creep Fitted Curve: DuPont (3/4-in.) High-Paste

ACI 209 recommends this method of normalization to correct for the effects of varying strength among mixtures. Analyzing the specific creep strains from the remaining mixtures provides a method of documenting the effects of paste content, aggregate size, and aggregate type on the creep behavior without strength affecting the data.

8.1.7 Creep Coefficient

The creep coefficient is defined as the creep strain divided by the elastic strain at a particular duration of loading. The DuPont (3/4-in.) high-paste creep strain was normalized with the mean elastic strain of all four creep cylinders (370 microstrain, Table 8.1), and the resulting fitted curve can be seen in Figure 8.4. The AASHTO specifications (5.4.2.3.2-1, Equation 2.12) estimate a creep coefficient that varies with load duration. On the basis of the cure duration before loading (14 days), relative humidity (RH = 45 percent), design strength of the concrete

(4,000 psi), and volume-to-surface ratio (V/S = 1.5), the calculated creep coefficient curve was included in Figure 8.4.

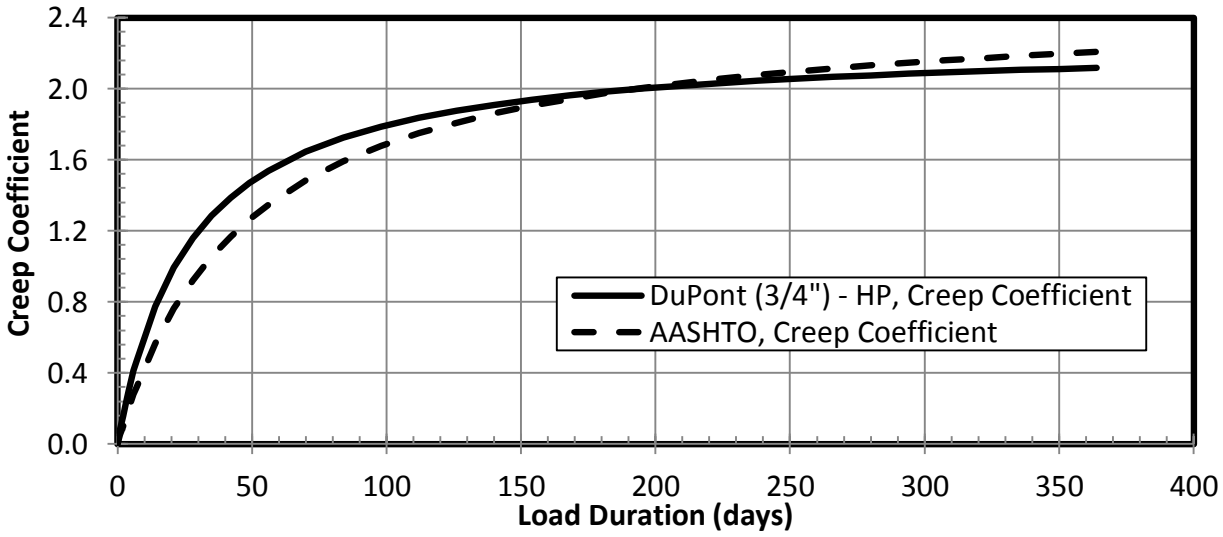

Figure 8.4: AASHTO Predicted Creep Coefficient: DuPont (3/4-in.) High-Paste

The creep coefficients at Day 365 were 2.1 for the DuPont (3/4-in.) high-paste mixture and 2.2 for AASHTO specifications (a difference of only 4.2 percent). This result implies that the creep strain at one year is greater than twice the magnitude of the elastic strain for an applied load of approximately 35 percent of the Day 14 compressive strength. The creep coefficients estimated by AASHTO under-predicted the initial rate of strain gain of the measured creep samples. For example, the ratio of Day 28 to Day 365 creep coefficient for the AASHTO curve was 0.42, whereas it was 0.55 for the DuPont (3/4-in.) high-paste mixture (a difference of 24 percent).

The accuracy of creep calculations based on the creep coefficient depends greatly on the calculated elastic deformation. To illustrate this dependence, the creep strains were determined from elastic strain values based on three sets of assumptions:

- The first elastic strain was calculated by using the AASHTO predicted elastic modulus (Section 5.4.2.4-1, Equation 2.7) based on the design strength of the mixture (4,000 psi) along with the applied stress (Table 8.1).

- The second elastic strain was calculated by using the predicted elastic modulus value (Section 5.4.2.4-1, Equation 2.7) from the measured Day 14 compressive strength (4,900 psi) along with the applied stress (Table 8.1).
- The third elastic strain value was the measured strain value from the initial loading.

The creep strains from the DuPont (3/4-in.) high-paste mixture were then modified by multiplying by the ratio of 1,600 psi to the applied stress of 1,810 psi (Table 8.1). The resulting creep strains from the three AASHTO curves are compared with the DuPont (3/4-in.) high-paste creep strains in Table 8.6 and Figure 8.5.

Table 8.6: Estimated AASHTO Creep Strains: DuPont (3/4-in.) High-Paste

	Elastic Modulus (ksi)	Elastic Strain (microstrain)	Fitted ε_{365} (microstrain)	Fitted ε_{365} (% Difference)	Coef. Of Variation
AASHTO – Design Strength	3,640	440	970	28.9%	18.3%
AASHTO – Predicted Elastic Modulus	4,070	390	870	20.7%	11.7%
AASHTO – Measured Elastic Strain	4,900	330	720	4.2%	4.7%
DuPont (3/4") High Paste	4,900	330	690		

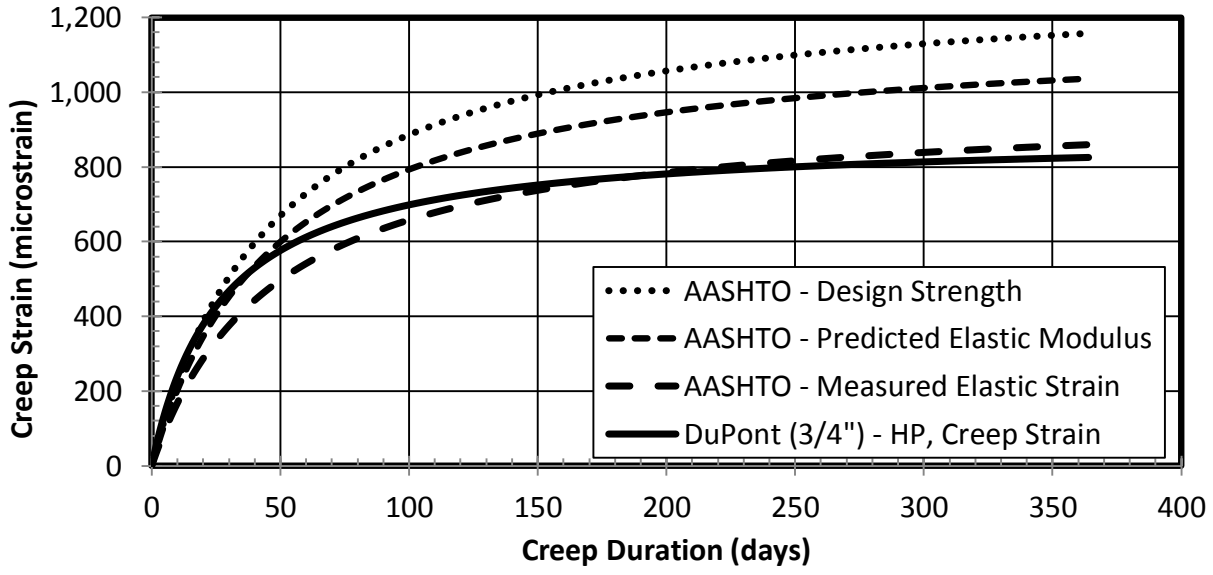

Figure 8.5: AASHTO Predicted Creep Strains: DuPont (3/4-in.) High-Paste Mixture

The figure shows that the accuracy of the calculated creep strains increased with increasing knowledge of the concrete elastic modulus. For example, the estimated Day 365 creep strain was 20.7 percent greater than the measured values when the measured compressive strength was known. This percentage difference is consistent with the results of Section 6.1.1, in which the measured elastic moduli for DuPont (3/4-in.) mixtures was found to be on average 19 percent greater than the AASHTO predicted values (Table 6.2). Knowledge of the elastic modulus at loading is essentially the same as having measured the elastic strain, so the predicted AASHTO creep strains are significantly improved. This figure suggests that modifications to the creep coefficient or elastic modulus specifications are required to improve the estimated creep strains if the actual strength and/or elastic modulus are unknown.

8.2 LABORATORY DATA FOR ALL CREEP MIXTURES

The same process that was followed the DuPont (3/4-in.) high-paste mixture (Section 8.1) was repeated for the other five creep mixtures. A summary of the results is provided in this section, and the details of the individual results are contained in Appendix D.

8.2.1 Elastic Strain

The initial elastic strains for each creep rig were evaluated by using the same criteria as defined in Section 8.1.1, and a total of eight data points (out of 48) were altered. The applied stresses were then calculated by multiplying the mean creep strain for each creep rig with the respective Day 14 elastic modulus from standardized testing (ASTM C469). The average elastic strains for the unsealed creep cylinders, the calculated applied stresses, and the targeted stresses are listed in Table 8.7. The percentage differences between the applied and targeted stresses are included in the table.

Table 8.7: Estimated and Measured Elastic Strain: All Creep Mixtures

	Elastic Strain (microstrain)	Applied Stress (psi)	Targeted Stress (psi)	Percentage Difference
DuPont (3/4") - HP	370	1,810	1,750	8.4%
DuPont (3/4") - LP	330	1,410	1,300	5.1%
DuPont (3/8") - HP	390	1,740	1,670	4.0%
DuPont (3/8") - LP	410	1,910	1,810	5.2%
Sullivan Road- HP	440	1,690	1,630	3.6%
Sullivan Road - LP	390	1,550	1,540	0.8%

The applied stresses on the creep rigs were consistently larger than the targeted stress. The average percentage difference was 4.1 percent for all six of the creep mixtures, which is likely attributable to the precision of the pressure gauge used to set the loads. The precision of the applied stress was within ± 16 psi (led to an average percentage difference of 1.0 percent).

8.2.2 Time-Dependent Deformations

A summary of the Day 365 time-dependent strains from the unsealed creep and drying shrinkage curves is provided in Table 8.8. The reported creep strains do not include the elastic strains. The data were fit to Equation 8.2. The individual plots for the total deformations of each of the concrete mixtures can be seen in Appendix D.

Table 8.8: Summary of Elastic and Plastic Strains: All Creep Mixtures

		Fitted ε_{365} (microstrain)		
	f_{14} (psi)	Elastic Strain	Drying Shrinkage	Unsealed Cylinder
DuPont (3/4") - HP	4,990	370	750	1,570
DuPont (3/4") - LP	3,710	330	500	1,210
DuPont (3/8") - HP	4,770	390	790	1,560
DuPont (3/8") - LP	5,170	410	650	1,570
Sullivan Road - HP	4,650	440	620	1,520
Sullivan Road - LP	4,410	390	600	1,340

The drying shrinkage strains for the high-paste mixtures consistently exceeded the corresponding strains for the low-paste mixtures. With the exception of DuPont (3/8-in.)

mixtures, the elastic and creep strains were also greater for the high-paste mixtures than for the low-paste mixtures. The elastic and creep strains were greater for the DuPont (3/8-in.) low-paste mixture than for the high-paste mixture. This difference can partially be attributed to the higher Day 14 compressive strength for the low-paste mixture. The higher strength resulted in a greater stress applied to the low-paste samples. The increased stress applied to the low-paste mixture would have caused larger elastic and creep deformations than those for the high-paste mixture.

8.2.3 Drying Shrinkage

The drying shrinkage strains from the unloaded, unsealed cylinders were fit to Equation 8.2. Table 7.3 lists the fitted Day 365 strains and optimized coefficients for the six creep mixtures. As mentioned in Section 7.2, the fitted drying shrinkage curves for the cylinders and beams were compared to evaluate the effects of varying the curing duration before air drying and the volume-to-surface ratio. With the exception of the DuPont (3/4-in.) high-paste mixture, the fitted Day 365 strains for the shrinkage beams exceeded the fitted Day 365 strains for the cylinders by an average of 14.2 percent. This suggests that the shorter curing period had a lower effect than the larger volume-to-surface ratio.

The fitted drying shrinkage curves for the high- and low-paste mixtures are shown plotted together in Figure 8.6 for the DuPont (3/4-in.) aggregate, in Figure 8.7 for the DuPont (3/8-in.) aggregate, and in Figure 8.8 for the Sullivan Road aggregate.

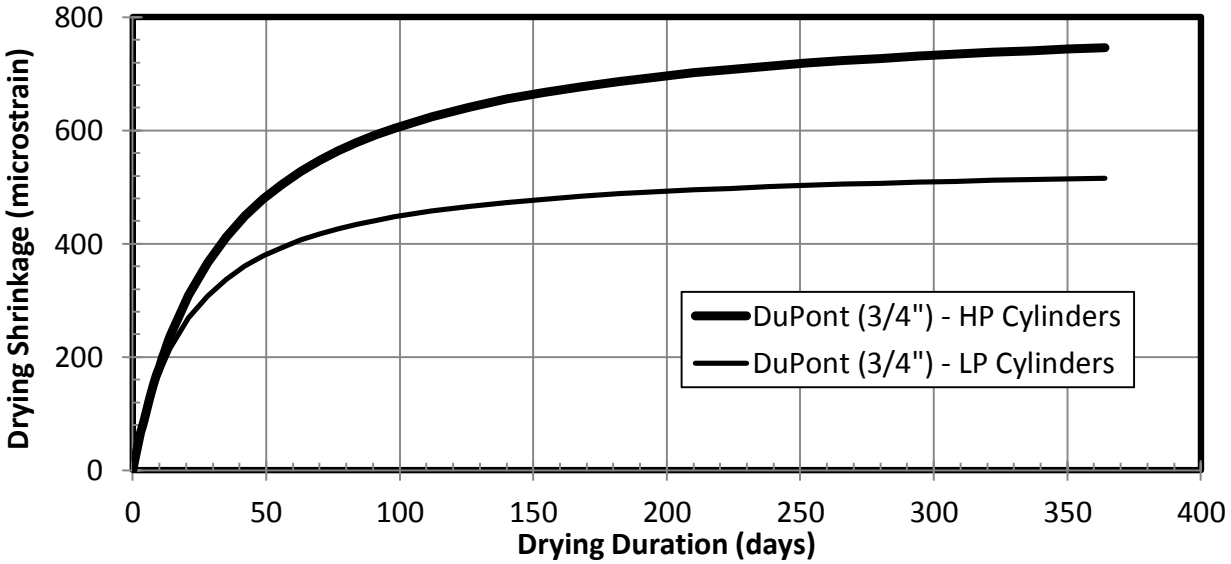

Figure 8.6: Drying Shrinkage Cylinder Curve Fits: DuPont (3/4-in.) Mixtures

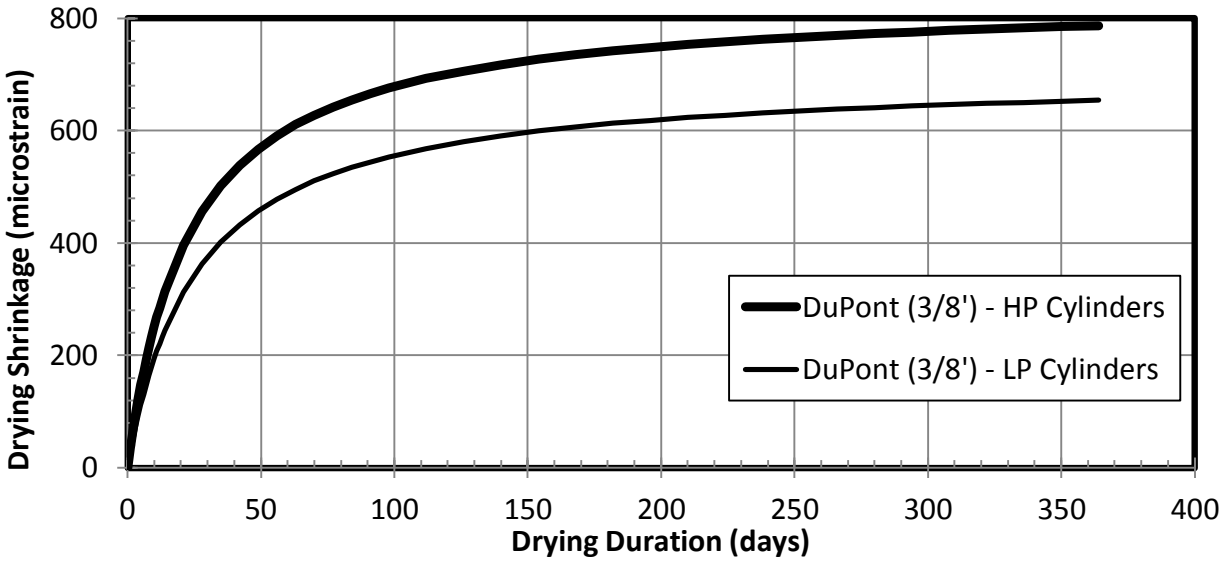

Figure 8.7: Drying Shrinkage Cylinder Curve Fits: DuPont (3/8-in.) Mixtures

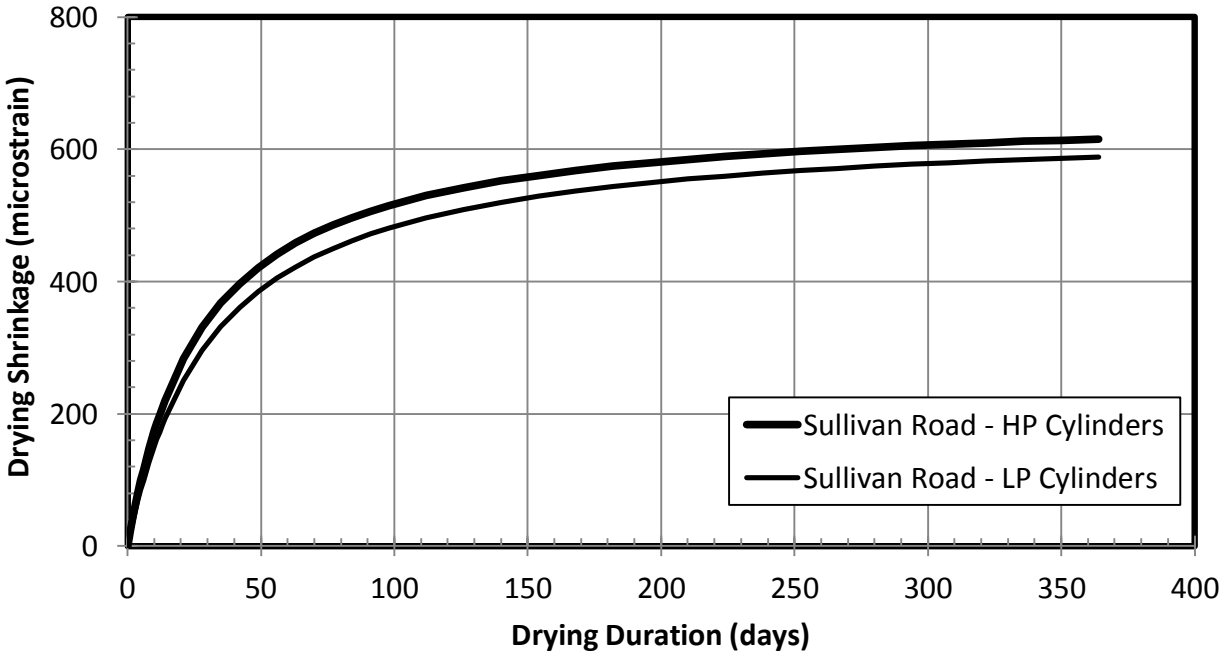

Figure 8.8: Drying Shrinkage Cylinder Curve Fits: Sullivan Road Mixtures

As expected, the shrinkage strains for the high-paste mixtures exceeded the strains for the low-paste mixtures for the drying shrinkage cylinders. All six of the creep high-mixtures had faster initial rates of strain gain than the low-paste mixtures. After a year's duration, the Day 365 fitted drying strains from the high-paste mixtures were on average 17.4 percent greater than

those of the low-paste mixtures. This comparison shows a consistent effect of the paste content on the drying shrinkage strains. This effect is not accounted for by the AASHTO specifications (5.4.2.3.3-1), which does not consider mixture proportions.

8.2.4 Creep Strains

The creep strains for each concrete mixture were fit to Equation 8.2. The optimized coefficients and fitted Day 365 strains for each creep mixture are listed in Table 8.9. The creep rigs had a targeted stress of 35 percent of the Day 14 compressive strength; therefore, the loadings for each rig were different. Since the creep rigs did not have similar loadings, there was no comparison of the measured creep strain data.

Table 8.9: Optimized Fitted Creep Curve Coefficients: All Mixtures

	f_{14} (psi)	t_{50} (Days)	ε_{Ult} (microstrain)	Fitted ε_{365} (microstrain)	$\varepsilon_{28} / \varepsilon_{365}$
DuPont (3/4") - HP	4,990	26.9	850	790	0.55
DuPont (3/4") - LP	3,710	21.7	730	690	0.62
DuPont (3/8") - HP	4,770	30.4	850	780	0.53
DuPont (3/8") - LP	5,170	22.0	980	920	0.60
Sullivan Road - HP	4,650	15.4	940	900	0.72
Sullivan Road - LP	4,410	17.6	790	750	0.70

8.2.5 Specific Creep

The specific creep was determined for each mixture by dividing the creep strains by the applied stress (in psi), which was determined by the measured elastic strain values. The specific creep optimized coefficients are listed in Table 8.10. The specific creep curves are plotted for all of the creep mixtures in Figure 8.9.

Table 8.10: Optimized Coefficients for Specific Creep: All Mixtures

	t_{50} (Days)	Day 365	ε_{28} / ε_{365}
DuPont (3/4") - HP	27.0	0.43	0.55
DuPont (3/4") - LP	21.9	0.49	0.60
DuPont (3/8") - HP	29.9	0.45	0.52
DuPont (3/8") - LP	22.1	0.48	0.59
Sullivan Road - HP	15.4	0.53	0.68
Sullivan Road - LP	17.5	0.48	0.65

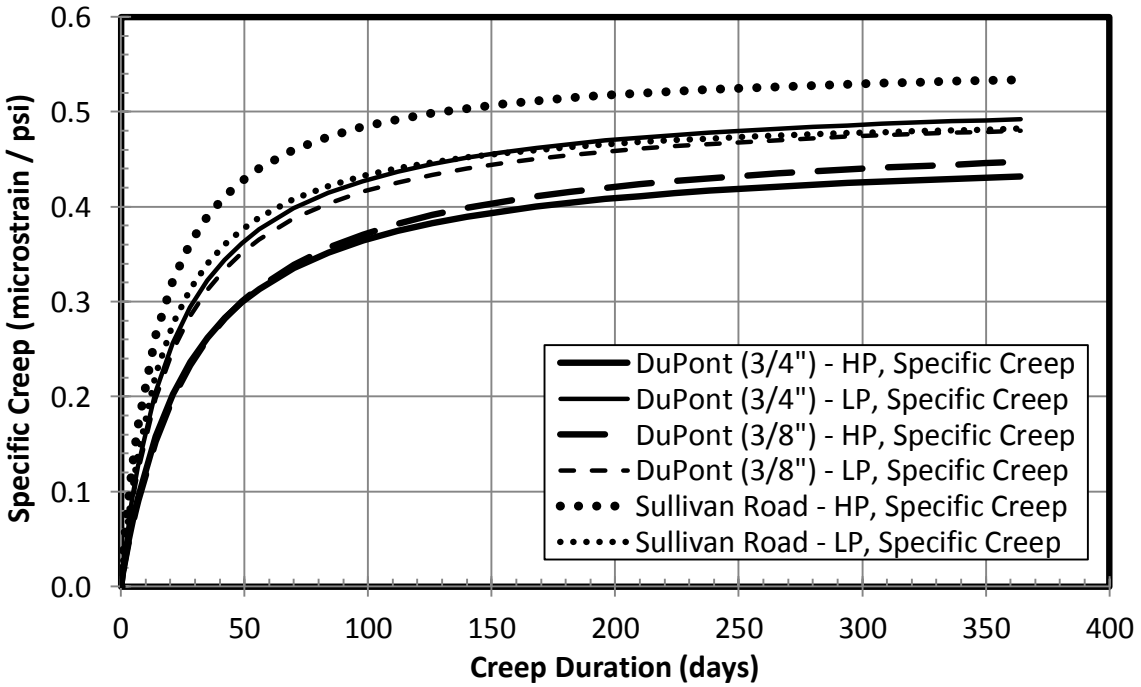

Figure 8.9: Specific Creep Fitted Curves: All Creep Mixtures

The three low-paste mixtures had similar specific creep curves (average difference of 2.4 percent). The DuPont (3/4-in. and 3/8-in.) high-paste mixtures had similar curves (average difference of 1.5 percent) that were approximately 16 percent smaller than the low-paste specific creep values. The Day 365 specific creep strains ranged from 0.43 to 0.53, with an average of 0.48 and a coefficient of variation of 7.5 percent. The ratio of Day 28 to Day 365 of the normalized strains ranged from 0.52 to 0.68, with an average ratio of 0.60 and a coefficient of variation of 9.9 percent. Figure 8.9 shows that variations in aggregate size had little effect on the

specific creep. Excluding the Sullivan Road high-paste mixture, increases in paste content tended to decrease the specific creep.

8.2.6 Creep Coefficient

The creep coefficient (defined in Section 8.1.7) was determined by normalizing the creep strains by the average measured elastic strain for each mixture. The creep coefficients for all six of the creep mixtures can be seen in Table 8.11 and Figure 8.10.

Table 8.11: Creep Coefficients: All Creep Mixtures

	Creep Coefficient (Day 365)	$\varepsilon_{28} / \varepsilon_{365}$
DuPont (3/4") - HP	2.12	0.55
DuPont (3/4") - LP	2.16	0.60
DuPont (3/8") - HP	1.92	0.52
DuPont (3/8") - LP	2.35	0.59
Sullivan Road - HP	2.04	0.68
Sullivan Road - LP	1.90	0.65
Average	2.08	0.60
St. Deviation	0.17	0.06
Coef. Of Variation	8.1%	9.9%

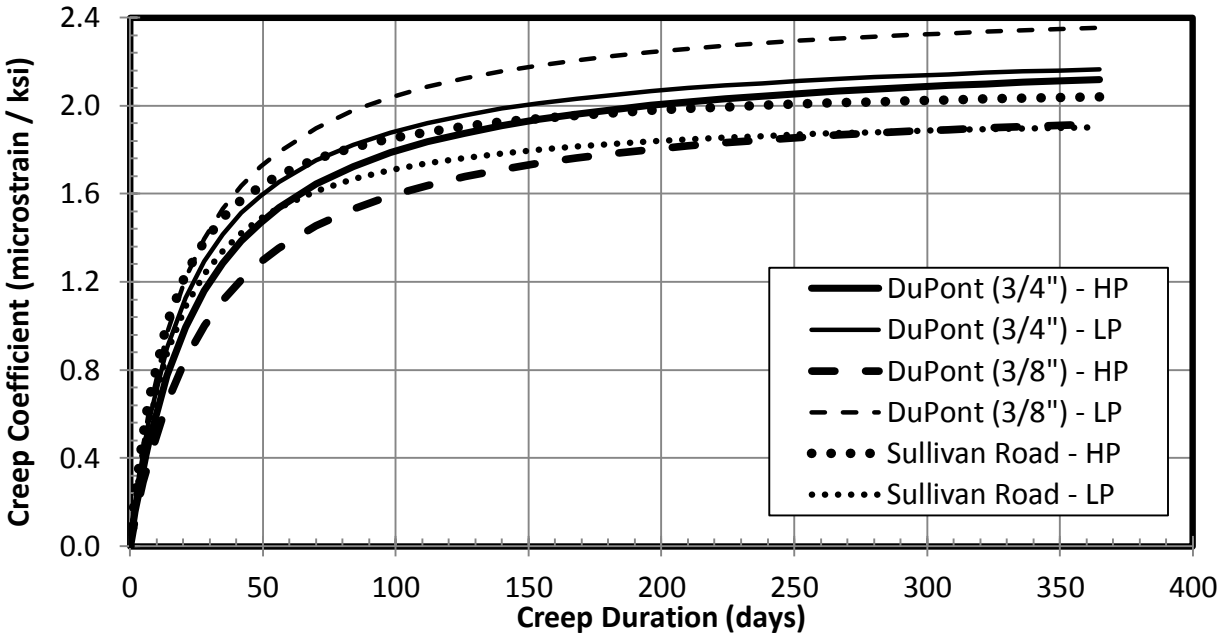

Figure 8.10: Creep Coefficient: All Creep Mixtures

The plot shows that all six of the fitted curves for the laboratory mixtures were similar. The fitted Day 365 coefficients ranged from 1.90 to 2.35, with an average coefficient of 2.08. The ratio of Day 28 to Day 365 for the coefficients ranged from 0.55 to 0.68, with an average ratio of 0.60. The creep coefficient after a year's loading duration had a coefficient of variation that was approximately 8 percent for six concrete mixtures, despite the variations in compressive strengths, elastic strains, paste contents, aggregate size, and aggregate type.

The aggregate source appeared to affect the ratio of Day 28 to Day 365 creep coefficients. The DuPont aggregates (3/4-in. and 3/8-in.) had an average ratio of 0.56, and the Sullivan Road aggregate had an average ratio of 0.66 (a difference of 14.9 percent). There was no consistent pattern for the effect of variations in paste content on the creep coefficients.

A comparison of the creep coefficient curves for the laboratory mixtures and the estimated curve from AASHTO specifications (5.4.2.3.2-1, Equation 2.12) are provided in Appendix D. The results are consistent with those detailed in Section 8.1.7. Namely, the creep coefficients at one year were well estimated by the AASHTO specifications. The difference between the predicted and measured Day 365 creep coefficients ranged from 1.7 percent to 16.2 percent, with an average difference of 8.0 percent. However, the measured creep coefficient curves and estimated AASHTO creep coefficient curves did not match well for any mixtures at

early ages. The difference in Day 28 to 365 ratios from the measured and estimated values ranged from 21.7 percent to 41.2 percent, with an average difference of 31.6 percent. By taking the aggregate source into account in the AASHTO specifications, it may be possible to improve the accuracy of the estimated creep coefficients at early ages.

The method of analyzing the creep strain variability, as detailed in Section 8.1.7, was repeated for all six of the creep mixtures. The method calculated three distinct creep strain values by dividing an applied stress of 1,600 psi (40 percent of the 4,000 psi design strength) by various elastic moduli (the measured elastic modulus, the predicted elastic modulus from the Day 14 compressive strength, and the predicted elastic modulus from the design strength of 4,000 psi). The estimated creep strain curves for each of the elastic strain values and the measured creep strain curve for each mixture can be seen in Appendix D. The differences from the measured and estimated creep strain and the average coefficient of variation for each of the AASHTO curves are listed in Table 8.12 for the creep mixtures.

Table 8.12: Predicted AASHTO Creep Strain Curve Differences: All Mixtures

		ε_{365} Percentage Difference			Average Coefficient of Variation		
	Fitted ε_{365}	Design Strength	Predicted Elastic Modulus	Measured Elastic Modulus	Design Strength	Predicted Elastic Modulus	Measured Elastic Modulus
DuPont (3/4") - HP	790	28.7%	20.4%	4.0%	18.3%	11.7%	4.7%
DuPont (3/4") - LP	690	18.7%	21.7%	4.4%	10.7%	12.6%	6.2%
DuPont (3/8") - HP	780	26.2%	19.4%	9.4%	16.7%	11.2%	5.2%
DuPont (3/8") - LP	920	20.7%	9.8%	1.5%	11.9%	6.8%	8.7%
Sullivan Road - HP	900	11.7%	4.8%	6.9%	8.9%	8.3%	8.2%
Sullivan Road - LP	750	20.0%	16.1%	12.6%	11.9%	9.9%	8.6%
Average	810	21.0%	15.4%	6.5%	13.1%	10.1%	6.9%

The results suggest that to improve the accuracy of AASHTO prediction curves, the measured compressive strength and elastic modulus should be known for each application. If standardized tests cannot be performed, then the AASHTO specifications for estimating the elastic modulus (Section 5.4.2.4-1, Equation 2.7) need to be improved.

8.3 CREEP CURVE EXTRAPOLATION VARIABILITY

Error was caused by shortening the monitored creep duration. The creep strains for the DuPont (3/4-in.) high-paste samples at various durations were fit to Equation 8.2 and extrapolated to a year's duration. The average percentage difference between the creep strains monitored for a year and the different durations are listed in Table 8.13. The fitted curves for each of the different monitored durations are shown in Figure 8.11.

Table 8.13: Percentage Difference from Varying Creep Monitor Durations

Monitored Duration (days)	Fitted ε_{365} (percentage difference)	Average Strains (percentage difference)
270	9.4%	7.1%
180	14.2%	11.0%
90	22.8%	18.3%
56	28.9%	23.7%
28	34.6%	28.9%

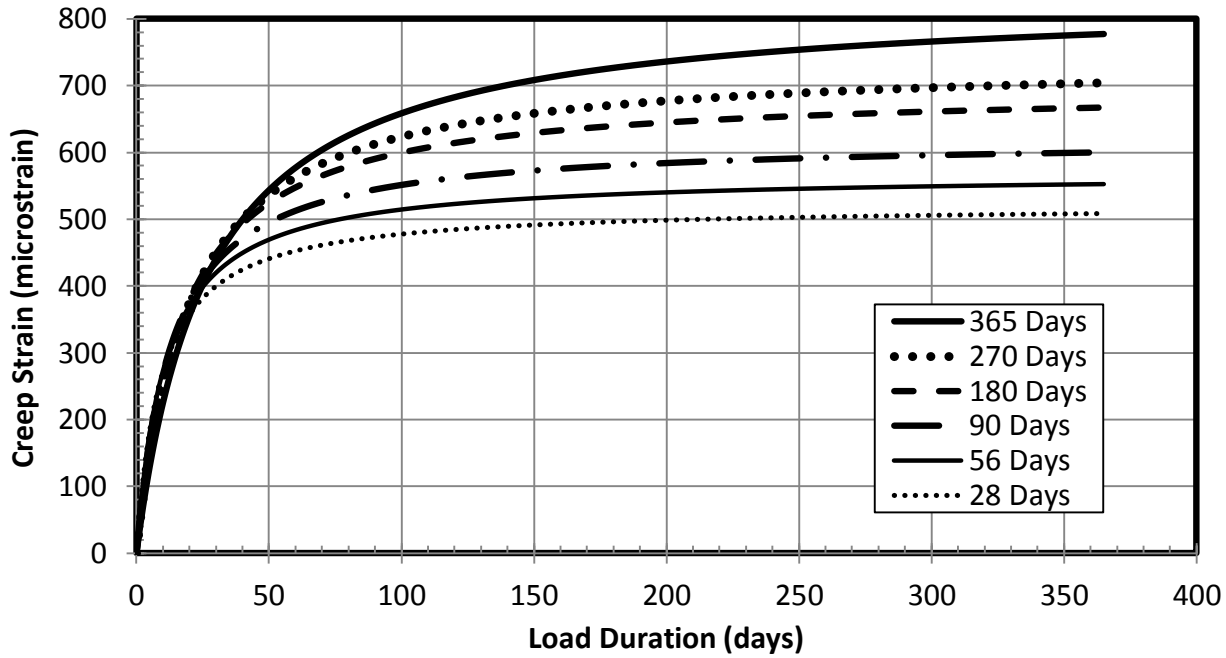

Figure 8.11: Strain Extrapolation Error: DuPont (3/4-in.) High-Paste

The initial rate of strain gain was identical for each of the different cure durations used; only the Day 365 strain varied for the different monitored durations. The average percentage difference between the measured and extrapolated values decreased with increasing monitor duration. The method of extrapolating the creep strain was found to achieve approximate strain values (around 10 percent difference) within half the year's duration. To improve the accuracy of the extrapolated curves, a constant coefficient was determined for each mixture to multiply with the fitted curve. A coefficient of 1.1 for 180 days of monitoring and a coefficient of 1.2 for 56 days of monitoring were found to minimize the errors of the extrapolated Day 365 strains and average percentage differences. Figure 8.12 plots the 365 and the modified 180 days of monitoring curve fits for the DuPont (3/4-in.) high-paste mixture. Figure 8.13 shows the 365, 56, and modified 56 days of monitoring curves for the DuPont (3/4-in.) high-paste mixture.

The results from extrapolating the creep strains for the remaining mixtures can be seen in Appendix D. The modified creep strain values for the 180 days of monitoring had an average percentage difference from the year-long loading duration of 6.8 percent, with a difference in the Day 365 strain value of 3.6 percent. The modified creep strains from 56 days of monitoring had an average percentage difference of 6.7 percent, with a difference in the Day 365 strain values of 4.9 percent.

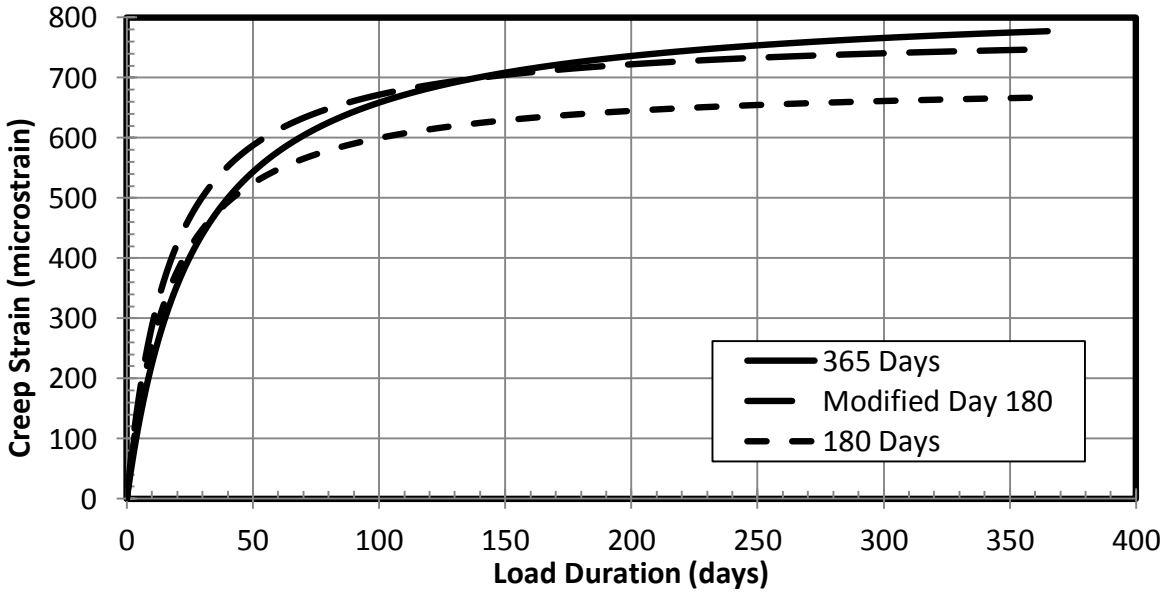

Figure 8.12: Modified 180 Days of Creep Monitoring: DuPont (3/4-in.) High-Paste

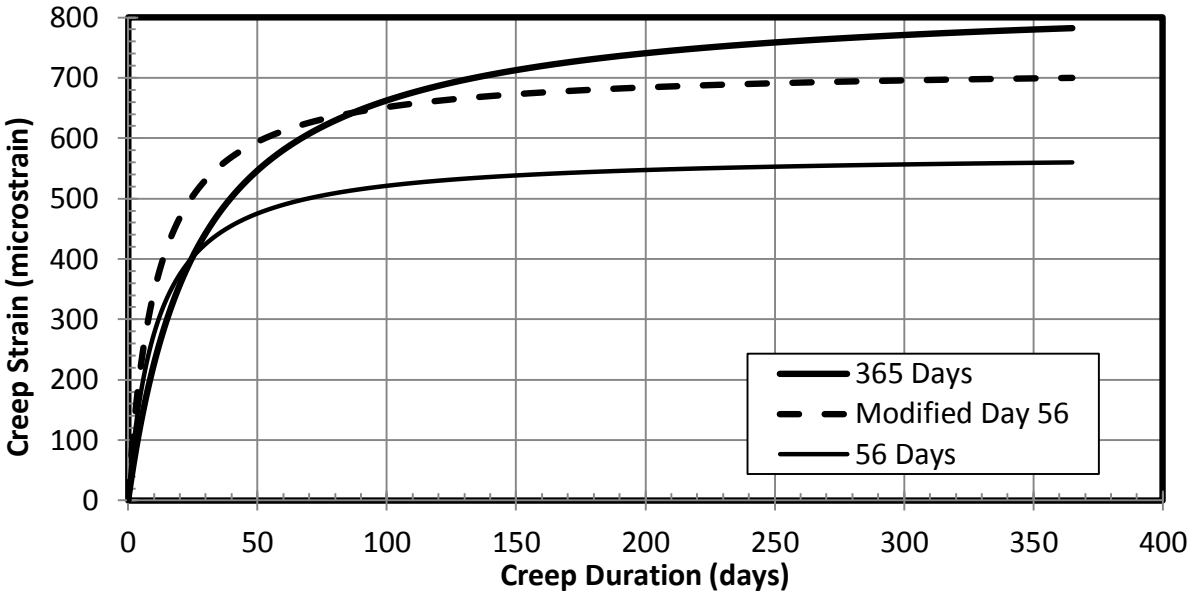

Figure 8.13: Modified 56 Days of Creep Monitoring: DuPont (3/4-in.) High-Paste

8.4 ANALYSIS OF CREEP RESULTS

Variations in the aggregate type, compressive strength, and paste content significantly affected the creep strains (Table 8.9).Modeling the specific creep data allowed for a direct comparison of different creep mixtures by removing the effects of different applied stresses. The specific creep data showed that the effects of aggregate size and type on specific creep were minimal, With the exception of the Sullivan Road high-paste mixture, the paste content had a significant impact (Figure 8.9) on specific creep. For concrete mixtures with lower paste contents, the specific creep values were larger for the entire loading duration than mixtures with higher paste contents.

AASHTO specifications (5.4.2.3.2-1, Equation 2.12) estimate year-long creep coefficients well but under-estimate the initial values (figures 8.4, D.7, D.8, D.9, D.10, and D.11). This may become a concern for structures that have larger creep deflections at earlier ages than expected, as predicted by AASHTO specifications, when those deformations are to be expected. When the creep coefficient is converted into an estimation of the creep strain, knowledge of the measured compressive strength and elastic modulus from standardized testing would greatly improve the accuracy of the calculated strain values (Table 8.12).

The measured values for the time-dependent strains (drying shrinkage and creep data) can be modeled well with Equation 8.2 (figures 8.1, D.2, D.3, D.4, D.5, and D.6). The fitted curves can be used to extrapolate beyond the monitored duration to estimate the future values. This extrapolation can reduce the required monitoring time for modeling creep strains, and a coefficient can be used to multiply the fitted curves and improve the accuracy. For monitoring durations of 180 days, a coefficient of 1.1 consistently improved the extrapolated creep data (figures 8.12, D.17, D.18, D.19, D.20, and D.21). Monitoring durations of 56 days can be improved consistently by using a coefficient of 1.2 for extrapolated creep strains (figures 8.13, D.22, D.23, D.24, D.25, and D.26).

Chapter 9: Summary of Findings and Recommendations

This chapter summarizes the finding and recommendations based on the evaluation of key performance characteristics for (1) twenty-eight laboratory mixtures, consisting of four mixtures (high strength, low strength, high paste and low paste) for seven aggregate types, and (2) concrete mixtures sampled from five WSDOT bridge projects.

The compressive strength, tensile strength, elastic modulus, drying shrinkage, and creep parameters were the key performance characteristics that were considered. In this chapter, a section is devoted to each characteristic. Within each section, a subsection is devoted to the effects of the concrete mixture proportions (paste content and water-cementitious ratio) and coarse aggregate source, to summarize the accuracy of the current relevant specifications, and to make recommendations.

9.1 COMPRESSIVE STRENGTH

Compressive strengths were measured for the 28 laboratory mixtures at 7, 14, 28 and 56 days. Compressive strengths of the field mixtures were measured at 28 and 56 days.

9.1.1 Findings

For a given concrete age, the compressive strength of a mixture depended mainly on its water-cementitious ratio and to a lesser extent, on the aggregate source.

- The compressive strength consistently decreased as the water-cementitious ratio increased, as expected. This effect was observed consistently for the laboratory mixtures (figures 4.2 and 4.7) and field mixtures (Figure 4.12).
- The compressive strength did not vary consistently with paste content (Figure 4.8)
- The strength of most (but not all) of the mixtures was insensitive to the aggregate type. The exceptions to this insensitivity were that the strengths of the high-strength mixtures were significantly lower for mixtures made with the Rock Island and Santosh aggregates (Figure 4.6). As a result, compared with other aggregate sources, the Rock Island aggregate source (and to a lesser extent, the Santosh aggregate source) were less sensitive to variations in the water-cementitious ratio (Figure 4.7). This insensitivity suggests that

it might be challenging to make higher-strength concrete with aggregates from the Rock Island and Santosh sources.

The rate of strength gain was evaluated by normalizing the compressive strengths at 7 days by the compressive strengths at 28 days.

- The normalized strength at 7 days was consistently higher for the higher-strength mixes (w/cm = 0.30 for ¾ in. aggregate) than for the low-strength mixes (w/cm = 0.49). This difference was observed for all aggregate types (Figure 4.8) and for the five field projects (Table 4.4).
- The normalized strength at 7 days was insensitive to variations in paste content and aggregate type (Figure 4.10).

9.1.2 Evaluation of Specifications

The time dependence of the compressive strength was modeled well by the ACI 209.2R-08 specifications (A-17, Equation 2.1), but only if the equation constants were optimized. For the laboratory and field mixtures, the optimized values of the K1 and K2 constants were 2.4 and 0.90, respectively. In contrast, ACI 209.2R-08 suggests values of K1 and K2 of 4.0 and 0.85, respectively. The concrete mixtures cast for this research gained strength significantly faster at early ages than suggested by the specifications. It is likely that variations in cement type and cement refinement process since the development of the ACI 209.2R-08 equation have led to an acceleration in the rate of strength gain.

9.1.3 Recommendations

WSDOT should consider estimating early strength gain using parameters that are representative of current materials used in Washington state. Further testing would be needed to evaluate the accuracy of Equation 2.1 for estimating compressive strengths for cure durations beyond fifty-six days.

9.2 TENSILE STRENGTH

Split-tension and flexural-strength tests were performed at 28 and 56 days for the five WSDOT project field mixtures.

9.2.1 Findings

The following conclusions were drawn from the results of split-tension and flexural tests:

- The flexure strengths (figures 5.2 and 5.3) and split-tensile strengths (figures 5.7 and 5.8) increased with increasing compressive strength, as expected.
- The flexural strength of the mixtures was approximately equal (on average) to 1.58 times the split-tension strength (figures 5.9 and 5.10). The correlation between the two strengths was fit well by Equation 5.2, and the results are similar to the correlation suggested by ASTM STP 169D (Equation 2.6), which has a factor of 1.54.
- The variability of the strengths of the split tension specimens (average variation of 8.3%) generally exceeded that of the flexural strength samples (average variation of 4.0%).

The effects of paste content and aggregate source could not be evaluated from the data, because the sample size was too small, and the split-tension strengths of the cylinders varied too much among nominally identical samples.

9.2.2 Evaluation of Specifications

The AASHTO code specifications for normal-weight concrete (5.4.2.6, Equation 2.2) greatly underestimated the flexural strengths of the field samples (lower by an average of 33%). In contrast, the AASHTO specifications C5.4.2.6 (Equation 2.3), which was developed for high-strength concrete, over-predicted the field sample flexure strengths (greater by an average of 13%).

Equation 5.1, developed based on the test results, fit the mean flexural strength of the field mixtures, with an average difference of 8.3%. This equation is repeated in Equation 9.1.

$$\sigma_{FLEX} \text{ psi} = 420 \times \sqrt[3]{f_c} \text{ (ksi)} \qquad \text{(Equation 9.1)}$$

9.2.3 Recommendations

Split-tension cylinders are easier to handle than flexural beams, so instead of performing flexure tests, the modulus of rupture can be predicted from split-tension tests using Equation 5.2, within a typical error of 7.1%. Due to the variability of the split-tension results, it is

recommended that a minimum of three split-tension samples be cast per test. Alternately, the flexural strength could be estimated with Equation 9.1.

9.3 ELASTIC MODULUS

The elastic modulus was measured at 7, 14, 28 and 56 days for four mixtures for each of the seven aggregate sources. The elastic modulus was also measured at 28 and 56 days for the five sets of field-collected samples.

9.3.1 Findings

The following findings were reached regarding variations in the elastic modulus at a particular age.

- The elastic modulus consistently decreased with increasing water-to-cementitious ratio (figures 6.1, 6.8 and 6.14).
- The elastic modulus consistently increased with increasing compressive strength (figures 6.2, 6.7 and 6.15)
- The effect of the paste content on the elastic modulus was not consistent. The elastic modulus increasing paste content for some aggregate sources. For some other aggregate sources, the higher-paste mixtures had lower elastic moduli (Figure 6.9).

The following findings were reached regarding rate at which the elastic modulus increased.

- The rate of stiffness gain (ratio of Day 7 to Day 28 of the elastic moduli) was not affected by variations in the water-cementitious ratio or aggregate source (figures 6.12 and 6.18). For all high-strength and low-strength mixes, as well as the field samples, the elastic modulus at 7 days was close to 90% of the elastic modulus at 28 days.
- The paste content did not consistently affect the rate of stiffness gain (figures 6.13 and 6.19).

9.3.2 Evaluation of Specifications

Regardless of compressive strength, paste content or aggregate source, the elastic moduli for all the laboratory mixtures exceeded the values predicted by the AASHTO specifications (5.4.2.4-1, Equation 2.7) by 10.4%, on average (figures 6.10 and 6.11).

Surprisingly, this discrepancy was not identified for the field mixtures, even though the laboratory and field mixtures used similar paste contents and aggregates from the same sources. The average difference between the measured and calculated elastic moduli for the field mixtures was only 4.2%.

A possible explanation for this difference is that steel molds were used for the laboratory mixtures, and plastic molds were used for the field mixtures. Alternately, it is possible that transportation slightly reduced the elastic modulus of the field samples. The cause of the differences could not be confirmed within the scope of this study.

Equation 2.7 estimated the elastic modulus for higher strength mixtures more accurately than lower strength mixtures (Figure 6.3). By accounting for the effect of the water-cementitious ratio and paste content on the elastic modulus in Equation 6.3, the average difference between the estimated and measured elastic modulus was 6.9%, which was slightly better than AASHTO predictions (AASHTO specifications had an average difference of 7.8%).

9.3.3 Recommendations

Further research would be needed to explain the discrepancy between elastic moduli for the laboratory cast and field-cast mixtures.

9.4 SHRINKAGE

Drying shrinkage specimens (3 in. by 4 in. by 16 in.) were monitored for 365 days for all four mixes for each of the seven aggregate sources.

9.4.1 Findings

The drying shrinkage strain increased with:

- increasing water-to-cementitious ratio (figure 7.5),
- increasing paste content (figures 7.6 and 7.9), and
- decreasing volume-to-surface ratio (figures 7.3, 7.10, 7.11 and 7.12), and

- decreasing compressive strength (figures 7.7 and 7.8)

The correlation between drying shrinkage and compressive strength is likely attributable to the correlation between compressive strength and water-to-cementitious ratio

With one exception, the shrinkage strains were similar for all of the ¾-in. aggregates (figures 7.8 and 7.9). The exception was the Santosh aggregate source for which the four mixtures had the highest shrinkage strains of all the mixes for each paste content.

9.4.2 Evaluation of Specifications

When the AASHTO specifications (5.4.2.3.3-1, Equation 2.9) were applied based on the design strength of 4000 psi), the specifications greatly overestimated the measured time-related shrinkage stains (by approximately 45%, Figure 7.3). The AASHTO drying shrinkage strain predictions improved when the measured Day 28 compressive strengths were used, but the predicted and measured strain still differed typically by about 20% (Table 7.3).

Two methods were developed to improve predictions of long-term deformations (one year drying duration). The first method extrapolates long-term deformations from short duration tests by optimizing the t_{50} and $\epsilon_{Ult.}$ constants with the following equation.

$$\epsilon_{time} = \frac{time}{t_{50} + time} \times \epsilon_{Ult.} \qquad \text{(Equation 9.2)}$$

Testing was performed for a minimum drying period of 56 days, and then increasing the extrapolated strain values (using Equation 9.2) by 10% to estimate the long-term deformations. This method resulted in average an error of 8.9% for the mixtures tested (Table 7.10).

A second method was developed to predict long-term deformations directly from key mixture characteristics. Equation 7.2 predicted one-year drying strains to an accuracy of 6.6% for the mixtures tested (Table 7.7), and the form of the equation can be seen in Equation 9.3. Further research for specific aggregate sources would vary the optimized values (K1, K2, and K3), and could improve the accuracy of Equation 7.2 for different locations.

$$\epsilon_{365} = K_1 \times PC \times W/CM + K_2 \; f_{Day\,28}^{\;K_3} \qquad \text{(Equation 9.3)}$$

9.4.3 Recommendations

WSDOT should consider the use of alternate methods for establishing the long-term shrinkage strains for mixtures made with local materials.

9.5 CREEP

Creep tests were conducted for a year for three aggregate sources (DuPont 3/4", DuPont Pea Gravel and Sullivan Road) for both low- and high-paste mixes. Each stack of cylinders was subjected to a concrete compressive load of approximately 35% of the day 14 compressive strength. The total deformations of pairs of cylinders were then attributed to elastic, drying shrinkage and creep deformations.

9.5.1 Findings

Based on the results of the six creep tests, the following conclusions were drawn.

- The elastic, drying shrinkage and creep strains all varied according to the aggregate type, compressive strength, and paste content (tables 8.8 and 8.9).
- The elastic deformations (Table 8.7) and the shrinkage deformations (Fig. 8.6, 8.7 and 8.8) measured for the cylinders in the creep rigs were comparable to those expected based on elastic modulus and beam shrinkage tests.
- The specific creep (ratio of creep strain to applied stress) varied little for the range of mixtures considered. At day 365, the specific creep ranged from 0.43 to 0.53 (Table 8.10) with an average of 0.48 and a coefficient of variation of 7.2%.
- The creep coefficient (ratio of creep strain) was also insensitive to changes in the mixture properties. At day 365, the creep coefficient ranged from 1.90 to 2.30 (Table 8.11) with an average of 2.08 and a coefficient of variation of 8.1%.

9.5.2 Evaluation of Specifications

The AASHTO specification estimate the long term creep deformations based on specified values of the creep coefficient. Using design values of the concrete compressive strength, and calculated values of the elastic modulus and creep coefficient, the measured creep strains consistently exceeded (on average, by 21%) the values predicted following the AASHTO specifications, which suggest values of the elastic modulus and creep coefficient. The average

error reduced to 15.4% when the actual compressive strength was included in the calculation. The error further reduced to 6.5% when the measured elastic modulus was included in the calculation (figures 8.5, D.12, D.13, D.14, D.15, and D.16).

Therefore, the creep coefficients specific by the AASHTO specifications are consistent with the measured creep deformations. The errors in the estimates of creep strains appear to stem mainly from differences between assumed and measured values of the concrete compressive strength and elastic modulus.

Long-term (one-year) predictions of creep strains can be made based on data from shorter testing durations.). For example, based on Equation 8.2, fitted for a loading duration of 56 days, and then increased the extrapolated one-year predictions by 20% resulted in average creep strain errors of 6.7% (figures 8.13, D.22, D.23, D.24, D.25, and D.26).

9.5.3 Recommendations

Estimates of long-term creep deformations could be best improved by making accurate estimates of the actual concrete strength (as opposed to specified strength) and estimates of the actual elastic modulus.

Acknowledgments

This study was made possible through the time and effort of the faculty members at the University of Washington and the employees of the Washington State Department of Transportation. Special thanks to Ron Lewis, Kim Willoughby, DeWayne Wilson, and Jugesh Kapur for their support. Yiming Liu of the Materials Testing Laboratory at the University of Washington helped provide the safety training required to operate all of the equipment for this research. Lastly, thanks to Spencer Livermore and Bradley Maier for their assistance in casting laboratory and field concrete samples. Only through the contributions of these individuals was successful completion of this research possible.

Bibliography

2010 Annual Book of ASTM Standards, Concrete and Aggregates, Volume 04.02. Baltimore, MD: ASTM International, 2010.

AASHTO LRFD Bridge Design Specifications. Washington, DC: American Association of State Highway and Transportation Officials, 2012.

Building Code Requirements for Structural Concrete (ACI 318-08) and Commentary. Farmington Hills, MI: American Concrete Institute, 2008.

Guide for Modeling and Calculating Shrinkage and Creep in Hardened Concrete, ACI 209.2R-08. Farmington Hills, MI: American Concrete Institute, 2008.

Mehta, Kumar and Monteiro, Paulo. *Concrete Microstructure, Properties, and Materials*, Third Edition. New York, NY: McGraw-Hill Companies, Inc., 2006.

Neville, A. *Properties of Concrete*. London, UK: Pitman Publishing LTD., 1975.

Prediction of Creep, Shrinkage, and Temperature Effects in Concrete Structures, ACI 209R-92. . Farmington Hills, MI: American Concrete Institute, 2008.

Significance of Tests and Properties of Concrete and Concrete-Making Materials, ASTM STP-169D. Bridgeport, NJ: ASTM International, 2006.

Appendix A: Compressive Strength Test Results

A.1: SUMMARY OF MEASURED COMPRESSIVE STRENGTHS

The measured compressive strength results from the four test dates are shown in this section for each laboratory mixture. The compressive strengths from DuPont (3/4-in.) mixture are excluded in this section, but can be seen in Table 4.1 and Figure 4.1. The following list of tables and figures detail the measured compressive strengths for laboratory aggregate: Table A.1 and Figure A.1 for DuPont (3/8-in.), Table A.2 and Figure A.2 for Okanogan Valley, Table A.3 and Figure A.3 for Sullivan Road, Table A.4 and Figure A.4 for Pasco, Table A.5 and Figure A.5 for Rock Island, and Table A.6 and Figure A.6 for Santosh mixtures.

Table A.1: Measured Compressive Strengths: DuPont (3/8-in.)

Mixture	Paste Content (%)	Water-Cementitious Ratio	Day 7 (psi)	Day 14 (psi)	Day 28 (psi)	Day 56 (psi)
High Paste	33.2	0.38	4,310	4,770	5,460	5,630
Low Paste	26.1	0.38	4,440	5,170	5,690	6,250
High Strength	28.2	0.33	4,570	4,950	5,610	5,560
Low Strength	29.3	0.49	2,690	3,390	3,850	4,000

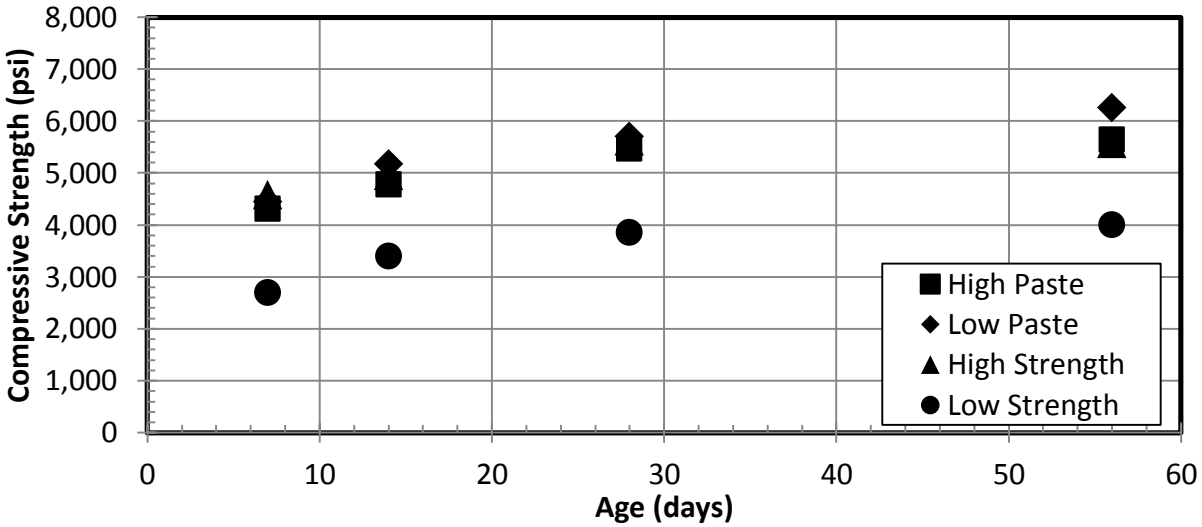

Figure A.1: Compressive Strengths: DuPont (3/8-in.) Mixtures

Table A.2: Measured Compressive Strengths: Okanogan Valley

Mixture	Paste Content (%)	Water-Cementitious Ratio	Day 7 (psi)	Day 14 (psi)	Day 28 (psi)	Day 56 (psi)
High Paste	30.5	0.38	4,710	5,180	5,340	5,970
Low Paste	24.0	0.38	3,200	3,710	4,180	4,440
High Strength	27.0	0.30	5,730	5,580	6,060	7,090
Low Strength	27.0	0.49	3,120	3,760	4,200	4,520

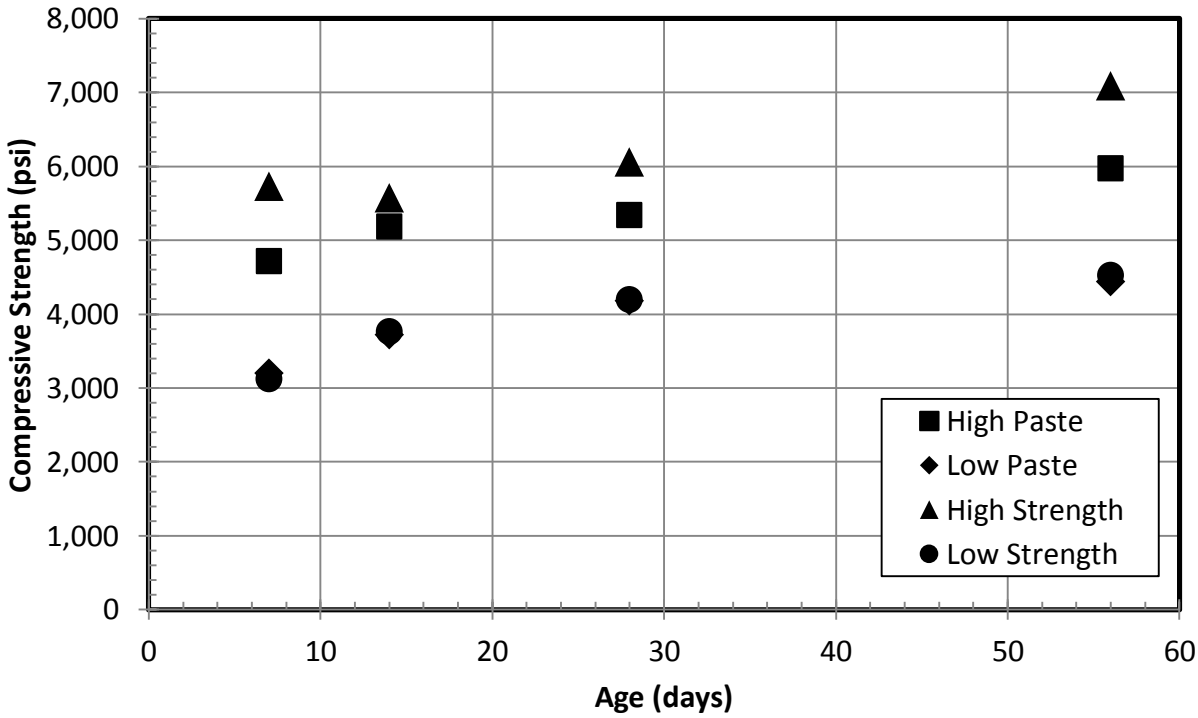

Figure A.2: Compressive Strengths: Okanogan Valley Mixtures

Table A.3: Measured Compressive Strengths: Sullivan Road

Mixture	Paste Content (%)	Water-Cementitious Ratio	Day 7 (psi)	Day 14 (psi)	Day 28 (psi)	Day 56 (psi)
High Paste	30.5	0.38	4,080	4,650	4,720	5,260
Low Paste	24.0	0.38	3,950	4,410	4,830	5,370
High Strength	27.0	0.30	5,820	6,370	6,750	7,300
Low Strength	27.0	0.49	2,980	3,490	3,810	4,340

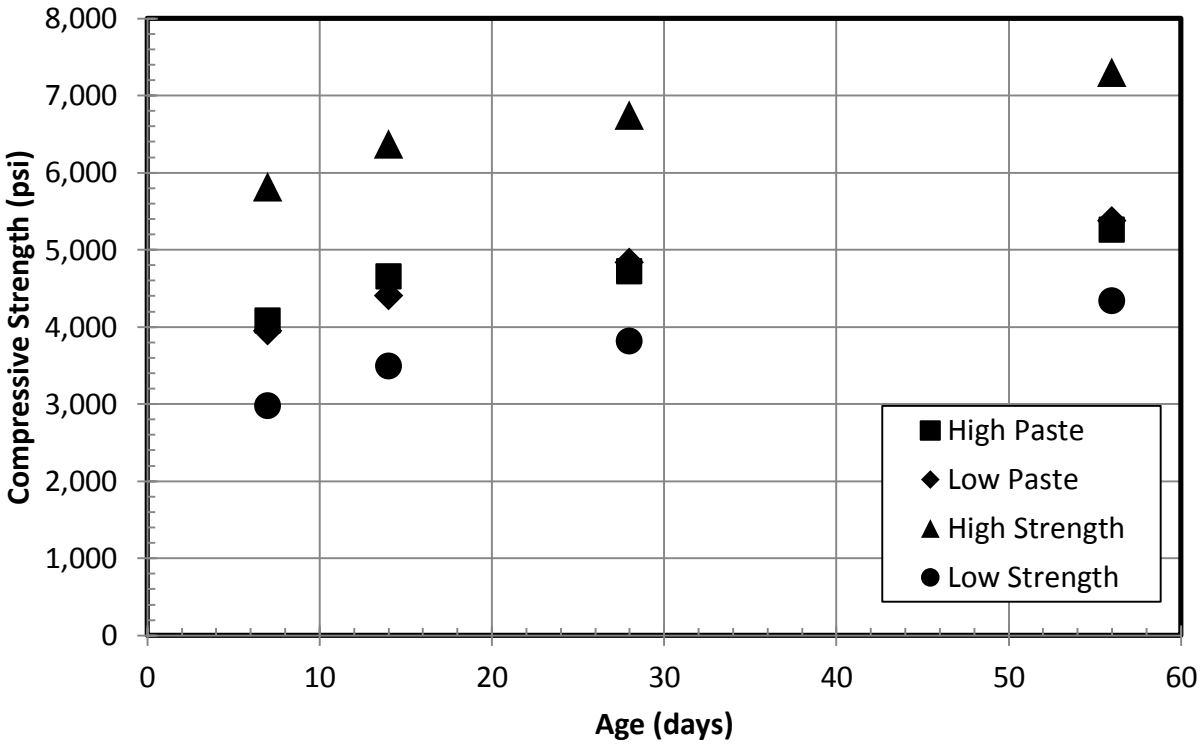

Figure A.3: Compressive Strengths: Sullivan Road Mixtures

Table A.4: Measured Compressive Strengths: Pasco

Mixture	Paste Content (%)	Water-Cementitious Ratio	Day 7 (psi)	Day 14 (psi)	Day 28 (psi)	Day 56 (psi)
High Paste	30.5	0.38	3,670	4,130	4,640	4,650
Low Paste	24.0	0.38	3,630	3,940	4,040	4,040
High Strength	27.0	0.30	4,940	5,330	5,450	6,170
Low Strength	27.0	0.49	2,470	2,900	3,060	3,540

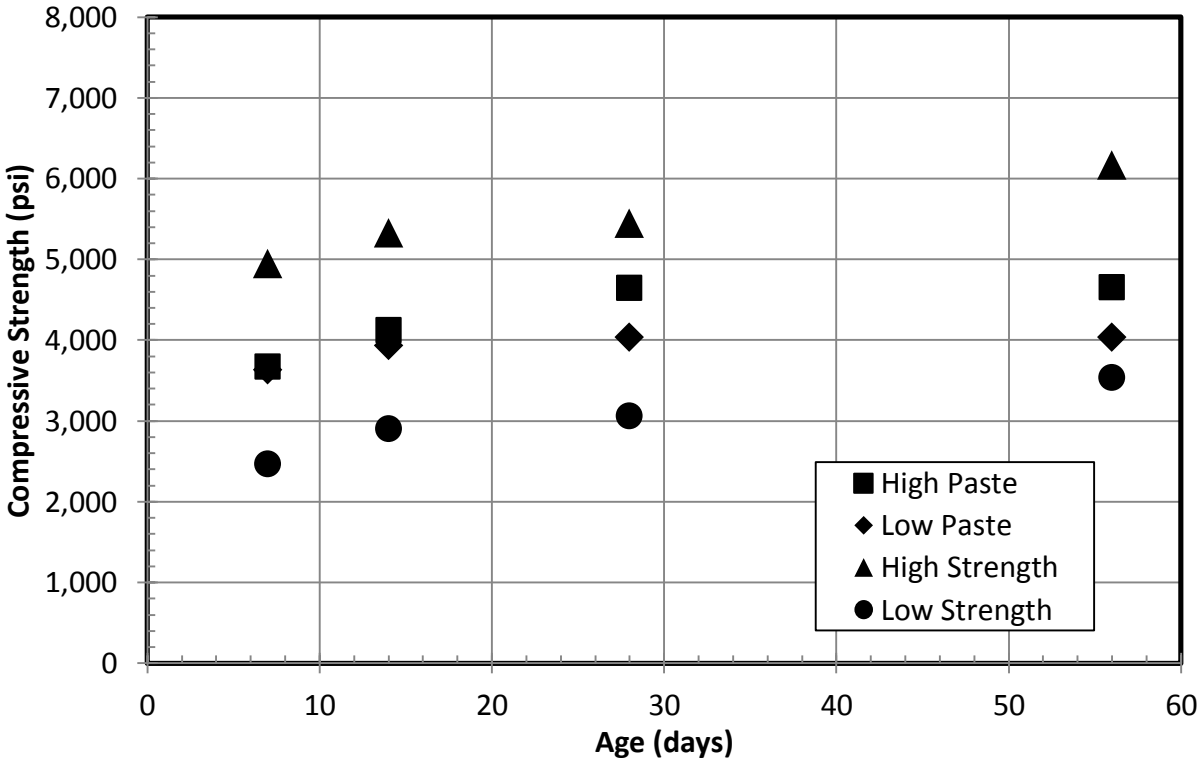

Figure A.4: Compressive Strengths: Pasco Mixtures

Table A.5: Measured Compressive Strengths: Rock Island

Mixture	Paste Content (%)	Water-Cementitious Ratio	Day 7 (psi)	Day 14 (psi)	Day 28 (psi)	Day 56 (psi)
High Paste	30.5	0.38	3,440	3,880	4,320	4,400
Low Paste	24.0	0.38	3,760	3,710	4,460	4,630
High Strength	27.0	0.30	4,000	4,020	4,520	4,700
Low Strength	27.0	0.49	3,480	3,930	4,280	4,760

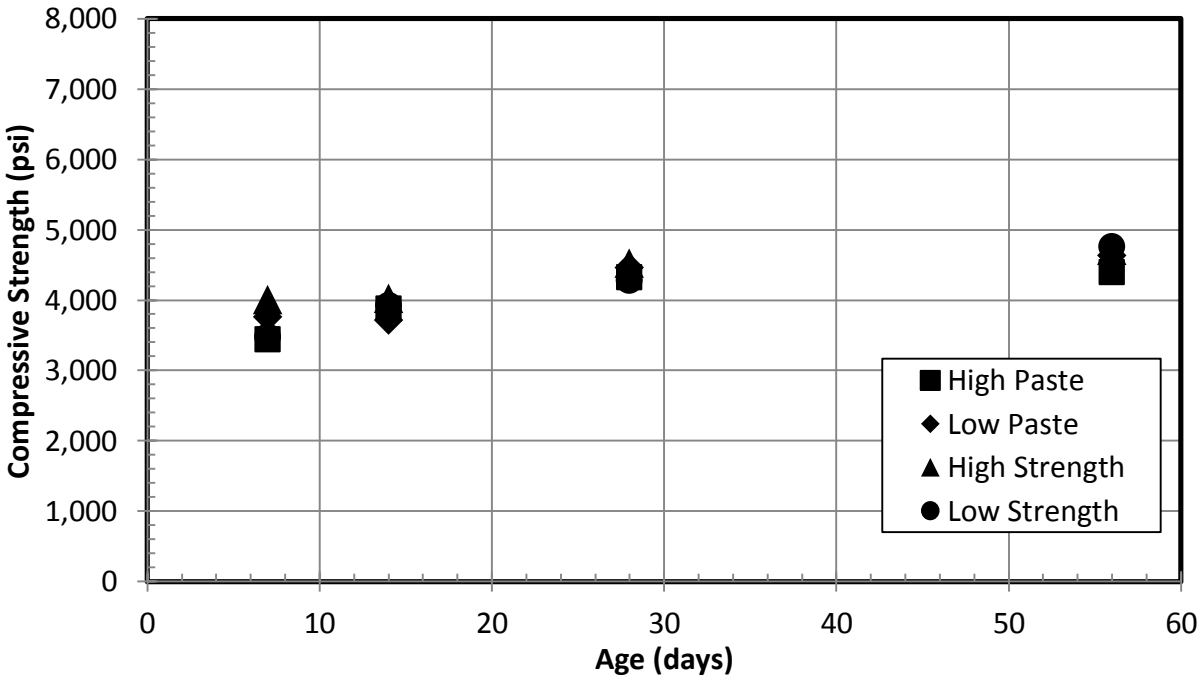

Figure A.5: Compressive Strengths: Rock Island Mixtures

Table A.6: Measured Compressive Strengths: Santosh

Mixture	Paste Content (%)	Water-Cementitious Ratio	Day 7 (psi)	Day 14 (psi)	Day 28 (psi)	Day 56 (psi)
High Paste	30.5	0.38	2,690	3,040	3,170	3,380
Low Paste	24.0	0.38	2,680	2,920	3,190	3,580
High Strength	27.0	0.30	4,160	4,350	4,630	4,890
Low Strength	27.0	0.49	2,470	2,510	3,340	3,640

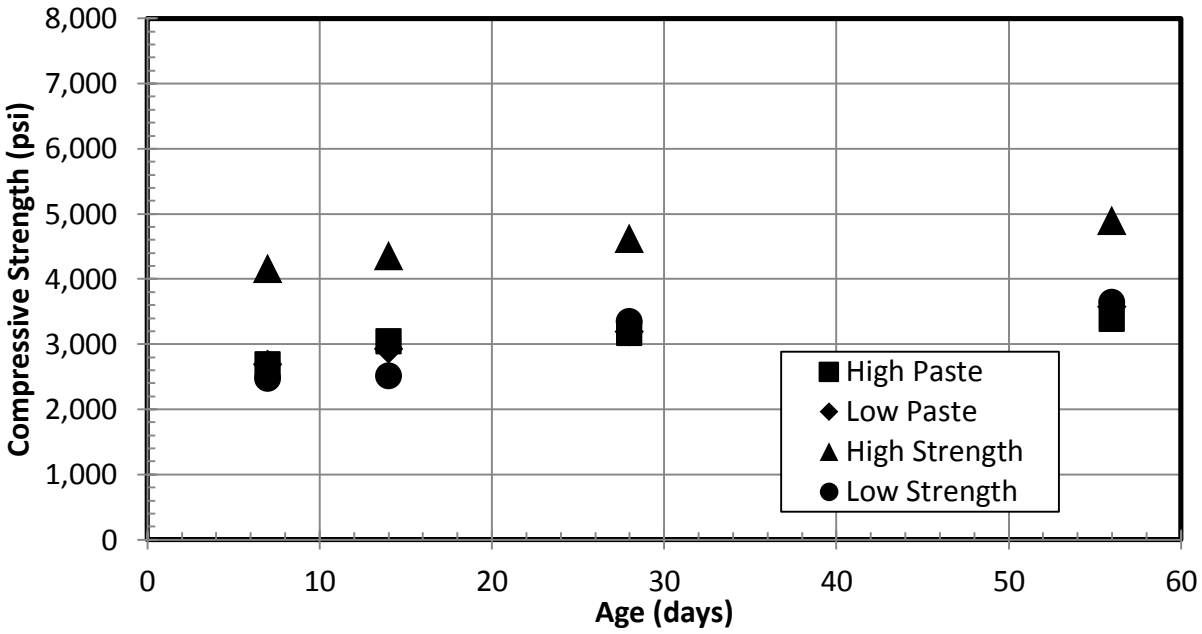

Figure A.6: Compressive Strengths: Santosh Mixtures

The measured Day 28 compressive strengths were plotted against the water-cementitious ratios for each laboratory aggregate sources. The Day 28 strengths versus the water-cementitious ratios of the DuPont (3/4-in.) mixtures are excluded from this section, but can be seen in Figure 4.2. The following list of figures show the Day 28 strengths against the water-cementitious ratios for each of the four laboratory mixtures: Figure A.7 for DuPont (3/8-in.), Figure A.8 for Okanogan Valley, Figure A.9 for Sullivan Road, Figure A.10 for Pasco, Figure A.11 for Rock Island, and Figure A.12 for Santosh mixtures.

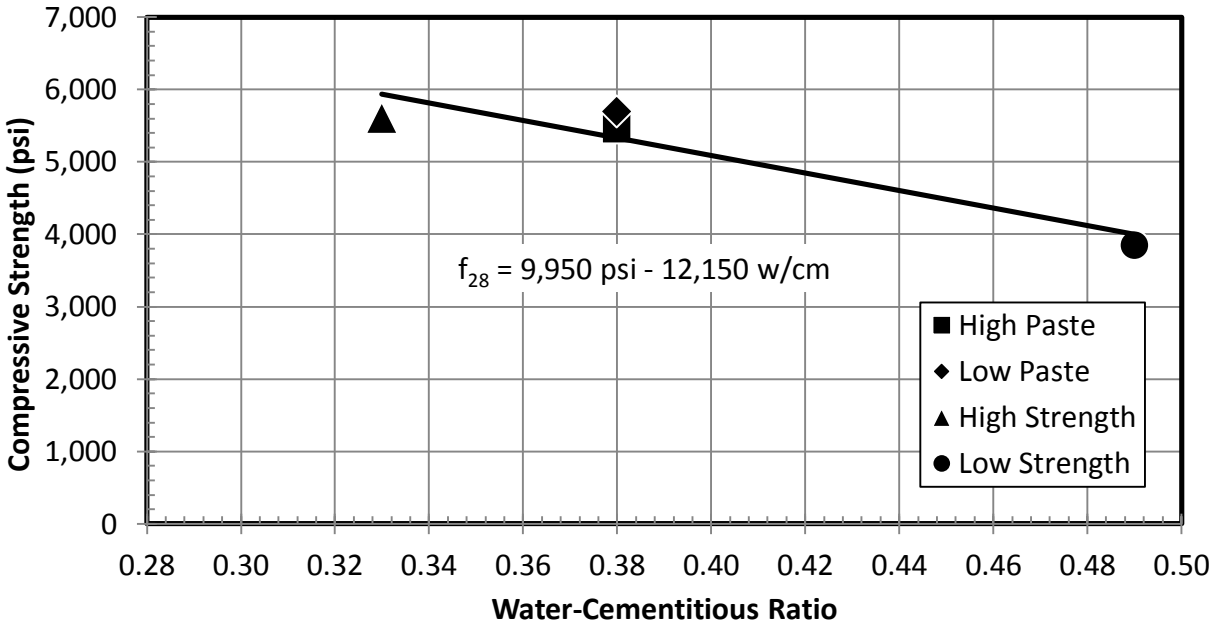

Figure A.7: Day 28 Comp. Strength vs. W/CM Ratio: DuPont (3/8-in.) Mixtures

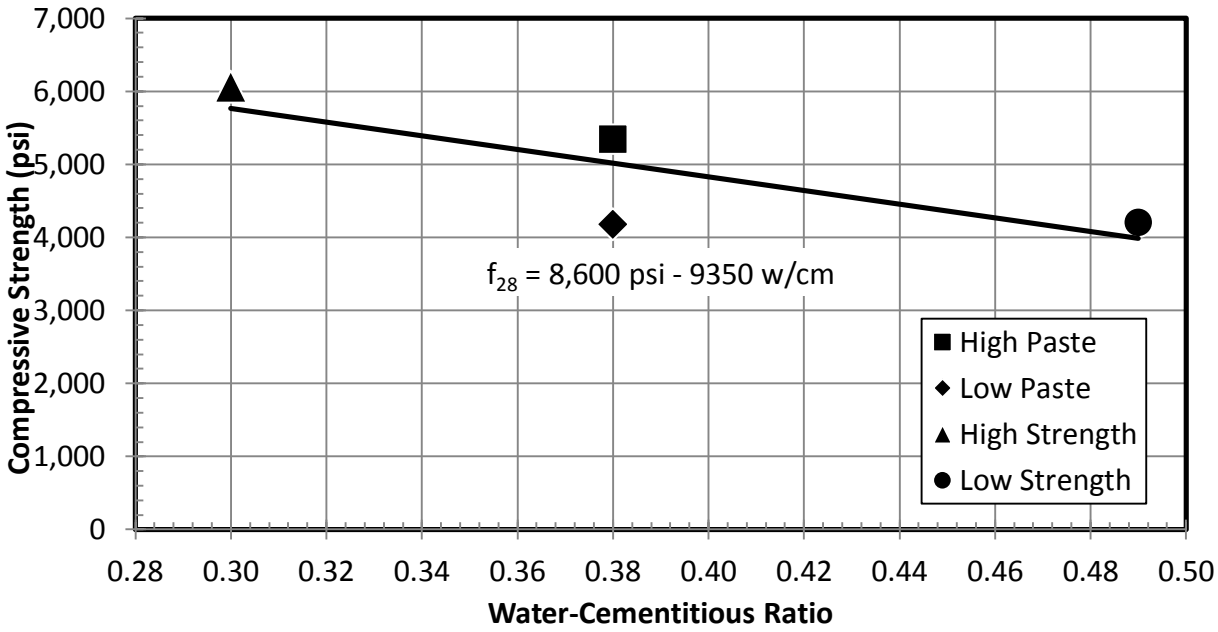

Figure A.8: Day 28 Comp. Strength vs. W/CM Ratio: Okanogan Valley Mixtures

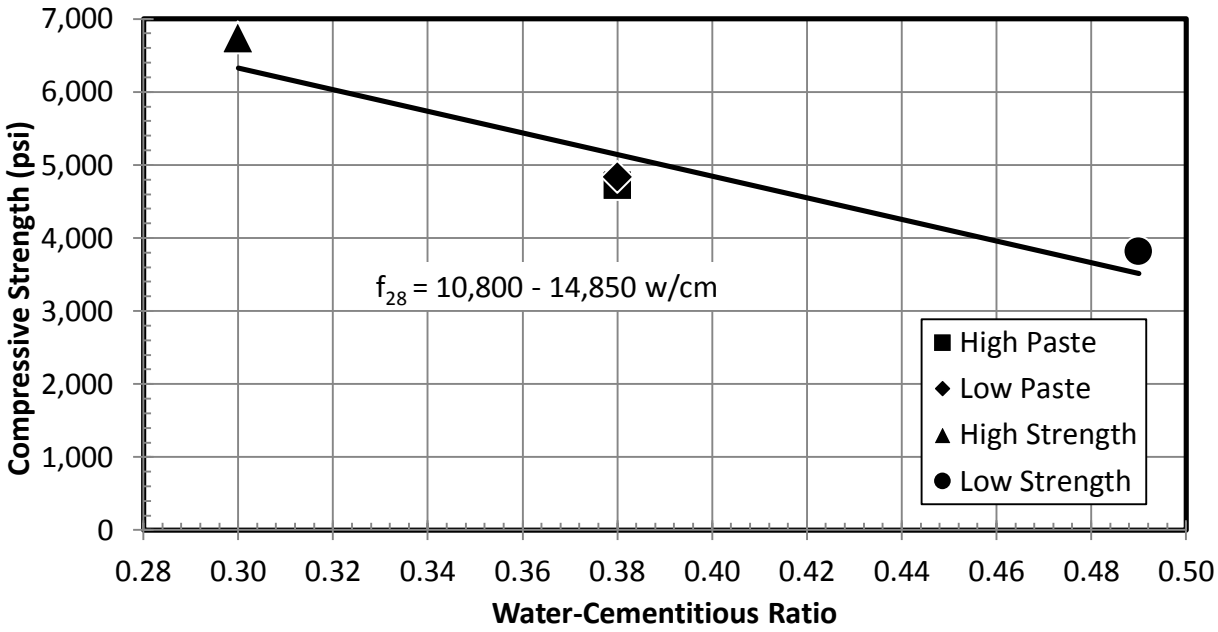

Figure A.9: Day 28 Comp. Strength vs. W/CM Ratio: Sullivan Road Mixtures

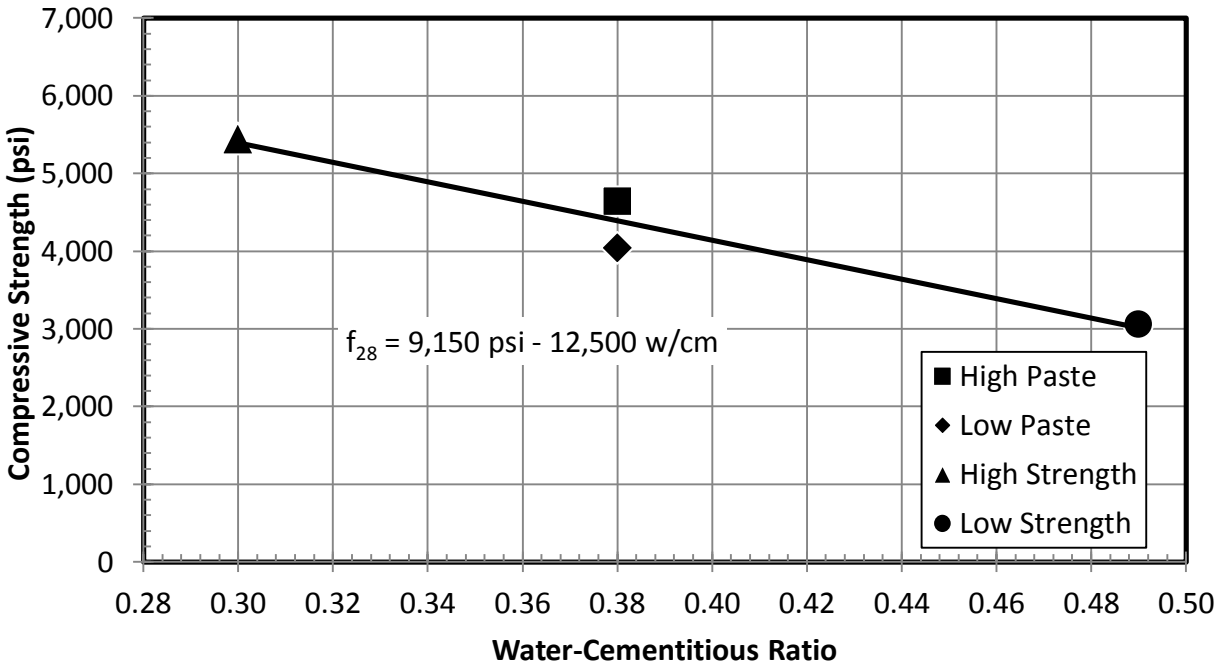

Figure A.10: Day 28 Comp. Strength vs. W/CM Ratio: Pasco Mixtures

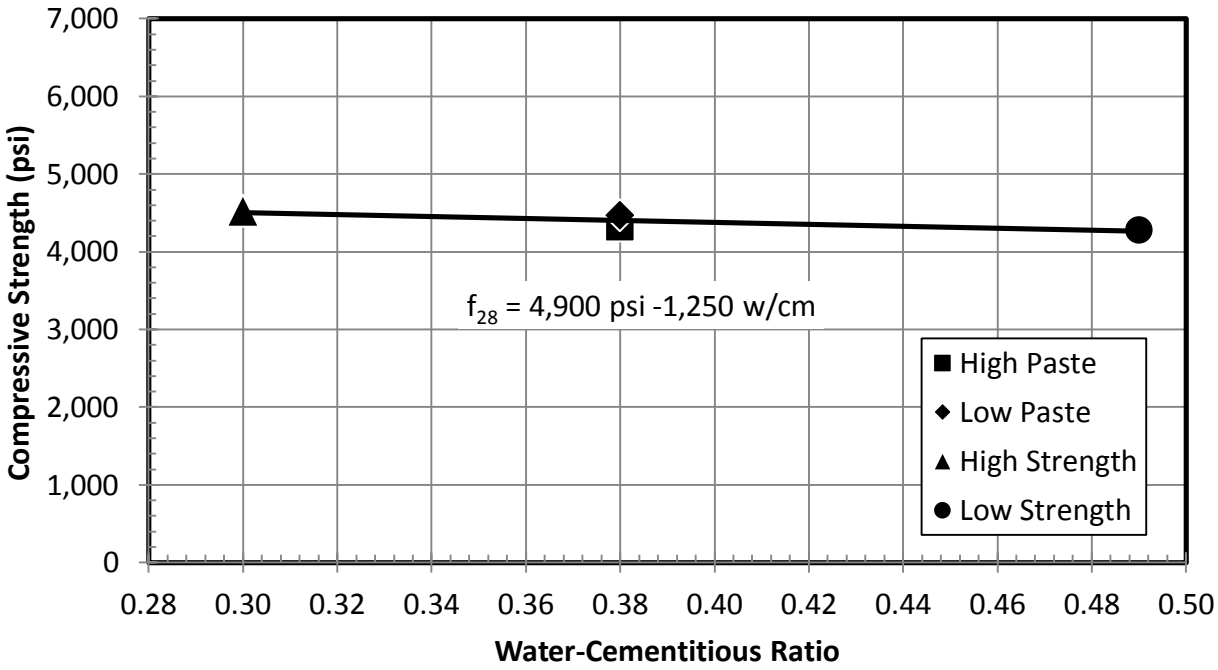

Figure A.11: Day 28 Comp. Strength vs. W/CM Ratio: Rock Island Mixtures

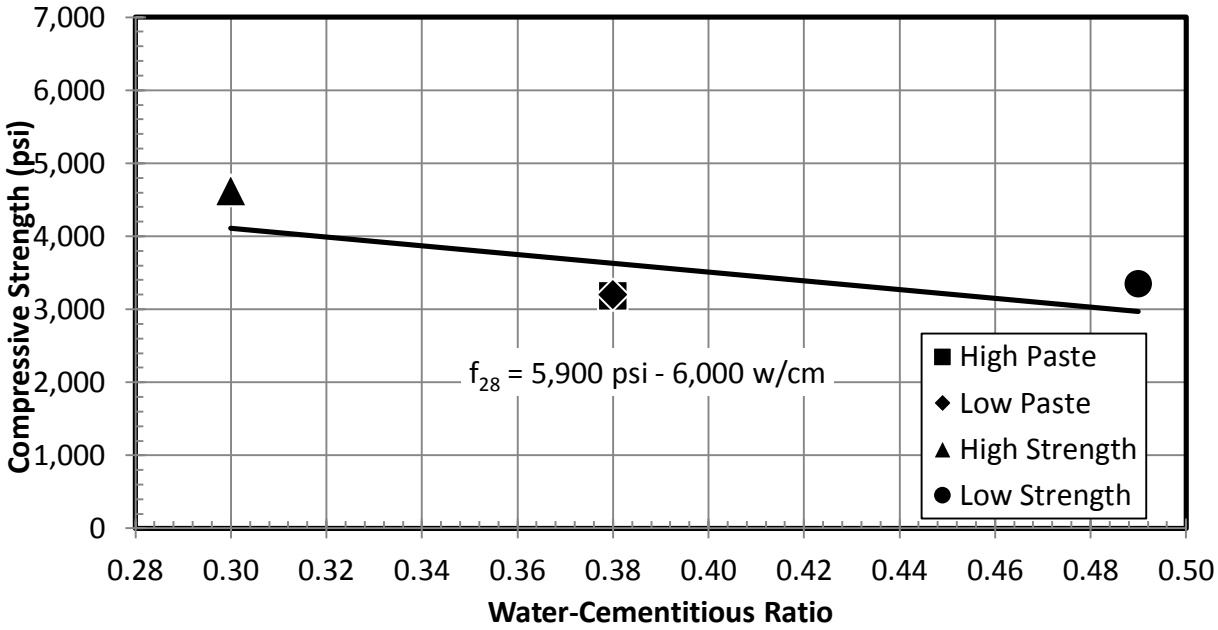

Figure A.12: Day 28 Comp. Strength vs. W/CM Ratio: Santosh Mixtures

A.2: RATE OF STRENGTH GAIN

The compressive strengths for each mixture were normalized by the Day 28 strength and fit to Equation 2.1. The optimized K1 and K2 values are listed in Table A.7 for all of the laboratory mixtures, with the exclusion of the DuPont (3/4-in.) mixtures. The fitted curves of the four laboratory mixtures (high and low paste and high and low strength) are shown for each laboratory aggregate source. The curves from DuPont (3/4-in.) mixture are excluded in this section, but can be seen in Figure 4.4. The following list of figures shows the fitted curves for each aggregate source: Figure A.13 for DuPont (3/8-in.), Figure A.14 for Okanogan Valley, Figure A.15 for Sullivan Road, Figure A.16 for Pasco, Figure A.17 for Rock Island, and Figure A.18 for Santosh mixtures.

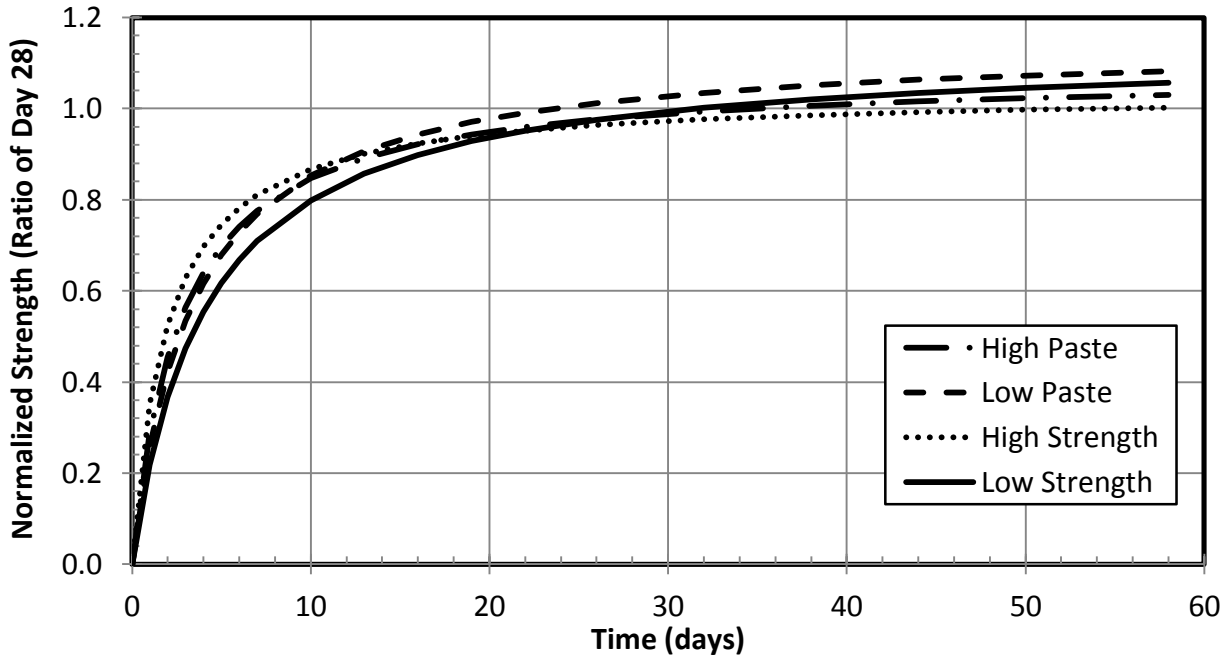

Figure A.13: Rate of Strength Gain Fitted Curves: DuPont (3/8-in.) Mixtures

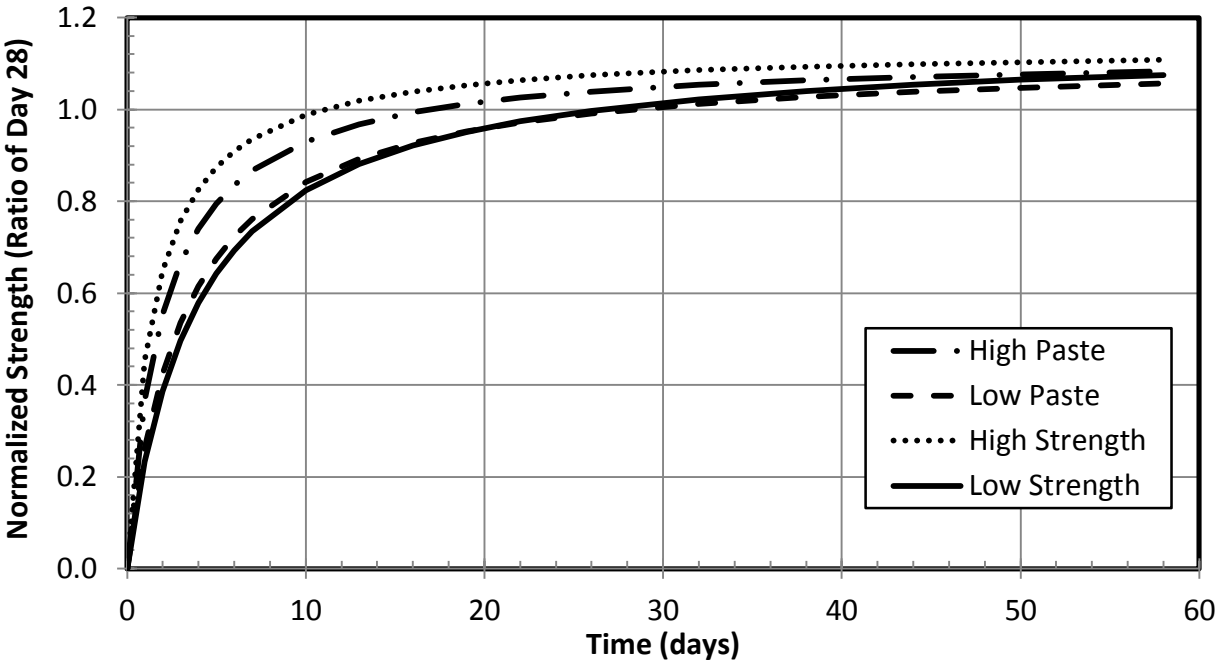

Figure A.14: Rate of Strength Gain Fitted Curves: Okanogan Valley Mixtures

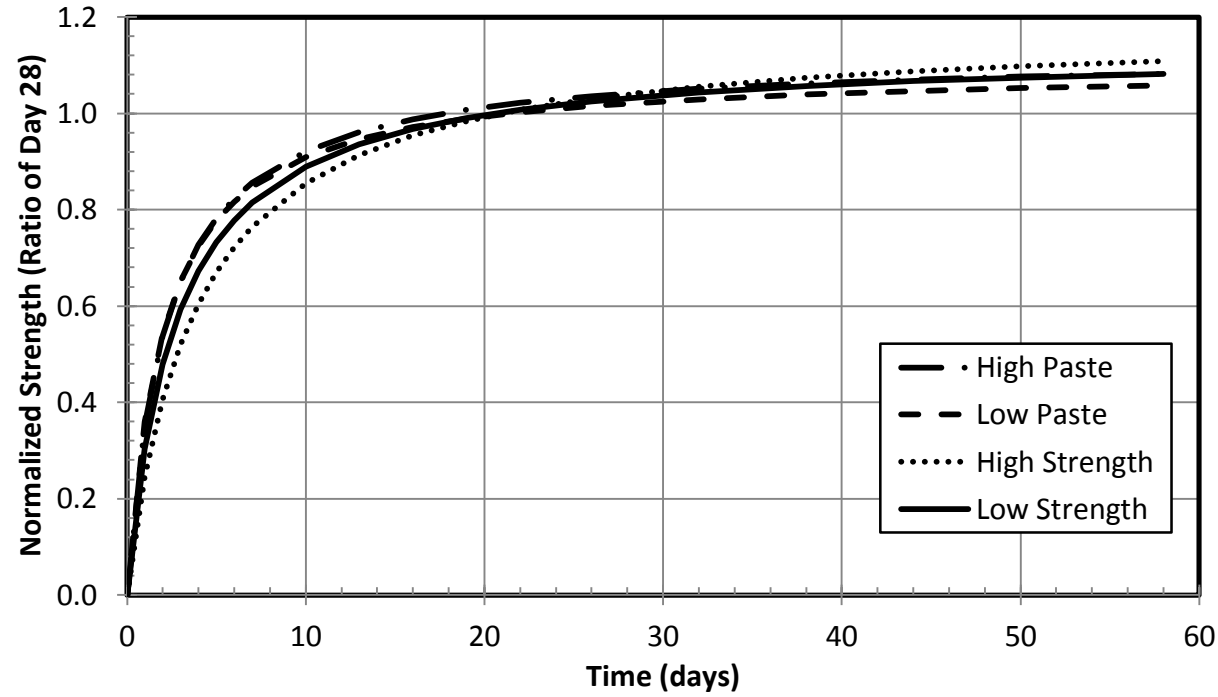

Figure A.15: Rate of Strength Gain Fitted Curves: Sullivan Road Mixtures

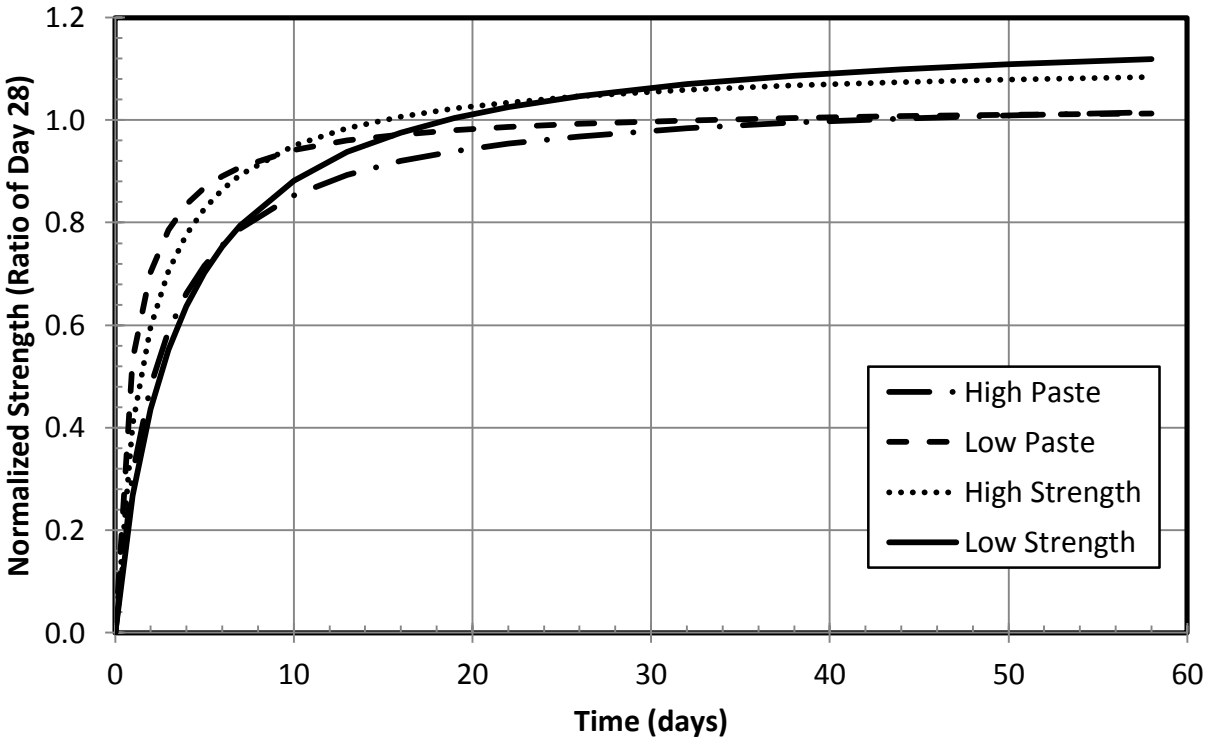

Figure A.16: Rate of Strength Gain Fitted Curves: Pasco Mixtures

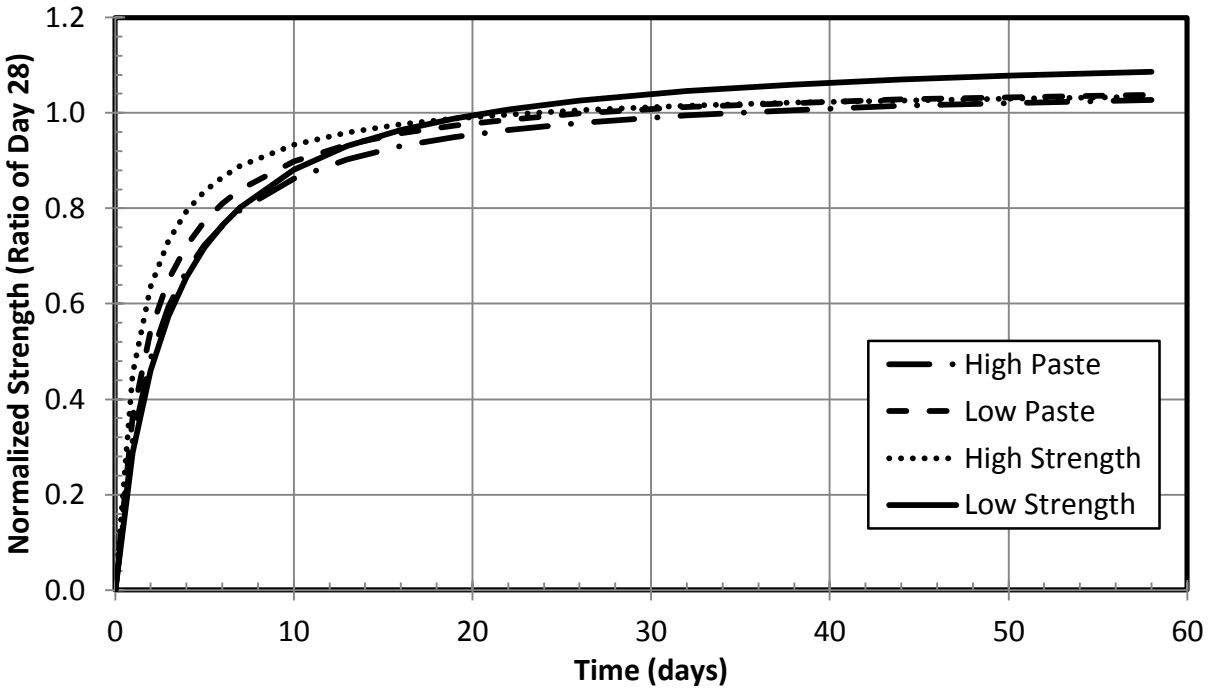

Figure A.17: Rate of Strength Gain Fitted Curves: Rock Island Mixtures

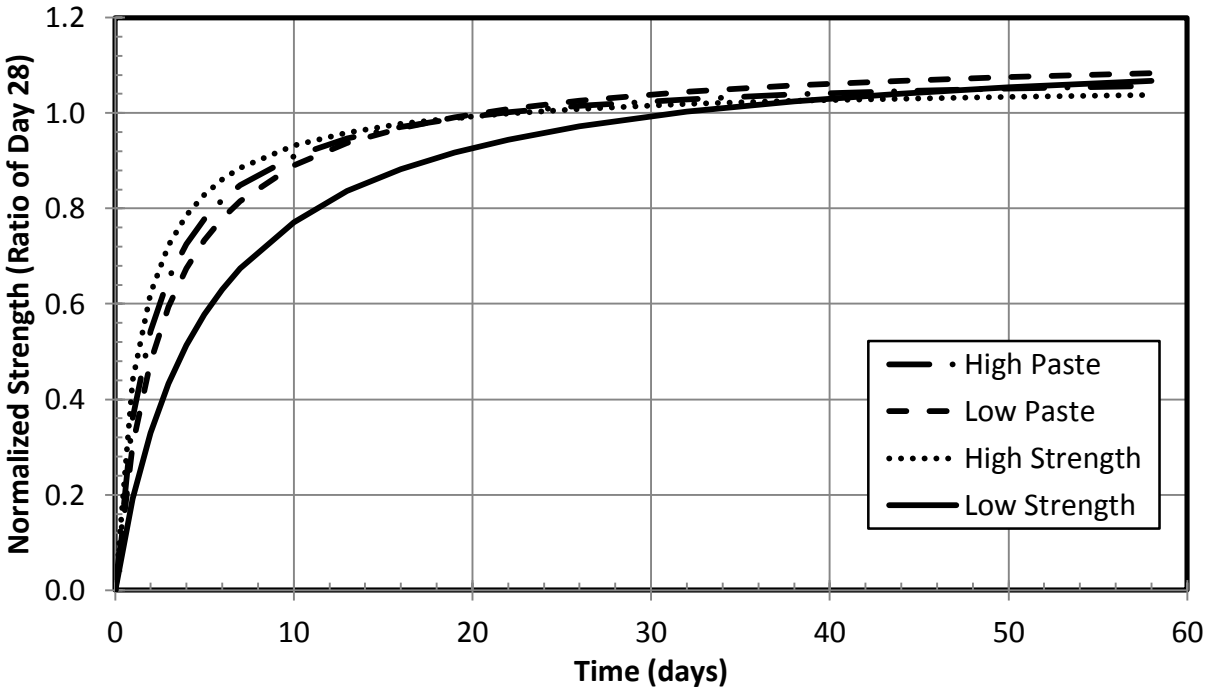

Figure A.18: Rate of Strength Gain Fitted Curves: Santosh Mixtures

Appendix B: Elastic Modulus Test Results

B.1: SUMMARY OF MEASURED ELASTIC MODULI

The measured elastic modulus values from the four test dates are shown in this section for each laboratory mixture. The elastic moduli from DuPont (3/4-in.) mixture are excluded in this section, but are listed in Table 6.1. The following set of tables list the measured elastic moduli for each laboratory aggregate: Table B.1 for DuPont (3/8-in.), Table B.2 for Okanogan Valley, Table B.3 for Sullivan Road, Table B.4 for Pasco, Table B.5 for Rock Island, and Table B.6 for Santosh mixtures.

Table B.1: Measured Elastic Moduli: DuPont (3/8-in.) Mixtures

Mixture	Paste Content (%)	Water-Cementitious Ratio	Day 7 (psi)	Day 14 (psi)	Day 28 (psi)	Day 56 (psi)
High Paste	33.2	0.38	4,040	4,470	4,680	4,590
Low Paste	26.1	0.38	4,530	4,660	4,500	4,850
High Strength	28.2	0.33	3,910	4,170	4,400	4,720
Low Strength	29.3	0.49	3,010	3,170	3,400	3,660

Table B.2: Measured Elastic Moduli: Okanogan Valley Mixtures

Mixture	Paste Content (%)	Water-Cementitious Ratio	Day 7 (psi)	Day 14 (psi)	Day 28 (psi)	Day 56 (psi)
High Paste	30.5	0.38	4,230	4,420	4,410	5,000
Low Paste	24.0	0.38	3,820	4,100	4,150	4,500
High Strength	27.0	0.30	4,460	4,580	4,830	5,290
Low Strength	27.0	0.49	3,870	4,000	4,380	4,380

Table B.3: Measured Elastic Moduli: Sullivan Road Mixtures

Mixture	Paste Content (%)	Water-Cementitious Ratio	Day 7 (psi)	Day 14 (psi)	Day 28 (psi)	Day 56 (psi)
High Paste	30.5	0.38	3,620	3,830	4,040	4,300
Low Paste	24.0	0.38	3,760	3,980	4,000	4,360
High Strength	27.0	0.30	4,790	5,090	5,250	5,570
Low Strength	27.0	0.49	3,670	3,710	4,180	4,230

Table B.4: Measured Elastic Moduli: Pasco Mixtures

Mixture	Paste Content (%)	Water-Cementitious Ratio	Day 7 (psi)	Day 14 (psi)	Day 28 (psi)	Day 56 (psi)
High Paste	30.5	0.38	3,810	3,900	4,050	4,310
Low Paste	24.0	0.38	3,610	4,090	4,280	4,600
High Strength	27.0	0.30	4,510	4,840	4,950	4,930
Low Strength	27.0	0.49	3,310	3,640	3,590	3,760

Table B.5: Measured Elastic Moduli: Rock Island Mixtures

Mixture	Paste Content (%)	Water-Cementitious Ratio	Day 7 (psi)	Day 14 (psi)	Day 28 (psi)	Day 56 (psi)
High Paste	30.5	0.38	3,100	3,660	3,860	3,990
Low Paste	24.0	0.38	3,710	3,670	4,020	4,240
High Strength	27.0	0.30	3,560	3,820	3,980	4,140
Low Strength	27.0	0.49	3,480	3,350	4,130	4,340

Table B.6: Measured Elastic Moduli: Santosh Mixtures

Mixture	Paste Content (%)	Water-Cementitious Ratio	Day 7 (psi)	Day 14 (psi)	Day 28 (psi)	Day 56 (psi)
High Paste	30.5	0.38	3,200	3,350	3,660	3,760
Low Paste	24.0	0.38	3,390	3,480	3,840	3,880
High Strength	27.0	0.30	3,870	4,000	4,230	4,350
Low Strength	27.0	0.49	3,350	3,410	3,760	3,950

B.2: DAY 28 ELASTIC MODULI VS. WATER-CEMENTITIOUS RATIOS

The effect of the water-cementitious ratio on the elastic modulus for each laboratory mixture is shown in the follow set of figures. The results of the elastic moduli verses the water-cementitious ratios from DuPont (3/4-in.) mixture are excluded in this section, but are shown in Figure 6.1. The following figures show the measured Day 28 elastic moduli against the water-cementitious ratios for each laboratory mixture: Figure B.1 for DuPont (3/8-in.), Figure B.2 for Okanogan Valley, Figure B.3 for Sullivan Road, Figure B.4 for Pasco, Figure B.5 for Rock Island, and Figure B.6 for Santosh mixtures.

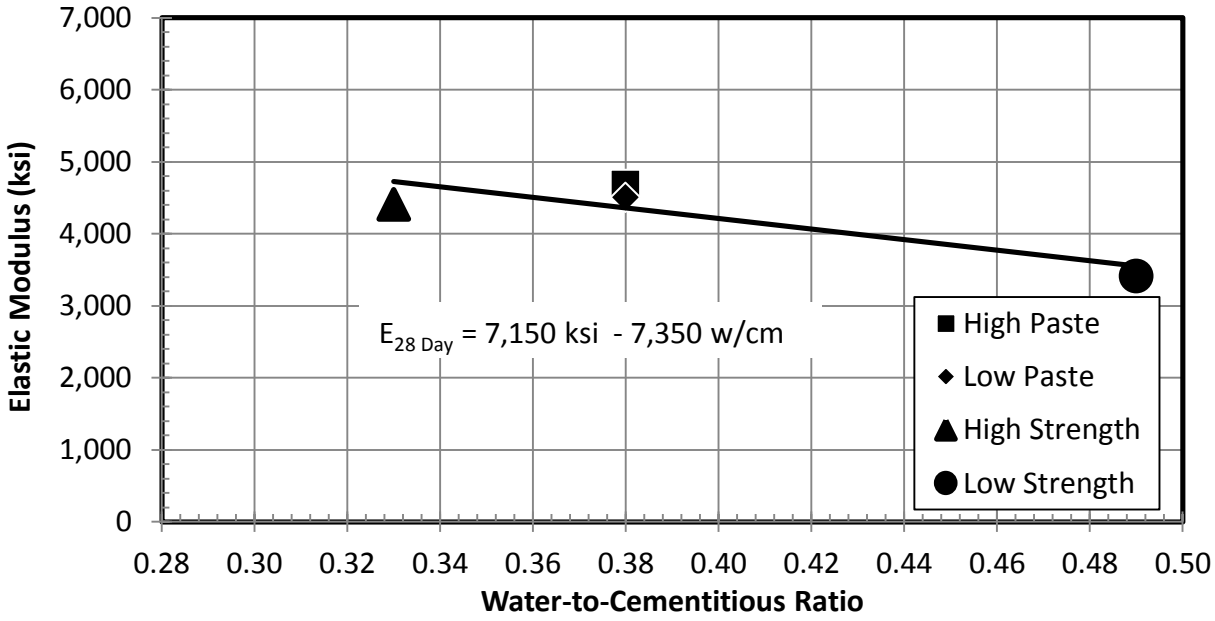

Figure B.1: Day 28 Elastic Modulus vs. W/CM Ratio: DuPont (3/8-in.) Mixtures

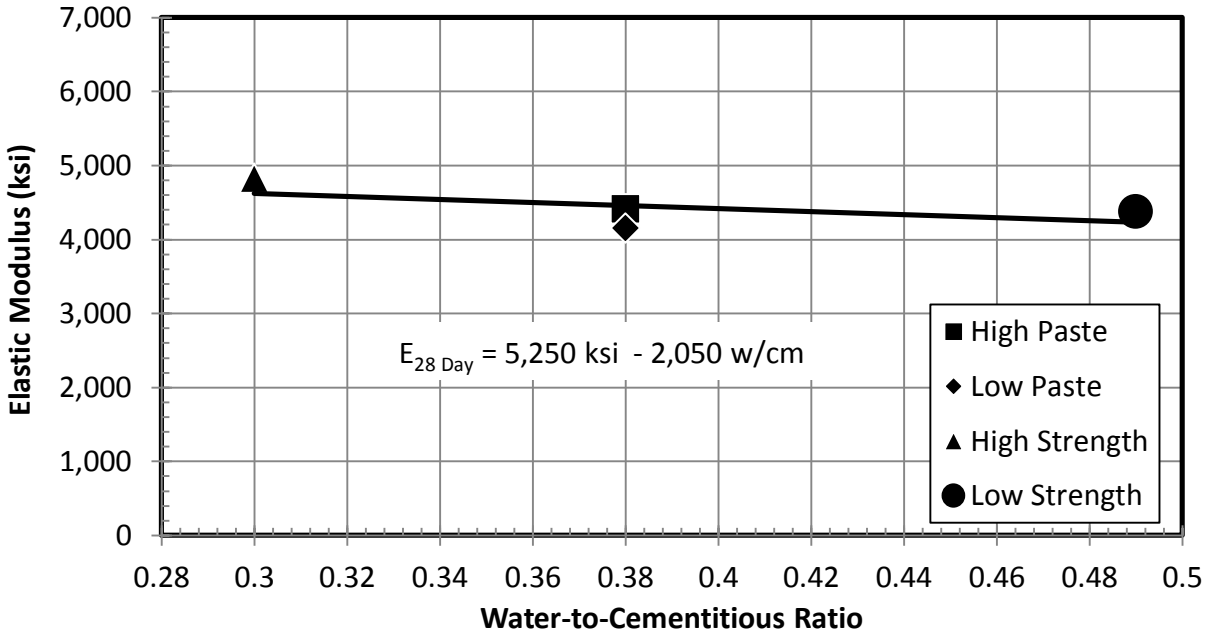

Figure B.2: Day 28 Elastic Modulus vs. W/CM Ratio: Okanogan Valley Mixtures

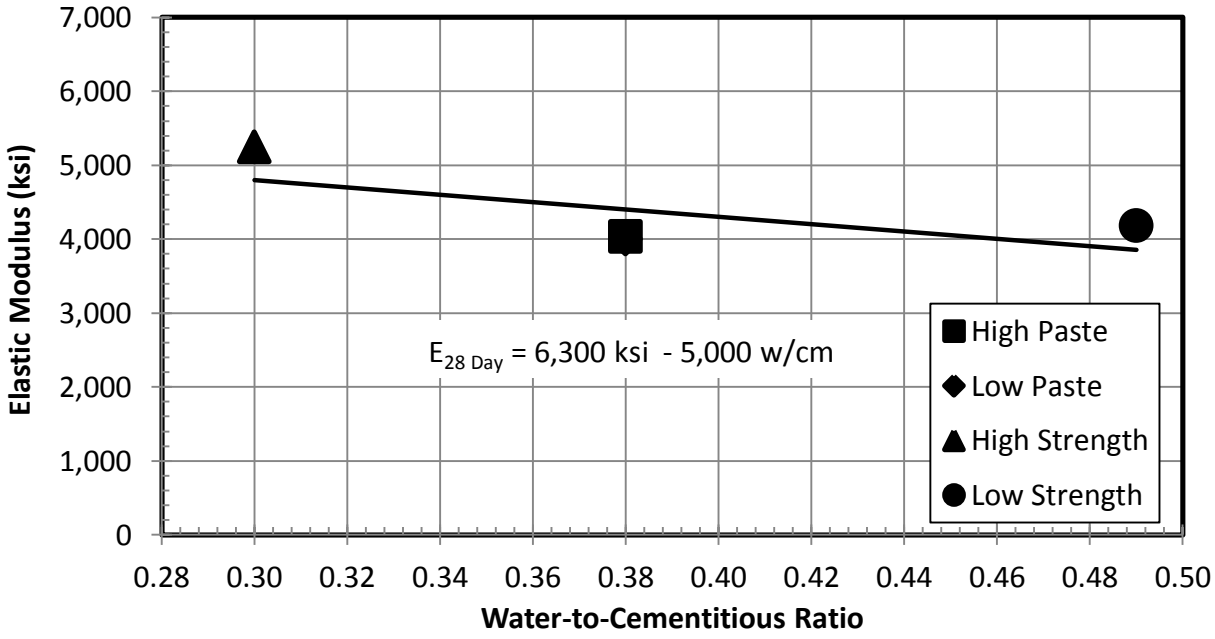

Figure B.3: Day 28 Elastic Modulus vs. W/CM Ratio: Sullivan Road Mixtures

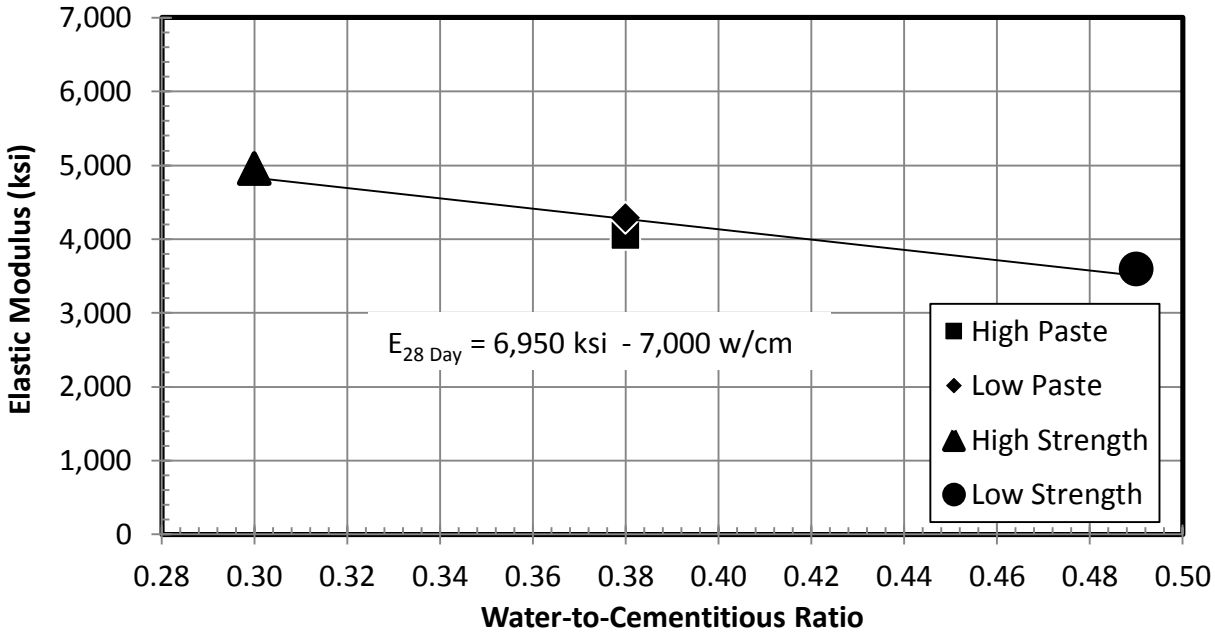

Figure B.4: Day 28 Elastic Modulus vs. W/CM Ratio: Pasco Mixtures

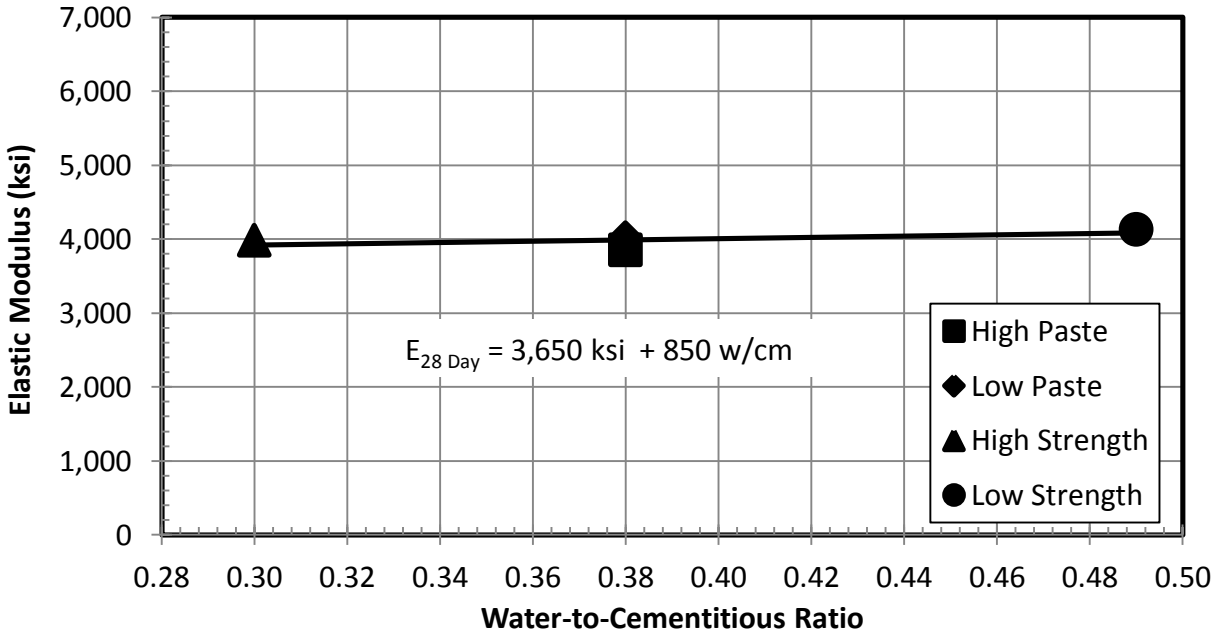

Figure B.5: Day 28 Elastic Modulus vs. W/CM Ratio: Rock Island Mixtures

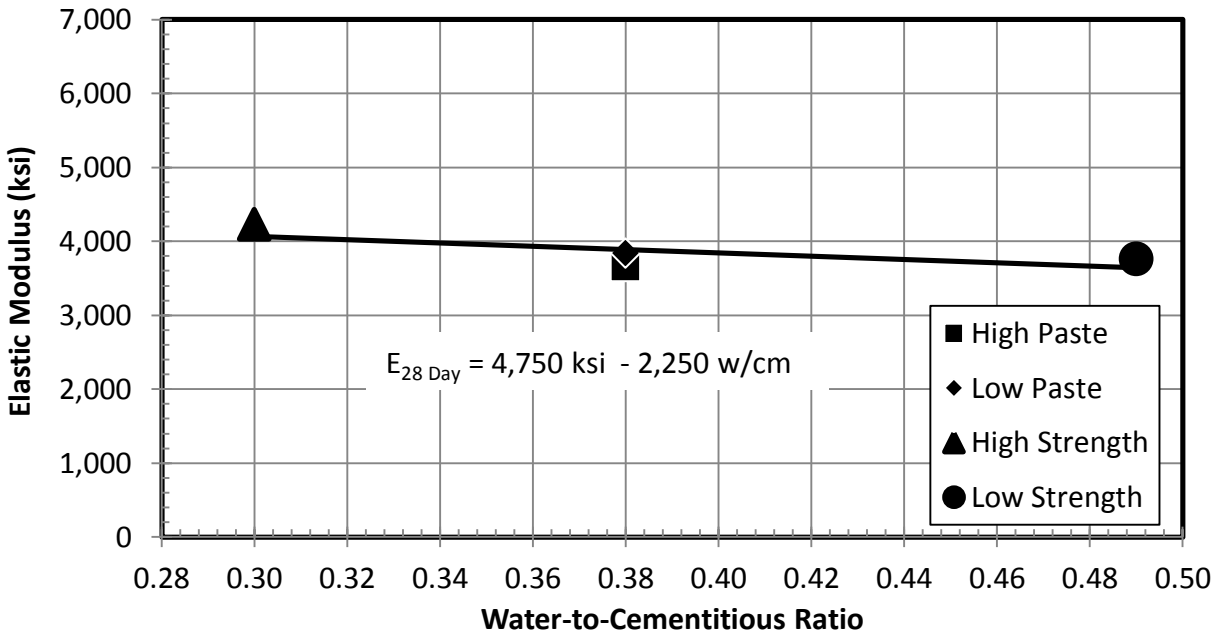

Figure B.6: Day 28 Elastic Modulus vs. W/CM Ratio: Santosh Mixtures

B.3: MEASURED ELASTIC MODULI VS. COMPRESSIVE STRENGTHS

The effect of the compressive strength on the elastic moduli of the four testing days from each laboratory mixture is shown in the follow set of figures. The figures will include the predicted elastic moduli from the AASHTO specifications (5.4.2.4-1, Equation 2.7). The results of the elastic moduli verses the compressive strengths from DuPont (3/4-in.) mixture are excluded in this section, but are shown in Figure 6.2. The following lists the figures with the elastic moduli plotted against the compressive strengths of the four testing days (the Day 28 elastic modulus symbol are increased in size and have a hollow fill) for each laboratory aggregate: Figure B.7 for DuPont (3/8-in.), Figure B.8 for Okanogan Valley, Figure B.9 for Sullivan Road, Figure B.10 for Pasco, Figure B.11 for Rock Island, and Figure B.12 for Santosh mixtures.

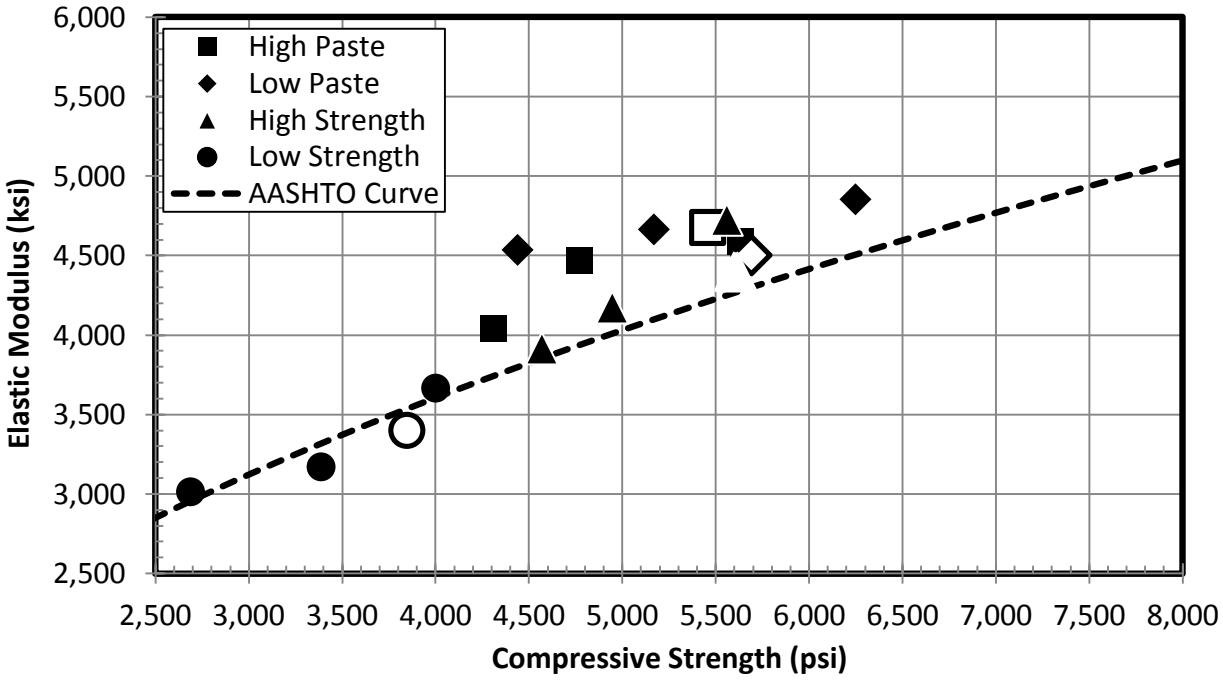

Figure B.7: Elastic Modulus vs. Compressive Strength: DuPont (3/8-in.) Mixtures

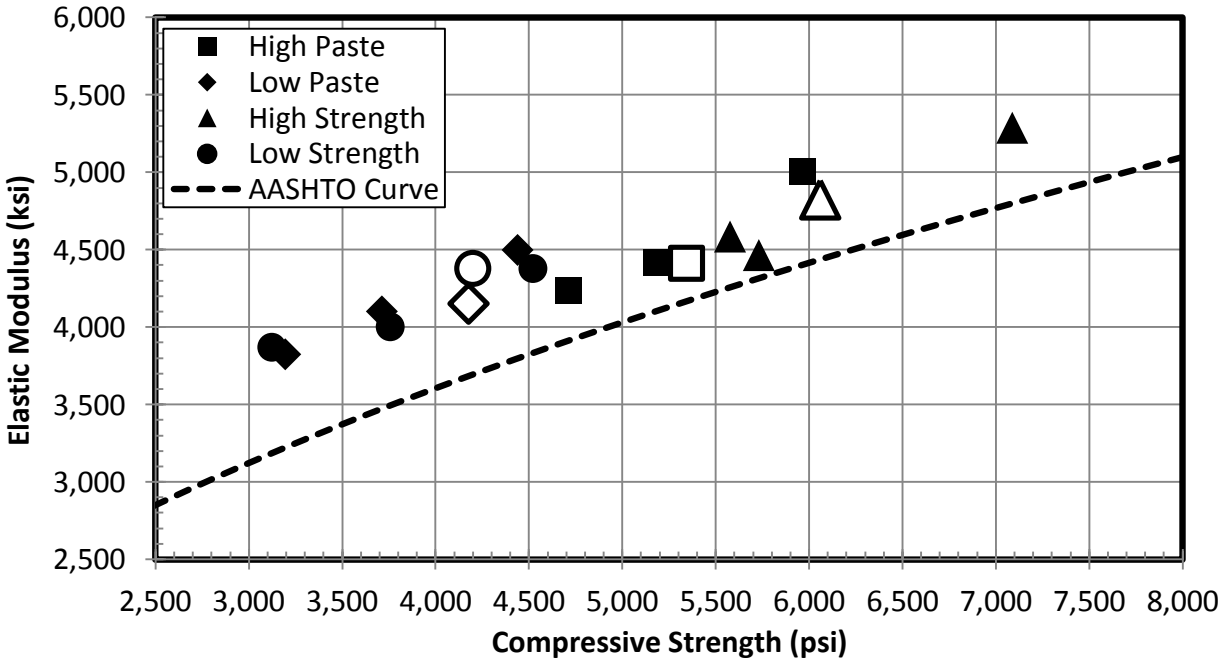

Figure B.8: Elastic Modulus vs. Compressive Strength: Okanogan Valley Mixtures

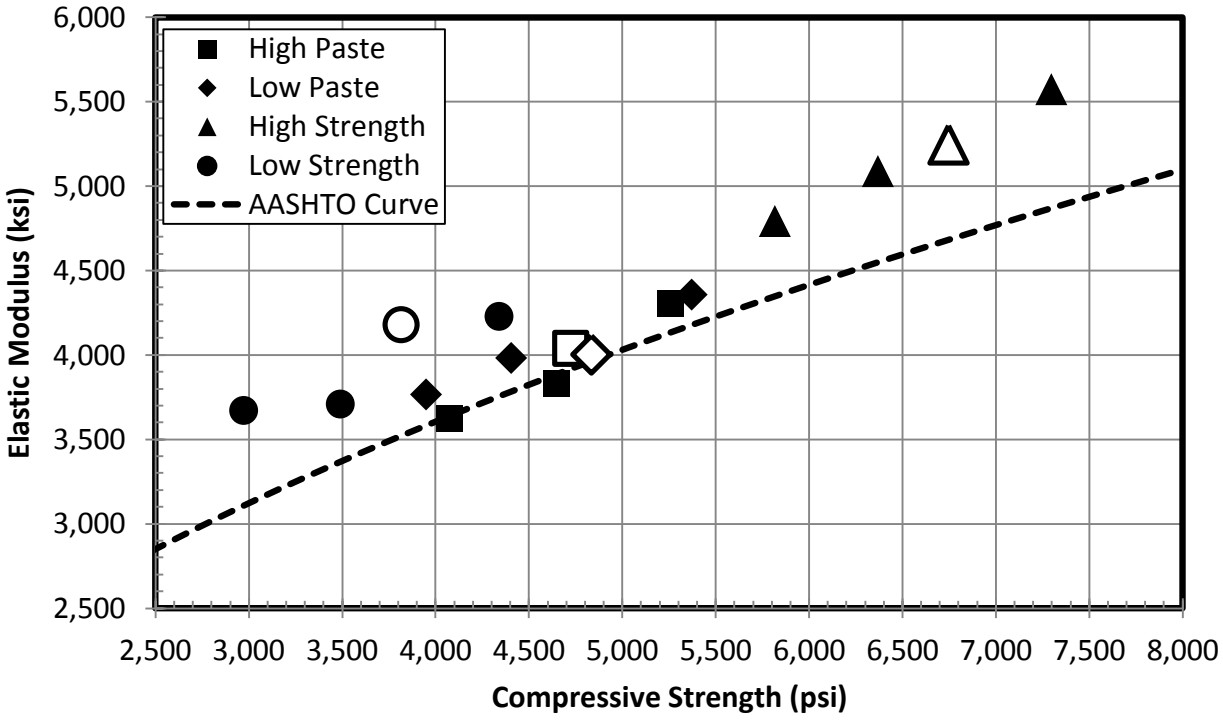

Figure B.9: Elastic Modulus vs. Compressive Strength: Sullivan Road Mixtures

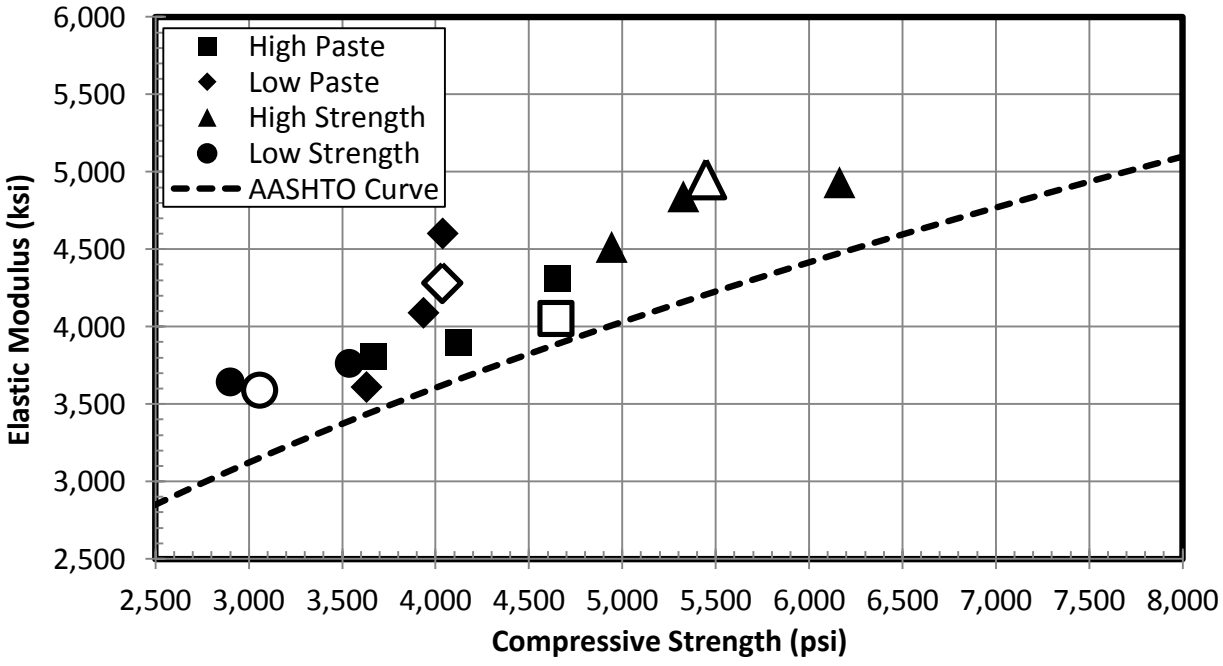

Figure B.10: Elastic Modulus vs. Compressive Strength: Pasco Mixtures

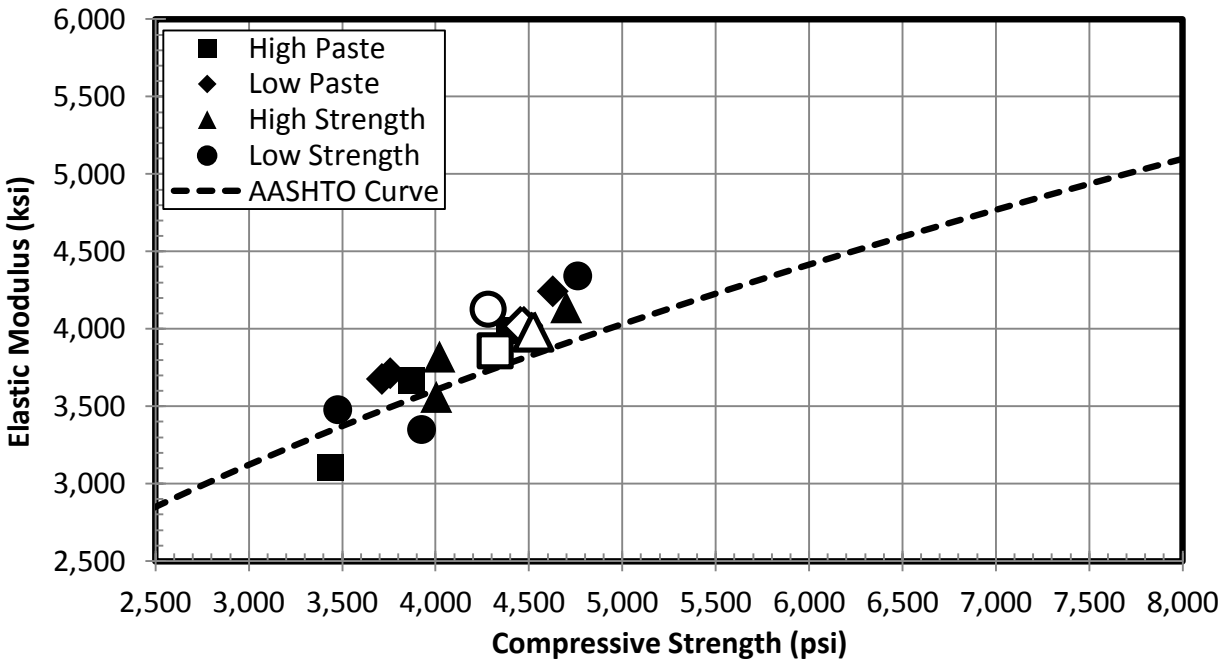

Figure B.11: Elastic Modulus vs. Compressive Strength: Rock Island Mixtures

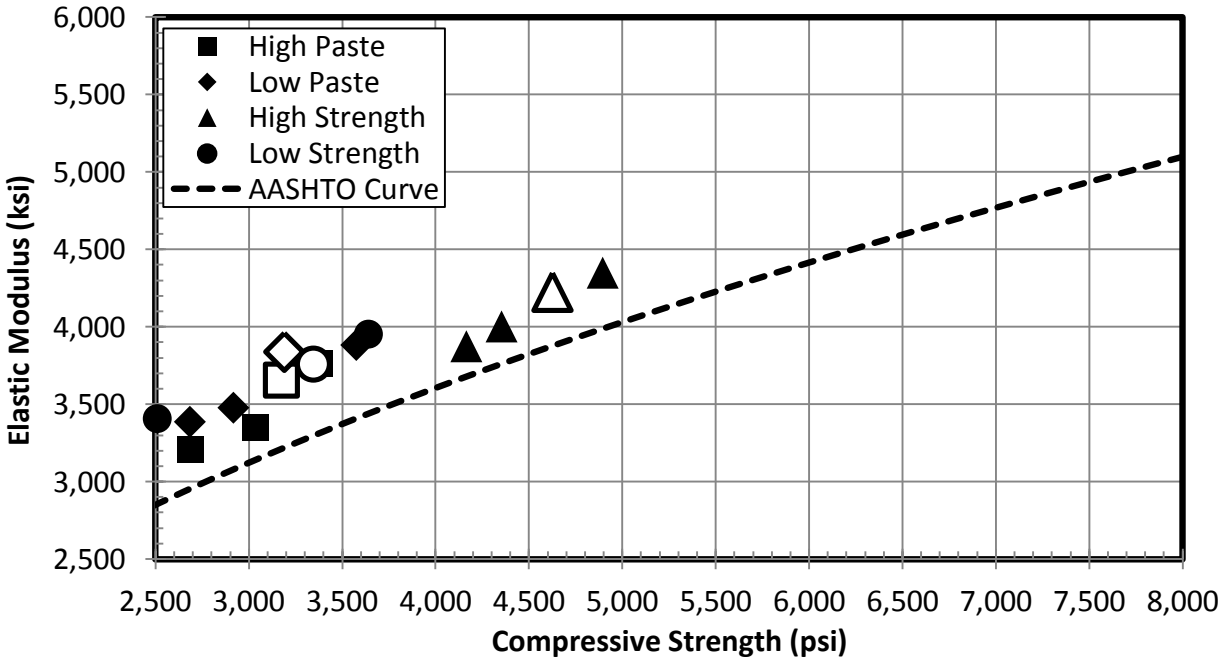

Figure B.12: Elastic Modulus vs. Compressive Strength: Santosh Mixtures

B.4: RATE OF STIFFNESS GAIN

The elastic moduli from the four testing dates were normalized by dividing by the Day 28 elastic modulus for each laboratory mixture. The normalized data was fit to Equation 6.2. The fitted curves for the elastic moduli from DuPont (3/4-in.) mixture are excluded in this section, but are shown in Figure 6.6. The optimized values and curve fits of the elastic moduli are listed in the following tables and figures for each laboratory aggregate: Table B.7 and Figure B.13 for DuPont (3/8-in.), Table B.8 and Figure B.14 for Okanogan Valley, Table B.9 and Figure B.15 for Sullivan Road, Table B.10 and Figure B.16 for Pasco, Table B.11 and Figure B.17 for Rock Island, and Table B.12 and Figure B.18 for Santosh mixtures.

Table B.7: Optimized Constants for DuPont (3/8-in.) Aggregate

Mixture	E_{28} (ksi)	K1	K2	E_7/E_{28}	E_{56}/E_{28}
High Paste	4,680	1.2	0.98	0.86	0.98
Low Paste	4,500	0.3	0.95	1.01	1.08
High Strength	4,400	1.5	0.93	0.89	1.07
Low Strength	3,400	1.6	0.93	0.89	1.08
Average	4,250	1.1	0.94	0.91	1.05
St. Deviation	580	0.6	0.02	0.06	0.05
Coef. of Variation	13.6%	50.4%	2.4%	7.1%	4.5%

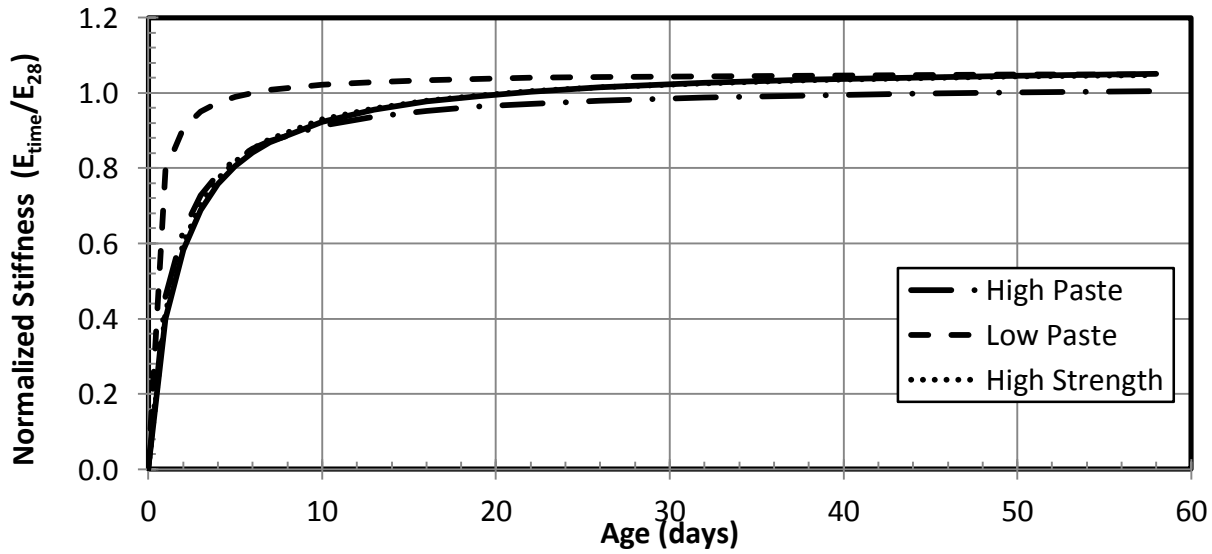

Figure B.13: Rate of Stiffness Gain Fitted Curves: DuPont (3/8-in.) Mixtures

Table B.8: Optimized Constants for Okanogan Valley Aggregate

Mixture	E_{28} (ksi)	K1	K2	E_7/E_{28}	E_{56}/E_{28}
High Paste	4,190	1.1	0.91	0.96	1.13
Low Paste	4,050	1.2	0.93	0.92	1.08
High Strength	4,870	1.4	0.92	0.92	1.10
Low Strength	4,460	1.2	0.98	0.88	1.00
Average	4,390	1.2	0.93	0.92	1.08
St. Deviation	360	0.1	0.03	0.03	0.06
Coef. of Variation	8.2%	10.4%	3.2%	3.3%	5.3%

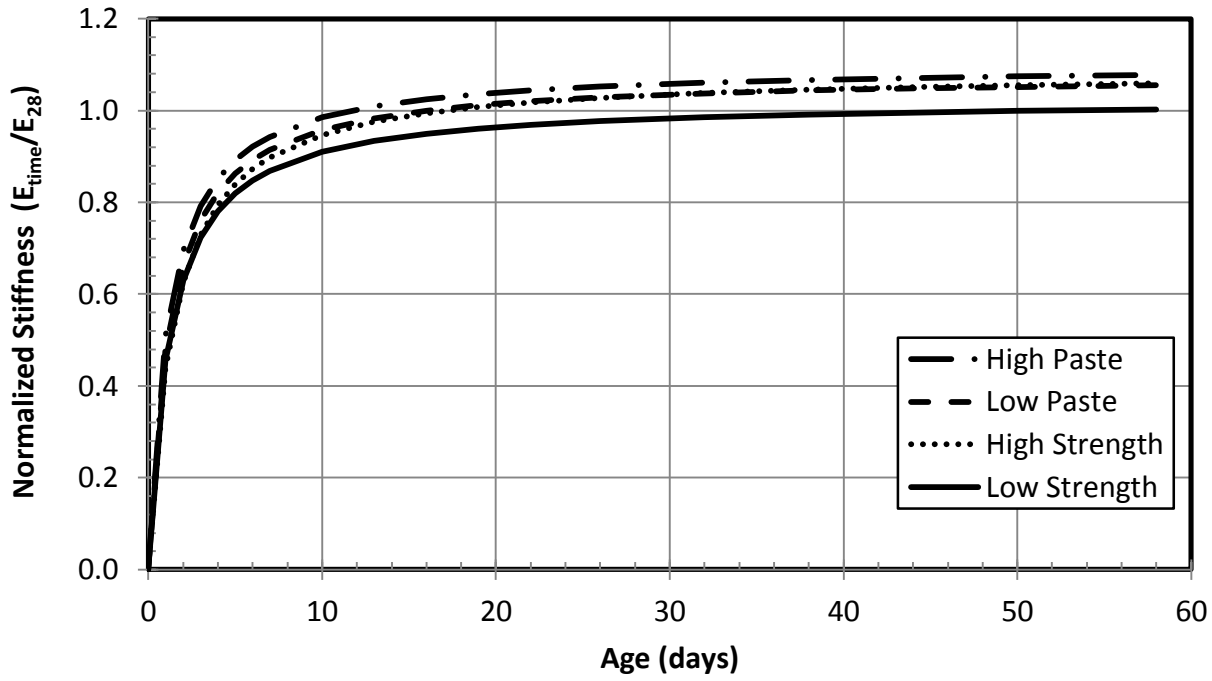

Figure B.14: Rate of Stiffness Gain Fitted Curves: Okanogan Valley Mixtures

Table B.9: Optimized Constants for Sullivan Road Aggregate

Mixture	E_{28} (ksi)	K1	K2	E_7/E_{28}	E_{56}/E_{28}
High Paste	4,040	1.4	0.93	0.90	1.07
Low Paste	4,000	1.0	0.93	0.94	1.09
High Strength	5,250	1.2	0.94	0.91	1.06
Low Strength	4,180	1.3	0.97	0.88	1.01
Average	4,370	1.2	0.94	0.91	1.06
St. Deviation	590	0.2	0.02	0.03	0.03
Coef. of Variation	13.5%	12.7%	2.2%	2.9%	3.1%

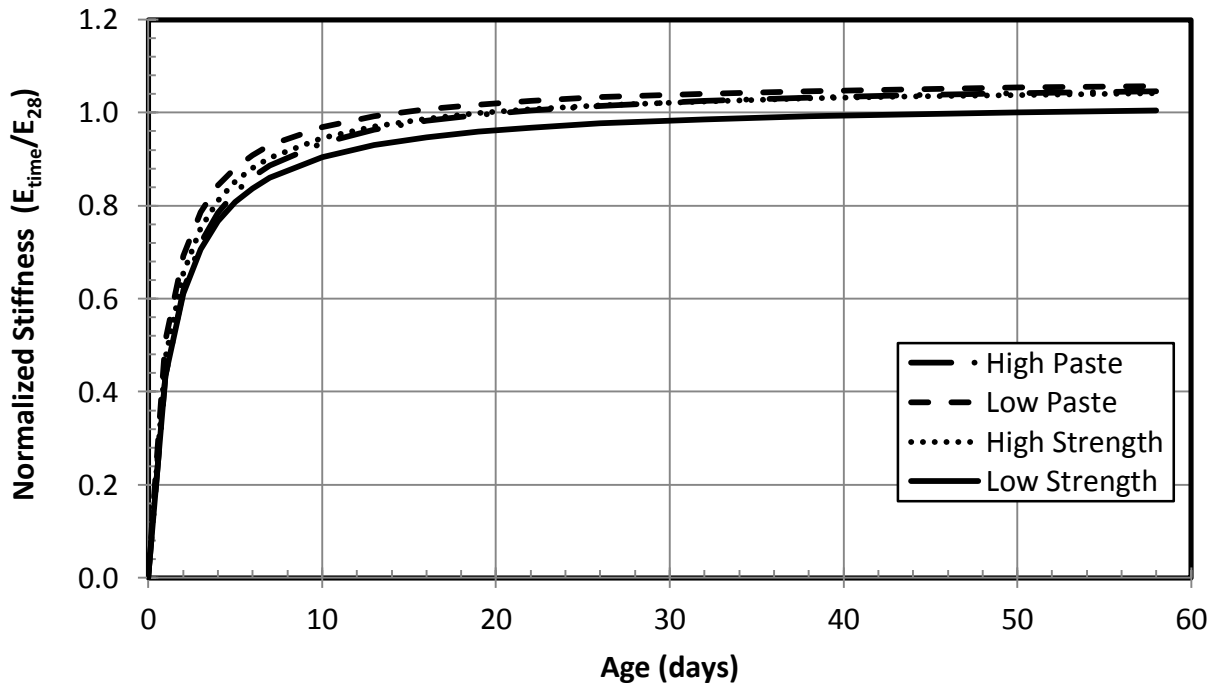

Figure B.15: Rate of Stiffness Gain Fitted Curves: Sullivan Road Mixtures

Table B.10: Optimized Constants for Pasco Aggregate

Mixture	E_{28} (ksi)	K1	K2	E_7/E_{28}	E_{56}/E_{28}
High Paste	4,050	0.9	0.95	0.94	1.06
Low Paste	4,280	2.0	0.91	0.84	1.07
High Strength	4,950	0.8	0.98	0.91	1.00
Low Strength	3,590	1.0	0.94	0.92	1.05
Average	4,220	1.2	0.95	0.90	1.04
St. Deviation	570	0.6	0.03	0.04	0.03
Coef. of Variation	13.5%	47.4%	2.8%	4.7%	3.3%

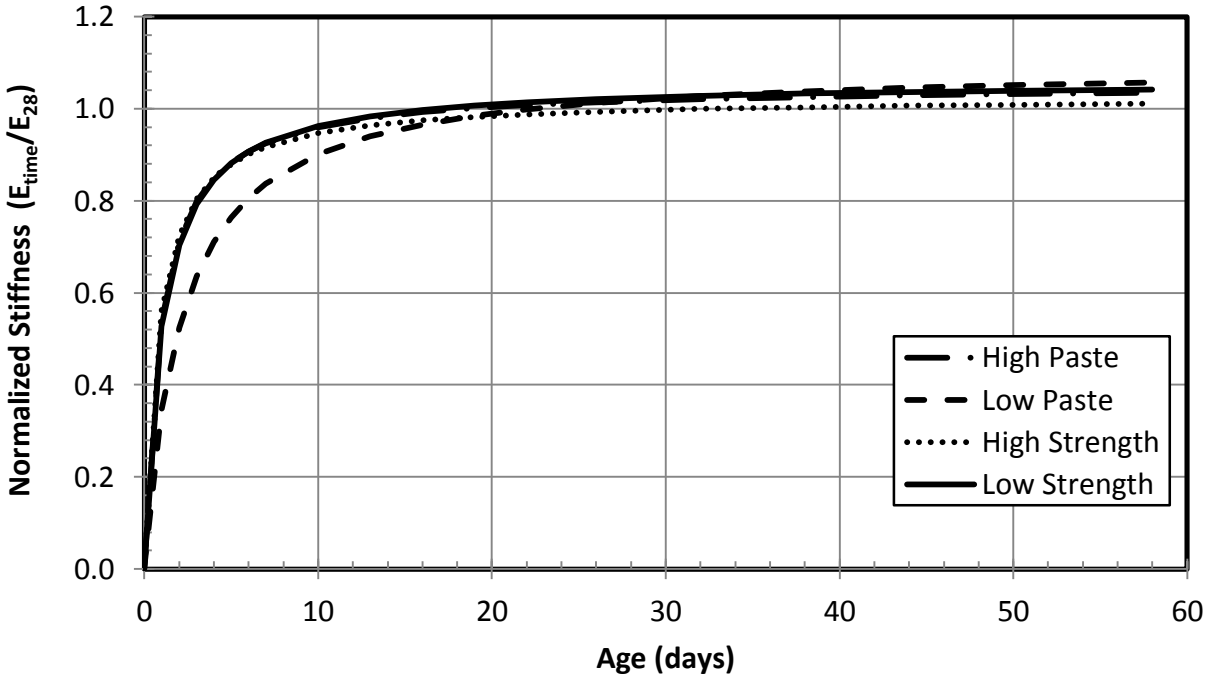

Figure B.16: Rate of Stiffness Gain Fitted Curves: Pasco Mixtures

Table B.11: Optimized Constants for Rock Island Aggregate

Mixture	E_{28} (ksi)	K1	K2	E_7/E_{28}	E_{56}/E_{28}
High Paste	3,860	2.2	0.92	0.80	1.03
Low Paste	4,020	1.2	0.95	0.92	1.06
High Strength	3,980	1.3	0.95	0.89	1.04
Low Strength	4,130	2.3	0.94	0.84	1.05
Average	4,000	1.7	0.94	0.87	1.04
St. Deviation	110	0.6	0.01	0.05	0.01
Coef. of Variation	2.8%	33.7%	1.3%	6.2%	1.0%

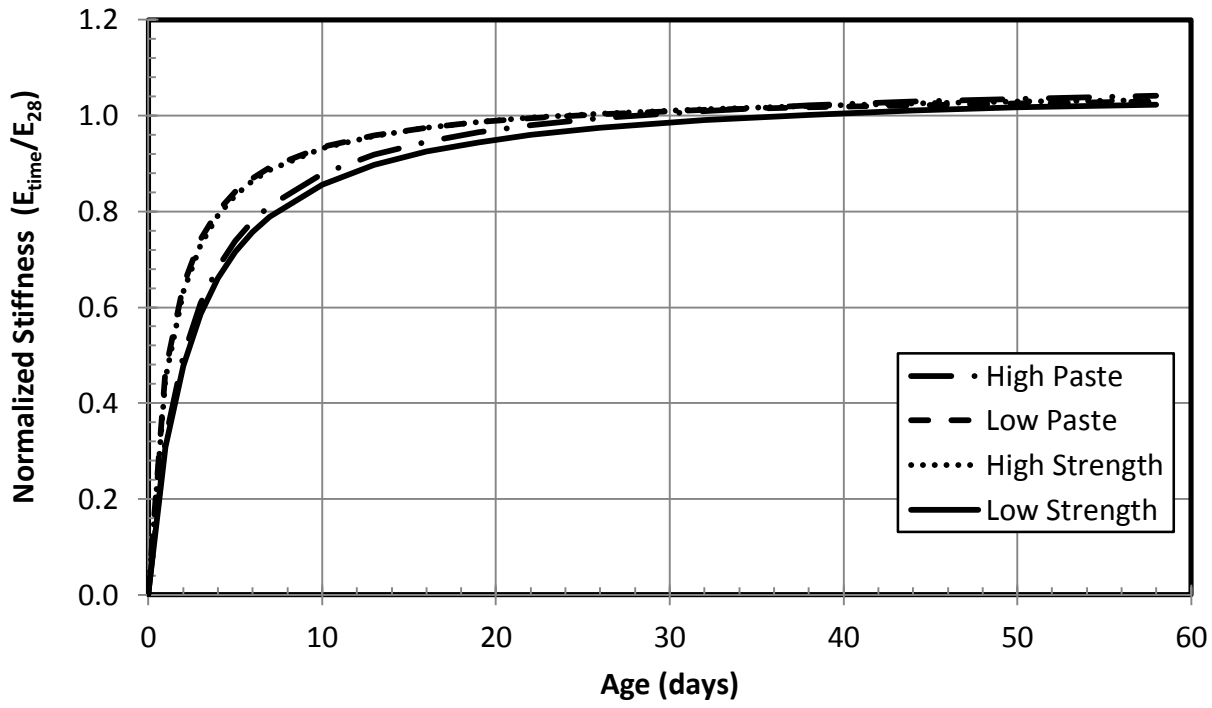

Figure B.17: Rate of Stiffness Gain Fitted Curves: Rock Island Mixtures

Table B.12: Optimized Constants for Santosh Aggregate

Mixture	E_{28} (ksi)	K1	K2	E_7/E_{28}	E_{56}/E_{28}
High Paste	3,660	1.4	0.96	0.88	1.03
Low Paste	3,840	1.2	0.97	0.88	1.01
High Strength	4,230	0.9	0.96	0.92	1.03
Low Strength	3,760	1.4	0.95	0.89	1.05
Average	3,870	1.3	0.96	0.89	1.03
St. Deviation	250	0.2	0.01	0.02	0.02
Coef. of Variation	6.5%	18.1%	1.2%	2.0%	1.6%

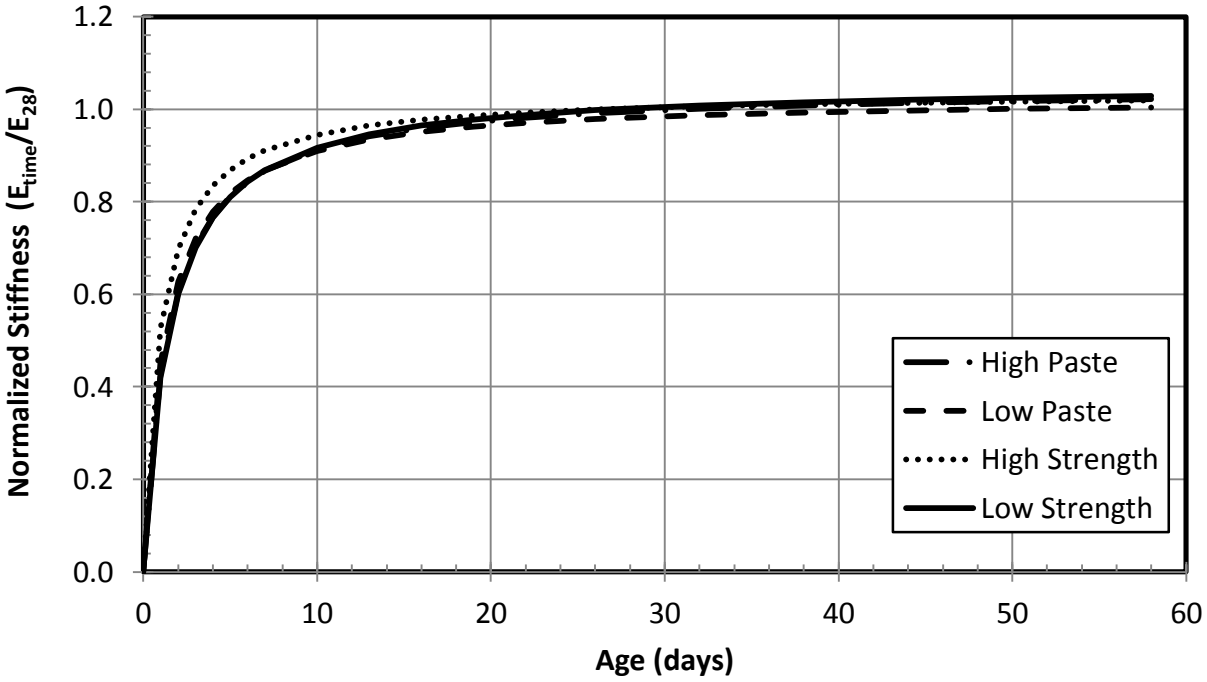

Figure B.18: Rate of Stiffness Gain Fitted Curves: Santosh Mixtures

Appendix C: Dry Shrinkage Results

C.1: DRYING SHRINKAGE FITTED CURVES

The fitted drying shrinkage curves from the four laboratory mixtures of each aggregate source are plotted in the following figures. The fitted drying shrinkage curves from DuPont (3/4-in.) mixture are excluded in this section, but can be seen in Figure 7.2. The following list of figures depicts the fitted curves for the four laboratory mixtures of each aggregate source: Figure C.1 for DuPont (3/8-in.), Figure C.2 for Okanogan Valley, Figure C.3 for Sullivan Road, Figure C.4 for Pasco, Figure C.5 for Rock Island, and Figure C.6 for Santosh mixtures.

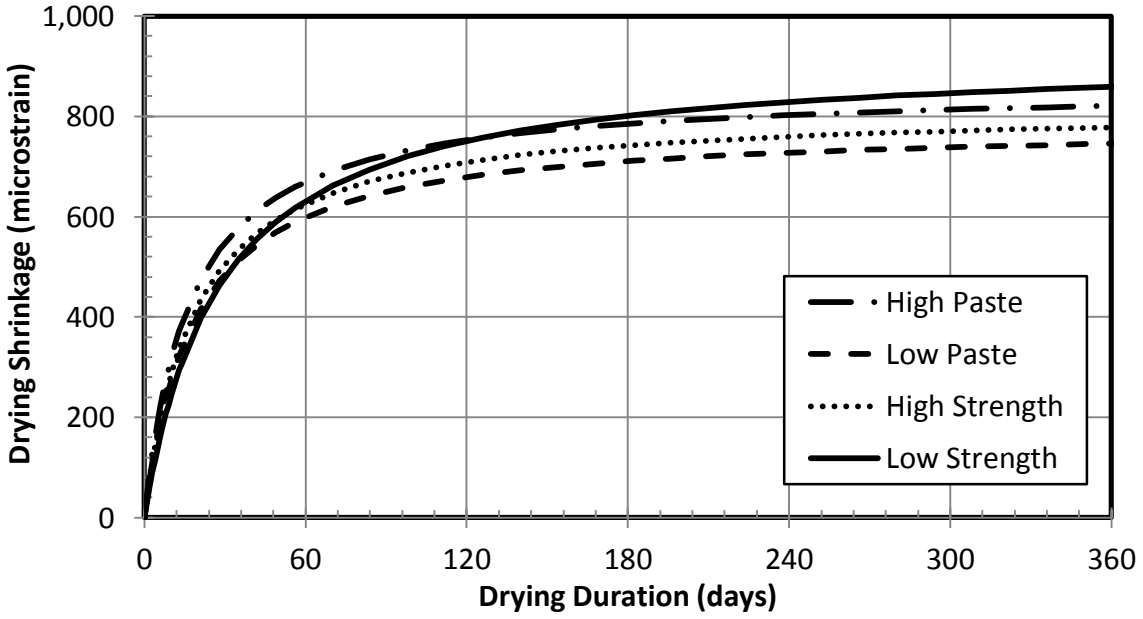

Figure C.1: Fitted Dry Shrinkage Data: DuPont (3/8-in.) Mixtures

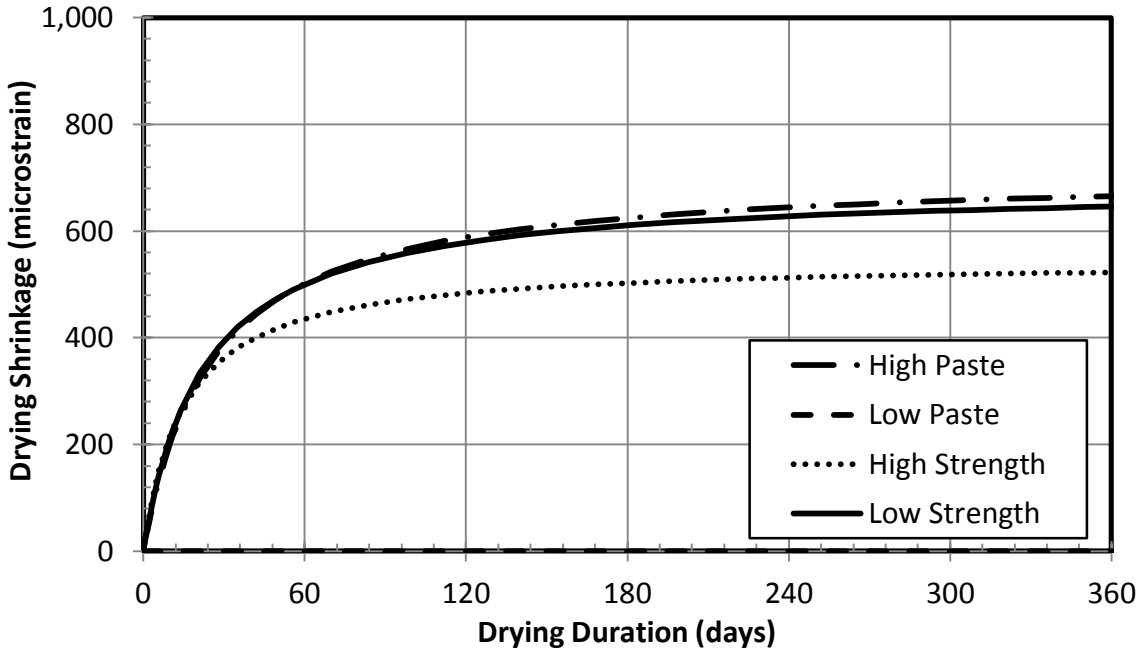

Figure C.2: Fitted Dry Shrinkage Data: Okanogan Valley Mixtures

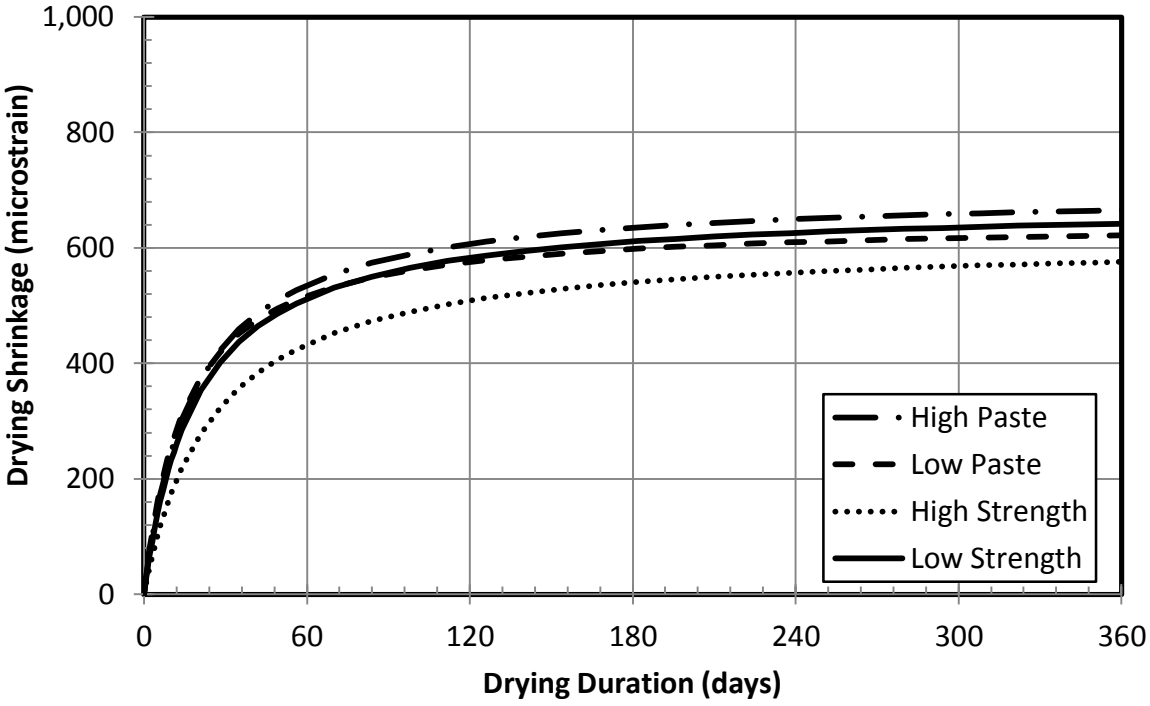

Figure C.3: Fitted Dry Shrinkage Sullivan Road Mixtures

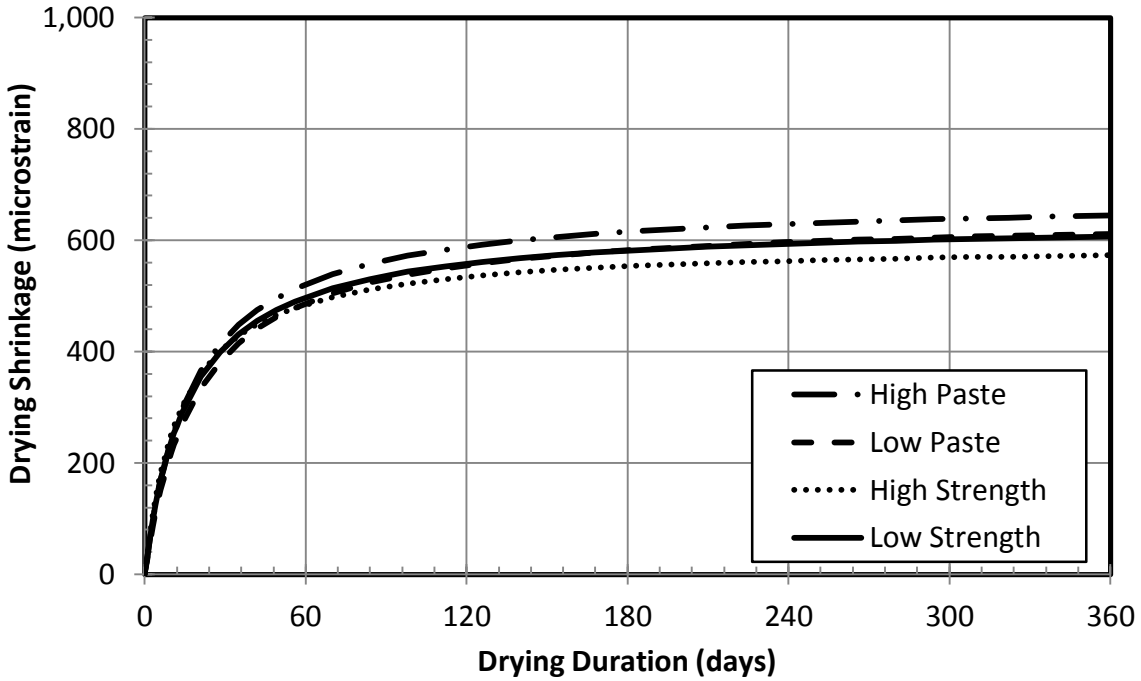

Figure C.4: Fitted Dry Shrinkage Data: Pasco Mixtures

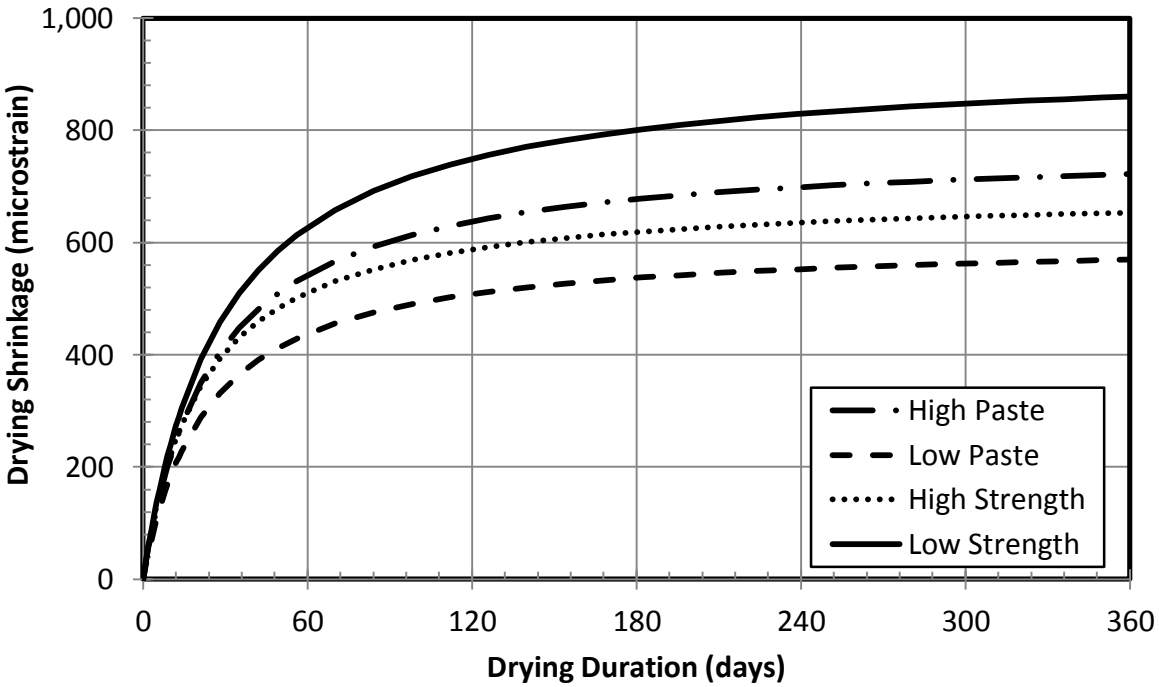

Figure C.5: Fitted Dry Shrinkage Data: Rock Island Mixtures

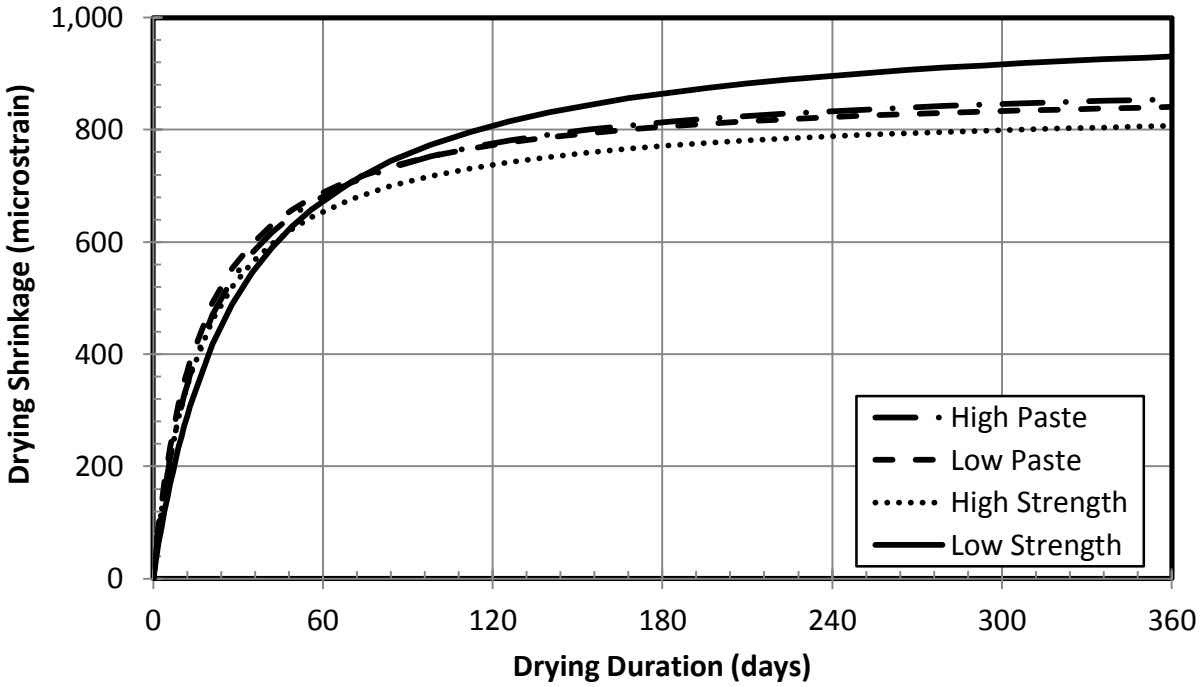

Figure C.6: Fitted Dry Shrinkage Data: Santosh Mixtures

C.2: DRYING SHRINKAGE FITTED CURVE VS. AASHTO PREDICTED CURVE

The fitted curves from the drying shrinkage beams and cylinders of the creep mixtures are compared against AASHTO specifications (5.4.2.3.3, Equation 2.9) in the following figures. The fitted curves from the drying shrinkage beams and cylinders of the DuPont (3/4-in.) high-paste mixture are excluded in this section, but can be seen in Figure 7.4. The following list of figures depicts the fitted curves for the drying shrinkage beams and cylinders for creep mixtures: Figure C.7 for DuPont (3/4-in.) low-paste, Figure C.8 for DuPont (3/8-in.) high-paste, Figure C.9 for DuPont (3/8-in.) low-paste, Figure C.10 for Sullivan Road high-paste, and Figure C.11 for Sullivan Road low-paste mixture.

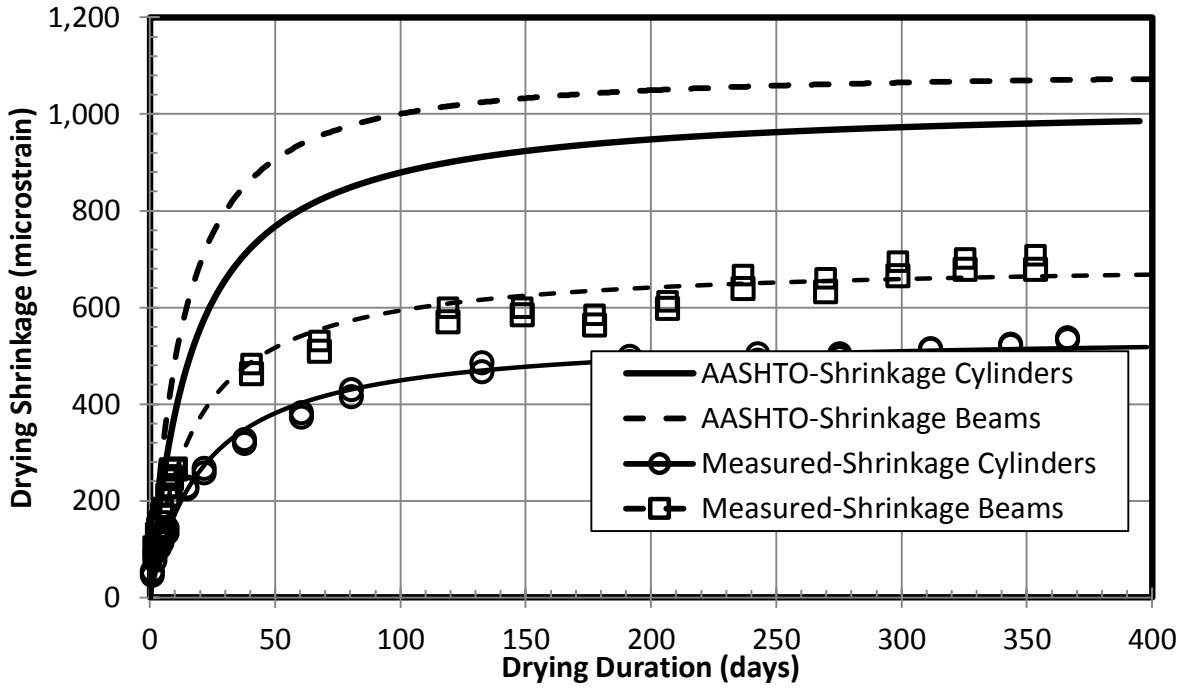

Figure C.7: AASHTO Drying Shrinkage Strains: DuPont (3/4-in.) Low-Paste

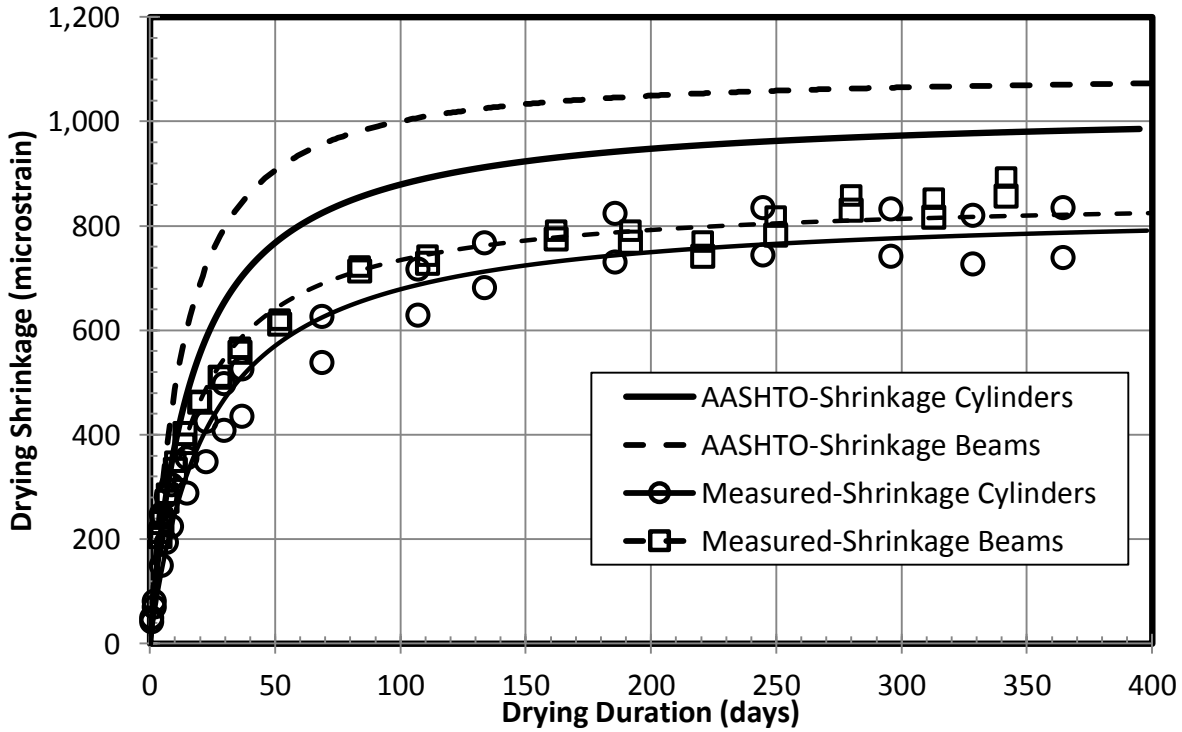

Figure C.8: AASHTO Drying Shrinkage Strains: DuPont (3/8-in.) High-Paste

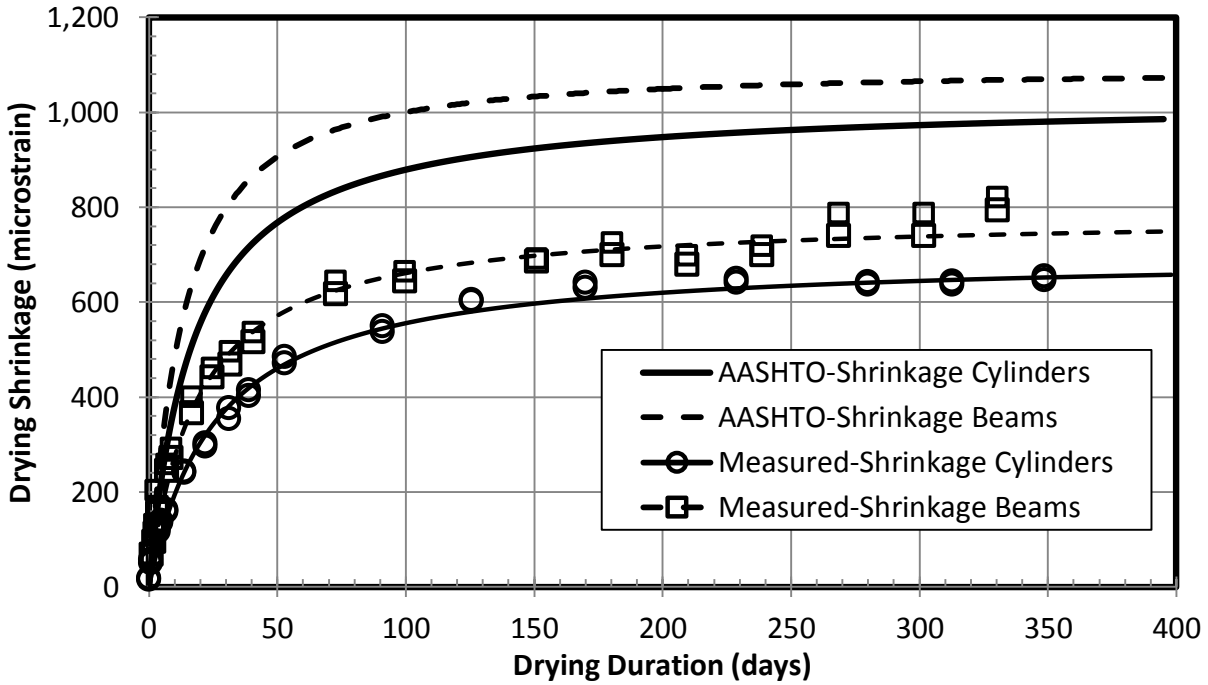

Figure C.9: AASHTO Drying Shrinkage Strains: DuPont (3/8-in.) Low-Paste

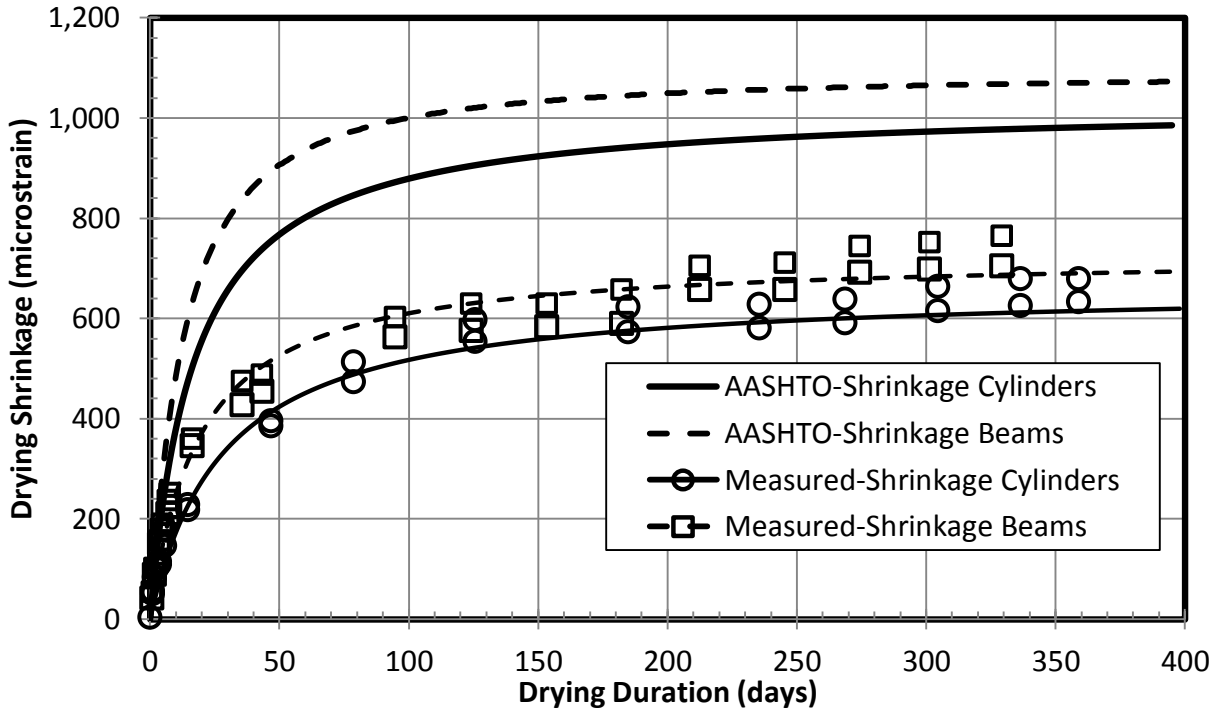

Figure C.10: AASHTO Drying Shrinkage Strains: Sullivan Road High-Paste

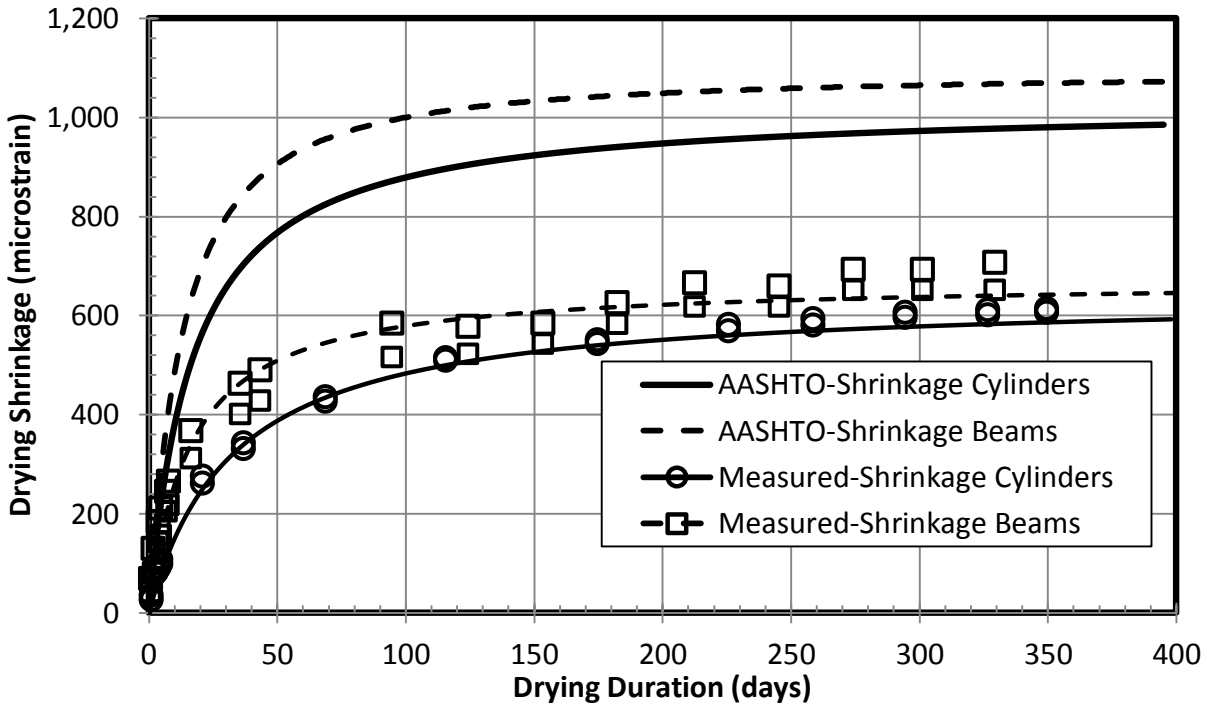

Figure C.11: AASHTO Drying Shrinkage Strains: Sullivan Road High-Paste

Appendix D: Creep Results

D.1: INITIAL GAUGE LENGTHS

The sealed and unsealed creep samples (two of each sample) were placed into the rig after fourteen days of curing. The gauge lengths of each creep sample were then measured, as per ASTM C512, to determine the starting lengths of each set of gauges. The creep samples were then loaded to the targeted thirty-five percent of the Day 14 compressive strength with a hydraulic ram. Once the required load was applied to the creep rig, locking nuts were fastened to maintain the stress on the samples. The lengths of each set of gauges were then measured again to record the deformation due to the application of the axial load on the samples.

The process of applying the load, fastening the nuts, and then measuring each set of gauges took around five minutes. This time allowed early creep deformations to take place between the first loading and initial readings. In order to remove that early creep from the measured data, the initial gauge lengths were extrapolated from the monitored values to a time of zero. This initial length also removes the elastic deformations, so only the time-dependent deformations are measured. To show an example of this process, the extrapolated initial length is shown from DuPont (3/4-in.) high-paste mixture (Unsealed Cylinder #1, north gauge set) in Figure D.1.

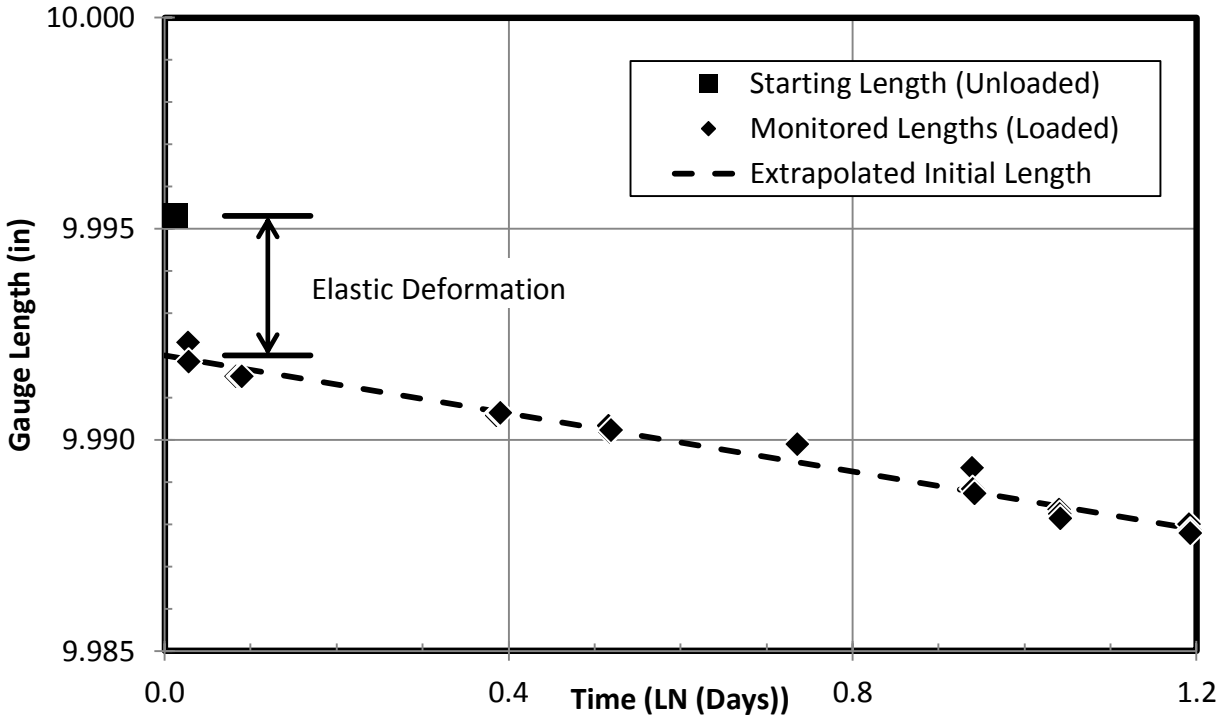

Figure D.1: Extrapolated Initial Lengths: DuPont (3/4-in.) High-Paste Mixture

D.2: TIME-DEPENDENT DEFORMATIONS

The monitored time-dependent strains and fitted curves from the creep (sealed and unsealed) and drying shrinkage cylinders are shown in this section for each aggregate source. The time-dependent strains from DuPont (3/4-in.) high-paste mixture are excluded in this section, but can be seen in Figure 8.1. The following list of figures depicts the monitored time-depended strains and fitted curves for each cylinder type and aggregate source: Figure D.2 for DuPont (3/4-in.) low-paste, Figure D.3 for DuPont (3/8-in.) high-paste, Figure D.4 for DuPont (3/8-in.) low-paste, Figure D.5 for Sullivan Road high-paste, and Figure D.6 for Sullivan Road low-paste mixture.

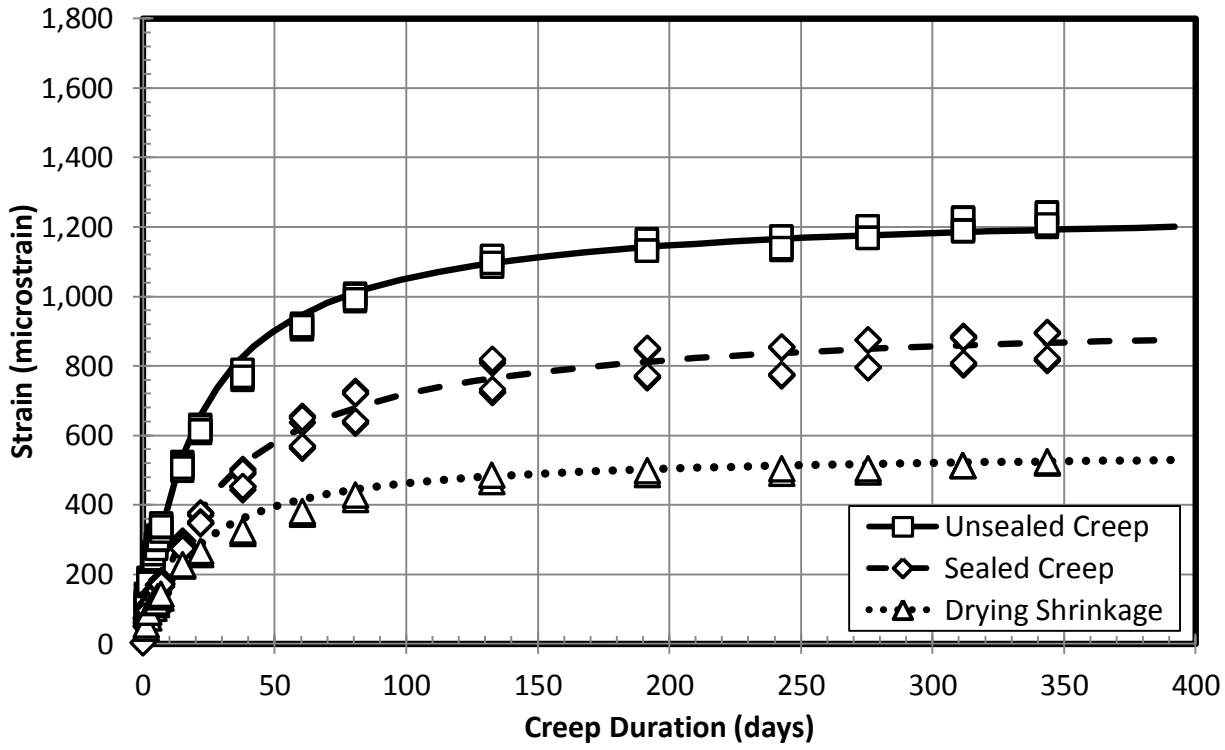

Figure D.2: Long-Term Deformations: DuPont (3/4-in.) Low-Paste

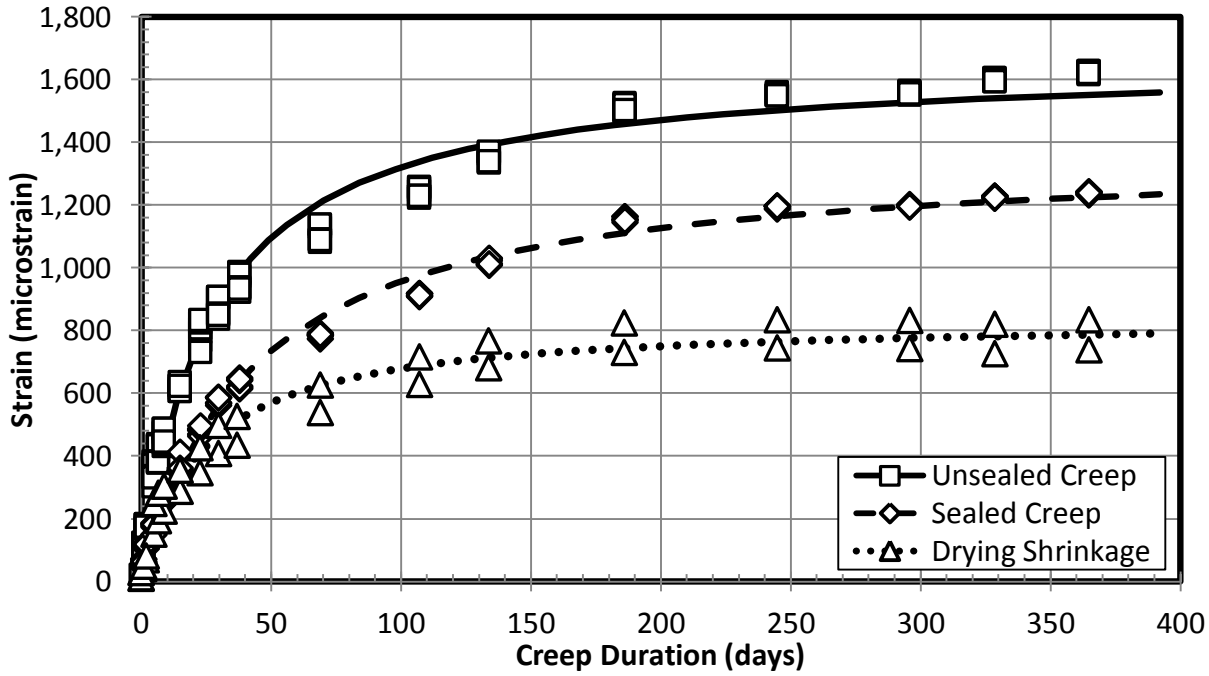

Figure D.3: Long-Term Deformations: DuPont (3/8-in.) High-Paste

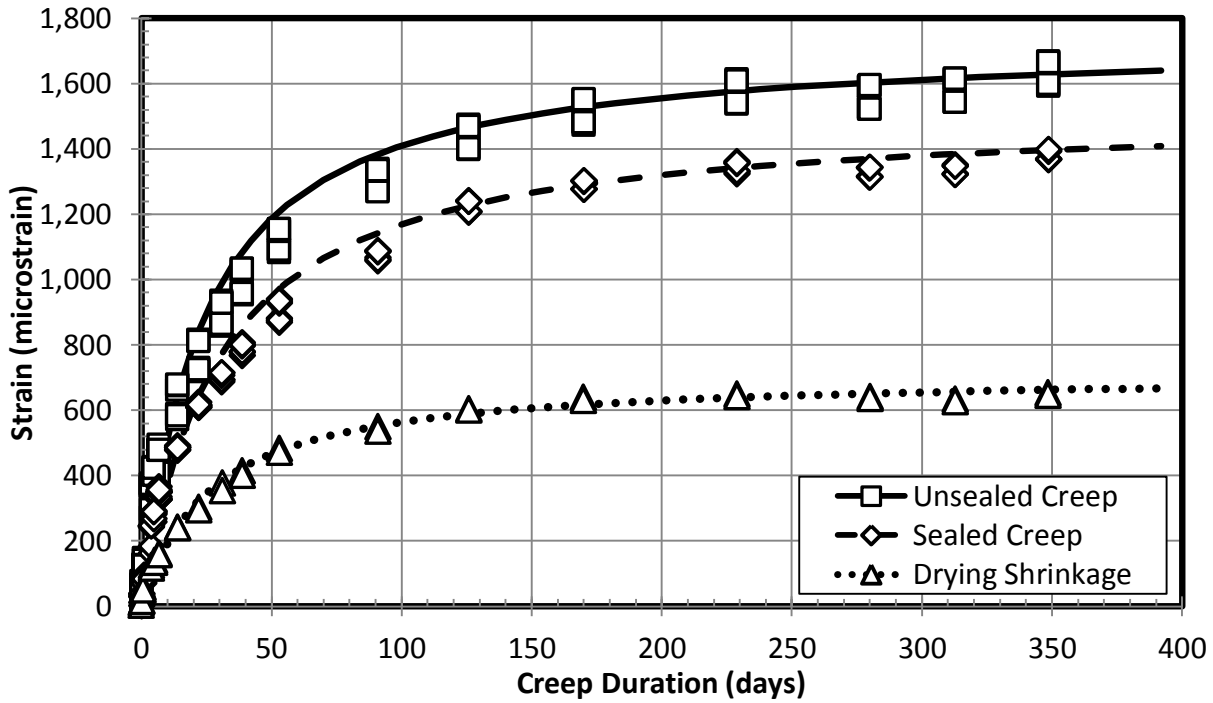

Figure D.4: Long-Term Deformations: DuPont (3/8-in.) Low-Paste

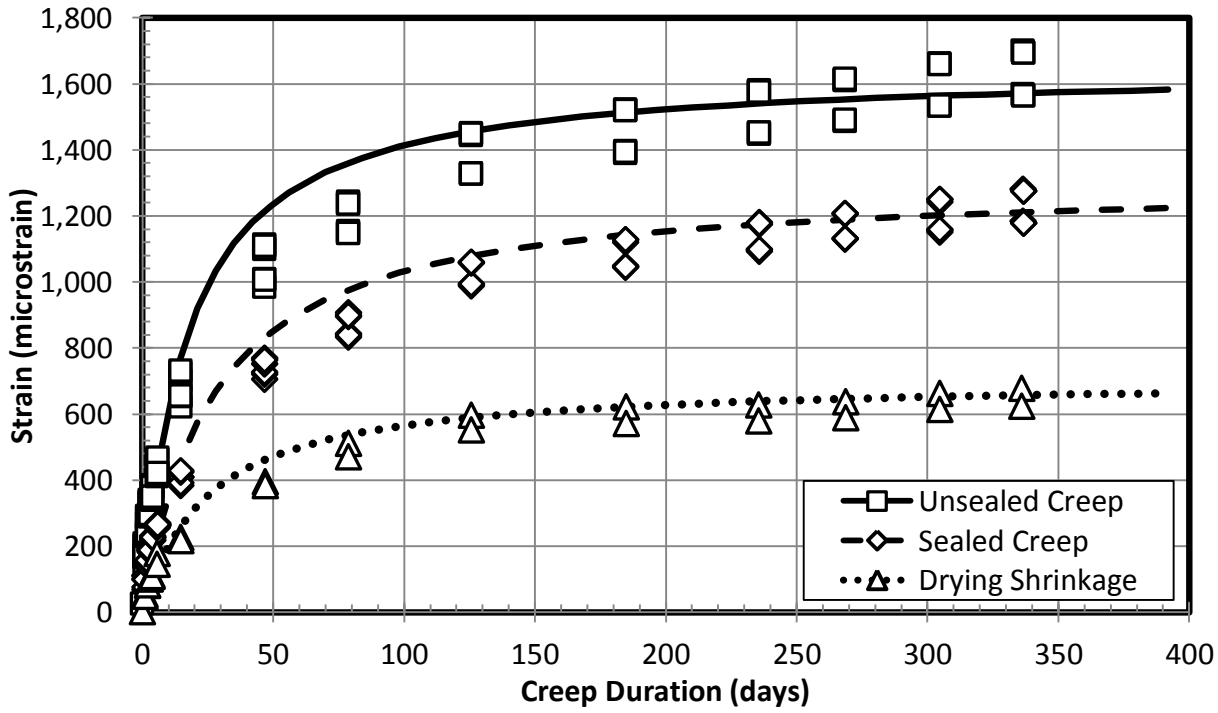

Figure D.5: Long-Term Deformations: Sullivan Road High-Paste

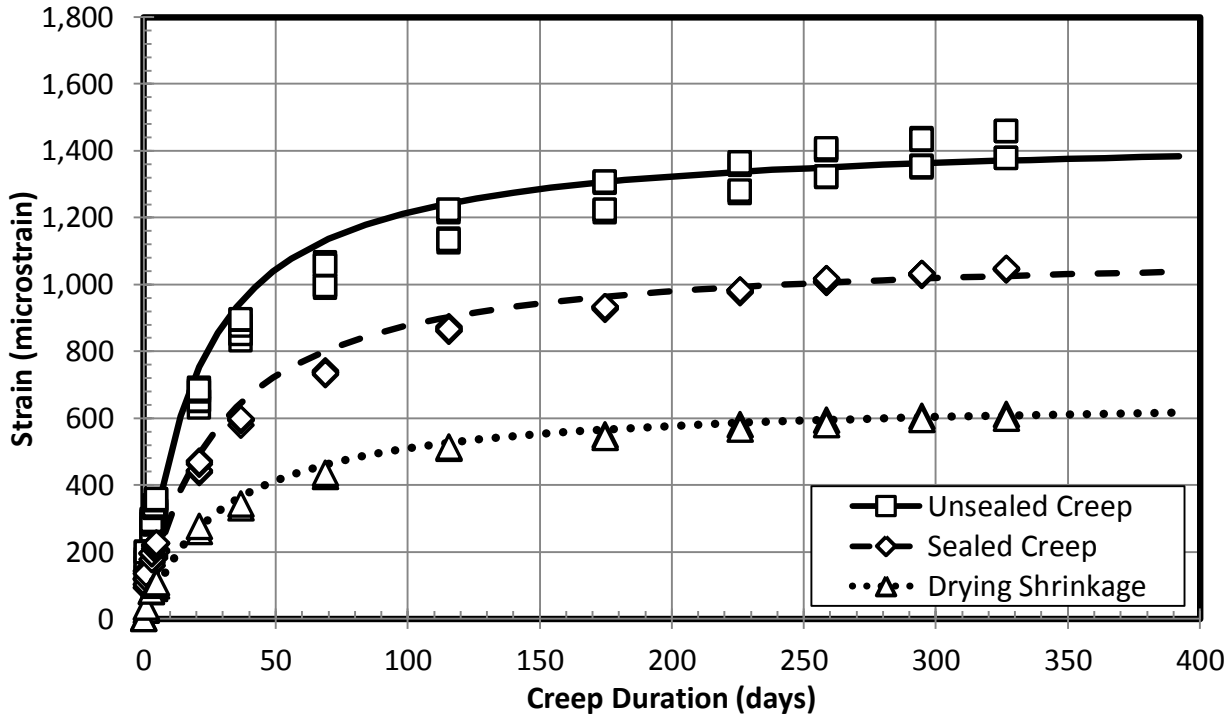

Figure D.6: Long-Term Deformations: Sullivan Road Low-Paste

D.3: MEASURED VS. AASHTO CREEP COEFFICIENT CURVES

The fitted curves for the creep strains are compared with the AASHTO creep specifications (Section 5.4.3.2, Equation 2.12) for each creep mixture. The fitted curve for the DuPont (3/4-in.) high-paste mixture is excluded in this section, but can be seen in Figure 8.4. The following list of figures depicts the fitted curves of the measured and predicted creep strains for each creep mixture: Figure D.7 for DuPont (3/4-in.) low-paste, Figure D.8 for DuPont (3/8-in.) high-paste, Figure D.9 for DuPont (3/8-in.) low-paste, Figure D.10for Sullivan Road high-paste, and Figure D.11 for Sullivan Road low-paste mixture.

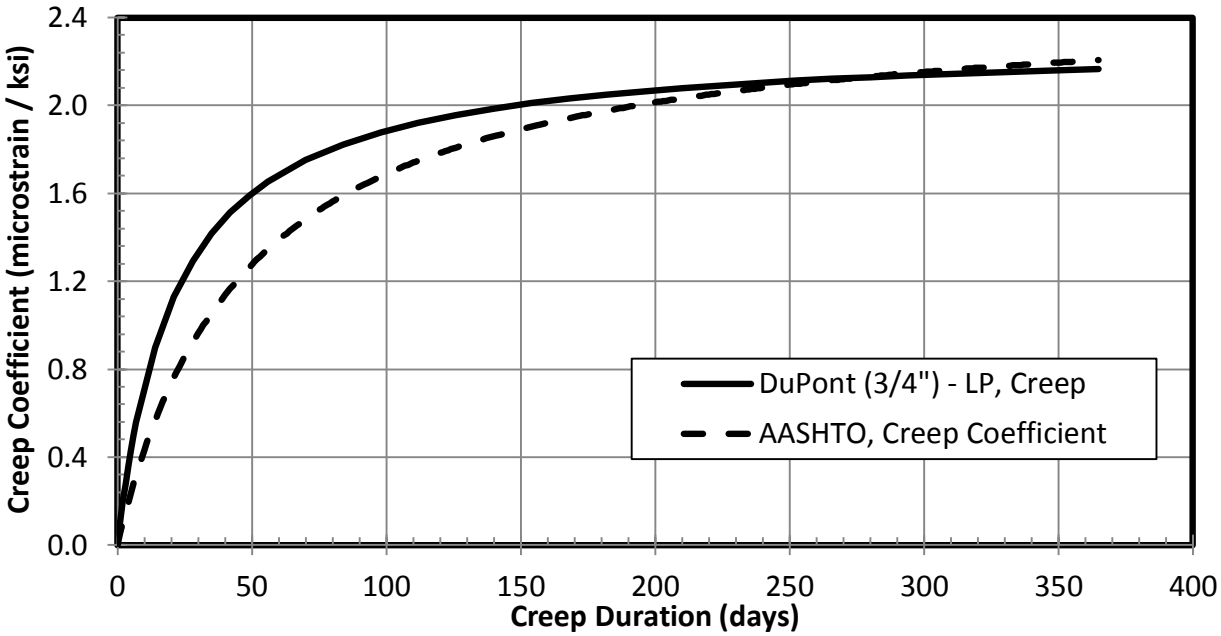

Figure D.7: AASHTO Predicted Creep Coefficient: DuPont (3/4-in.) Low-Paste

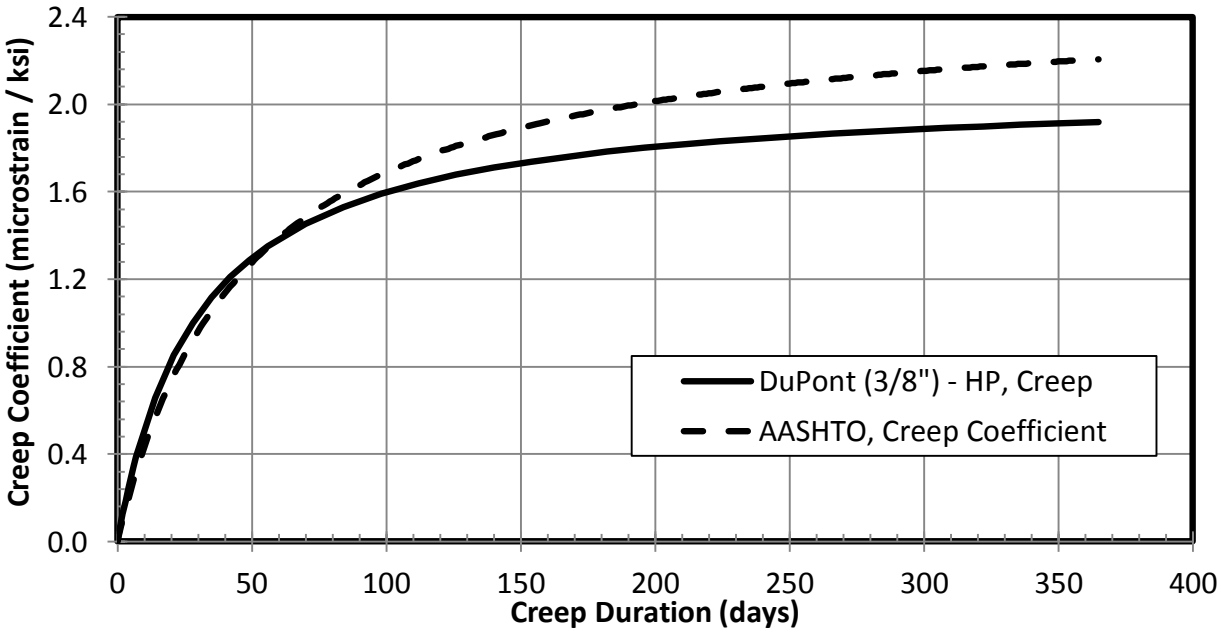

Figure D.8: AASHTO Predicted Creep Coefficient: DuPont (3/8-in.) High-Paste

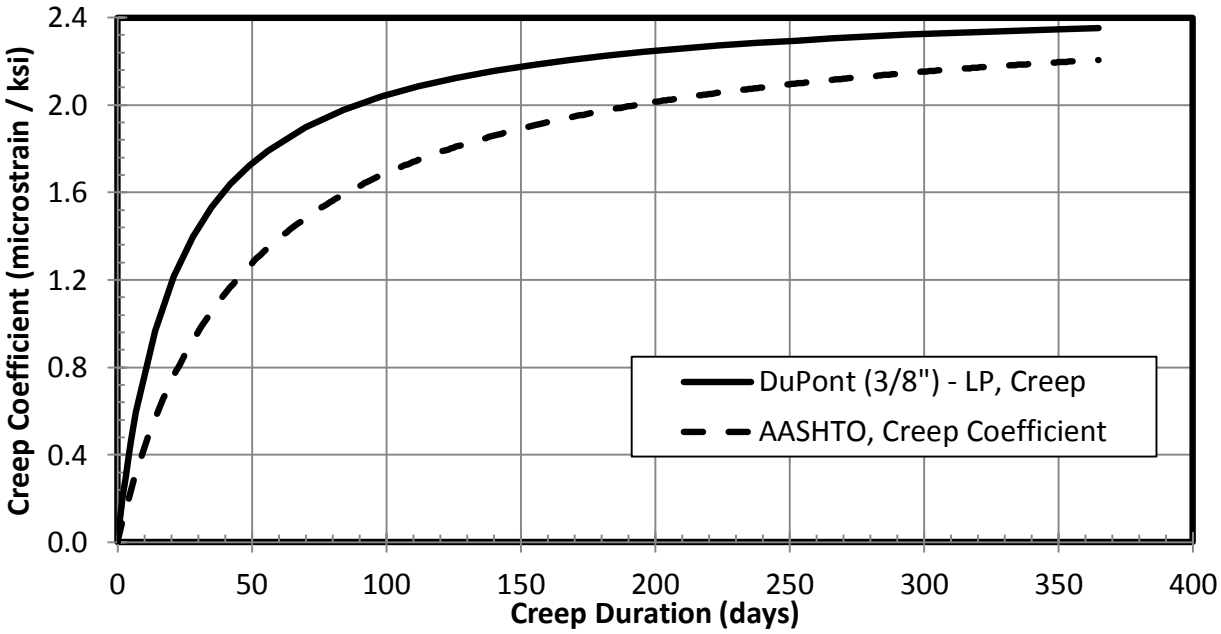

Figure D.9: AASHTO Predicted Creep Coefficient: DuPont (3/8-in.) Low-Paste

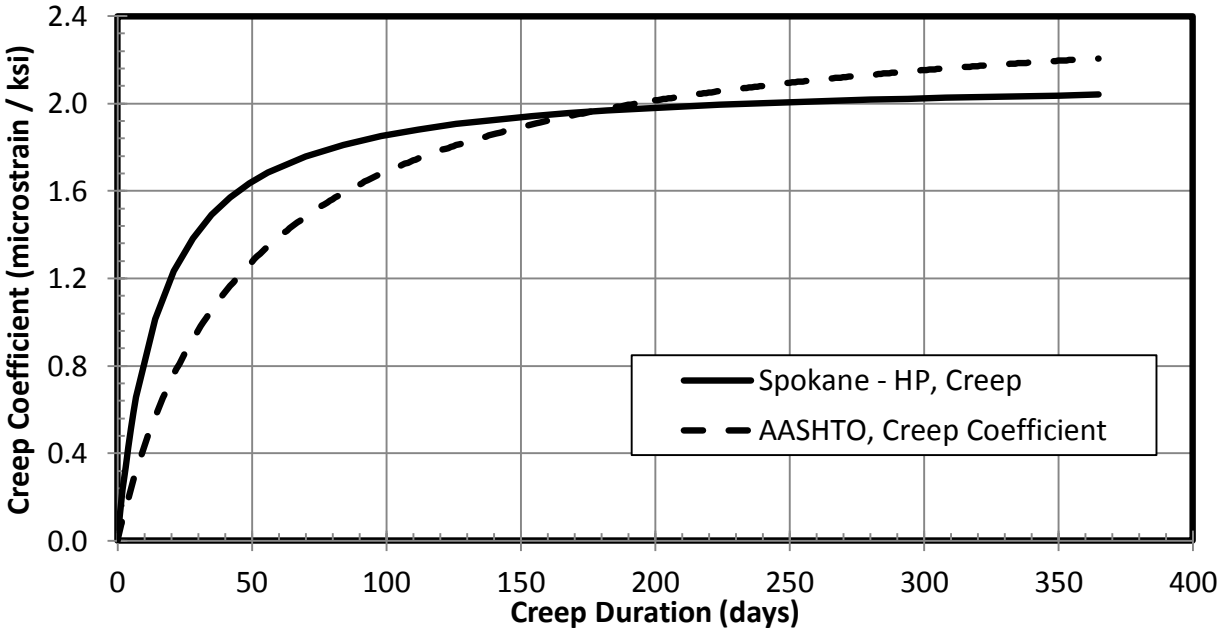

Figure D.10: AASHTO Predicted Creep Coefficient: Sullivan Road High-Paste

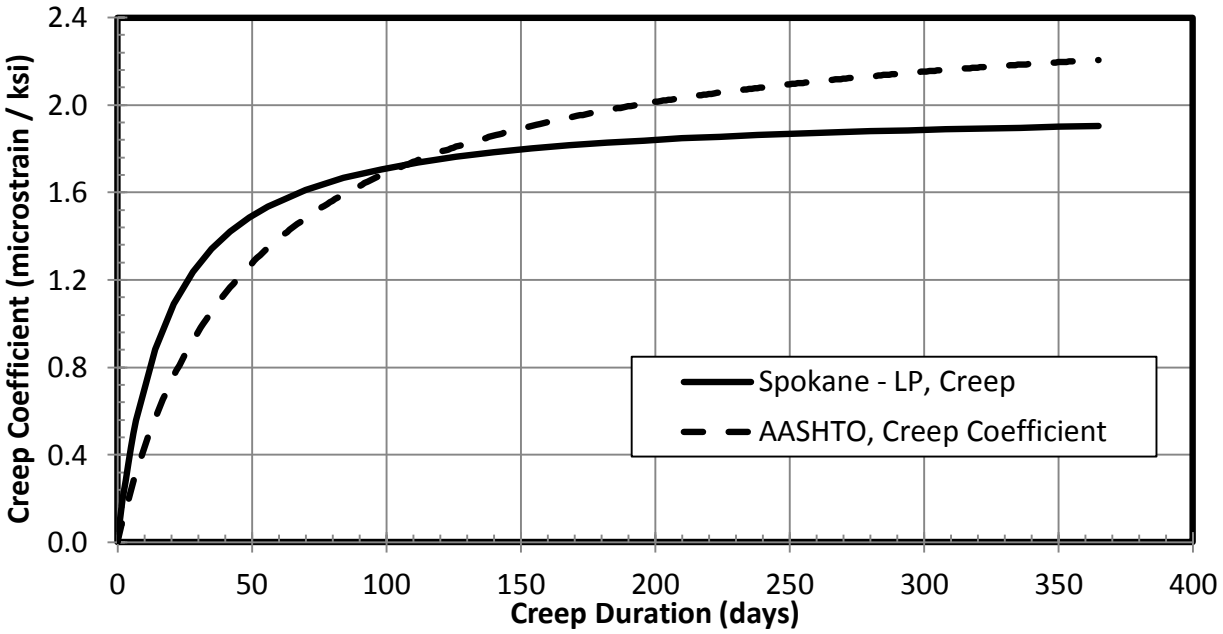

Figure D.11: AASHTO Predicted Creep Coefficient: Sullivan Road Low-Paste

D.4: MEASURED VS. AASHTO CREEP STRAIN EVALUATION

Creep coefficient is calculated by dividing the creep strain with the elastic strain from the initial loading on the concrete. The AASHTO creep coefficient specifications (5.4.3.2, Equation 2.12) can be used to estimate the creep strain at any loading duration. The accuracy of creep strain prediction from AASHTO depends greatly on the calculated elastic deformation. To illustrate this dependence, the creep strains were determined from elastic strain values based on three sets of assumptions:

- The first elastic strain was calculated using the AASHTO predicted elastic modulus (5.4.2.4-1, Equation 2.7) based on the design strength of the mixture (4,000 psi) along with the applied stress (Table 8.7).
- The second elastic strain was calculated using the predicted elastic modulus value (5.4.2.4-1, Equation 2.7) from the measured Day 14 compressive strength (Table 8.8) along with the applied stress (Table 8.7).
- The third elastic strain value was the measured strain value from the initial loading (Table 8.8).

The measured creep strains from each mixture were then modified by multiplying by the ratio of 1,600 psi to the applied stress (Table 8.7). The resulting creep strains from the three AASHTO curves are compared with the measured creep strain curves. The data from the DuPont (3/4-in.) high-paste mixture are excluded in this section, but can be seen in Figure 8.5. The following list of figures compare the measured creep strain curve against the three AASHTO creep curves for each creep mixture: Figure D.12 for DuPont (3/4-in.) low-paste, Figure D.13 for DuPont (3/8-in.) high-paste, Figure D.14 for DuPont (3/8-in.) low-paste, Figure D.15 for Sullivan Road high-paste, and Figure D.16 for Sullivan Road low-paste mixture.

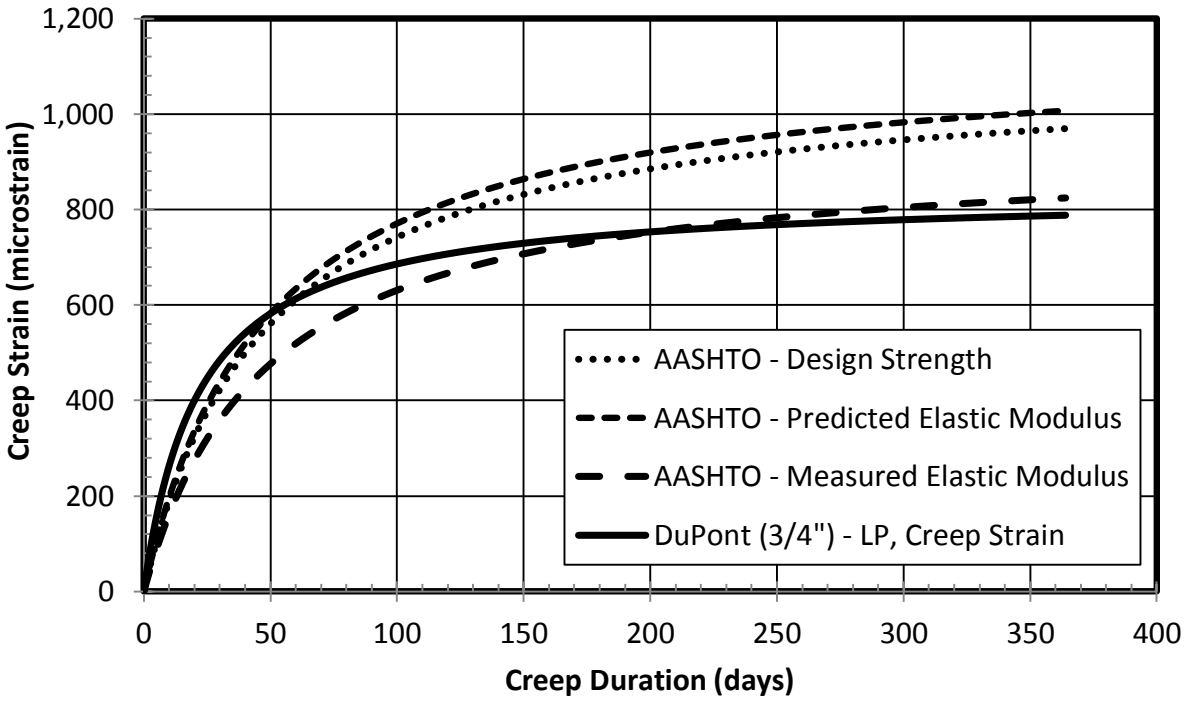

Figure D.12: AASHTO Predicted Creep Strains: DuPont (3/4-in.) Low-Paste

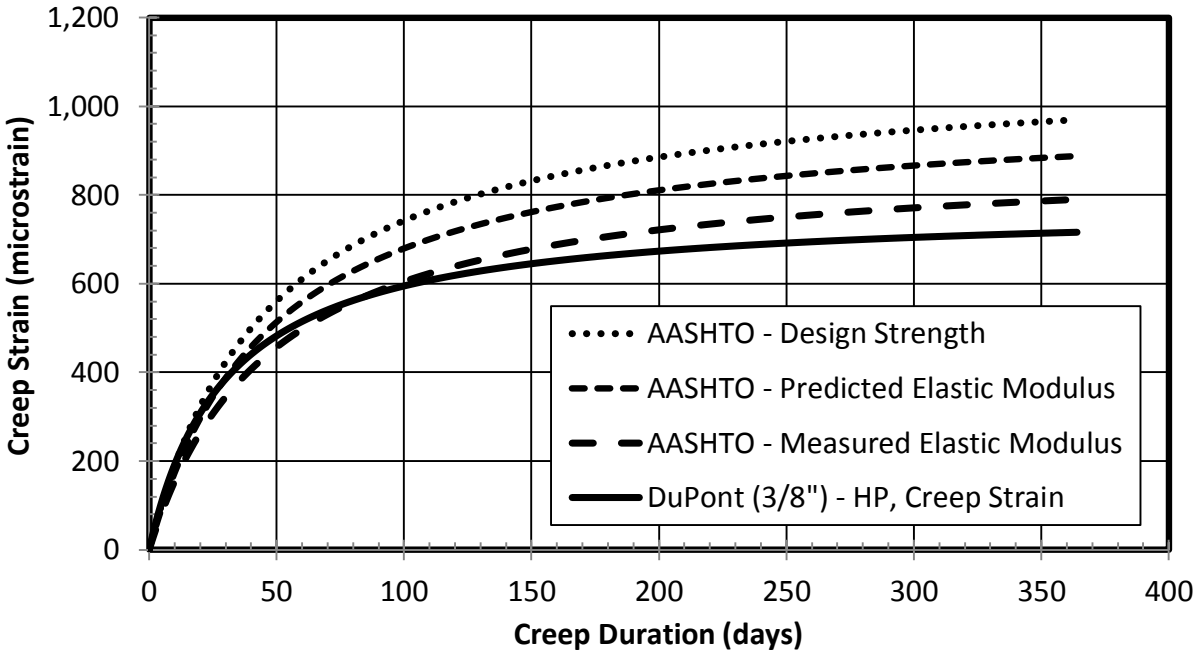

Figure D.13: AASHTO Predicted Creep Strains: DuPont (3/8-in.) High-Paste

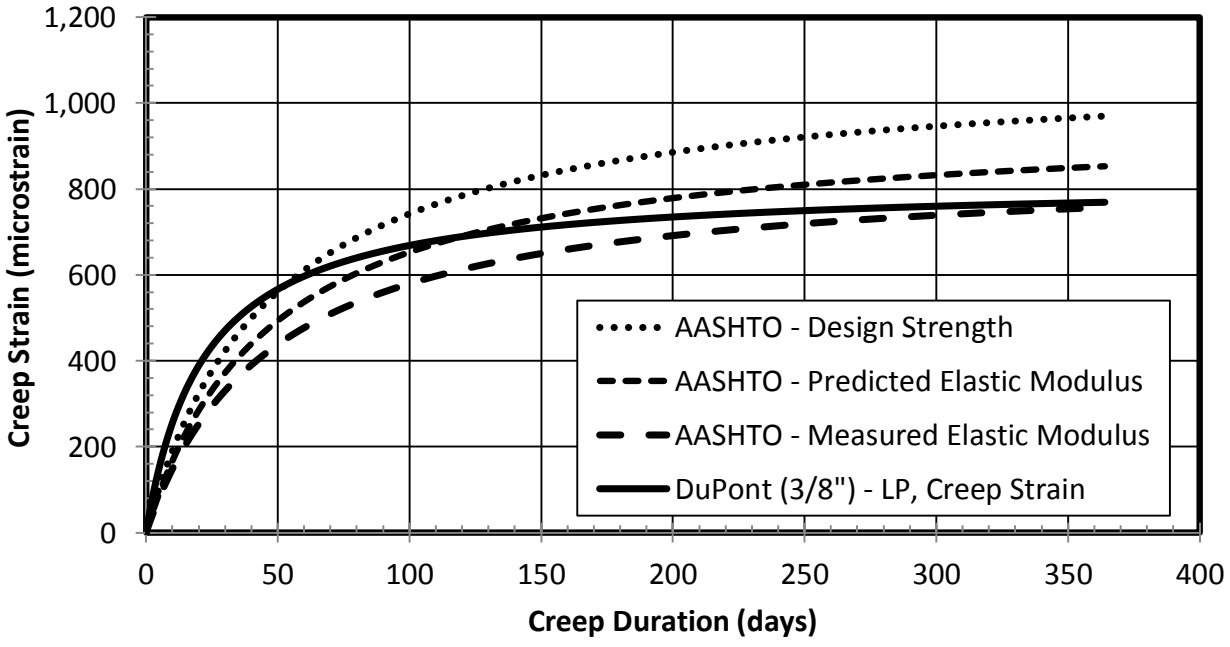

Figure D.14: AASHTO Predicted Creep Strains: DuPont (3/8-in.) Low-Paste

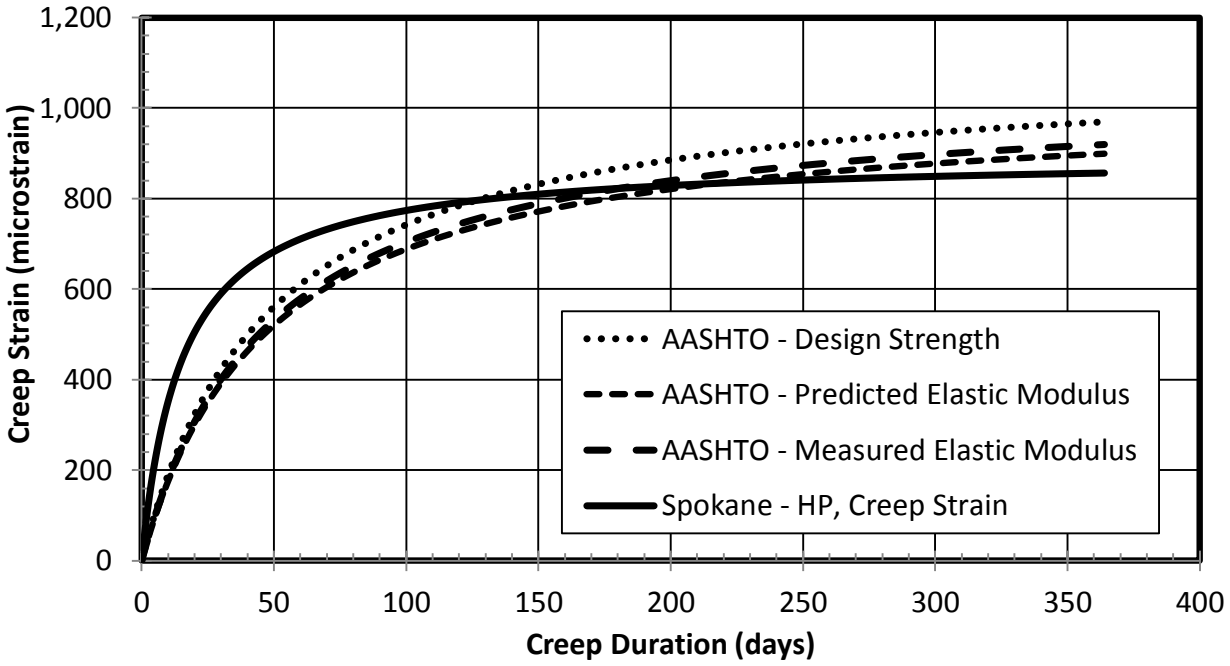

Figure D.15: AASHTO Predicted Creep Strains: Sullivan Road High-Paste

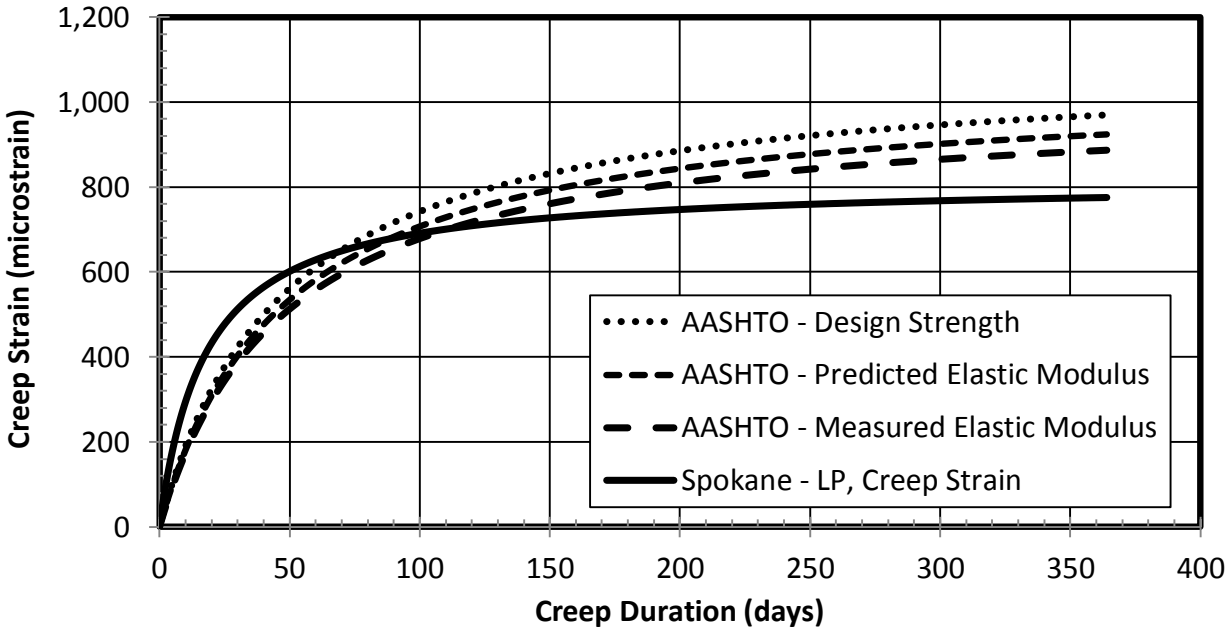

Figure D.16: AASHTO Predicted Creep Strains: Sullivan Road Low-Paste

D.5: IMPROVING EXTRAPOLATED CREEP STRAIN ACCURACY

Variations in the monitored loading duration for the creep strains were documented for this research. By monitoring for a shorter duration and extrapolating the creep strains out to a

year, strain values can be predicted with a lower required testing duration. As Section 8.3 describes, longer testing durations improved the accuracy of the extrapolated creep strain values. To offset this inaccuracy of shorter monitoring durations, a coefficient was determined based on the laboratory creep data to multiply the fitted creep curves (optimized from Equation 8.2). For 180 days of creep strain monitoring, a coefficient of 1.1 provided the most consistent improvement to the extrapolated strain values. For 56 days of monitoring, a coefficient of 1.2 improved the creep data the best.

The improvement of the fitted creep curves from DuPont (3/4-in.) high-paste mixture is excluded in this section, but can be seen in figures 8.12 and 8.13. The following list of figures shows the improvement to the modified creep curves from 180 days of monitored data for each creep mixture: Figure D.17 for DuPont (3/4-in.) low-paste, Figure D.18 for DuPont (3/8-in.) high-paste, Figure D.19 for DuPont (3/8-in.) low-paste, Figure D.20 for Sullivan Road high-paste, and Figure D.21 for Sullivan Road low-paste mixture.

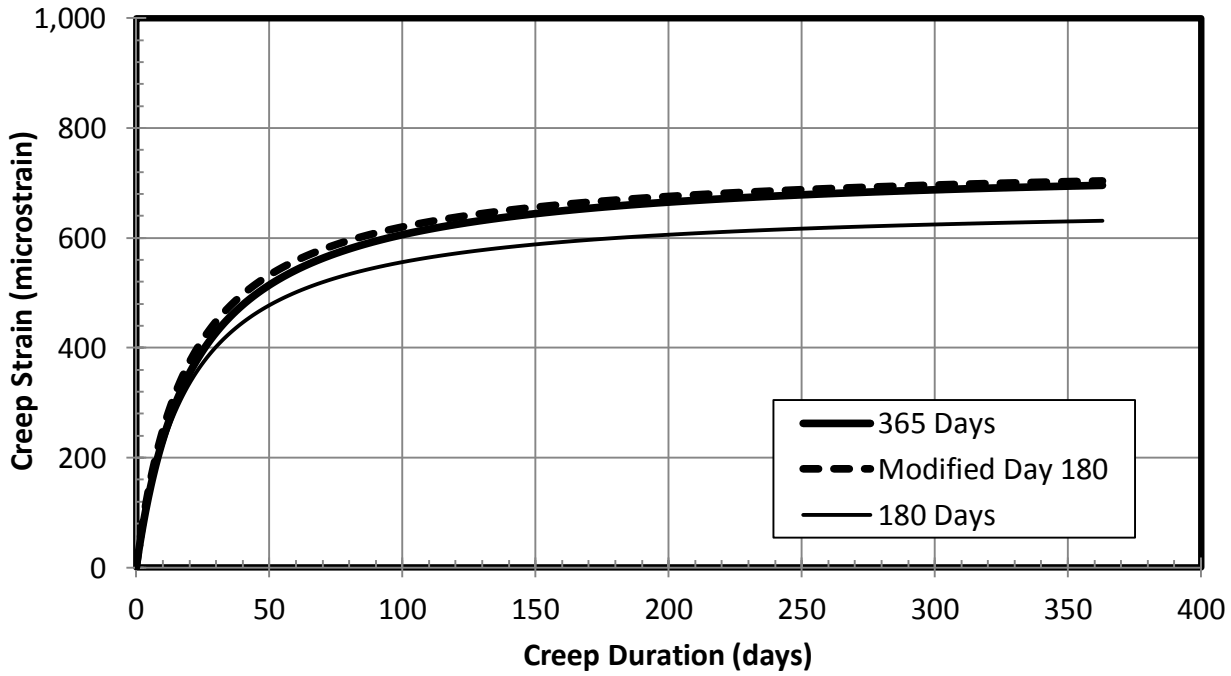

Figure D.17: Modified Day 180 Creep Strain Curves: DuPont (3/4-in.) Low-Paste

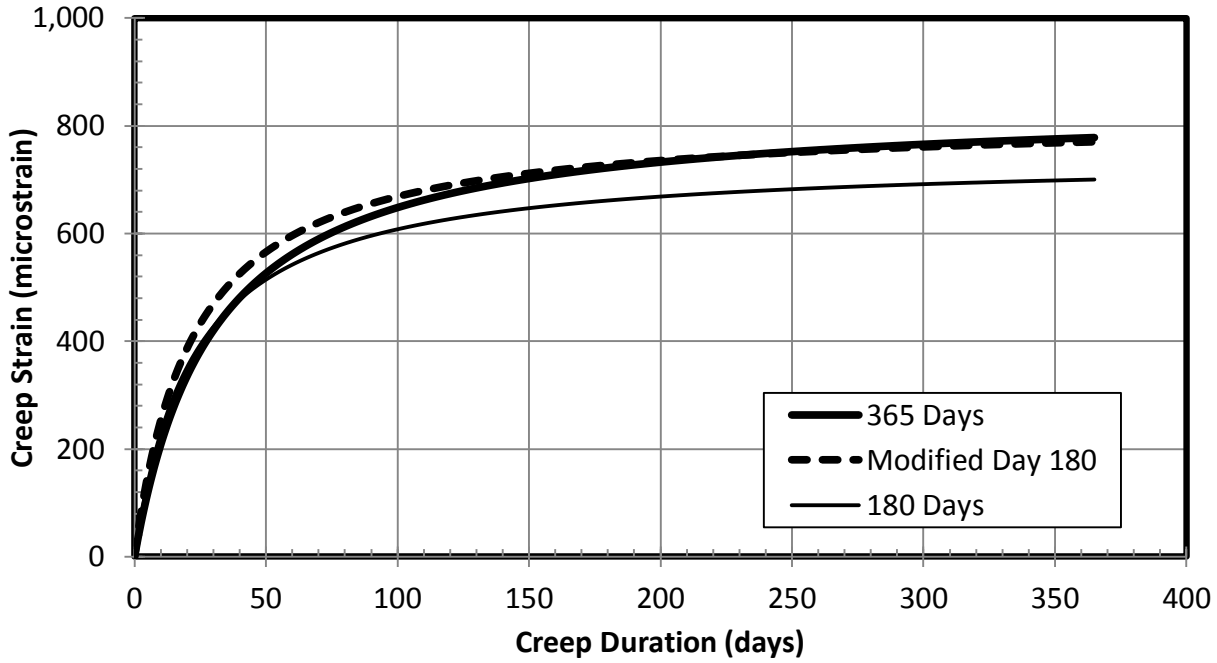

Figure D.18: Modified Day 180 Creep Strain Curves: DuPont (3/8-in.) High-Paste

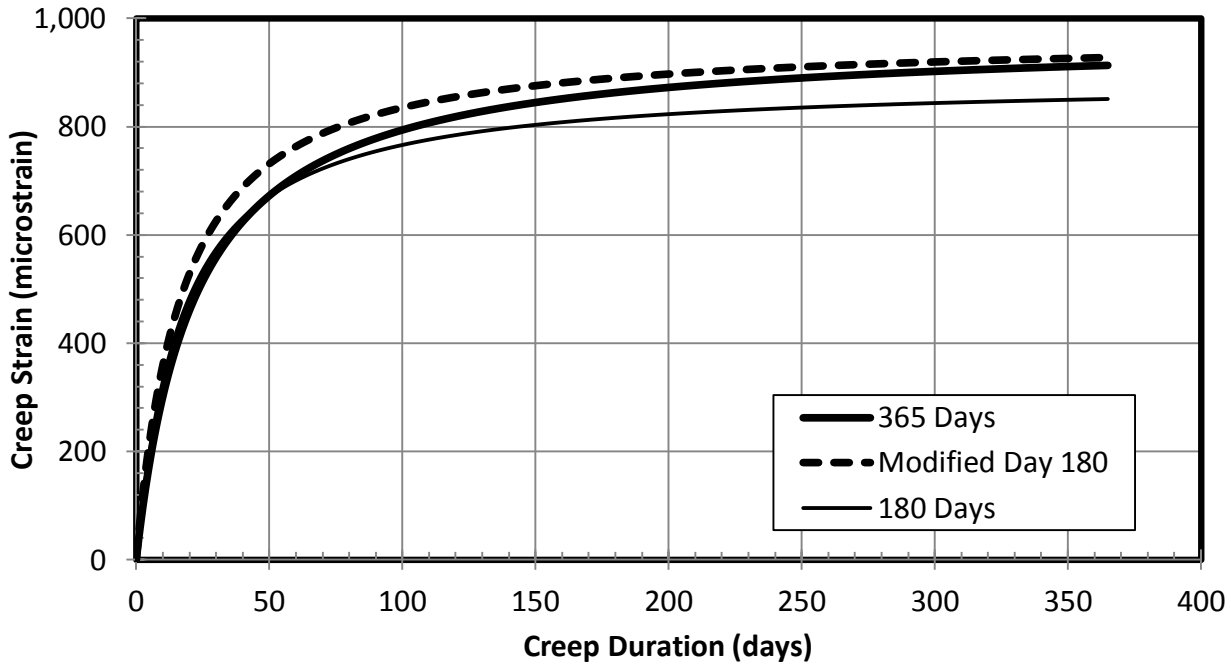

Figure D.19: Modified Day 180 Creep Strain Curves: DuPont (3/8-in.) Low-Paste

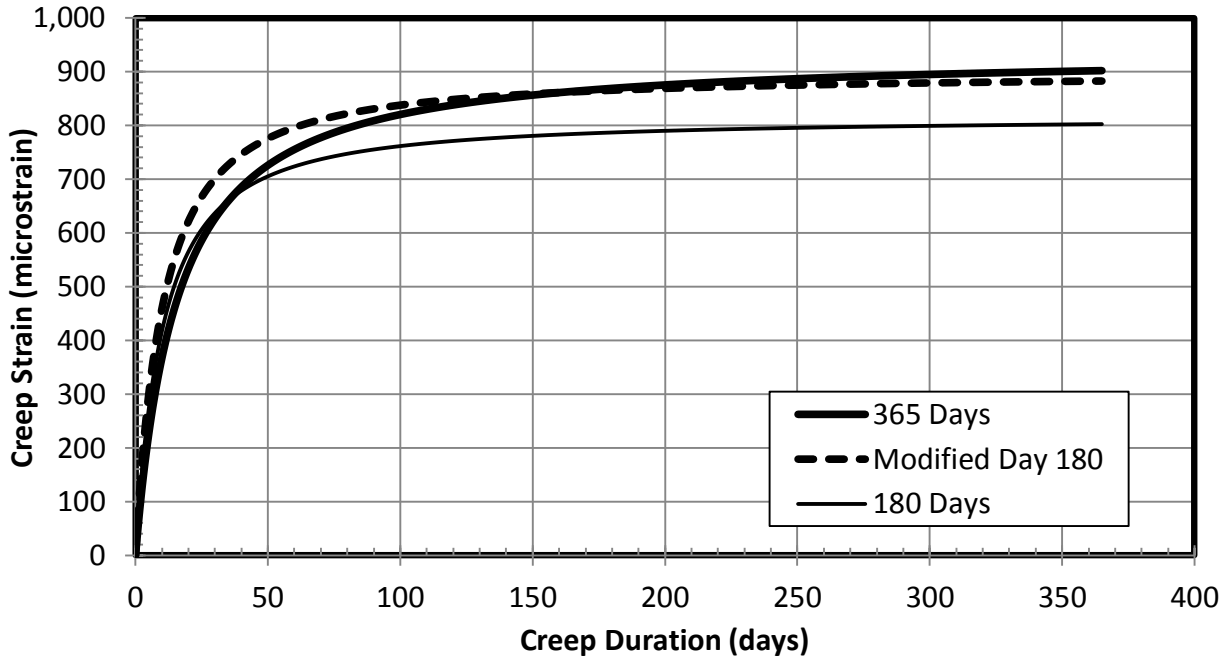

Figure D.20: Modified Day 180 Creep Strain Curves: Sullivan Road High-Paste

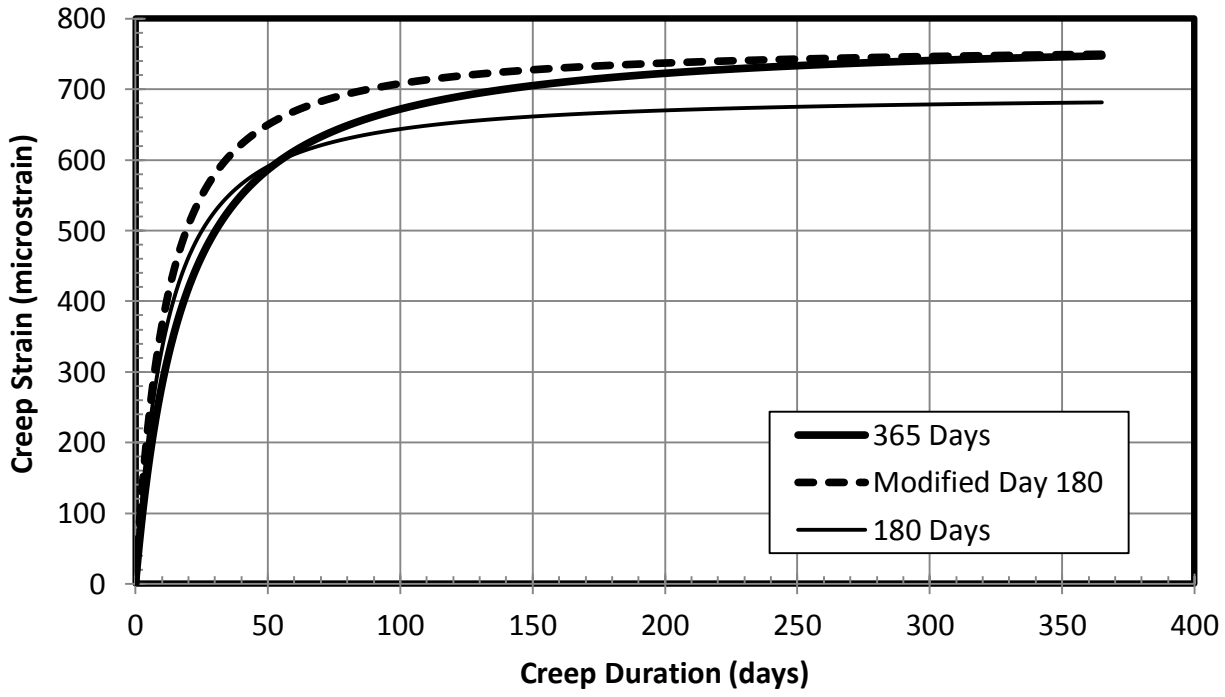

Figure D.21: Modified Day 180 Creep Strain Curves: Sullivan Road Low-Paste

The following list of figures shows the improvement to the modified creep curves from 56 days of monitored data for each creep mixture: Figure D.22 for DuPont (3/4-in.) low-paste, Figure D.23 for DuPont (3/8-in.) high-paste, Figure D.24 for DuPont (3/8-in.) low-paste, Figure D.25 for Sullivan Road high-paste, and Figure D.26 for Sullivan Road low-paste mixture.

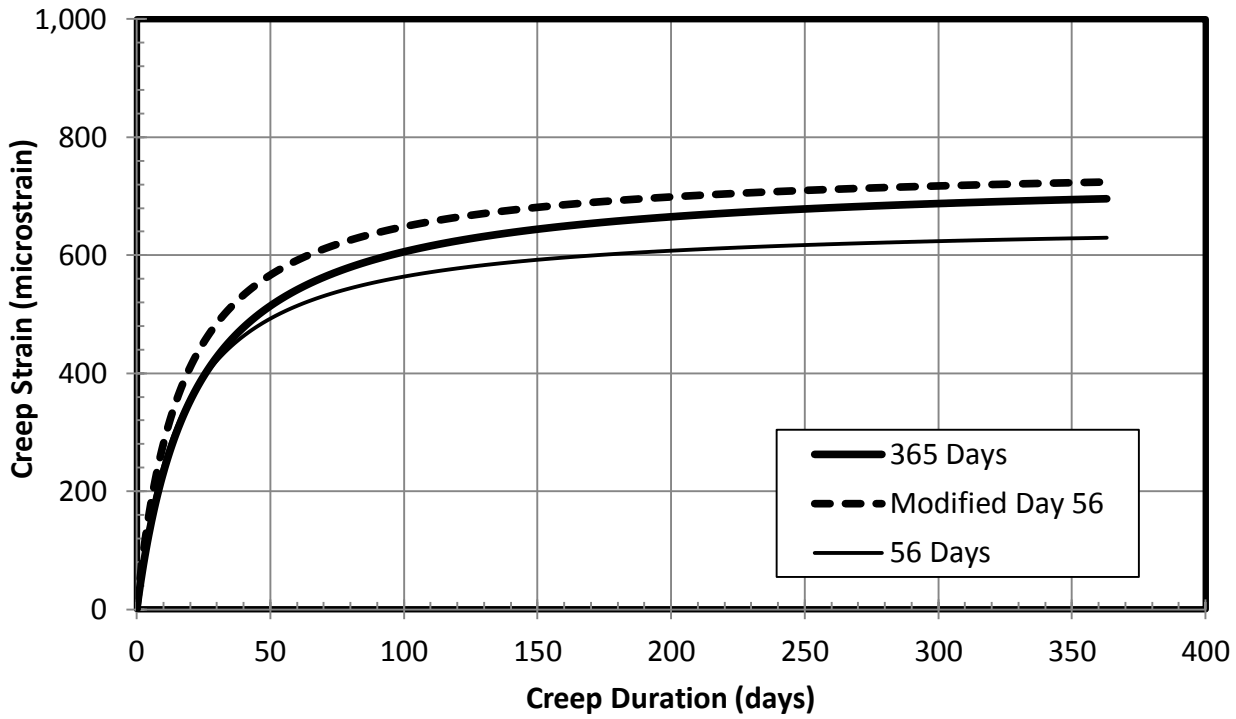

Figure D.22: Modified Day 56 Creep Strain Curves: DuPont (3/4-in.) Low-Paste

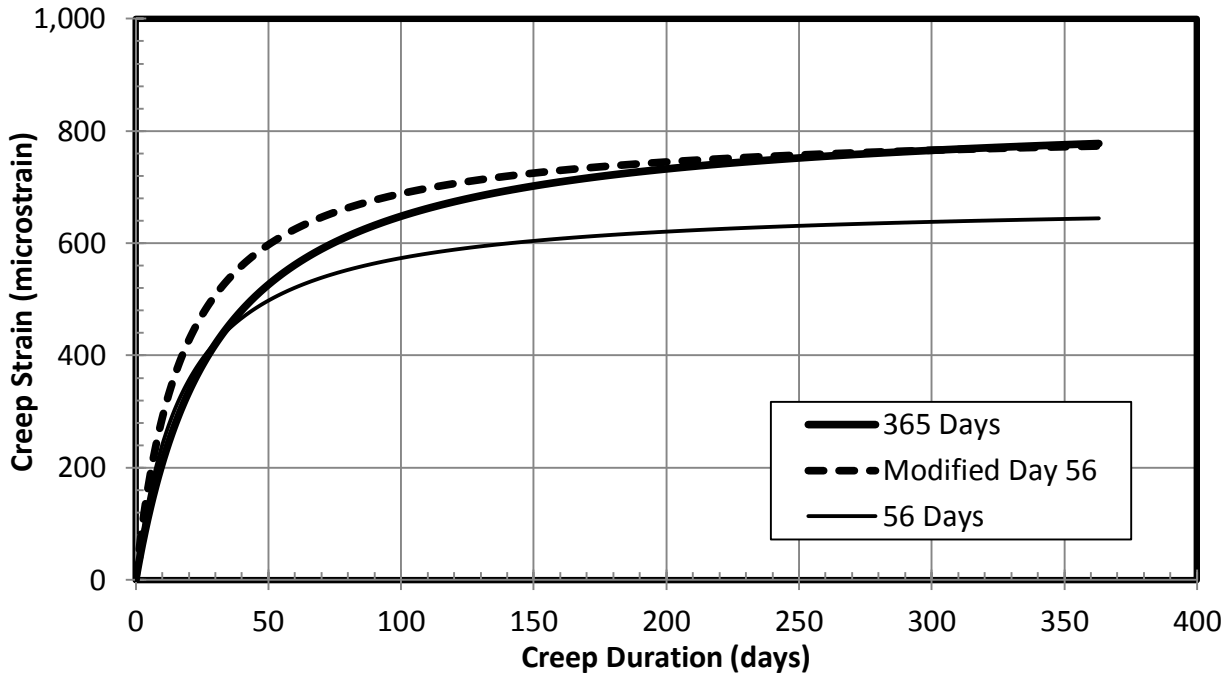

Figure D.23: Modified Day 56 Creep Strain Curves: DuPont (3/8-in.) High-Paste

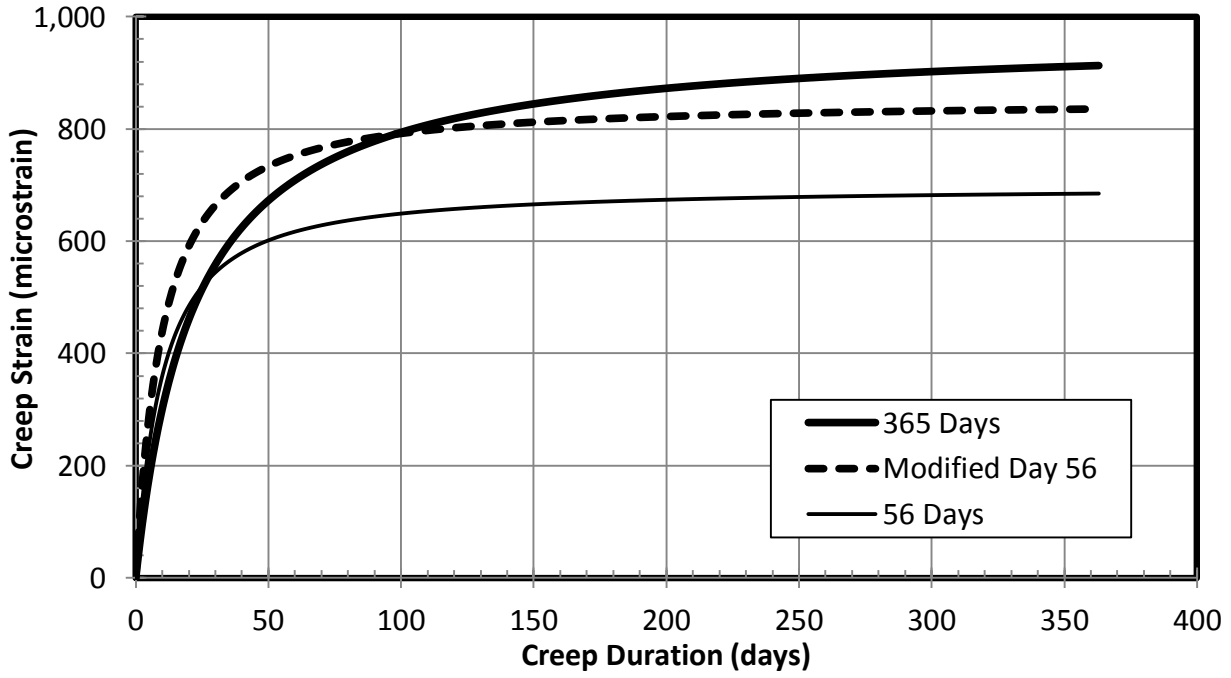

Figure D.24: Modified Day 56 Creep Strain Curves: DuPont (3/8-in.) Low-Paste

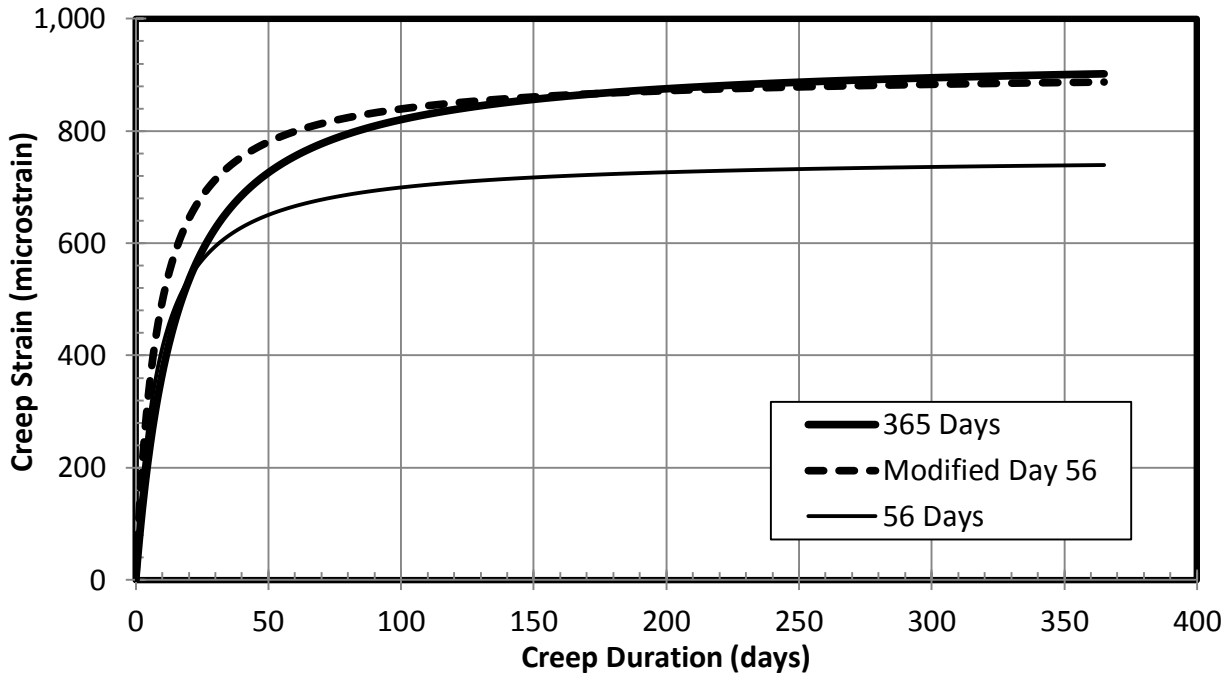

Figure D.25: Modified Day 56 Creep Strain Curves: Sullivan Road High-Paste

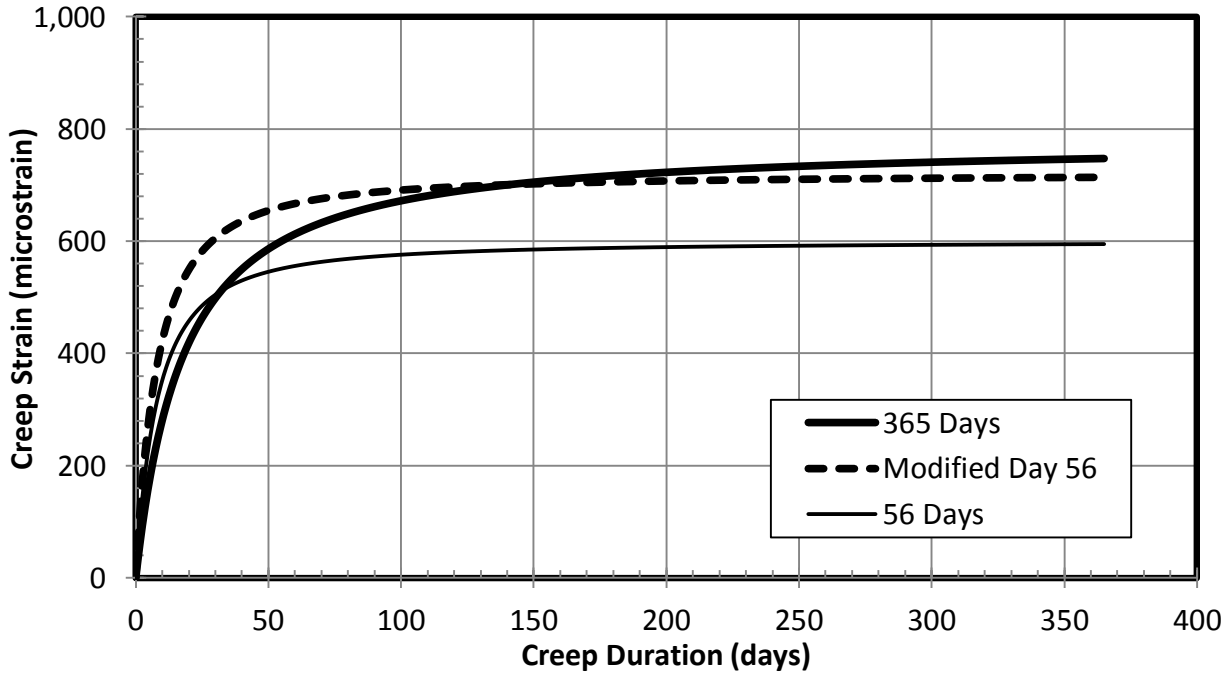

Figure D.26: Modified Day 56 Creep Strain Curves: Sullivan Road Low-Paste